

Immunostimulatory Properties of Nucleic Acid Nanoparticles

by

Justin Ross Halman

A dissertation submitted to the faculty of
The University of North Carolina at Charlotte
in partial fulfillment of the requirements
for the degree of Doctor of Philosophy in
Nanoscale Science

Charlotte

2020

Approved by:

Dr. Kirill Afonin

Dr. Kausik Chakrabarti

Dr. Ian Marriott

Dr. Yuri Nesmelov

Dr. Juan Vivero-Escoto

Dr. Andy Bobyarchick

ABSTRACT

JUSTIN ROSS HALMAN. Immunostimulatory Properties of Nucleic Acid Nanoparticles.
(Under the direction of DR. KIRILL AFONIN)

Nucleic acids (DNA and RNA) are ubiquitous biomolecules found throughout all living organisms. They can act as genetic information storage and messengers, enzymes, molecular switches, and much more. Although DNA is used almost exclusively for its ability to store information, discoveries in the roles of RNA in development and homeostasis through complex molecular interactions are ever-expanding. The myriad of roles that nucleic acids can perform makes them ideal therapeutic candidates, as well as molecular machines, and their inherent structure makes investigating their use as materials a worthwhile endeavor. Combining these applications, nucleic acid nanoparticles have the ability to assume any designable structure, varying in shape, size, and composition. This degree of structural customizability, made possible by both Watson-Crick canonical interactions and non-canonical, further enhance the ability to fine-tune a given nanoparticles resulting physicochemical properties. Additionally, their inherent structures make them able to simultaneously carry several different pharmaceuticals including nucleic acid-based agents such as RNA interference inducers, aptamers, and immunostimulatory sequences, as well as small molecules and fluorescent entities. This combination of customizability, biocompatibility, and therapeutic activity makes nucleic acid nanoparticles a highly promising approach for treating complex diseases. Despite rapid advances in the field of therapeutic nucleic acids, unexpected deleterious immune responses have halted both clinical trials and research, leading to hesitation towards their advancement into clinical use. This dissertation aims to elucidate the link between structure and composition of nucleic acid nanoparticles and their ability to produce an immune response in cells. Furthermore, the investigation of chemical modifications, existing both naturally in cells as well as artificially for therapies, is explored for its use in enhancing the stability of nucleic acid nanoparticles while altering their immunostimulatory capabilities. Finally, an approach of dynamic, response activated nucleic acid nanoparticles is explored.

Acknowledgements

There are so many people to thank and acknowledge for their support throughout this PhD process. First and foremost, I would like to thank my advisor, Dr. Kirill Afonin, who taught me so much throughout these years, and provided me a push in the right direction when needed. I'd also like to thank my committee as well as the professors at UNC Charlotte who have helped make me the scientist I am today. Additionally, I would like to thank the members of the Afonin lab, with whom I have spent long hours talking, joking, and occasionally doing research with. Whether through discussions or collaborations, research is very much a team sport and I would be lost without their support.

I would also like to thank my family who have supported me far beyond just my years in graduate school. Mom, Dad, and Alexander, everything that I have accomplished thus far has only been made possible with your encouragement, and occasional (and deserved) chastising. Lastly, I need to also thank Morgan Chandler, who falls under both lab mate and family. Thank you for your love and support, spending long hours in lab with me and going on all of our adventures; I can't wait to see what comes next.

Table of Contents

LIST OF TABLES	VII
TABLE OF FIGURES	VIII
LIST OF ABBREVIATIONS.....	XIV
1 CHAPTER 1: INTRODUCTION	1
1.1 NUCLEIC ACIDS IN MOLECULAR BIOLOGY	1
1.1.1 Structure and interactions of nucleic acids	1
1.1.2 Functions of nucleic acids	4
1.1.3 Chemical modifications of nucleic acids	8
1.1.4 Natural immune response to nucleic acids	11
1.2 NUCLEIC ACID THERAPEUTICS.....	13
1.2.1 Anti-sense oligonucleotides and RNA interference.....	13
1.2.2 Aptamers as therapeutics	15
1.2.3 Immunostimulation from nucleic acids as a therapeutic approach	17
1.3 NUCLEIC ACID NANOTECHNOLOGY	18
1.3.1 Rational design and computed assisted strategies	19
1.3.2 Therapeutic nucleic acid nanotechnology.....	23
1.3.3 Delivery of therapeutic nucleic acid with nanotechnology.....	25
1.4 DISSERTATION SUMMARY	28
1.5 REFERENCES	30
2 CHAPTER 2: FUNCTIONALLY-INTERDEPENDENT SHAPE-SWITCHING NANOPARTICLES WITH CONTROLLABLE PROPERTIES	50
2.1 INTRODUCTION.....	50
2.2 METHODS.....	52
2.2.1 Nanoparticle assembly and purification.	52
2.2.2 UV-melting experiments.	53
2.2.3 Kinetics of re-association determination.	54
2.2.4 Primary human peripheral blood mononuclear cell and whole blood culture for analysis of interferon and cytokine secretion.	55
2.2.5 Nuclease digestion assays.....	55
2.2.6 Computational predictions and 3D modeling.....	56
2.2.7 Activation of FRET	57
2.2.8 AFM imaging and sample preparation	57
2.2.9 Transfection of human cell lines.....	58
2.2.10 Fluorescent microscopy.....	59
2.2.11 Flow Cytometry.....	59
2.2.12 Cell proliferation assay.....	59
2.2.13 Statistics.....	60
2.3 RESULTS AND DISCUSSION.....	61
2.3.1 Complementary nanoparticles have controlled rates of re-association and fine-tunable thermodynamic, chemical, and immunogenic properties	61
2.3.2 Re-association of complementary DNA nanoparticles triggers co-transcriptional formation of RNA nanoparticles.....	69
2.3.3 Re-association of complementary DNA nanoparticles triggers activation of embedded split RNA aptamers	71
2.3.4 Re-association of complementary nanoparticles triggers activation of energy transfer and RNA interference in cells	72
2.3.5 Other examples of complementary nanoparticles.....	75
2.4 CONCLUSION.....	78
2.4.1 Sequences used in this project	79
2.5 REFERENCES	87

3	CHAPTER 3: PROGRAMMABLE NUCLEIC ACID-BASED POLYGONS WITH CONTROLLED NEUROIMMUNOMODULATORY PROPERTIES FOR PREDICTIVE QSAR MODELING	91
3.1	INTRODUCTION.....	91
3.2	METHODS.....	93
3.2.1	Assembly of polygons and their characterization.....	93
3.2.2	3D modeling.....	93
3.2.3	Atomic force microscopy (AFM).....	94
3.2.4	Dynamic Light Scattering (DLS).....	94
3.2.5	Degradation assay in fetal bovine serum (FBS).....	94
3.2.6	Equilibrium dissociation constant (KD) measurements.....	95
3.2.7	Structural integrity of polygons associated with Lipofectamine 2000 (L2K).....	95
3.2.8	Transfections.....	95
3.2.9	Cell Viability.....	96
3.2.10	Relative uptake efficiencies in hHu.....	96
3.2.11	Enzyme-linked Immunosorbent Assay (ELISA).....	97
3.2.12	Limulus Amoebocyte Lysate (LAL) assay.....	97
3.2.13	Statistics.....	97
3.2.14	Quantitative Structure-Activity Relationship (QSAR) modeling.....	98
3.2.15	QSAR approach.....	98
3.2.16	Descriptors.....	98
3.2.17	Machine learning method.....	98
3.2.18	Model construction and validation.....	99
3.2.19	Evaluation of the model prediction accuracy.....	99
3.3	RESULTS AND DISCUSSION.....	100
3.4	CONCLUSION.....	109
3.4.1	Sequences used in this project.....	113
3.5	REFERENCES.....	117
4	CHAPTER 4: A CATIONIC AMPHIPHILIC CO-POLYMER AS A CARRIER OF NUCLEIC ACID NANOPARTICLES (NANPs) FOR CONTROLLED GENE SILENCING, IMMUNOSTIMULATION, AND BIODISTRIBUTION	121
4.1	INTRODUCTION.....	121
4.2	METHODS.....	123
4.2.1	Synthesis of PgP and NANPs.....	123
4.2.2	Nuclease protection assay of PgP/DNA duplex polyplexes.....	123
4.2.3	Physical characterization of NANPs.....	124
4.2.4	Fluorescent microscopy and cellular uptake.....	124
4.2.5	Specific gene silencing and cell viability.....	125
4.2.6	Immunostimulation in vitro.....	126
4.2.7	Hemolysis assay in vitro.....	127
4.2.8	Biodistribution of PgP/NANP polyplexes after systemic injection.....	127
4.2.9	Statistics.....	128
4.3	RESULTS.....	129
4.3.1	PgP/DNA stability, binding, and nuclease protection assay.....	129
4.3.2	Intracellular uptake of PgP/RNA or PgP/DNA complexes.....	130
4.3.3	Characterization of PgP/NANP polyplexes.....	131
4.3.4	Gene silencing with PgP/NANP(GFP or RhoA) polyplexes.....	133
4.3.5	Hemocompatibility and immunotoxicity of PgP/NANP polyplexes.....	134
4.3.6	Biodistribution of PgP/NANP polyplexes after systemic in vivo administration.....	138
4.4	DISCUSSION.....	139
4.5	CONCLUSION.....	141
4.5.1	Sequences used in this project.....	142
4.6	REFERENCES.....	146
5	CHAPTER 5: CONCLUSIONS.....	150

List of Tables

Table 1. Endotoxin in the test samples was measured by kinetic turbidity LAL. Spike recovery between 50 and 200% indicates that the tested nanoparticle did not interfere with the assay and the value of endotoxin shown in the middle column is valid.	104
Table 2. Model accuracy estimated during 5-fold cross validation procedure.	108
Table 3. Descriptor's contribution into the Random Forest models. Bold and italic font represents the most important descriptors.	109
Table 4. The data set for 16 polygons used for QSAR modeling.	112
Table 5. Immunogenic values experimentally observed and predicted with QSAR model based on physicochemical descriptors.	113
Table 6. Hemocompatibility of various PgP/NANP polyplexes at N/P ratio of 30/1 on rat erythrocytes in vitro. % hemolysis= (A sample-A PBS) / (A Tritonx-100-A PBS) X 100	141

Table of Figures

Figure 1. Functions of DNA and RNA in molecular biology. DNA is used almost exclusively for storage of genetic information, whereas RNA has diverse functions some of which are schematically shown.	5
Figure 2. Chemical modifications of DNA and RNA effect their folding and molecular interactions.	9
Figure 3. Schematic demonstrating the main receptors and proteins in coordinating an immune response to foreign nucleic acids.	11
Figure 4. (A) Schematic representation of DNA and RNA nanoparticles. (B) Schematic representation of several nanocarriers. (C) Surface modifications of nanoparticles allowed for enhanced targeting and tunable physicochemical properties.	26
Figure 5. Schematics depicting the design principles of complementary nucleic acid nanoparticles.	50
Figure 6. Fine-tunable isothermal re-association of complementary shape-switching nanoparticles. (A) Schematic representation of re-association between the complementary cube and anti-cube nanoparticles. (B) 3D models of nanoparticles. (C) AFM images of RNA, RNA/DNA, DNA cubes and RNA anti-cube. (D) Experimental and predicted melting temperatures of nanoparticles controlled by their compositions and native-PAGE with corresponding assemblies. Error bars indicate s.d.; N=3 (E) Relative re-association rates of RNA, RNA/DNA, and DNA cubes with DNA anti-cubes measured at 25 °C and native-PAGE with corresponding re-associations visualized after 30 mins of incubation. Error bars indicate s.d.; N=3. (F) Relative stabilities of nanoparticles in the presence of DNase, RNase, and human blood serum. Results are normalized to corresponding non-treated samples. Error bars indicate s.d.; N=3. (G) Immunostimulatory properties of RNA, RNA/DNA, and DNA shape-switching nanoparticles delivered using Lipofectamine 2000. Error bars indicate s.d.; N=2. Statistically significant results (compared to PC) are indicated with asterisks (p -value < 0.05). For IL-1 β and TNF α all results are statistically significant. In (D-E), note that the higher number of RNA strands per nanoparticle weakens the extent of total staining.	60
Figure 7. Melting temperatures measured by UV-melt for varying compositions of cube and anti-cube RNA, RNA/DNA, and DNA nanoparticles. EtBr total staining native-PAGE show the assemblies of corresponding compositions. Error is presented as s.d.; N=3.	61
Figure 8. Predicted free energy of nucleic acid cube structures (at 250 nM concentration) as a function of temperature.	62
Figure 9. Computationally predicted secondary structures of RNA cube, DNA anti-cube and hybrid duplexes formed during their re-association. As described in the Methods section, secondary structure predictions were generated using HyperFold for a variety of different temperatures and different combinations of RNA and DNA strands. The depicted secondary structures are idealized secondary structures, but they are also identical to the secondary structures for low temperatures (10 °C). At higher temperatures, the predicted cube structures are similar, but some helices (especially helices consisting of only 4 or 6 base pairs) are predicted to be unfolded. This tendency is more pronounced for DNA strands compared to RNA strands.	63

Figure 10. Relative rates of re-association measured for different compositions of nanoparticles using native-PAGE. In all experiments with DNA anti-cube (blue), gel purified anti-cube was fluorescently labeled with Cy5. For RNA anti-cube (green), RNA cube was labeled with Alexa 488. All re-association constants are summarized below. Error is presented as s.d.; N=3 65

Figure 11. Isothermal re-association of complementary DNA nanoparticles activates co-transcriptional production of RNA nanoparticles. (A) Schematics of re-association between the complementary DNA cubes and anti-cubes carrying split and therefore inactive T7 RNA polymerase promoters. The re-association of DNA cubes in transcription mixture releases DNA templates with active promoters and allows for co-transcriptional assembly of RNA cubes. (B-C) Native-PAGE and fluorescence experiments visualizing re-association of shape-switching purified DNA cubes and DNA anti-cubes, resulting in formation of DNA templates with activated T7 RNA polymerase promoters and further co-transcriptional assembly of RNA cubes. (D) Co-transcriptionally assembled RNA cubes eluted from native-PAGE and imaged by AFM. (E) RNA cubes can only be formed co-transcriptionally using DNA anti-cubes decorated with six complete T7 RNA Polymerase promoters (A6P) and not from DNA cubes (C6P) due to the directionality of the promoter sequences. (F) Native-PAGE showing the co-transcriptional production of RNA cubes from DNA anti-cubes with six promoters. Following 4 hours of incubation, all transcription mixtures were treated with DNase to remove any residual DNA. 66

Figure 12. Design and working principles of complementary nanoparticles activating the in vitro transcription upon their re-association. 67

Figure 13. Denaturing 8M urea PAGE demonstrates the relative yields of transcribed individual ssDNA strands of cubes and anti-cube with dsDNA promoter for T7 RNA Polymerase and schematics explaining the process. The bands are visualized by UV shadowing 68

Figure 14. Activation of functional aptamers with isothermal re-association of shape-switching nanoparticles. (A) Schematics of isothermal re-association and re-assembly of aptamers. (B) Total EtBr and DFHBI-1T stained native-PAGE demonstrates fiber formation and aptamer activation on re-association of cognate cubes. (C) AFM images of the aptamer containing fibers. (D) Re-association and fiber formation can be traced by measuring fluorescence of DFHBI-1T in vitro. Error bars indicate s.d.; N=3. 69

Figure 15. Fiber formation and simultaneous activation of multiple BROCCOLI aptamers. Schematics of activation of aptamers and total EtBr and DFHBI-1T stained native-PAGE demonstrates fiber formation and aptamer activation when stained with DFHBI-1T 70

Figure 16. Activation of RNA interference and intracellular FRET with complementary shape-switching nanoparticles. (A) Schematics of isothermal re-association and activation of FRET and RNAi. (B) In vitro re-association of fluorescently labeled cubes and anti-cubes with split DS RNAs was visualized by native-PAGE. (C) FRET time traces during re-association of fluorescently labeled Alexa 488 and Alexa 546 cubes and anti-cubes carrying split Dicer Substrate RNAs (DS RNAs). (D) For intracellular FRET experiments, human prostate cancer (PC-3) cells were co-transfected with fluorescently labeled cubes and anti-cubes and images were taken on the next day. (E) Cell viability assay for HeLa cells transfected with nanoparticles (at 5 nM final) designed to release two DS RNAs against PLK1 and BCL2. Error bars indicate s.d.; N=3. Statistically significant results (compared to control cells) are indicated with asterisks (p-value < 0.05). (F-G) GFP knockdown assays for human breast cancer cells expressing enhanced GFP (MDA-MB-231/GFP). Prior to transfection, formation of the nanocubes was verified by total EtBr staining of native-PAGE. Three days after the transfection of cells, GFP expression was analyzed with

fluorescent microscopy (**F**) and flow cytometry (**G**). As the control, pre-formed DS RNAs (at 2 nM final) against PLK1, BCL2, and GFP were used for HeLa and MDA-MB-231 cells respectively. At concentrations higher than 10 nM, some gene silencing was observed for cubes carrying antisense DS RNAs (data not shown). Note that the individual cubes and anti-cubes cause no decrease in GFP production. gMFI corresponds to the geometric mean fluorescence intensity. Error bars denote SEM. 71

Figure 17. Activation of FRET with complementary shape switching nanoparticles. (**A**) *In vitro* re-association of fluorescently labeled cubes and anti-cubes with split Dicer Substrate (DS) RNAs was visualized by native-PAGE. (**B**) Fluorescence time traces show no re-association between the fluorescently labeled Alexa 488 and Alexa 546 cubes and anti-cubes carrying split DS RNAs when associated with Lipofectamine 2000 (L2K). (**C**) For intracellular FRET experiments, human prostate cancer (PC-3) and breast cancer (MDA-MB-231) cells were co-transfected with fluorescently labeled cubes and anti-cubes and images were taken the next day. Numbers at each image correspond to (1) differential interference contrast images, (2) Alexa 488 emission, (3) Alexa 546 emission, (4) bleed-through corrected FRET image. 73

Figure 18 Ring and anti-ring nanoparticles do not re-associate but cognate monomers form rings and fibers. (**A**) Schematics of isothermal re-association of triangles and anti-triangles. AFM of triangles and anti-triangles and native-PAGE of re-associated anti-triangles with triangles after 30 mins of incubation. (**B**) AFM images of RNA rings and anti-rings and native-PAGE showing that they do not interact. (**C**) The individual monomers of rings and anti-rings form the mixture of hexameric rings and fiber-like structures as shown by native-PAGE and AFM. 74

Figure 19. Assembly of RNA and DNA ring monomers show no assembly for nanorings due to lack of kissing loop interactions 75

Figure 20. Contrary to assembled rings, individual ring monomers and anti-ring monomers form a mixture of ring and fiber structures as shown by native-PAGE. (**A**) Assemblies of non-functionalized monomers. Two different assembly protocols explained in methods were tested. Depending on the kissing loop sequence the formation either of fibers (*e.g.*, A and anti-A) or rings (*e.g.*, F and anti-F) can be promoted. (**B**) Assembly of monomers functionalized with DS RNAs and Alexa 488 led to the formation of functional fibers and rings. 77

Figure 21. Programmable nucleic acid RNA (**A**) and DNA (**B**) polygons. Each panel presents energy minimized 3D models of RNA and DNA nanoparticles (identical sequences are colored the same), with corresponding AFM images, hydrodynamic radii measured by DLS (presented as +/- SEM), and ethidium bromide total staining native-PAGE results. 100

Figure 22. Cell culture experiments with programmable polygons. Human microglia-like cell lines were transfected with polygons at a final concentration of 5 nM and 25 nM. (**A**) 3D models of tested polygons with RNA strands shown in grey and DNA strands in blue. (**B**) Assemblies all polygons visualized by agarose gel. (**C**) Structural integrity of polygons associated with Lipofectamine 2000 (L2K) confirmed by the release studies with Triton X100. The results are analyzed by native-PAGE and visualized by AFM. (**D**) Relative cellular uptakes assessed by flow cytometry and (**E**) cell viability assays. (**F-G**) 24 hours post transfection with 16 RNA, DNA and RNA/DNA polygons, cell supernatants were collected and levels of IFN- β (**F**) and IL-6 (**G**) production were assessed by specific-capture ELISA. In C, E, and F, results were normalized to transfection reagent alone treated cells (L2K) and presented as the mean +/- SEM. Statistically significant results are indicated with asterisks (p value < 0.05). 101

Figure 23. (A) 3D models of polygons with corresponding sequence annotations. (B) Self-assembly properties of RNA polygons in the presence and absence of central (blue) strands evaluated on 7% non-denaturing PAGE. Lanes 1 – 3 correspond to monomer, dimer and trimer stepwise association of RNA strands. Lane 4 corresponds to triangle with strand rT1. Lanes 5 and 6 correspond to square with and without central strand rS1. Lanes 7 and 8 correspond to pentagon with and without central strand rP1. Lanes 9 and 10 correspond to hexagon with and without central strand rH1. (C) Self-assembly properties of RNA polygons from the same mixture of short strands (rT2, rT3, rT4, rS5, rP6, rH7) and different central strands. Lane M is a DNA step ladder (Low Molecular Weight from NEB). Lanes 2, 4, 6, and 7 are corresponding assembly of Triangle, Square, Pentagon and Hexagon formations driven by the presence of rT1, rS1, rP1, and rH1, respectively. Lanes 1, 3, 5, and 8 are corresponding pre-assembled control RNA polygons. 102

Figure 24. Experiments confirming structural integrity of DNA polygons associated with Lipofectamine 2000 (L2K). L2K complexes with polygons were prepared and then treated with Triton X100. All samples were analyzed by ethidium bromide total staining native-PAGE and visualized by AFM..... 104

Figure 25. Human microglia-like cell lines were transfected with nanoparticles at a final concentration of 5nM and 25nM. 24 hours post transfection cell supernatants were collected and levels of IL-8, were assessed by specific-capture ELISA. Results are normalized to L2K control and presented as the mean +/- SEM..... 105

Figure 26. Examples of model accuracy estimations for IFN- β , IL-6, and IL-8 datasets obtained by 5-fold Cross Validation procedure..... 107

Figure 27. Schematic representation of quantitative structure-activity relationship (QSAR) modeling used in this project. 107

Figure 28. Human microglia-like cell lines were transfected with nanoparticles at a final concentration of 5 nM and 25 nM using the transfection reagents jetPrime (A-B) or Mirus TransIT-X2 (B-C) and following the manufacturer's protocols. 24 hours post transfection with RNA, DNA and RNA/DNA polygons, cell supernatants were collected and levels of IL-6 (A, C) and IFN- β (B, D) production were assessed by specific-capture ELISA. Results were normalized to transfection reagent alone treated cells. Data shown is an N=1. 110

Figure 29. Examples of experimental determination of dissociation constants (K_D), melting temperatures (T_m), and stabilities in blood serum (τ). (A) For equilibrium dissociation constant (K_D) assay: fixed amounts of IR-700 labeled dT2 was titrated with increasing amount of unlabeled strands corresponding to triangle, tetragon, pentagon, and hexagon. The assembled polygons were subjected to 7% native-PAGE analysis shown on left. Titration curve fitting data is demonstrated on the right with corresponding apparent K_D values (+/- SEM). (B) Representative UV-melting curves for RNA polygons. Sigmoidal curves exhibited one transition at $T_m \sim 80^\circ\text{C}$ in all cases. The exact melting temperatures for polygons were determined from first derivative plots of corresponding melting curves. (C) Time dependent degradation profiles for RNA polygons (at 1 μM) in 2% (v/v) FBS at 37 $^\circ\text{C}$ 111

Figure 30. Experimental design of the current work. 129

Figure 31. Binding of DNA to PgP leads to protection from nuclease activity. (A) Schematic showing electrostatically-driven PgP binding to nucleic acids, (B) gel retardation of various

PgP/DNA polyplexes prepared using various PgP/DNA ratios (N/P ratio), and (C-D) nuclease protection assay of PgP/DNA polyplexes after incubation with DNase I..... 129

Figure 32. Intracellular uptake of PgP/DS RNA polyplexes assessed in MDA-MB-231 human breast cancer cells. (A) Visualization of intracellular uptake of polyplexes by confocal microscope; (B) Co-localization of polyplexes with early endosomal marker Rab5 confirms an endocytic pathway of internalization; (C) Flow cytometry measuring the effect of temperature on intracellular uptake of polyplexes (**** denotes $p < 0.0005$); (D) Fluorescent microscopy and bright-field overlay of MDA-MB-231 human breast cancer cells transfected with either PgP/DS RNA-A1488 or PgP/DNA-A1488 at either 4 °C or 37 °C, 6 hours after transfection..... 131

Figure 33. Characterization of various functionalized NANPs by AFM and native-PAGE: (A) RNA rings functionalized with six Dicer substrate (DS) RNAs, (B) RNA cubes functionalized with six DS RNAs, and (C) DS functionalized RNA fibers. (D) Native-PAGE results confirm the integrity of NANPs upon heparin-assisted release from PgP polyplexes..... 132

Figure 34. Specific gene silencing with PgP/NANP(GFP) polyplexes and cell viability assays tested against GFP expressing breast cancer cells (MDA-MB-231/GFP). Fluorescent microscopy (A) shows representative images of GFP knockdown by PgP/NANP(GFP) polyplexes. (B) GFP knockdown efficiency by cubes (PgP/cubes(GFP)), rings (PgP/rings(GFP)), and fibers (PgP/fibers(GFP)) are compared to free DS RNAs(GFP) and negative control (siNT), PgP only (0.1 mg/mL) used as an additional control. (N=3, **** denotes statistically significant vs. untreated cells with $p < 0.0005$, # denotes statistical significance vs. cubes with $p < 0.05$). (C) Cell viability by PgP/NANP(GFP) polyplexes (N=3, * denotes statistical significance with $p < 0.05$, ** with $p < 0.005$, *** with $p < 0.005$)..... 134

Figure 35. (A) AFM images of RhoA NANPs and (B,C) specific gene silencing with PgP/NANP polyplexes targeting RhoA in rat neuroblastoma cells (B35). In all experiments, cubes (PgP/cubes(RhoA)), rings (PgP/rings(RhoA)), fibers (PgP/fibers(RhoA)), and individual DS RNAs(RhoA) are compared. Negative control siRNA (siNT) and DS RNA transfected with Lipofectamine 3000 (L3K) are used as controls. Intracellular uptake of fluorescently labeled PgP/Ring-A1488 by confocal microscopy (A) and RhoA gene silencing assessed by RT PCR (B). 135

Figure 36. Blood compatibility and immunostimulation with PgP/NANP(GFP) polyplexes. In all experiments, cubes (PgP/cubes(GFP)), rings (PgP/rings(GFP)), fibers (PgP/fibers(GFP)), and individual DS RNAs(GFP) are compared. (A) Hemolysis assay was conducted using primary rat erythrocytes and demonstrated no lysis. (B-C) Immunostimulation of PgP/NANP(GFP) polyplexes measured via ELISA of inflammatory cytokines and type I interferons in hügla cells. (D) IRF and NF- κ B stimulation as measured by luciferase production and SEAP production, respectively, in THP1-Dual™ cells, and (E) TLR stimulation from polyplexes as measured by SEAP secretion from HEK-Blue™ hTLR7 cells. In B and C, statistical significance relevant to cells, poly I:C, and ring is denoted by *, #, and & respectively (*/# $p < 0.05$, **/##/ && $p < 0.005$, ### $p < 0.001$, **** $p < 0.0001$). (D) The role of IRF and NF- κ B stimulation were measured using THP1-Dual™ cells. Statistical significance compared to cells denoted by *** with $p < 0.0005$ and **** with $p < 0.0001$). (E) HEK-Blue™ hTLR7 cells were transfected with the various PgP/NANP complexes and the TLR stimulation was measured using QUANTI-Blue™ detection media (* denotes $p < 0.005$). 136

Figure 37. hTLR3 stimulation as measured by HEK-Blue™ hTLR3 cells. Positive control Poly I:C stimulates a response whereas none of the PgP/NANPs trigger hTLR3 activation. In all

experiments, cubes (PgP/cubes(GFP)), rings (PgP/rings(GFP)), fibers (PgP/fibers(GFP)), and individual DS RNAs(GFP) are compared..... 137

Figure 38. Biodistribution of various PgP/NANPs after systemic injection via tail vein in mice. The results were analyzed *in vivo* (A), and *ex vivo* (B-C). Significant difference ($p < 0.05$) when compared to PgP/DS RNA for PgP/NANPs' accumulation in lungs (*) and in livers (#) are shown. 139

List of abbreviations

3WJ	3-way junction
AB	Assembly buffer
AdoCbl	5'-deoxy-5'-adenosylcobalamin
AL488	Alexa Fluor 488
AL546	Alexa Fluor 546
APS	Aminopropyl silatrane
ASO	Anti-sense oligonucleotide
BBB	Blood brain barrier
bPEI	Branched polyethyleimine
BSA	Bovine serum albumin
cGAS	Cyclic GMP-AMP synthase
CNS	Central nervous sytem
CO ₂	Carbon dioxide
CpG	Cytosine phosphate guanosine
CV	Cross validation
DAMP	Damage associated molecular pattern
ddH ₂ O	Double deionized water
DFHBI-1T	(5Z)-5-[(3,5-Difluoro-4-hydroxyphenyl)methylene]-3,5-dihydro-2-methyl-3-(2,2,2-trifluoroethyl)-4 <i>H</i> -imidazol-4-one
DiR	1,1-dioctadecyl-3,3,3,3-tetramethyl indo tricarbocyanine iodide
DMEM	Delbuco's modified eagle medium
DNA	Deoxyribonucleic acid
DS	Dicer substrate
dsRNA	Double-stranded RNA
DTT	Dithiothreitol
E. Coli	Escherichia coli
ELISA	Enzyme linked immunosorbent assay
EMEM	Eagle's minimum essential medium
EU	Endotoxin unit
FBS	Fetal bovine serum
FDA	Food and drug administration
FRET	Förster resonance energy transfer
GC content	Guanine cytosine content
GFP	Green fluorescent protein
gMFI	Geometric mean fluorescence
H ₂ SO ₄	Sulfuric acid
HEPES	(4-(2-hydroxyethyl)-1-piperazineethanesulfonic acid)
HIV	Human immunodeficiency virus
Hz	Hertz
IFN I	Type one interferon
IFN- α	Interferon alpha
IFN- β	Interferon beta
IL-1B	Interleukin 1B
IL-6	Interleukin 6
IL-8	Interleukin 8
IR	Infrared
IWB	Iowa black quencher
KCl	Potassium chloride
K _D	Dissociation constant

kDa	Kilodaltons
kHz	Kilohertz
KOH	Potassium hydroxide
L2K	Lipofectamine 2000
LAL	Limulus amoebocyte assay
Li	Lithium
lncRNA	Long non-coding ribonucleic acid
LPS	Lipopolysaccharide
MDA5	Melanoma differentiation-associated protein 5
MgCl ₂	Magnesium chloride
MIP-1 α	Macrophage inflammatory protein alpha
miRNA	Micro ribonucleic acid
mRNA	Messenger ribonucleic acid
MSN	Mesoporous silica nanoparticle
MW	Molecular weight
N/m	Newtons per meter
N/P	Amine to phosphate ratio
NaCl	Sodium chloride
NANP	Nucleic acid nanoparticle
ncRNA	Non-coding ribonucleic acid
nM	Nanomolar
Nm	Nanometer
ODN	Oligodeoxynucleotide
OOB	Out of bag
PAGE	Polyacrylamide gel electrophoresis
PAMAM	Poly (β -amino esters), and polyamidoamine
PAMP	Pathogen associated molecular pattern
PBMC	Peripheral blood mononuclear cell
PC physicochemical	Physicochemical
PCL	Polycaprolactone
PCR	Polymerase chain reaction
pDNA	Plasmid deoxynucleic acid
PEG	Polyethylene glycol
PEI	Polyethyleneimine
Pg picogram	Picogram
PgP	Poly (lactide-co-glycolide)-graft-polyethylenimine
PLGA	Poly(lactic-co-glycolic acid)
PRR	Pattern recognition motif
PSMA	Prostate-specific membrane antigen
PTGS	Post-transcriptional gene silencing
QSAR	Quantitative structure activity relationship
RF	Random forest
RIG	Retinoic inducible gene
RISC	Ribonucleic acid induced silencing complex
RNA	Ribonucleic acid
RNAi	Ribonucleic acid interference
rNTP	Ribonucleotide triphosphate
rRNA	Ribosomal ribonucleic acid
RT	Room temperature
RT-PCR	Reverse transcriptase polymerase chain reaction
scaRNA	Small Cajal body-associated ribonucleic acid

SD	Standard deviation
SELEX	System evolution of ligand by exponential enrichment
SEM	Standard error of the mean
shRNA	Short hairpin ribonucleic acid
siRNA	Small interfering ribonucleic acid
ssDNA	Single stranded deoxyribonucleic acid
ssRNA	Single stranded ribonucleic acid
STING	Stimulator of interferon genes
sxRNA	Structurally interacting ribonucleic acid
T7 RNAP	R7 ribonucleic acid polymerase
τ	Serum stability half-life
TB	Tris-borate buffer
TBE	Tris-borate ethylenediaminetetraacetic acid buffer
TLR	Toll-like receptor
T _m	Melting temperature
TMB	Tetramethylbenzidine
TNA	Therapeutic nucleic acid
TNF α	Tumor necrosis factor alpha
tRNA	Transfer ribonucleic acid
μ L	Microliter
μ M	Micromolar
UTR	Untranslated region
UV	Ultraviolet
w/v	Weight by volume
WC	Watson-Crick

1 Chapter 1: Introduction

1.1 Nucleic acids in molecular biology

1.1.1 Structure and interactions of nucleic acids

DNA and RNA are biological polymers that have evolved to perform principle biological functions. The main and most appreciated roles are as storage and conduits of genetic information across all forms of life. The unique chemical structure of nucleic acids is widely conserved throughout biology, with only minor idiosyncrasies to accommodate additional functionalities. Although the chemical differences between DNA and RNA seem insignificant, alterations in their properties that result from these changes make them two entirely different players in the cast of molecular biology.

The role of DNA in molecular biology is almost exclusively for the storage of genetic information. In eukaryotes, DNA is mainly contained in the nuclei of cells where it is stored and protected. The DNA can then be selectively unwound and transcribed into RNA, a complex and interesting process which is not the focus of this dissertation. RNA is a more versatile molecule, which acts as the conduit between DNA and protein, an enzyme, a scaffold, and a regulator of gene expression. This section serves to introduce the main functions of nucleic acids, as well as outline the chemical and physical features that dictate their functions.

The anatomy of nucleic acids evolved both to fit its niche in biology. The chemical structure can be separated into three main components, the phosphate backbone, pentose sugar, and nucleobase.¹⁻³ The negatively charged at neutral pH phosphate backbone is identical for both DNA and RNA (though sometimes modified in bacterial species to form phosphorothioate bonds, to be discussed later). The phosphate backbone links covalently to the sugar group, a β -D-ribofuranose in RNA and a β -2'-deoxy-D-ribofuranose in DNA. The consequences of the additional 2'-hydroxyl group in RNA makes it very distinct from DNA molecules. Firstly, the 2'-hydroxyl group is polar, which makes RNA more chemically reactive than DNA. Additionally, the 2'-hydroxyl group causes the ribose to form a different orientation, changing the overall helix. This different shape,

referred to as a sugar pucker, has vast implications of the secondary structure of RNA, and allows it to form several higher order structures. Specifically, the sugar pucker has implications for the helix itself, causing RNA to form what is known as an A-form helix. The C3'-endo sugar conformation, induced by the 2'-hydroxyl, causes shorter phosphate-phosphate distances in the backbone, resulting in a more compact helix.⁴⁻⁵ In contrast, the resulting C2'-endo structure that forms for DNA causes a B-form helix, which is less compact. Additionally, the two forms of helices result in different lengths and number of base pairs (bp) required per full helical turn; B-form helices achieve one full turn with 10.5 bases, whereas A-form helices achieve a full helical turn after 11 bases.⁶ The third and rarest helix of nucleic acids, Z-DNA, is a left handed helix with several unique properties including a narrower helix and greater rise per turn.⁷ The final feature of nucleic acids is the nucleobase, which are derivatives of nitrogen containing heteroaromatic molecules -- purines and pyrimidines. Purine bases (adenine and guanine) contain double rings while pyrimidine bases (cytosine, thymine (DNA), and uracil (RNA)) contain single rings. The planar nucleobases are responsible for inter-strand interactions through hydrogen bonding, wherein adenine binds to thymine (DNA) or uracil (RNA), and cytosine binds to guanine. It is through these hydrogen bonds that DNA binds to its complementary strand and forms a double helix structure. DNA is also capable of forming additional bonds known as Hoogsteen interactions which are essential in the formation of, for example, G-quadruplexes and triple helices.⁸⁻⁹ Alternatively, the structure of RNA allows for a plethora of other interactions which allow it to form unique structures (discussed below), leading to a multitude of additional functionalities.¹⁰⁻¹³

The annealing of complementary nucleic acid strands and helix formation is driven by several forces: hydrogen bonding between nucleotides, hydrophobic and hydrophilic forces of the bases and phosphate backbones, respectively, and aromatic pi-pi stacking of the bases. These forces lead to the self-assembly double helix structures, which vary based on the strands which compose them (DNA or RNA). Furthermore, metal ions play a large role in the formation and stabilization of complex DNA and RNA structures. Particularly, sodium, potassium, and magnesium are used

to counteract the negative charges in the phosphate groups of nucleic acids and act as a glue of sorts to enable compact structures and helices.¹⁴⁻²² Of the metal ions integral in nucleic acid folding and stability, magnesium has been identified as the most crucial. The combination of size and charge (high charge density) enables magnesium to stabilize the nucleic acid helix by direct electrostatic interactions with the phosphate backbone, and via coordination of water around the phosphate backbone for favorable hydrogen bonding.²³⁻²⁷ In the first scenario, magnesium's size allows it to fit in the groove of the nucleic acid, and its divalence allows for electrostatic interaction with two negatively charged phosphates simultaneously. In the second scenario, magnesium interacts electrostatically with the oxygens in water, coordinating six water molecules around the ion. This complex directs the hydrogens of water to face outwards, which then hydrogen bond to the phosphate backbone to stabilize the structure.

Whereas DNA is often limited to its double helix, the combination of nucleobases and ribose group enable RNA to fold into more unique and complex structures.²⁸ The hierarchy of nucleic acid structure can be defined in three orders: the primary structure refers to the linear sequence of nucleotides, the secondary structure is the helices formed through base pairing, and the tertiary structure is the overall compact and highly organized structures assumed by RNA. The non-canonical RNA interactions which make secondary and tertiary structure possible are defined by twelve basic geometric families demarcated by their location of interaction (Watson-Crick, Hoogsteen, or Sugar Edge) and their directionality (parallel or anti-parallel). Overall, these interactions lead to extraordinarily diverse and complex structures capable of a wide range of functions. Three categories of structure are used when defining nucleic acids: primary is described as the specific sequence of nucleotides which comprise the strand, secondary structures are helices which form through canonical WC base pairing, and tertiary structure with interactions which result from RNAs ability to form non-canonical interactions while folding into compact and highly organized structures.²⁹ Overall, the complexity of structures formed by RNA can rival those of protein.

1.1.2 Functions of nucleic acids

While the natural functions of DNA lie solely in the storage of genetic information (with minor exceptions such as, for example, neutrophil extracellular traps), RNA is a fantastically versatile molecule, whose functions are vast and still not completely known today. The central dogma of molecular biology states that DNA is transcribed into RNA, RNA is translated into protein, and protein will go on to perform function. Although this is correct, it woefully understates the versatility of RNA in molecular biology, and limits RNA to its earliest understood function. Most of the understood functions of nucleic acids are outlined in Figure 1.

RNA is most popularly known for its function as a conduit of genetic information via messenger RNA (mRNA) which codes for proteins. Eukaryotic mRNAs can be identified by a number of chemical hallmarks, including the presence of a 5' 7-methyl guanosine cap, and a polyadenosine 3' tail, which both serve to protect the transcript from exonuclease activity³⁰⁻³¹. Furthermore, the 5' 7-methyl guanosine cap plays a major role in translation initiation.³² The structure of mRNAs can be defined by a number of features; read 5' to 3', those features are: the 5' cap, the 5' untranslated region (UTR),³³⁻³⁴ the coding region, the 3' UTR,³⁵⁻³⁶ and the polyadenosine tail.³⁷⁻³⁸ The UTRs are not translated into protein (as its name suggests), but can serve various roles in gene expression such as mRNA stability, localization, and translation efficiency. Beyond (and often embedded in) mRNA, RNA has a myriad of functions in biology which help to regulate cell metabolism and protein expression.³⁹⁻⁴⁰ RNA is unique in that it is able to perform the actions of both information conduit as well as enzyme activities.⁴¹ Several classes of natural non-coding RNAs include ribozymes,⁴²⁻⁴³ riboswitches,⁴⁴⁻⁴⁵ long non-coding RNAs (lncRNAs), short-interfering RNAs (siRNAs),⁴⁶ short hairpin RNAs (shRNAs),⁴⁶ and small nucleolar RNAs (snRNAs),⁴⁷ just to name a few. All of these classes perform a function involved in cell maintenance and metabolism but are not directly translated into protein. It is now understood that the complexity of higher order life is due to the number of non-coding RNAs transcribed, and not

always correlated genome size or number of proteins.

Ribozymes are RNAs which are able to perform a catalytic function.⁴⁸⁻⁴⁹ There are several properties of RNA (resulting from the chemical differences of DNA and RNA discussed) that enable them to perform these activities. Firstly, ssRNAs ability to fold into tertiary structures, an ability which allows for specific conformations for the formation of active and binding sites. Secondly, RNA can bind metal ions to use in catalytic activities. The 2' hydroxyl group on the ribose of RNA makes it far more reactive than DNA. For example, deprotonation of the hydroxyl group generates a single negative oxygen which is highly reactive and can cause self-cleavage of

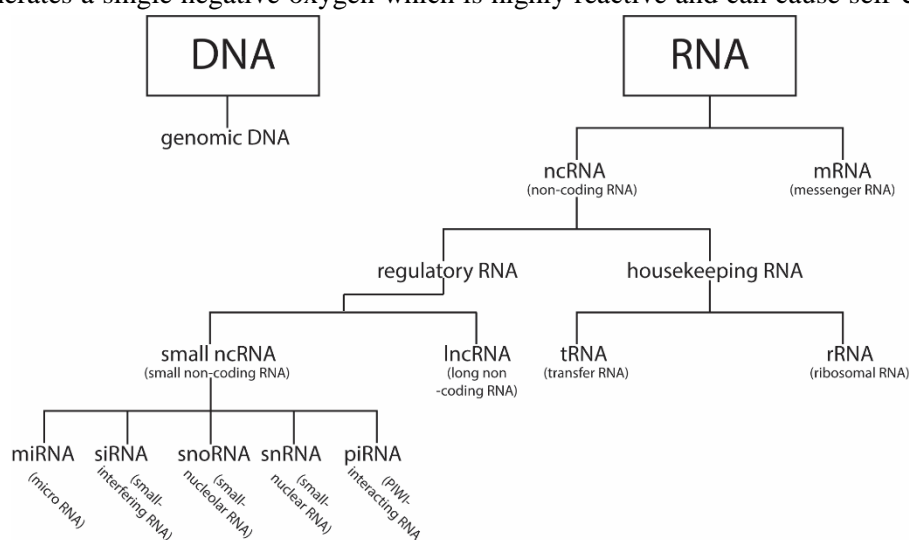


Figure 1. Functions of DNA and RNA in molecular biology. DNA is used almost exclusively for storage of genetic information, whereas RNA has diverse functions some of which are schematically shown.

the RNA by reacting with the phosphate backbone. Thirdly, the ability for RNA nucleobases to accept and donate protons can allow ribozymes to perform acid-base catalysis. Although ribozymes are widespread in biological activity and morphology, most (but certainly not all) ribozymes activity function by breaking the ester bond in the phosphodiester backbone. These ribozymes can be separated into two distinct groups, small and large, which is defined by those containing fewer or greater than 200 nucleotides, respectively.⁵⁰ The ability to self-cleave allows for regulated post-transcription control of RNA. For example, the Hammerhead ribozyme, found in various viruses, self-cleaves the RNA product of rolling-circle transcription to generate high efficiency mRNAs.⁵¹⁻

The most important ribozyme, the ribosome, is utilized ubiquitously throughout nature.⁵³⁻
⁵⁴ The ribosome is a biological complex composed of roughly 65% RNA and 35% protein, whose assembly requires a variety of further structural and catalytic RNAs including small Cajal body-associated RNAs (scaRNAs) and small nucleolar RNAs (snoRNAs).⁵⁵⁻⁵⁶ The catalytic activities of the ribosome include intricate interactions between ribosomal RNA and proteins. The ribosomal RNA (rRNA) in conjunction with transfer RNA (tRNA) is able to catalyze the synthesis of peptides.⁵⁷ The importance of the ribosome (and its associated RNAs) is vital to molecular biology, and it is necessary to acknowledge RNA's role in the synthesis of proteins beyond that of mRNA.

Riboswitches, as well as recently discovered class of structurally interacting RNAs (sxRNAs) describe an additional functionality of RNA beyond mRNA in which the confirmation of an RNA changes in response to a specific input to modulate an RNA's activity.⁵⁸⁻⁵⁹ Often times this is used in biology to maintain proper concentrations of certain molecules. The structures function by altering their secondary or tertiary structure in response to binding a target ligand.⁶⁰ For example, one of the first riboswitches discovered regulates the expression of vitamin *btuB*, an enzyme necessary for the production of vitamin B12.⁶¹ The expression of *btuB* is regulated by the cellular concentration of coenzyme B₁₂ (5'-deoxy-5'-adenosylcobalamin or AdoCbl); that is, in conditions of high concentration of AdoCbl, the translation of *btuB* is retarded, and in low concentration production is increased.⁶² It was discovered that structural changes were induced in the *btuB* mRNA by binding of AdoCbl to the 5'-UTR, and these structural changes alter the gene expression. Several similar riboswitches have been identified to alter the expression of a number of proteins, and many have been developed for therapeutic purposes.⁶³⁻⁶⁴

Beyond ribosomes (and their associated ncRNAs), ncRNAs exist for epigenetic regulation, cellular metabolism and protein expression.⁶⁵⁻⁶⁷ Short ncRNAs (generally 22-30 bp) play a vital role in gene silencing and post-transcriptional control over protein expression.⁶⁸ Short ncRNAs play a vital role in both regulation of expression of self-proteins as well as defense versus viral

infections by a process known as RNA interference (RNAi), a vital post-transcriptional gene silencing (PTGS) process. There are several subclasses of RNA molecules that can induce RNAi, including (but not limited to) siRNA and microRNA (miRNA).⁶⁹ miRNAs function by achieving post-transcriptional modulation of the activity of mRNA transcripts, including blocking translation, or cleaving the mRNA transcript itself.⁷⁰⁻⁷² Interestingly, miRNAs are located in both intergenic and coding regions of the genome, and within genes can be found in introns or exons, acting as endogenous regulators of gene expression.⁷³ miRNAs begin as a single stranded folded pri-miRNA that are later processed by the enzyme Drosha to yield pre-miRNAs to be exported into the cytoplasm.⁷⁴⁻⁷⁶ Interestingly, miRNAs are an endogenous means of post-transcriptional control, allowing a cell to maintain proper expression of countless RNA transcripts; however, it has been shown that miRNAs can be transferred between cells via extracellular bodies such as exosomes.⁷⁷⁻⁷⁸ To this effect, miRNAs represent an endogenous means of RNA-controlled expression through target specific steric mRNA hinderance, degradation, or cleavage.⁷⁰ Once in the cytoplasm, pre-miRNAs are processed by Dicer and loaded into the RISC and proceed to bind to their target mRNA, akin to the fate of siRNA.⁷⁶ Different from siRNAs, miRNAs are only partially complementary to their target genes, and can repress translation by both cleaving and non-cleaving mechanisms.⁷⁹⁻⁸¹ Furthermore, miRNAs differ from siRNAs in their target promiscuity; miRNAs can have several mRNA targets whereas siRNAs generally only have one.⁸¹⁻⁸³

Alternatively, siRNAs compose the exogenous facet of RNAi, with a small set of endogenous siRNAs controlling self-expression.⁸⁴⁻⁸⁵ In their final form, siRNAs are generally 21-23 bp dsRNAs with 2 nucleotide 3' overhangs.⁸⁶ To generate these molecules, the endonuclease Dicer cleaves longer RNAs to their functional product.⁸⁷ siRNAs are generally derived from exogenous sources and later cleaved and processed in the cytoplasm; it has been shown that siRNAs are processed from viruses, transposons, or foreign genes as a mean of defense against exogenous threats.^{86, 88-89} It has been further demonstrated that Dicer facilitates the loading of the siRNA into the RNA induced silencing complex (RISC), the cellular machinery which carries out the

silencing.⁹⁰ The RISC is composed of several proteins tasked at separating the guide strand (active) from the passenger strand (inactive).⁹¹ Specifically, the distinction between guide and passenger strand is determined by the stability of the 3' end of the siRNA, where the strand with the less thermodynamically stable 3' end is selected as guide.⁹² From Dicer, the siRNA is loaded into the RISC by binding to the RNA binding protein TRBP.⁹³ The siRNAs (now associated with the RISC) bind with fully complementary to their target mRNA, and through the nuclease activity of Argonaute 2, cause cleavage and degradation of their mRNA target.⁹⁴⁻⁹⁵ siRNAs are highly specific and generally target only one specific gene; however, mutations or mismatches can occur which may result in off-target silencing or reduced efficiency.⁹⁶ In fact, only a few copies of siRNA per cell are needed to achieve sufficient gene knockdown.⁹⁷ The simplicity and ubiquity of siRNA makes them ideal tools in laboratories for experimentation, and in the clinic for therapeutic use.

Overall, RNAs comprise of a versatile and diverse set of biological tools which are necessary for every living organism. Although they are known mainly to serve as a conduit of genetic information between DNA and protein, their enzymatic activities give unique roles in cellular metabolism and homeostasis. An additional subset of RNA, Long-ncRNAs, exist as a heterogenous subset of RNAs which perform a number of functions in epigenetic regulation.⁹⁸ This class of RNAs are united only by their length, as their functionality is widely varied. Bringing the subsets together, RNAs are responsible for the synthesis of proteins, as well as the control over their expression. The above paragraphs only skim the surface of the complex and vital roles that RNA play in molecular biology. It is for this reason that RNAs are continuously being targeted as potential therapeutics and will always play an active role in modern medicine.

1.1.3 Chemical modifications of nucleic acids

Chemical modifications of nucleic acids are pervasive throughout biology and with great variety.⁹⁹ Although researchers have identified a number of key functions, the purpose and mechanisms of many remain unknown; for example, the N⁶-methyladenosine (m⁶A) modification has recently been demonstrated to drive stem cell differentiation, as well as correlate with circadian

rhythms in eukaryotes, but with over 18,000 evolutionarily confirmed modified sites, it is speculated that this only makes up a fraction of its purpose.¹⁰⁰⁻¹⁰² Largely, chemical modifications play a role in gene expression and regulation, nucleic acid stability, and immune recognition.¹⁰³⁻¹⁰⁴ So as to not understate its importance, this section serves only as a minor foray into its depth of chemically modified nucleic acids, focusing on the aspects more relevant to this dissertation. Several of these modifications are depicted in Figure 2.

In eukaryotes, nucleic acids undergo chemical modifications in a dynamic manner from synthesis to degradation.¹⁰⁵⁻¹⁰⁶ The DNA of eukaryotes undergoes constant remodeling to modulate expression patterns of all genes. DNA is generally kept in two morphological states: heterochromatin, in which the DNA is tightly packed around histones and is difficult to transcribe, and euchromatin, in which the DNA is more loosely packed and is able to be readily transcribed.¹⁰⁷ Chemically, this is achieved through a series of reactions which result in the methylation of the

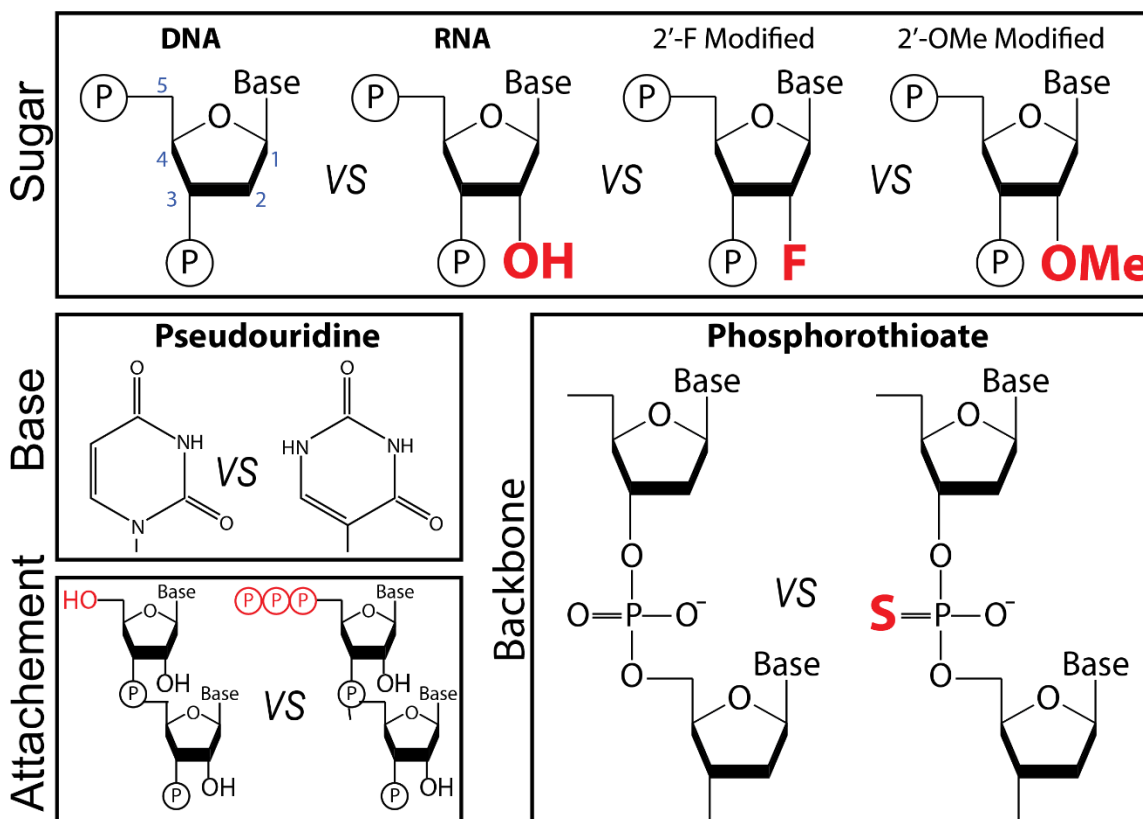


Figure 2. Chemical modifications of DNA and RNA effect their folding and molecular interactions.

DNA. For most animals, DNA methylation occurs by the addition of a methyl group to the 5 position on the cytosine base (5-methyl cytosine). Consequently, the DNA methylation functions by blocking the interaction with DNA binding proteins, initiating transcriptional silencing.¹⁰⁸ Furthermore, DNA methylation encourages the conversion from euchromatin to heterochromatin, further repressing expression.¹⁰⁹⁻¹¹⁰ This process works in tandem with histone methylation and acetylation to control gene expression at the transcriptional level.¹¹⁰⁻¹¹¹

The library of RNA modifications is diverse in both chemistry and function. With respect to chemistry, eukaryotic RNA modifications occur on either the ribose or the base, as well as at the extreme ends of the strand (capping).¹¹² These modifications play a large role in modifying RNA stability, enhancing catalysis, enabling immune recognition, and modulating translation efficiency.¹¹³⁻¹¹⁵ Although several modifications are well understood, there still exists a dearth of knowledge for many. For example, pseudouridine is the most abundant base replacement modification in which uridine is replaced with an isomer.¹¹⁶ Pseudouridine is found in tRNA, mRNA, rRNA, and snRNA, with varying function for each.¹¹⁷ In tRNA and rRNA, it has been proposed that pseudouridines facilitate the formation of specific structural motifs, though this has still not been explicitly proven.¹¹⁸ Alternatively, 2'OMe modifications on the ribose of RNA are also one of the most abundant modifications; however, discovery of their function has largely evaded scientists, and its purpose remains unclear beyond its enhancing of stability and flexibility.¹¹⁹⁻¹²²

Beyond the transcriptome, chemical modifications of nucleic acids have been adopted for nucleic acid therapeutics. Modifications which increase melting temperature, enhance resistance from nuclease activity, and either purposefully evade or provoke the immune system have garnered much attention. The aforementioned 2'OMe modification is utilized because of the above properties, as well as 2'Fluorine modified RNA.¹²³ Backbone modifications such as phosphorothioate are used in to enhance stability, while CpG motifs are used in conjunction with them to provoke an immune response.¹²⁴⁻¹²⁵

1.1.4 Natural immune response to nucleic acids

The presence of foreign nucleic acids within a cell is often indicative of either damage to neighboring cells or infection by a pathogen. As such, eukaryotic cells have developed a suite of

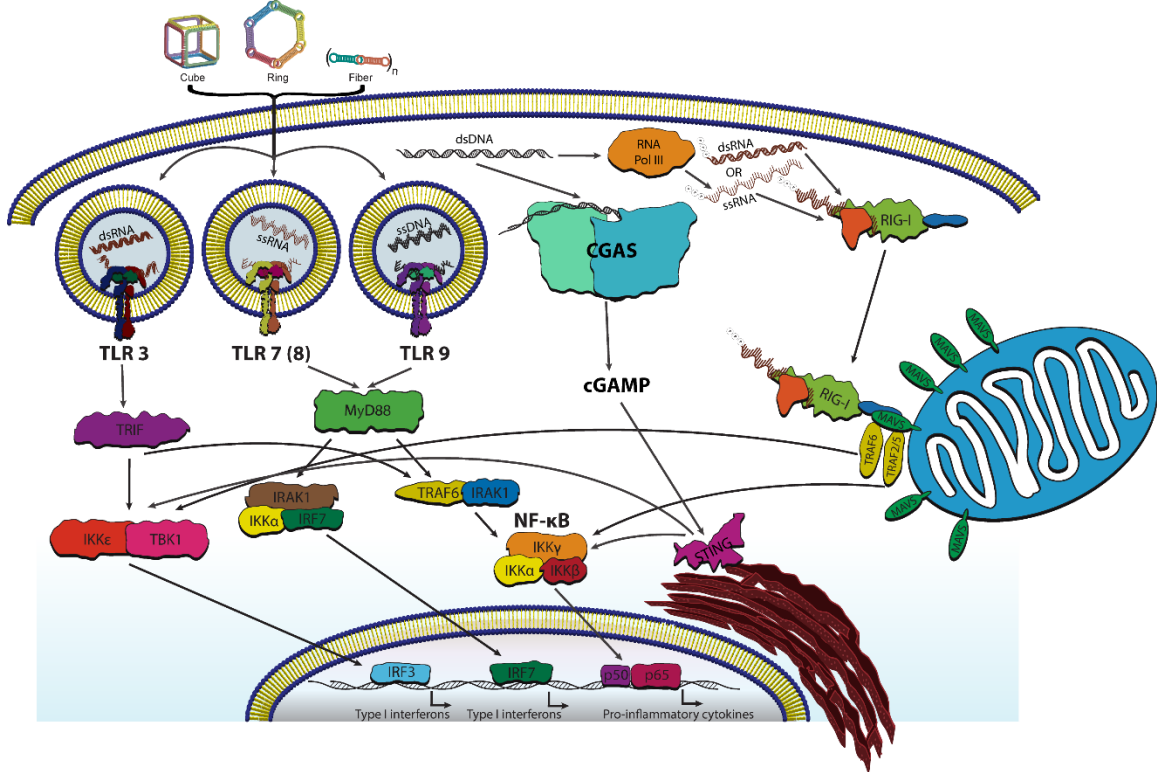


Figure 3. Schematic demonstrating the main receptors and proteins in coordinating an immune response to foreign nucleic acids.

pattern recognition receptors (PRRs) to bind to pathogen associated molecular patterns (PAMPs) or damage associated molecular patterns (DAMPs) for the detection and response to nucleic acids¹²⁶⁻¹²⁹. These sensors can be divided into two categories: endosomal and cytosolic. In the endosome, membrane bound proteins, called Toll-like receptors, function to bind specific nucleic acids motifs and signal for the expression of type I interferons and/or pro-inflammatory cytokines.¹²⁷ In the cytoplasm, a larger and more diverse array of proteins comprise a comprehensive defense system.¹³⁰ Several of the pathways and receptors are displayed in Figure 3.

The Toll-like receptors are a series of transmembrane proteins responsible for detecting PAMPs and DAMPs such as nucleic acids, flagellum, and lipopolysaccharide.¹²⁸⁻¹²⁹ In the endosome, TLR 3, 7, 8, and 9 are responsible for detecting DNA and RNA in human biology. TLR

3 is detects dsRNA,¹³¹ TLR 7 and 8 detect ssRNA,¹³²⁻¹³³ and TLR 9 detects CpG DNA.¹³⁴⁻¹³⁵ Each receptor has specific requirements for the type of nucleic it can detect. TLR 3 preferentially binds dsRNA of 40-50 bp in acidic conditions.¹³⁶ Once the dsRNA binds to the ectodomain of the receptor, a conformational change of the protein on the other side of the endosomal membrane leads to a pathway activating type I interferons.¹³⁷ Alternatively, TLR 7 and 8 bind to ssRNA with preference to uridine rich sequences.¹³⁸ The binding then activates the MyD88 pathway which signals downstream for the expression of both type one interferons as well as proinflammatory cytokines.¹³⁹⁻¹⁴⁰ Additionally, TLR 9 is activated by CpG motifs in ssDNA, and its stimulation also leads to the expression of type one interferons and pro-inflammatory cytokines.¹⁴¹

Detection of pathogenic or foreign nucleic acids in the cytoplasm is achieved by a more diverse set of receptors which interplay for a comprehensive system.¹⁴²⁻¹⁴⁷ Much like the endosomal receptors, the cytosolic receptors each have their own specific targets. Retinoic-acid-inducible-gene-I (RIG-I)¹⁴⁸ is a cytosolic receptor that has specificity for RNAs containing a 5' triphosphate, which is indicative of a viral RNA.¹⁴² RIG-I has interplay with RNA polymerase III, which converts foreign DNA to RNA for downstream detection.¹⁴⁹ This makes RIG-I a direct sensor of RNA, and an indirect sensor of DNA. Melanoma-differentiated gene 5 (MDA5) is a cytosolic receptor that specifically targets longer dsRNAs.¹⁵⁰⁻¹⁵¹ Although more is known about the ligands of RIG-I than MDA5, research has demonstrated a clear discrimination of the two by length, with RIG-I detecting shorter sequences, and MDA5 detecting longer sequences.¹⁵² Furthermore, MDA5 has a preference for RNAs with higher-order structures.¹⁵³ The final of the major cytosolic RNA receptors, Laboratory of Genetics and Physiology 2 (LGP2), likely has strong interplay with RIG-I and MDA5, as it lacks adaptor domains for further downstream signaling.¹⁵⁴ Contradicting studies have shown that LGP2 acts as both a positive and negative regulator of the other cytosolic receptors RIG-I and MDA5.¹⁵⁵⁻¹⁵⁶

Another sensor of DNA, cyclic GMP-AMP Synthase (cGAS) works in tandem to respond to foreign DNA.¹⁵⁷ cGAS functions by binding to dsDNA and synthesizing cyclic GMP-AMP

(cGAMP), which then acts as a potent activator of stimulator of interferon genes (STING), which proceeds downstream to produce pro-inflammatory cytokines and type one interferons.¹⁵⁸

The discussed receptors comprise the bulk of the cellular immune response to foreign nucleic acids, with interplay and crosstalk between them highly important for coherent function.¹⁵⁹⁻
¹⁶² Together, these receptors their cascade proteins make an immune response possible against nucleic acids.

1.2 Nucleic acid therapeutics

1.2.1 Anti-sense oligonucleotides and RNA interference

RNAi is a post-transcriptional phenomenon that results in temporary reduced expression of a particular protein and in general, RNAi has evolved for two purposes: immune defense and gene expression regulation. Alternatively, anti-sense oligonucleotides (ASO) are ssRNA or chemical analogs that operate via selective binding to their reverse complement mRNA and reduce their translation by steric hinderance, either blocking translation directly, or altering mRNAs splicing.

First identified in the late 1970s, ASOs have been well-studied and improved over the decades.¹⁶³ This approach of inhibiting translation of target mRNAs is unique in that the ASOs can be composed of either DNA or RNA, so long as it binds effectively to their target mRNA.¹⁶⁴⁻¹⁶⁶ This binding can alter translation in several ways, either directly or indirectly. Firstly, ASOs can operate by directly blocking translation via steric hinderance.¹⁶⁷⁻¹⁶⁸ These are often designed to bind to their target mRNA near the start codon of a gene, blocking interaction between the mRNA and the ribosome. Secondly, ASOs can function by inhibiting splicing in diseased genes. For example, an ASO can bind to and block a splice site in a gene with a mutated splicing site, disabling the splicing and maturation of the target mRNA, thus inhibiting its further translation into protein.¹⁶⁹⁻
¹⁷² Thirdly, ASOs can operate by preventing the 5' cap on mRNA from forming.¹⁷³ 7-methyl guanosine is necessary for both nuclease protection as well as translation initiation. Finally, ASOs (specifically DNAs) can function by recruiting RNase H to the target ASO/mRNA hybrid, thus

inducing mRNA degradation.^{168, 174} RNase H is an enzyme which selectively degrades RNA in a DNA/RNA hybrid; therefore, this is a highly effective method because after mRNA degradation, the intact DNA ASO is released to repeat this action and further reduce translation.

Several ASOs have been approved for clinical use, with many more in clinical trials. Currently, there are six FDA approved ASO-based therapies for a range of diseases. The first ASO, approved by the FDA in the late twentieth century, was fomiviseran, a phosphorothioate DNA oligonucleotide designed for the treatment of cytomegalovirus retinitis.¹⁷⁵⁻¹⁷⁶ Additional approved ASO therapies target diseases such as hypercholesterolemia, liver diseases, muscular dystrophy, macular degeneration, and spinal atrophy.¹⁷⁷⁻¹⁸² Interestingly, these pharmaceuticals use the same treatment (ASO inhibition of translation) for treating very different ailments.

Beyond antisense therapies, RNAi has been extensively investigated for the treatment of various diseases. As a therapeutic, RNAi drugs including siRNA, miRNA, and short-hairpin RNAs (shRNAs) can be used to knockdown target genes of mutated proteins, induce cell death, or regulate cellular pathways. Despite its efficacy, there are only two currently FDA approved siRNA-based therapies: Patisiran, an siRNA used to treat polyneuropathy,¹⁸³⁻¹⁸⁴ and Givisoran, an siRNA used to treat acute hepatic porphyria.¹⁸⁵⁻¹⁸⁶ Although only two siRNA-based therapies have been FDA approved, there are several more RNAi inducers in clinical trials, which have great promise for treating complex diseases.¹⁸⁷ While siRNAs are often transfected directly, or transfected as longer dsRNAs that can be processed by the enzyme dicer, shRNAs are introduced in the form of DNA to be transcribed for their action.¹⁸⁸⁻¹⁸⁹

The broad-acting nature of miRNAs makes them ideal candidates for the treatment of various diseases as well. This includes both using miRNAs as therapeutics, or targeting the endogenous miRNAs.¹⁹⁰ The expression of various genes can be modified by using synthetic miRNA mimics, which have the same effect as their endogenous counterparts including downregulating coding genes or transcription factors.¹⁹¹⁻¹⁹² As a therapeutic, miRNA mimics have been considered for cancers due to their role in regulating tumor growth,¹⁹³ as well as anti-viral

activity.¹⁹⁴ Considering their role in protein expression and epigenetics, the inhibition of miRNAs for therapeutic activity has also been investigated. Using anti-miRNAs (antagomirs), an anti-sense adjacent approach was designed to reduce the efficacy of endogenous miRNAs.¹⁹⁵ Both transfection of miRNA and inhibition of specific miRNAs have confirmed effective for treating the same disease, demonstrating the depth and width of miRNA activity in cellular regulation.^{194, 196}

While the principle has remained the same, improvements and alternative administration strategies to ASOs and RNAi inducers have led to more effective delivery, stability, and therapeutic efficacy. As with most oligonucleotide-based therapies, the main challenges include stability, delivery, and reducing off-target effects. One potent strategy for enhancing stability and therefore circulation time is the inclusion of chemical modifications to ASOs and siRNAs.¹⁹⁷⁻¹⁹⁹ The inclusion of phosphorothioate bonds to replace phosphodiester in the backbone of DNA is a popular strategy for ASOs as it greatly enhances their resistance versus nucleases. In both ASOs and siRNAs alike, modifying the sugar and bases can achieve enhanced stability, but several modifications have been shown to reduce silencing efficacy due to hinderance in RISC loading for siRNAs; therefore, careful consideration of chemical modifications is paramount for successful therapeutic design. Alternatively, carriers can be used to help deliver ASOs and siRNAs to their intended target cells. There are several nanoformulations aimed for the delivery of therapeutic nucleic acids.²⁰⁰⁻²⁰³ These carriers can be silica, lipid, polymer, or metal based. Several of these carriers have made it to clinical trials, yet safety and potency issues have limited others.

1.2.2 Aptamers as therapeutics

Aptamers are single stranded oligonucleotides which are designed to have a high affinity for a specific target. Interestingly, aptamers can be designed to bind to nearly any target molecule, including sugars, dyes, proteins, or even whole cells. In fact, aptamers are often thought of as the nucleic acid mimic of antibodies, due to their high affinity for a specific target. Aptamers are designed through a process known as systematic evolution of ligands by exponential enrichment (SELEX).²⁰⁴⁻²⁰⁶ SELEX is a process in which an immense library of randomized nucleic acids is

incubated with a target ligand and surveyed for potential interactions. Due to the vast and diverse structures that nucleic acids can assume, the strands will have varying degrees of interactions with the target ligand. By repeatedly narrowing the library by removing non-interacting strands and strands interacting with non-intended targets, a small panel strands with high specificity towards the target molecule can be generated. The result is an oligonucleotide which binds with high affinity and specificity to a target, which can then be utilized either in medicine or biological research.

In the biomedical field, aptamers can be used in a number of ways to either directly treat a disease or act as a targeting moiety for enhanced delivery.²⁰⁷⁻²⁰⁸ The most common methods in which aptamers are used therapeutically is their binding and inactivation or blocking of a specific receptor (similar to monoclonal antibodies),²⁰⁹ or their ability to deliver a therapeutic agent specifically to a target cell.²¹⁰ These methods of therapy can be achieved both extracellularly or in cells, depending on the specific target and this strategy is common for aptamers selected to target cancers.²¹¹ For example, prostate-specific membrane antigen (PSMA) is overexpressed on cancer cells when compared to healthy prostate cells.²¹² As such, PSMA is used when specifically targeting cancer cells, and several aptamers have been designed against it.²¹³⁻²¹⁴ PSMA aptamers have been conjugated to various pharmaceutical agents, including peptides and chemotherapeutics.²¹⁵⁻²¹⁶ Additionally, these aptamer/drug conjugates have been loaded onto nanoparticles for enhanced delivery and targeting.²¹⁷⁻²¹⁹ A library of aptamers has been selected and now available for targeting other cancer associated antigens or mutated receptors.

Extracellularly, aptamers have been designed for thrombosis and the treatment of vascular disease. Aptamers have been designed against thrombin, von Willebrand Factor, and Factor IXa, all of which are important for normal clotting in humans.²²⁰⁻²²⁴ As an example, thrombin binding aptamers have been designed to delay clotting time and have been shown to work extensively *in vitro* and *in vivo*. Furthermore, by using the reverse complement, the aptamers can be “turned off” and clotting is returned to normal.²²⁵⁻²²⁶

Together, aptamers present a powerful tool for the targeting or direct treatment of complex

diseases. Their ability to bind directly to a specific target, as well as their ability to be readily conjugated to other therapeutics make them prime candidates for treating a number of diseases.

1.2.3 Immunostimulation from nucleic acids as a therapeutic approach

Immunomodulatory nucleic acids are just starting to find their niche in modern medicine and are being highly studied in research laboratories to treat a variety of diseases. Modulating the immune system is a common approach in medicine; vaccines are used to generate specific antibodies and create lasting immunity (more potently with the help of adjuvants), and engineering immune cells to work as anti-tumoral agents is now a promising approach. Alternatively, nucleic acids are only able to stimulate the innate immunity, and don't produce memory cells, but can aid in adaptive responses if other receptors are stimulated.²²⁷ By targeting any number of specific cell receptors, immunomodulatory nucleic acids can provoke an immune response to produce inflammation, cause specific cell proliferation, or start a cascade of cytokines for further action.²²⁸

Stimulating nucleic acid receptors in immune cells can have a number of effects on their proliferation and gene expression. As such, one strategy for enhancing immune activity is the delivery of TLR agonists to immune cells. It has been demonstrated that TLR stimulation in dendritic cells leads to their activation and maturation, while TLR stimulation in B cells leads to enhanced differentiation into anti-body secreting plasma cells.²²⁹⁻²³⁰ In plasmacytoid dendritic cells, TLR stimulation leads to increased secretion of type I interferons, as well as an increase in the expression of co-stimulatory molecules such as CD80 and CD86.²³¹⁻²³² Due to the complex interwoven nature of the immune system, this is expected to initiate a broad range of downstream effects including the further secretion of cytokines from neighboring cells, expansion of T-cells, and activation of natural killer cells.²³³⁻²³⁵

The above consequences of TLR activation makes using immunomodulatory DNAs or RNAs to elicit an immune response in tumors a viable approach for turning the immune system against cancer. Researchers have demonstrated activation of natural killer cells by RNA-based TLR7 agonists (delivered via lipid based nanoparticles) were able to exhibit enhanced anti-tumoral

responses *in vivo*.²³⁶ They have also demonstrated enhanced cytotoxic T-lymphocyte activity via increased IFN- γ production. In another study, researchers showed that RIG-I activation (via RNA 5'-triphosphate) in combination with specific gene silencing using siRNAs delivered via polyethyleneimine (PEI) was able to produce anti-tumoral effects in cutaneous melanomas as well as colon carcinomas.²³⁷ Several other studies have shown the use of TLR9 agonists both alone and in tandem with other therapeutics to treat cancers. By itself, TLR9 agonists have been shown to upregulate expression of MHC molecules on malignant B cells, increasing their ability to stimulate T cells and providing a more robust response.^{230, 238} Combinatorial therapy with TLR9 agonists and both antibodies or chemotherapies have shown increased efficacy in treating non-Hodgkin's lymphoma and non-small cell lung cancer, respectively.²³⁹⁻²⁴⁵

Another major strategy for using nucleic acids in immunotherapy is the co-delivery of an immunostimulatory nucleic acid with an antigen peptide. This has been demonstrated to greatly enhance the proliferation of antigen-specific T cells against the target peptide. In one study, TLR9 agonist (unmethylated CpG DNA) was co-delivered with peptide MART-1 for the melanoma, and it resulted in a 10-fold increase in anti-gen specific CD8⁺ cells against the target antigen.²⁴⁶⁻²⁴⁷ In more recent developments, nanoparticles containing both peptide antigens and CpG oligonucleotides were shown to guarantee co-delivery of both for enhanced antigen presentation.²⁴⁸⁻²⁴⁹ Furthermore, another group demonstrated the use of gold nanoparticles to generate spherical nucleic acids, which showed enhanced immunomodulatory activity.²⁵⁰

Overall, nucleic acids can be used in a variety of strategies to combat complex diseases. The combination of specific targeting, gene silencing, and immunomodulation, which can all be combined in one molecule, make nucleic acids a prime candidate for the treatment of nearly any disease or disorder.

1.3 Nucleic Acid Nanotechnology

The combination of the aforementioned properties and functionalities has led to a new field called nucleic acid nanotechnology. This field uses the folding and bonding principles of DNA and

RNA to fold into rationally designed, unique, nanoscale architectures which are capable of performing a designated task.²⁵¹ Over the years, the field has evolved from simple assemblies with no function to complex, three-dimensional architectures that can be used as molecular machines, therapies, or scaffolds. These structures have shown advantages over traditional therapeutics such as biocompatibility, multivalence, tunable physicochemical properties, and have been trending towards relatively low cost.

1.3.1 Rational design and computed assisted strategies

Early designs of nucleic acid nanoassemblies focused mainly on organizing DNA into controlled structures such as branched junctions and lattices.²⁵²⁻²⁵⁴ In its nascence, these assemblies demonstrated some of the first uses of natural biomolecules in bottom-up assembly of nanoscale materials.²⁵²⁻²⁵³ As strategies advanced, simple functional DNA-based materials were designed, including nanomechanical devices and rudimentary DNA walkers.²⁵⁵⁻²⁵⁷ In the past decades, new classes and design methods of nucleic acid nanotechnology began to emerge.²⁵⁸⁻²⁵⁹ Novel architectures wowed the scientific community with familiar images of smiling faces, stars, and triangles self-assembled from DNA strands in a technique now known as DNA origami.²⁶⁰⁻²⁶¹ At the same time, early RNA nano-designs began making their debut, with RNA tectonics (or tecto-RNA) facilitating the design of novel RNA nanostructures through combining motifs.²⁶²

DNA origami and tecto-RNA demonstrated early abilities for precise bottom-up nucleic acid nanodesign.^{260, 263} Since then, the two fields, DNA and RNA nanotechnology, have move largely in tandem, with ever-increasingly complex designs being developed to answer critical questions in medicine, materials, and molecular biology.^{251, 264}

DNA origami works on the principle of using one large (initially virally derived using the M13mp18 virus) scaffold ssDNA to fold at the direction of numerous smaller staple ssDNAs.^{260, 265} Changing the staple strands and leaving the scaffold constant allows for the design of countless structures.²⁶⁰ Since then, a variety of two-dimensional structures generated by DNA origami have been demonstrated, including letters of the alphabet and various common symbols.²⁶⁶⁻²⁶⁷ Beyond

these structures, three-dimensional DNA assemblies have been designed, including those exclusively made of DNA, and those which can coordinate other molecules to fold into three-dimensional structures.²⁶⁸⁻²⁷⁰ For DNA-exclusive structures, several basic design strategies can be employed, including extending DNA origami through either stacking of two-dimensional sheets or combining smaller three-dimensional unit cells. Furthermore, wireframe DNA nanostructures have been designed by incorporating a triangulated three-dimensional mesh of dsDNA.²⁷¹

Expanding beyond DNA exclusive materials, the incorporation of various organic molecules, transition metals, polymers, lipids, intercalating agents, or even other nanoparticles can facilitate the generation of a greater library of nanostructures.²⁷²⁻²⁷⁵ These structures can be designed in two directions, either using DNA to organize the complementary material, or using the material to coordinate the DNA. These DNA-based supra-assemblies have applications in medicine and materials alike.

Analogous to DNA, RNA nanotechnology began with two-dimensional lattices and expanded thereafter.²⁷⁶ Despite their molecular similarities, consequences of the 2' hydroxyl group causes vast differences in the resulting molecule, demonstrated simply by their roles in molecular biology and RNA tertiary structures are complex and their prediction is problematic. As such, researchers take inspiration from natural biology, allowing natural evolution to guide their basic design. This idea was first brought forth through RNA tectonics, which aims at constructing libraries using RNA mosaic units to create molecules with designed shapes and properties.²⁶² In fact, a “Jigsaw Puzzle” RNA nanostructure, among the first reported RNA nano-designs, incorporated motifs taken from HIV genomes and ribosomal derived structures.²⁷⁶ In another approach, a library of RNA nanostructures was designed by simply orienting the bacteriophage phi29 motif in different orientations to produce dimers, trimers, tetramers, and beyond in different orientations.²⁷⁷⁻²⁸⁰ Despite the rigor of prediction, approaches used to construct DNA nanostructures can often times be applied to RNA nanostructures, such as junctions, branches, bundles, and twisted bundles. Furthermore, examples of RNA origami have been demonstrated,

expanding the domain of RNA nanotechnology.²⁸¹⁻²⁸²

RNA tectonics made generation of complex nanostructures a reality, but limitations still existed beyond using evolutionarily prepared motifs. As computational power has increased, the ability to predict intricacies in RNA structure has too. The simple nature of Watson-Crick base pairing makes predicting DNA structures a facile task; however, pseudoknots, non-canonical pairing, loop-loop, and other extraneous interactions makes predicting RNA structures a challenging feat. Furthermore, the contributions of metal ions to RNA stabilization needs to be accounted for, and can play a major role in structure formation. To address these challenges, many programmers and mathematicians have aided the field with programs to predict RNA secondary and tertiary structure. These programs, including Mfold²⁸³⁻²⁸⁵, Hyperfold²⁸⁶, NUPACK²⁸⁷⁻²⁸⁹, and Nanotiler²⁹⁰, have aided RNA nanotechnologists in streamlining rational design for various facets of research. Despite advances, perfecting RNA structure prediction eludes researchers.

With these advances, numerous DNA, RNA, and DNA/RNA hybrid nanostructures have been designed and assembled including two-dimensional long-range structures such as tiles, sheets, and bundles.^{254, 291-293} Additionally, RNA has the advantage of being assembled co-transcriptionally, when RNA structures fold and interact while individual RNA strands simultaneously being transcribed.. Three-dimensional designs have been demonstrated, with a variety of shapes and structures incorporating several RNA exclusive motifs or structures. For example, cubic RNA nanoparticles have been designed which use exclusively Watson-Crick base pairing, incorporating six individual RNA strands into a nanostructure of only 10 nm.²⁹⁴ Furthermore, a ring-like structure was designed incorporating HIV-like kissing loops which assume near-perfect 120° geometry.²⁹⁵⁻²⁹⁶

In another approach, the bacteriophage phi29 motif was used in numerous orientations to allow for the generation of dozens of shapes with well-defined and predicted properties and sizes via one-pot assembly.²⁹⁷ Several RNA structural motifs have been incorporated into nano-assemblies, allowing for a myriad of shapes including polygons, hearts, stars, and beyond.²⁹⁸⁻³⁰⁰ In

fact, using exclusively DNA and/or RNA, the repertoire of nanostructures that can be assembled is nearly infinite.³⁰¹ Some DNA and RNA nanoparticles are schematically demonstrated in Figure 4A.

Beyond static structures, DNA and RNA can be used to design dynamic machinery. The Watson-Crick base pairing predictability of nucleic acids allows for the generation of logic gates, switches, and various molecular machines.³⁰² Early designs used isothermal strand displacement to fuel reactions, generating desirable products downstream for biosensing or therapeutics, or to cause a physical or chemical change in a product.³⁰³⁻³⁰⁵ This has been achieved for simple hybridization reactions to generate new structures based on strand input.³⁰⁶⁻³⁰⁷ For example, DNA tweezers have been designed, using FRET as an output for their completed action.³⁰³ This approach has been used to generate a series of functional designs, wherein the generation of a therapeutic product is achieved through strand displacement caused by a related input.³⁰⁸⁻³¹¹ Furthermore, researchers have used strand displacement to cause shape-switching in nucleic acid nanostructures.^{309, 312-315} In addition to strand displacement, other strategies such as pH responsive,³¹⁶ biomarker-dependent,³¹⁷ and light-activated³¹⁸⁻³²⁰ dynamic nucleic acid-based structures have also been designed.

Outside of direct therapeutics, walkers and molecular machines have also been designed, using strand displacement to physically move cargo across a surface.³²¹⁻³²² Both single-step and multi-step walkers have been achieved, with increasingly complex strand displacement mechanisms to achieve a greater depth of motion.³²³ Expanding on this strategy, and taking advantage of advances in folding prediction, complex logic gates and cascade pathways have been designed, activating recoverable products for biosensing purposes.^{306, 324} These strategies have since been incorporated into nucleic acid nanostructures for further advancements.

Advancements in nucleic acid structure resolution and prediction have expanded the breadth of nucleic acid nanostructures. Beginning from simple junctions and branches, improvements have made the generation of complex three-dimensional structures a reality, using DNA origami, RNA tectonics, and rational design complemented by computed assisted structure

prediction. Furthermore, incorporating dynamic activity into these once static designs greatly expands the scope of their utilization, and further functionalization with therapeutics will aid in realizing their potential.

1.3.2 Therapeutic nucleic acid nanotechnology

As discussed earlier, several nucleic acid-based pharmaceuticals are currently approved by the US Food and Drug Administration (FDA), with several more in clinical trials.³²⁵⁻³²⁷ In addition to their therapeutic applications, anti-sense oligonucleotides, RNAi inducers, immunostimulatory oligonucleotides, and aptamers have become commonplace in laboratories as tools for molecular biology. Although these approaches hold great potential, hinderances such as off-target activity, immunostimulation, and degradation have retarded their procession from lab to clinic. Nucleic acid nanotechnology presents many opportunities to answer these issues. Incorporation of multiple therapeutics, capability of multivalence, and resistance versus degradation have all been achieved to enhance the therapeutic capability traditional therapeutic nucleic acids.

RNAi through various moieties has been shown to be effective for reducing expression of target proteins. RNAi inducers, such as siRNA, miRNA, and shRNA are prone to enzymatic degradation from intracellular and extracellular nucleases.³²⁸ Furthermore, off-target effects in non-target cells can be an issue in therapeutic RNAi inducers.³²⁹ Incorporation of RNAi inducers into nucleic acid nanostructures is an approach to remedying these issues. By simply extending the constituent strands of a NANP, incorporation of several different RNAi inducers is possible, thus creating a multivalent platform for a combinatorial approach. For example, pRNA-3WJ RNA nanoparticles were designed with incorporated siRNA against BRCA1 gene to treat gastric cancer.³³⁰ This strategy was further extended for other cancers and demonstrated effective treatment.³³¹⁻³³² In another study, RNA ring structures were designed to carry six different siRNAs against HIV-1.³³³ Furthermore, different nanostructures have been designed to incorporate many siRNAs, including against green fluorescent protein (GFP) and RhoA.^{312, 334-336} They have also been demonstrated to carry anti-miRNAs to regulate miRNA influence, such as anti-miR-21.³³⁷

In addition to rationally designed NANPs carrying RNAi inducers, RNA nanoparticles created by rolling circle transcription can generate mesh-like nanoparticles with repeats of transcribed siRNA.³³⁸⁻³³⁹ Often referred to as micro sponges, these densely packed RNA spheres or sheets can carry vast amounts of RNAi inducers in efficient nanoparticles. This was demonstrated for the efficient knockdown of luciferase and GFP, as well as several therapeutically relevant targets.³⁴⁰⁻³⁴² Varying the conditions in which the transcription takes place allows for tuning of the nanoparticles size, adding an additional layer of customizability to this technology.

Aptamers have been incorporated into NANPs for several reasons. Firstly, targeting of specific cells by aptamers could greatly reduce off-target effects. As such, surface markers on diseased cells are often one of the most commonly desired targets. Aptamers against various targets have been incorporated onto NANPs, including those against glioblastoma, breast cancer, prostate cancer, ovarian cancer, and lymphoma.^{331, 333, 343-344} In an analogous technology, folic acid has been conjugated onto NANPs, as many cancer cells have been shown to over express folic acid receptors, allowing for enhanced targeting.³⁴⁵ Aptamers incorporated into nucleic acid nanoparticles can also be used as a biosensor for detection of specific inputs.^{312, 315, 324} Beyond their targeting capabilities, the ability for aptamers to bind to a specific target makes them amenable for target inhibition. Using NANPs to carry multiple aptamers for targeted inhibition could enhance targeting and increase stability.

Nucleic acids can generate a robust immune response, starting from detection by either PRRs in the endosome or the cytoplasm. These conserved receptors, described in detail above, have evolved to detect specific molecular patterns, such as ssRNA, dsRNA, or CpG motifs. Although research has elucidated the mechanisms by which simple and natural nucleic acid structures are recognized, understanding the interactions between the immune system and engineered nucleic acid nanostructures has been of particular interest in recent years. Mentioned above are several approaches in which nucleic acid agonists are used to provoke a PRR dependent immune response for therapeutic function. Incorporation of immunostimulatory nucleic acids, such as CpG DNA,

have been incorporated into various NANPs.³⁴⁶⁻³⁴⁷ Beyond the addition of immunostimulatory motifs, immunorecognition of a NANP was found to be determined by its structure and composition. In one study, the surveying of an entire panel of NANPs revealed that globular, RNA-based NANPs are amongst the most immunostimulatory, with minimal effect from sequence.^{312, 348} Further studies used quantitative structure activity relationship (QSAR) to mathematically show a positive correlation between NANP stability and size to its immunostimulatory potential.³⁴⁹ Furthermore, it has been demonstrated that the addition of siRNAs to a given scaffold NANP can greatly increase its immunostimulation.³⁵⁰ These properties were found to be consistent for several carriers, including mesoporous silica nanoparticles and polymeric nanoparticles.³³⁴

1.3.3 Delivery of therapeutic nucleic acid with nanotechnology

Despite enhanced stability granted by engineered structures in NANPs, serum degradation and off-target effects remain an issue. To combat this, different synthetic and biological carriers have been utilized to deliver DNA and RNA functionalities, with the goal of enhancing cellular uptake, complex circulation, and nucleic acid stability for enhanced efficacy.³⁵¹ The breadth of therapeutic nanoparticles, even just those incorporating nucleic acids, is vast and cannot be covered in its entirety.

Several issues hinder effective therapeutic action for nucleic acids when administered in patients. The perils of an administered nucleic acid are many and varied, from difficulties traveling to their target organ, to assaults from ubiquitous nucleases.³⁵¹ Tissue barriers prevent complete circulation to target organs, and the negative overall charge on nucleic acids makes crossing these barriers challenging; as such, most non-active targeting therapeutics rely on the enhanced permeability and retention effect (for cancers).³⁵² The vascular endothelial barrier is amongst the most challenging for intravenously deliver nucleic acids, which can preclude the therapeutic nucleic acids from arriving at their target.³⁵³⁻³⁵⁴ In the case of successful circulation, larger nucleic acids (and other foreign entities) risk being detected by the reticuloendothelial system, leading to passivation by phagocytic cells.³⁵⁵ However, in most cases, the generally low mass of therapeutic

nucleic acids makes them susceptible to renal excretion.³⁵⁶ To address these challenges, various nanoscale carriers have been developed. These nanoparticles can be composed of various chemical make-ups, including lipid nanoparticles, polymeric nanoparticles, or inorganic nanoparticles, all of various flavors. Consequently, all of these nanoparticles have different properties, varying in size, charge, and loading capacity, all of which have consequences for their biodistribution and therapeutic efficacy. Several of these nanoparticles are demonstrated in figure 4B.

Lipid nanoparticles have received tremendous attention due to their ubiquity in nature, ability to self-assemble, and readiness to complex with nucleic acids; in fact, lipid nanoparticles

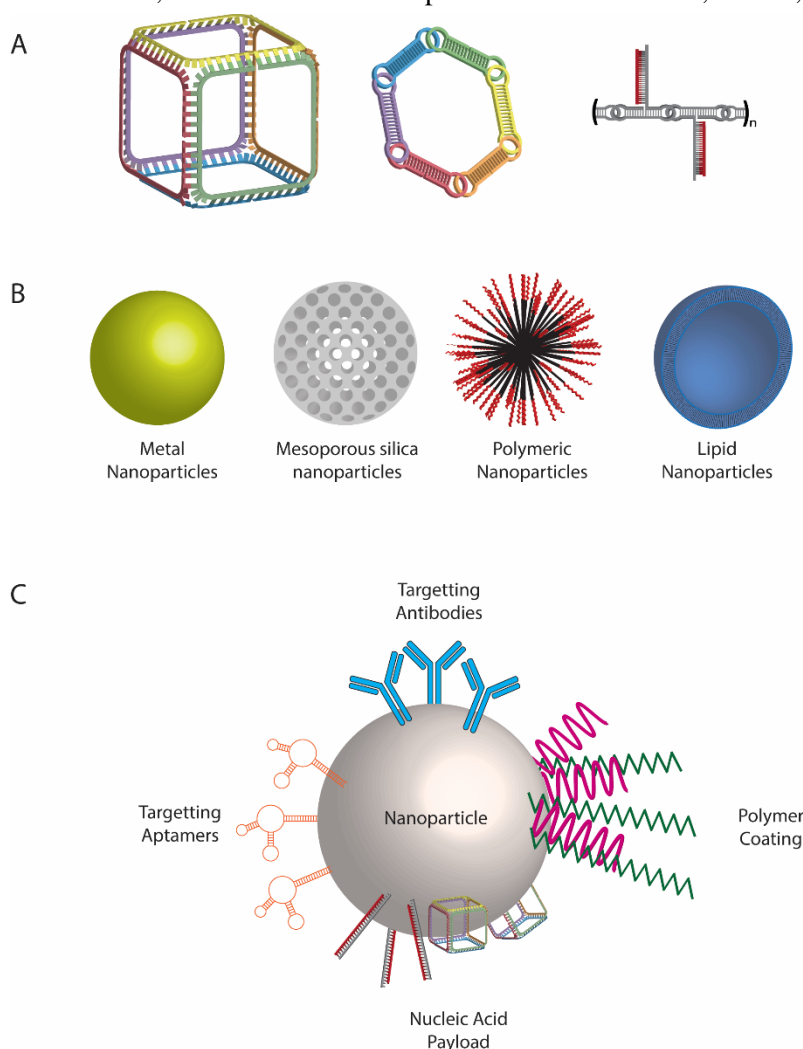


Figure 4. (A) Schematic representation of DNA and RNA nanoparticles. (B) Schematic representation of several nanocarriers. (C) Surface modifications of nanoparticles allowed for enhanced targeting and tunable physicochemical properties.

are amongst the highest investigated nanoparticles for the delivery of nucleic acids.³⁵⁷⁻³⁵⁸ There are several clinical trials involving the delivery of nucleic acid therapeutics with lipid nanoparticles.³⁵⁹⁻³⁶¹ Despite their popularity, several clinical trials have ended due to unexpected toxicity from these complexes.³⁶¹ The toxicity is speculated to be due both to immune responses, as well as interactions between the cationic lipids in the nanoparticle interacting with cellular membranes.³⁶²⁻³⁶³

Efforts have been made to lower their toxicity such as coating in PEG or using more neutral lipids.³⁶⁴ Additional studies have used antibodies for targeting specific ligands.³⁶⁵ Overall, several studies have shown effective delivery of nucleic acids using lipid particles, including delivery of siRNA targeting KRAS, several miRNAs, and anti-sense oligonucleotides.³⁶⁶⁻³⁶⁹ Despite advances, issues including toxicity, opsonization of serum proteins, and endosomal escape remain issues.

Polymeric nanoparticles have made progress towards effective delivery of therapeutic nucleic acids as well, though they have not yet reached the level of clinical trials.³⁷⁰ Thus far, various polymeric nanoparticles have been investigated, with the majority of those containing poly-co-glycolic acid (PLGA), polycaprolactone (PCL), polyethyleneimine (PEI), and/or polyethylene glycol (PEG).³⁷¹ Dendrimer nanoparticles composed of various polymers have been designed to grant additional control over size and composition.³⁷² Branched structures allow for tuning of their size and charge, which further modifies their loading capacity. Natural polymers have been used to synthesize nanoparticles for biomedical purposes including alginate, chitosan, starch, and cellulose nanoparticles.³⁷³ Like all nanoparticles, their physicochemical properties can be tuned to determine their bio-related properties such as circulation time, biodistribution, drug loading, and immune response. An advantage of polymeric (and lipid) nanoparticles is the ability to either encapsulate a therapeutic payload, or use the payload to decorate the surface of the nanoparticle³⁷⁴. Because polymers can be natural immunostimulants, they have the potential to add an additional layer of customizability.³⁷⁵

Inorganic nanoparticles encompass a broad range of materials, including mesoporous silica nanoparticles (MSNs), metal nanoparticles, ceramic nanoparticles, and more.³⁷⁶ Because of the

wide range of their make-up and properties, they can vary greatly in task and efficacy. Particularly, MSNs have been used due to their extraordinarily high surface area and tunability.³⁷⁷ Size, pore size, surface reactivity, and drug loading can be tuned for specific tasks. Researchers have demonstrated the use of MSNs conjugated to antibodies, loaded with chemotherapeutics, or loaded with nucleic acids to combat various diseases.³⁷⁸⁻³⁸¹ Furthermore, the chemistry to attach these therapies can be altered, resulting a trigger responsive release, or targeted treatments. Beyond MSNs, other inorganic nanoparticles such as iron-oxide, gold nanoparticles, and quantum dots have been used for the delivery of nucleic acids.³⁸² Each contains their own advantages and idiosyncrasies. For example, gold nanoparticles and quantum dots exhibit unique spectral properties which can be used as biosensors, including surface plasmon resonance or broad absorbance and narrow emission. Iron oxide nanoparticles can be engineered to have desirable magnetic properties for combinatorial magnetically induced thermal therapy.

Overall, the abundance of available nanoparticles is diverse, allowing for desirable properties no matter the application. Choosing the correct nanocarrier is of paramount importance for the desired application. Furthermore, modifications to these nanoparticles such as polymer coatings, and aptamer or antibody targeting have facilitated enhanced efficacy (Figure 4C.)

1.4 Dissertation summary

This dissertation aims to address key obstacles in the field of nucleic acid nanotechnology by identifying immunostimulatory properties of NANPs, advancing the delivery of therapeutic NANPs, and designing dynamic structures. These issues are prominent in the field of nucleic acid therapeutics, and extend into nucleic acid nanotechnology.

Chapter two is a study on a novel approach to dynamic NANPs. In this study, a NANP is designed to interact with its “anti-NANP” to undergo an isothermal strand displacement, causing a morphological shape change, as well as the activation of several functionalities. The anti-NANP is simply the reverse complement of the NANP, and assumes the same geometric shape and properties. Through this process, the activation of several functionalities is demonstrated to be

conditionally activated, including FRET, transcription, aptamer formation, and siRNA formation. Furthermore, its physicochemical and immunostimulatory properties are studied, and shown to be readily tuned by alteration of the NANP by substituting RNA for DNA.

Chapter three focuses on the immunostimulatory properties of NANPs. In this study, a limited library of polygons NANPs with similar design principles are compared. The set of sixteen NANPs compose of triangles, squares, pentagons, or hexagons composed of DNA, RNA or DNA/RNA hybrids. The physicochemical properties of the NANPs are measured and calculated, and a QSAR model is built based on preliminary immunostimulation results. Validation results verified the accuracy of the model, showing a positive correlation between NANP stability and mass with its immunostimulatory capabilities.

Chapter four describes the use of a polymeric nanoparticle for the delivery of a suite of NANPs. The polymeric nanoparticle, PgP, has previously been demonstrated to effectively deliver nucleic acid cargo for therapeutic function. In this study, NANPs carrying siRNA against GFP and RhoA are demonstrated to silence their targets with high efficiency. Furthermore, the immunostimulatory properties of the NANPs are surveyed. Finally, the biodistribution of each NANP/PgP complex is studied.

Together, these articles form a comprehensive sample on the current state of the field of DNA and RNA nanotechnology. In chapter five, concluding remarks are made, and a discussion of the field moving forward.

1.5 References

1. Watson, J. D.; Crick, F. H. C., Molecular structure of nucleic acids - a structure for deoxyribose nucleic acid. *Nature* **1953**, *171* (4356), 737-738.
2. Wang, A. H. J.; Quigley, G. J.; Kolpak, F. J.; Crawford, J. L.; Vanboom, J. H.; Vandermaer, G.; Rich, A., Molecular-structure of a left-handed double helical dna fragment at atomic resolution. *Nature* **1979**, *282* (5740), 680-686.
3. Strobel, S. A.; Doudna, J. A., RNA seeing double: Close-packing of helices in RNA tertiary structure. *Trends in Biochemical Sciences* **1997**, *22* (7), 262-266.
4. Šponer, J.; Mládek, A.; Šponer, J. E.; Svozil, D.; Zgarbová, M.; Banáš, P.; Jurečka, P.; Otyepka, M. J. P. C. C. P., The DNA and RNA sugar–phosphate backbone emerges as the key player. An overview of quantum–chemical, structural biology and simulation studies. **2012**, *14* (44), 15257-15277.
5. Nelson, J. W.; Martin, F. H.; Tinoco Jr, I. J. B. O. R. o. B., DNA and RNA oligomer thermodynamics: The effect of mismatched bases on double-helix stability. **1981**, *20* (12), 2509-2531.
6. Dickerson, R. E.; Drew, H. R.; Conner, B. N.; Wing, R. M.; Fratini, A. V.; Kopka, M. L. J. S., The anatomy of a-, b-, and z-dna. **1982**, *216* (4545), 475-485.
7. Rich, A.; Nordheim, A.; Wang, A. H.-J. J. A. r. o. b., The chemistry and biology of left-handed Z-DNA. **1984**, *53* (1), 791-846.
8. Bochman, M. L.; Paeschke, K.; Zakian, V. A. J. N. R. G., DNA secondary structures: stability and function of G-quadruplex structures. **2012**, *13* (11), 770-780.
9. Rhee, S.; Han, Z.-j.; Liu, K.; Miles, H. T.; Davies, D. R. J. B., Structure of a Triple Helical DNA with a Triplex– Duplex Junction. **1999**, *38* (51), 16810-16815.
10. Leontis, N. B.; Stombaugh, J.; Westhof, E., The non-Watson-Crick base pairs and their associated isostericity matrices. *Nucleic Acids Research* **2002**, *30* (16), 3497-3531.
11. Abu Almakarem, A. S.; Petrov, A. I.; Stombaugh, J.; Zirbel, C. L.; Leontis, N. B., Comprehensive survey and geometric classification of base triples in RNA structures. *Nucleic Acids Research* **2012**, *40* (4), 1407-1423.
12. Zgarbova, M.; Jurecka, P.; Banas, P.; Otyepka, M.; Sponer, J. E.; Leontis, N. B.; Zirbel, C. L.; Sponer, J., Noncanonical Hydrogen Bonding in Nucleic Acids. Benchmark Evaluation of Key Base-Phosphate Interactions in Folded RNA Molecules Using Quantum-Chemical Calculations and Molecular Dynamics Simulations. *Journal of Physical Chemistry A* **2011**, *115* (41), 11277-11292.
13. Leontis, N. B.; Lescoute, A.; Westhof, E., The building blocks and motifs of RNA architecture. *Current Opinion in Structural Biology* **2006**, *16* (3), 279-287.
14. Klein, D. J.; Moore, P. B.; Steitz, T. A., The contribution of metal ions to the structural stability of the large ribosomal subunit. *Rna* **2004**, *10* (9), 1366-1379.
15. Auffinger, P.; D'Ascenzo, L.; Ennifar, E., Sodium and Potassium Interactions with Nucleic Acids. In *Alkali Metal Ions: Their Role for Life*, Sigel, A.; Sigel, H.; Sigel, R. K. O., Eds. 2016; Vol. 16, pp 167-201.
16. Balaratnam, S.; Basu, S., Divalent Cation-Aided Identification of Physico-Chemical Properties of Metal Ions that Stabilize RNA G-Quadruplexes. *Biopolymers* **2015**, *103* (7), 376-386.
17. Cassone, G.; Kruse, H.; Sponer, J., Interactions between cyclic nucleotides and common cations: an ab initio molecular dynamics study. *Physical Chemistry Chemical Physics* **2019**, *21* (15), 8121-8132.
18. Fischer, N. M.; Poletto, M. D.; Steuer, J.; van der Spoel, D., Influence of Na⁺ and Mg²⁺ ions on RNA structures studied with molecular dynamics simulations. *Nucleic Acids Research* **2018**, *46* (10), 4872-4882.
19. Halder, A.; Roy, R.; Bhattacharyya, D.; Mitra, A., Consequences of Mg²⁺ binding on the

- geometry and stability of RNA base pairs. *Physical Chemistry Chemical Physics* **2018**, *20* (34), 21934-21948.
20. Kolev, S. K.; St Petkov, P.; Rangelov, M. A.; Trifonov, D. V.; Milenov, T. I.; Vayssilov, G. N., Interaction of Na⁺, K⁺, Mg²⁺ and Ca²⁺ counter cations with RNA. *Metallomics* **2018**, *10* (5), 659-678.
 21. Mandic, A.; Hayes, R. L.; Lammert, H.; Cheng, R. R.; Onuchic, J. N., Structure-Based Model of RNA Pseudoknot Captures Magnesium-Dependent Folding Thermodynamics. *Journal of Physical Chemistry B* **2019**, *123* (7), 1505-1511.
 22. Rozov, A.; Khusainov, I.; El Omari, K.; Duman, R.; Mykhaylyk, V.; Yusupov, M.; Westhof, E.; Wagner, A.; Yusupova, G., Importance of potassium ions for ribosome structure and function revealed by long-wavelength X-ray diffraction. *Nature Communications* **2019**, *10*.
 23. Serra, M. J.; Baird, J. D.; Dale, T.; Fey, B. L.; Retatagos, K.; Westhof, E. J. R., Effects of magnesium ions on the stabilization of RNA oligomers of defined structures. **2002**, *8* (3), 307-323.
 24. Misra, V. K.; Draper, D. E. J. B. O. R. o. B., On the role of magnesium ions in RNA stability. **1998**, *48* (2-3), 113-135.
 25. Zheng, H.; Shabalin, I. G.; Handing, K. B.; Bujnicki, J. M.; Minor, W. J. N. a. r., Magnesium-binding architectures in RNA crystal structures: validation, binding preferences, classification and motif detection. **2015**, *43* (7), 3789-3801.
 26. Fischer, N. M.; Polêto, M. D.; Steuer, J.; van der Spoel, D. J. N. a. r., Influence of Na⁺ and Mg²⁺ ions on RNA structures studied with molecular dynamics simulations. **2018**, *46* (10), 4872-4882.
 27. Bowman, J. C.; Lenz, T. K.; Hud, N. V.; Williams, L. D. J. C. o. i. s. b., Cations in charge: magnesium ions in RNA folding and catalysis. **2012**, *22* (3), 262.
 28. Batey, R. T.; Rambo, R. P.; Doudna, J. A., Tertiary motifs in RNA structure and folding. *Angewandte Chemie-International Edition* **1999**, *38* (16), 2327-2343.
 29. Zuker, M.; Jaeger, J. A.; Turner, D. H., A comparison of optimal and suboptimal rna secondary structures predicted by free-energy minimization with structures determined by phylogenetic comparison. *Nucleic Acids Research* **1991**, *19* (10), 2707-2714.
 30. Lutz, C. S., Alternative Polyadenylation: A Twist on mRNA 3' End Formation. *Acs Chemical Biology* **2008**, *3* (10), 609-617.
 31. Marcotrigiano, J.; Gingras, A. C.; Sonenberg, N.; Burley, S. K., Cocrystal structure of the messenger RNA 5' cap-binding protein (eIF4E) bound to 7-methyl-GDP. *Cell* **1997**, *89* (6), 951-961.
 32. Mitchell, S. F.; Walker, S. E.; Algire, M. A.; Park, E.-H.; Hinnebusch, A. G.; Lorsch, J. R. J. M. c., The 5'-7-methylguanosine cap on eukaryotic mRNAs serves both to stimulate canonical translation initiation and to block an alternative pathway. **2010**, *39* (6), 950-962.
 33. Hinnebusch, A. G.; Ivanov, I. P.; Sonenberg, N. J. S., Translational control by 5'-untranslated regions of eukaryotic mRNAs. **2016**, *352* (6292), 1413-1416.
 34. Cenik, C.; Derti, A.; Mellor, J. C.; Berriz, G. F.; Roth, F. P. J. G. b., Genome-wide functional analysis of human 5'untranslated region introns. **2010**, *11* (3), R29.
 35. Matoulkova, E.; Michalova, E.; Vojtesek, B.; Hrstka, R. J. R. b., The role of the 3'untranslated region in post-transcriptional regulation of protein expression in mammalian cells. **2012**, *9* (5), 563-576.
 36. Conne, B.; Stutz, A.; Vassalli, J.-D. J. N. m., The 3' untranslated region of messenger RNA: a molecular 'hotspot' for pathology? **2000**, *6* (6), 637-641.
 37. Dreyfus, M.; Régnier, P. J. C., The poly (A) tail of mRNAs: bodyguard in eukaryotes, scavenger in bacteria. **2002**, *111* (5), 611-613.
 38. Colgan, D. F.; Manley, J. L. J. G.; development, Mechanism and regulation of mRNA polyadenylation. **1997**, *11* (21), 2755-2766.
 39. Sriyothi, L.; Ponne, S.; Prathama, T.; Ashok, C.; Baluchamy, S. J. T.; Regulation, P.-t.,

Roles of Non-Coding RNAs in Transcriptional Regulation. **2018**, 55.

40. Palazzo, A. F.; Lee, E. S. J. F. i. g., Non-coding RNA: what is functional and what is junk? **2015**, 6, 2.
41. Uno, T.; Schultz, P. J. S., Expanding the scope of RNA catalysis. **1994**, 264 (5167), 1924-1927.
42. Walter, N. G.; Engelke, D. R. J. B., Ribozymes: catalytic RNAs that cut things, make things, and do odd and useful jobs. **2002**, 49 (5), 199.
43. Weinberg, C. E.; Weinberg, Z.; Hammann, C. J. N. a. r., Novel ribozymes: discovery, catalytic mechanisms, and the quest to understand biological function. **2019**, 47 (18), 9480-9494.
44. Breaker, R. R. J. C. S. H. p. i. b., Riboswitches and the RNA world. **2012**, 4 (2), a003566.
45. Garst, A. D.; Edwards, A. L.; Batey, R. T. J. C. S. H. p. i. b., Riboswitches: structures and mechanisms. **2011**, 3 (6), a003533.
46. Dana, H.; Chalbatani, G. M.; Mahmoodzadeh, H.; Karimloo, R.; Rezaiean, O.; Moradzadeh, A.; Mehmandoost, N.; Moazzen, F.; Mazraeh, A.; Marmari, V. J. I. j. o. b. s. I., Molecular mechanisms and biological functions of siRNA. **2017**, 13 (2), 48.
47. Kiss, T. J. C., Small nucleolar RNAs: an abundant group of noncoding RNAs with diverse cellular functions. **2002**, 109 (2), 145-148.
48. Lilley, D. M. J., The origins of RNA catalysis in ribozymes. *Trends in Biochemical Sciences* **2003**, 28 (9), 495-501.
49. Takagi, Y.; Warashina, M.; Stec, W. J.; Yoshinari, K.; Taira, K., Recent advances in the elucidation of the mechanisms of action of ribozymes. *Nucleic Acids Research* **2001**, 29 (9), 1815-1834.
50. Tanner, N. K., Ribozymes: the characteristics and properties of catalytic RNAs. *FEMS microbiology reviews* **1999**, 23 (3), 257-275.
51. de la Pena, M.; Garcia-Robles, I., Ubiquitous presence of the hammerhead ribozyme motif along the tree of life. *Rna* **2010**, 16 (10), 1943-1950.
52. Hammann, C.; Luptak, A.; Perreault, J.; de la Pena, M., The ubiquitous hammerhead ribozyme. *Rna-a Publication of the Rna Society* **2012**, 18 (5), 871-885.
53. Erlacher, M. D.; Polacek, N., Ribosomal catalysis - The evolution of mechanistic concepts for peptide bond formation and peptidyl-tRNA hydrolysis. *Rna Biology* **2008**, 5 (1), 5-12.
54. Simonovic, M.; Steitz, T. A., A structural view on the mechanism of the ribosome-catalyzed peptide bond formation. *Biochimica Et Biophysica Acta- Gene Regulatory Mechanisms* **2009**, 1789 (9-10), 612-623.
55. Nissen, P.; Hansen, J.; Ban, N.; Moore, P. B.; Steitz, T. A. J. S., The structural basis of ribosome activity in peptide bond synthesis. **2000**, 289 (5481), 920-930.
56. Wilson, D. N.; Cate, J. H. D. J. C. S. H. p. i. b., The structure and function of the eukaryotic ribosome. **2012**, 4 (5), a011536.
57. Beringer, M.; Bruell, C.; Xiong, L.; Pfister, P.; Bieling, P.; Katunin, V. I.; Mankin, A. S.; Böttger, E. C.; Rodnina, M. V. J. J. o. B. C., Essential mechanisms in the catalysis of peptide bond formation on the ribosome. **2005**, 280 (43), 36065-36072.
58. Mandal, M.; Breaker, R. R., Gene regulation by riboswitches. *Nature Reviews Molecular Cell Biology* **2004**, 5 (6), 451-463.
59. Winkler, W. C.; Breaker, R. R., Regulation of bacterial gene expression by riboswitches. In *Annual Review of Microbiology*, 2005; Vol. 59, pp 487-517.
60. Manzourolajdad, A.; Arnold, J. J. B. b., Secondary structural entropy in RNA switch (Riboswitch) identification. **2015**, 16 (1), 133.
61. Nahvi, A.; Sudarsan, N.; Ebert, M. S.; Zou, X.; Brown, K. L.; Breaker, R. R. J. C.; biology, Genetic control by a metabolite binding mRNA. **2002**, 9 (9), 1043-1049.
62. Nahvi, A.; Barrick, J. E.; Breaker, R. R., Coenzyme B-12 riboswitches are widespread genetic control elements in prokaryotes. *Nucleic Acids Research* **2004**, 32 (1), 143-150.

63. Mulhbachter, J.; St-Pierre, P.; Lafontaine, D. A., Therapeutic applications of ribozymes and riboswitches. *Current Opinion in Pharmacology* **2010**, *10* (5), 551-556.
64. Lee, C. H.; Han, S. R.; Lee, S. W., Therapeutic Applications of Aptamer-Based Riboswitches. *Nucleic Acid Therapeutics* **2016**, *26* (1), 44-51.
65. Uszczynska-Ratajczak, B.; Lagarde, J.; Frankish, A.; Guigo, R.; Johnson, R., Towards a complete map of the human long non-coding RNA transcriptome. *Nature Reviews Genetics* **2018**, *19* (9), 535-548.
66. Holoch, D.; Moazed, D., RNA-mediated epigenetic regulation of gene expression. *Nature Reviews Genetics* **2015**, *16* (2), 71-84.
67. Morris, K. V.; Mattick, J. S., The rise of regulatory RNA. *Nature Reviews Genetics* **2014**, *15* (6), 423-437.
68. De Fougères, A.; Manoharan, M.; Meyers, R.; Vornlocher, H. P., RNA interference in vivo: Toward synthetic small inhibitory RNA-based therapeutics. In *Rna Interference*, Engelke, D. R.; Rossi, J. J., Eds. 2005; Vol. 392, pp 278-296.
69. Agrawal, N.; Dasaradhi, P.; Mohammed, A.; Malhotra, P.; Bhatnagar, R. K.; Mukherjee, S. K. J. M. B. R., RNA interference: biology, mechanism, and applications. **2003**, *67* (4), 657-685.
70. Bartel, D. P., MicroRNAs: Genomics, biogenesis, mechanism, and function. *Cell* **2004**, *116* (2), 281-297.
71. Murchison, E. P.; Hannon, G. J., MiRNAs on the move: miRNA biogenesis and the RNAi machinery. *Current Opinion in Cell Biology* **2004**, *16* (3), 223-229.
72. Pillai, R. S., MicroRNA function: Multiple mechanisms for a tiny RNA? *Rna-a Publication of the Rna Society* **2005**, *11* (12), 1753-1761.
73. Olena, A. F.; Patton, J. G. J. o. c. p., Genomic organization of microRNAs. **2010**, *222* (3), 540-545.
74. Filippov, V.; Solovyev, V.; Filippova, M.; Gill, S. S. J. G., A novel type of RNase III family proteins in eukaryotes. **2000**, *245* (1), 213-221.
75. Lee, Y.; Ahn, C.; Han, J.; Choi, H.; Kim, J.; Yim, J.; Lee, J.; Provost, P.; Rådmark, O.; Kim, S. J. N., The nuclear RNase III Drosha initiates microRNA processing. **2003**, *425* (6956), 415-419.
76. Shukla, G. C.; Singh, J.; Barik, S. J. M.; pharmacology, c., MicroRNAs: processing, maturation, target recognition and regulatory functions. **2011**, *3* (3), 83.
77. Bhome, R.; Del Vecchio, F.; Lee, G.-H.; Bullock, M. D.; Primrose, J. N.; Sayan, A. E.; Mirnezami, A. H., Exosomal microRNAs (exomiRs): Small molecules with a big role in cancer. *Cancer letters* **2018**, *420*, 228-235.
78. Sanz-Rubio, D.; Martin-Burriel, I.; Gil, A.; Cubero, P.; Forner, M.; Khalyfa, A.; Marin, J. M., Stability of circulating exosomal miRNAs in healthy subjects. *Scientific reports* **2018**, *8* (1), 1-10.
79. MacFarlane, L.-A.; R Murphy, P. J. C. g., MicroRNA: biogenesis, function and role in cancer. **2010**, *11* (7), 537-561.
80. Ardekani, A. M.; Naeini, M. M. J. A. j. o. m. b., The role of microRNAs in human diseases. **2010**, *2* (4), 161.
81. Lam, J. K.; Chow, M. Y.; Zhang, Y.; Leung, S. W. J. M. T.-N. A., siRNA versus miRNA as therapeutics for gene silencing. **2015**, *4*, e252.
82. Liufu, Z.; Zhao, Y.; Guo, L.; Miao, G.; Xiao, J.; Lyu, Y.; Chen, Y.; Shi, S.; Tang, T.; Wu, C.-I. J. G. r., Redundant and incoherent regulations of multiple phenotypes suggest microRNAs' role in stability control. **2017**, *27* (10), 1665-1673.
83. Goljanek-Whysall, K.; Pais, H.; Rathjen, T.; Sweetman, D.; Dalmay, T.; Münsterberg, A. J. J. o. C. S., Regulation of multiple target genes by miR-1 and miR-206 is pivotal for C2C12 myoblast differentiation. **2012**, *125* (15), 3590-3600.
84. Snead, N. M.; Rossi, J. J., Biogenesis and function of endogenous and exogenous

- siRNAs. *Wiley Interdisciplinary Reviews: RNA* **2010**, *1* (1), 117-131.
85. Piatek, M. J.; Werner, A., Endogenous siRNAs: regulators of internal affairs. Portland Press Ltd.: 2014.
 86. Carthew, R. W.; Sontheimer, E. J. J. C., Origins and mechanisms of miRNAs and siRNAs. **2009**, *136* (4), 642-655.
 87. Song, M.-S.; Rossi, J. J. B. J., Molecular mechanisms of Dicer: endonuclease and enzymatic activity. **2017**, *474* (10), 1603-1618.
 88. Ding, S.-W.; Lu, R., Virus-derived siRNAs and piRNAs in immunity and pathogenesis. *Current opinion in virology* **2011**, *1* (6), 533-544.
 89. Mirkovic-Hösle, M.; Förstemann, K. J. P. o., Transposon defense by endo-siRNAs, piRNAs and somatic piRNAs in Drosophila: contributions of Loqs-PD and R2D2. **2014**, *9* (1).
 90. Bernstein, E.; Caudy, A. A.; Hammond, S. M.; Hannon, G. J. J. N., Role for a bidentate ribonuclease in the initiation step of RNA interference. **2001**, *409* (6818), 363-366.
 91. Wang, H.-W.; Noland, C.; Siridechadilok, B.; Taylor, D. W.; Ma, E.; Felderer, K.; Doudna, J. A.; Nogales, E. J. N. s.; biology, m., Structural insights into RNA processing by the human RISC-loading complex. **2009**, *16* (11), 1148.
 92. Noland, C. L.; Ma, E.; Doudna, J. A. J. M. c., siRNA repositioning for guide strand selection by human Dicer complexes. **2011**, *43* (1), 110-121.
 93. Chendrimada, T. P.; Gregory, R. I.; Kumaraswamy, E.; Norman, J.; Cooch, N.; Nishikura, K.; Shiekhattar, R. J. N., TRBP recruits the Dicer complex to Ago2 for microRNA processing and gene silencing. **2005**, *436* (7051), 740-744.
 94. Matranga, C.; Tomari, Y.; Shin, C.; Bartel, D. P.; Zamore, P. D. J. C., Passenger-strand cleavage facilitates assembly of siRNA into Ago2-containing RNAi enzyme complexes. **2005**, *123* (4), 607-620.
 95. Hutvagner, G.; Simard, M. J. J. N. r. M. c. b., Argonaute proteins: key players in RNA silencing. **2008**, *9* (1), 22-32.
 96. Dahlgren, C.; Zhang, H.-Y.; Du, Q.; Grahn, M.; Norstedt, G.; Wahlestedt, C.; Liang, Z. J. N. a. r., Analysis of siRNA specificity on targets with double-nucleotide mismatches. **2008**, *36* (9), e53-e53.
 97. Cruz, C.; Houseley, J. J. E., Endogenous RNA interference is driven by copy number. **2014**, *3*, e01581.
 98. Yao, R.-W.; Wang, Y.; Chen, L.-L. J. N. c. b., Cellular functions of long noncoding RNAs. **2019**, *21* (5), 542-551.
 99. Chen, K.; Zhao, B. S.; He, C. J. C. c. b., Nucleic acid modifications in regulation of gene expression. **2016**, *23* (1), 74-85.
 100. Yue, Y.; Liu, J.; He, C. J. G.; development, RNA N6-methyladenosine methylation in post-transcriptional gene expression regulation. **2015**, *29* (13), 1343-1355.
 101. Fustin, J.-M.; Doi, M.; Yamaguchi, Y.; Hida, H.; Nishimura, S.; Yoshida, M.; Isagawa, T.; Morioka, M. S.; Takeya, H.; Manabe, I. J. C., RNA-methylation-dependent RNA processing controls the speed of the circadian clock. **2013**, *155* (4), 793-806.
 102. Geula, S.; Moshitch-Moshkovitz, S.; Dominissini, D.; Mansour, A. A.; Kol, N.; Salmon-Divon, M.; Hershkovitz, V.; Peer, E.; Mor, N.; Manor, Y. S. J. S., m6A mRNA methylation facilitates resolution of naïve pluripotency toward differentiation. **2015**, *347* (6225), 1002-1006.
 103. Song, J. H.; Yi, C. Q., Chemical Modifications to RNA: A New Layer of Gene Expression Regulation. *Acs Chemical Biology* **2017**, *12* (2), 316-325.
 104. Nachtergaele, S.; He, C., The emerging biology of RNA post-transcriptional modifications. *Rna Biology* **2017**, *14* (2), 156-163.
 105. Li, X.; Zhu, P.; Ma, S.; Song, J.; Bai, J.; Sun, F.; Yi, C. J. N. c. b., Chemical pulldown reveals dynamic pseudouridylation of the mammalian transcriptome. **2015**, *11* (8), 592.
 106. Lu, X.; Han, D.; Zhao, B. S.; Song, C.-X.; Zhang, L.-S.; Doré, L. C.; He, C. J. C. r., Base-resolution maps of 5-formylcytosine and 5-carboxylcytosine reveal genome-wide DNA

- demethylation dynamics. **2015**, 25 (3), 386-389.
107. Huisinga, K. L.; Brower-Toland, B.; Elgin, S. C. J. C., The contradictory definitions of heterochromatin: transcription and silencing. **2006**, 115 (2), 110-122.
108. Suzuki, M. M.; Bird, A., DNA methylation landscapes: provocative insights from epigenomics. *Nature Reviews Genetics* **2008**, 9 (6), 465-476.
109. Moore, L. D.; Le, T.; Fan, G. J. N., DNA methylation and its basic function. **2013**, 38 (1), 23-38.
110. Javaid, N.; Choi, S. J. G., Acetylation-and methylation-related epigenetic proteins in the context of their targets. **2017**, 8 (8), 196.
111. Sterner, D. E.; Berger, S. L. J. M. M. B. R., Acetylation of histones and transcription-related factors. **2000**, 64 (2), 435-459.
112. Chen, K.; Zhao, B.; He, C. A., Nucleic Acid Modifications in Regulation of Gene Expression. *Cell Chemical Biology* **2016**, 23 (1), 74-85.
113. O'Reilly, D.; Kartje, Z. J.; Ageely, E. A.; Malek-Adamian, E.; Habibian, M.; Schofield, A.; Barkau, C. L.; Rohilla, K. J.; DeRossett, L. B.; Weigle, A. T. J. N. a. r., Extensive CRISPR RNA modification reveals chemical compatibility and structure-activity relationships for Cas9 biochemical activity. **2019**, 47 (2), 546-558.
114. Sloan, K. E.; Warda, A. S.; Sharma, S.; Entian, K.-D.; Lafontaine, D. L.; Bohnsack, M. T. J. R. b., Tuning the ribosome: The influence of rRNA modification on eukaryotic ribosome biogenesis and function. **2017**, 14 (9), 1138-1152.
115. Stepanov, G.; Zhuravlev, E.; Shender, V.; Nushtaeva, A.; Balakhonova, E.; Mozhaeva, E.; Kasakin, M.; Koval, V.; Lomzov, A.; Pavlyukov, M. J. G., Nucleotide modifications decrease innate immune response induced by synthetic analogs of snRNAs and snoRNAs. **2018**, 9 (11), 531.
116. Zhao, B. S.; He, C., Pseudouridine in a new era of RNA modifications. *Cell Research* **2015**, 25 (2), 153-154.
117. Charette, M.; Gray, M. W. J. I. I., Pseudouridine in RNA: what, where, how, and why. **2000**, 49 (5), 341-351.
118. Penzo, M.; Montanaro, L. J. B., Turning uridines around: Role of rRNA pseudouridylation in ribosome biogenesis and ribosomal function. **2018**, 8 (2), 38.
119. Motorin, Y.; Helm, M., RNA nucleotide methylation. *Wiley Interdisciplinary Reviews-Rna* **2011**, 2 (5), 611-631.
120. Bachelierie, J. P.; Cavaille, J., Guiding ribose methylation of rRNA. *Trends in Biochemical Sciences* **1997**, 22 (7), 257-261.
121. Decatur, W. A.; Fournier, M. J., rRNA modifications and ribosome function. *Trends in Biochemical Sciences* **2002**, 27 (7), 344-351.
122. Birkedal, U.; Christensen-Dalsgaard, M.; Krogh, N.; Sabarinathan, R.; Gorodkin, J.; Nielsen, H., Profiling of Ribose Methylations in RNA by High-Throughput Sequencing. *Angewandte Chemie-International Edition* **2015**, 54 (2), 451-455.
123. Patra, A.; Paolillo, M.; Charisse, K.; Manoharan, M.; Rozners, E.; Egli, M., 2'-Fluoro RNA Shows Increased Watson-Crick H-Bonding Strength and Stacking Relative to RNA: Evidence from NMR and Thermodynamic Data. *Angewandte Chemie-International Edition* **2012**, 51 (47), 11863-11866.
124. Hacker, G.; Redecke, V.; Hacker, H., Activation of the immune system by bacterial CpG-DNA. *Immunology* **2002**, 105 (3), 245-251.
125. Dalpke, A. H.; Heeg, K., CpG-DNA as immune response modifier. *International Journal of Medical Microbiology* **2004**, 294 (5), 345-354.
126. Wu, J. X.; Chen, Z. J., Innate Immune Sensing and Signaling of Cytosolic Nucleic Acids. In *Annual Review of Immunology, Vol 32*, Littman, D. R.; Yokoyama, W. M., Eds. 2014; Vol. 32, pp 461-488.
127. Majer, O.; Liu, B.; Barton, G. M., Nucleic acid-sensing TLRs: trafficking and regulation.

Current Opinion in Immunology **2017**, *44*, 26-33.

128. Barton, G. M.; Medzhitov, R., Toll-like receptor signaling pathways. *Science* **2003**, *300* (5625), 1524-1525.
129. Kawasaki, T.; Kawai, T., Toll-like receptor signaling pathways. *Frontiers in Immunology* **2014**, *5*.
130. Ori, D.; Murase, M.; Kawai, T. J. I. r. o. i., Cytosolic nucleic acid sensors and innate immune regulation. **2017**, *36* (2), 74-88.
131. Alexopoulou, L.; Holt, A. C.; Medzhitov, R.; Flavell, R. A., Recognition of double-stranded RNA and activation of NF-kappa B by Toll-like receptor 3. *Nature* **2001**, *413* (6857), 732-738.
132. Heil, F.; Hemmi, H.; Hochrein, H.; Ampenberger, F.; Kirschning, C.; Akira, S.; Lipford, G.; Wagner, H.; Bauer, S., Species-specific recognition of single-stranded RNA via toll-like receptor 7 and 8. *Science* **2004**, *303* (5663), 1526-1529.
133. Lund, J. M.; Alexopoulou, L.; Sato, A.; Karow, M.; Adams, N. C.; Gale, N. W.; Iwasaki, A.; Flavell, R. A., Recognition of single-stranded RNA viruses by Toll-like receptor 7. *Proceedings of the National Academy of Sciences of the United States of America* **2004**, *101* (15), 5598-5603.
134. Takeshita, F.; Leifer, C. A.; Gursel, I.; Ishii, K. J.; Takeshita, S.; Gursel, M.; Klinman, D. M., Cutting edge: Role of toll-like receptor 9 in CpG DNA-induced activation of human cells. *Journal of Immunology* **2001**, *167* (7), 3555-3558.
135. Tian, J.; Avalos, A. M.; Mao, S. Y.; Chen, B.; Senthil, K.; Wu, H.; Parroche, P.; Drabic, S.; Golenbock, D.; Sirois, C.; Hua, J.; An, L. L.; Audoly, L.; La Rosa, G.; Bierhaus, A.; Naworth, P.; Marshak-Rothstein, A.; Crow, M. K.; Fitzgerald, K. A.; Latz, E.; Kiener, P. A.; Coyle, A. J., Toll-like receptor 9-dependent activation by DNA-containing immune complexes is mediated by HMGB1 and RAGE. *Nature Immunology* **2007**, *8* (5), 487-496.
136. Leonard, J. N.; Ghirlando, R.; Askins, J.; Bell, J. K.; Margulies, D. H.; Davies, D. R.; Segal, D. M. J. P. o. t. N. A. o. S., The TLR3 signaling complex forms by cooperative receptor dimerization. **2008**, *105* (1), 258-263.
137. Ranjith-Kumar, C.; Miller, W.; Xiong, J.; Russell, W. K.; Lamb, R.; Santos, J.; Duffy, K. E.; Cleveland, L.; Park, M.; Bhardwaj, K. J. J. o. B. C., Biochemical and functional analyses of the human Toll-like receptor 3 ectodomain. **2007**, *282* (10), 7668-7678.
138. Zhang, Z.; Ohto, U.; Shibata, T.; Taoka, M.; Yamauchi, Y.; Sato, R.; Shukla, N. M.; David, S. A.; Isobe, T.; Miyake, K. J. C. r., Structural analyses of Toll-like receptor 7 reveal detailed RNA sequence specificity and recognition mechanism of agonistic ligands. **2018**, *25* (12), 3371-3381. e5.
139. de Marcken, M.; Dhaliwal, K.; Danielsen, A. C.; Gautron, A. S.; Dominguez-Villar, M. J. S. s., TLR7 and TLR8 activate distinct pathways in monocytes during RNA virus infection. **2019**, *12* (605).
140. Heil, F.; Hemmi, H.; Hochrein, H.; Ampenberger, F.; Kirschning, C.; Akira, S.; Lipford, G.; Wagner, H.; Bauer, S. J. S., Species-specific recognition of single-stranded RNA via toll-like receptor 7 and 8. **2004**, *303* (5663), 1526-1529.
141. Latz, E.; Visintin, A.; Espevik, T.; Golenbock, D. T. J. J. o. e. r., Mechanisms of TLR9 activation. **2004**, *10* (6), 406-412.
142. Hornung, V.; Ellegast, J.; Kim, S.; Brzozka, K.; Jung, A.; Kato, H.; Poeck, H.; Akira, S.; Conzelmann, K. K.; Schlee, M.; Endres, S.; Hartmann, G., 5'-triphosphate RNA is the ligand for RIG-I. *Science* **2006**, *314* (5801), 994-997.
143. Kato, H.; Takeuchi, O.; Sato, S.; Yoneyama, M.; Yamamoto, M.; Matsui, K.; Uematsu, S.; Jung, A.; Kawai, T.; Ishii, K. J.; Yamaguchi, O.; Otsu, K.; Tsujimura, T.; Koh, C. S.; Sousa, C. R. E.; Matsuura, Y.; Fujita, T.; Akira, S., Differential roles of MDA5 and RIG-I helicases in the recognition of RNA viruses. *Nature* **2006**, *441* (7089), 101-105.
144. Kawai, T.; Takahashi, K.; Sato, S.; Coban, C.; Kumar, H.; Kato, H.; Ishii, K. J.;

- Takeuchi, O.; Akira, S., IPS-1, an adaptor triggering RIG-I- and Mda5-mediated type I interferon induction. *Nature Immunology* **2005**, *6* (10), 981-988.
145. Pichlmair, A.; Schulz, O.; Tan, C. P.; Naslund, T. I.; Liljestrom, P.; Weber, F.; Sousa, C. R. E., RIG-I-mediated antiviral responses to single-stranded RNA bearing 5'-phosphates. *Science* **2006**, *314* (5801), 997-1001.
146. Yoneyama, M.; Kikuchi, M.; Matsumoto, K.; Imaizumi, T.; Miyagishi, M.; Taira, K.; Foy, E.; Loo, Y. M.; Gale, M.; Akira, S.; Yonehara, S.; Kato, A.; Fujita, T., Shared and unique functions of the DExD/H-box helicases RIG-I, MDA5, and LGP2 in antiviral innate immunity. *Journal of Immunology* **2005**, *175* (5), 2851-2858.
147. Yoneyama, M.; Kikuchi, M.; Natsukawa, T.; Shinobu, N.; Imaizumi, T.; Miyagishi, M.; Taira, K.; Akira, S.; Fujita, T., The RNA helicase RIG-I has an essential function in double-stranded RNA-induced innate antiviral responses. *Nature Immunology* **2004**, *5* (7), 730-737.
148. Loo, Y.-M.; Gale Jr, M. J. I., Immune signaling by RIG-I-like receptors. **2011**, *34* (5), 680-692.
149. Ablasser, A.; Bauernfeind, F.; Hartmann, G.; Latz, E.; Fitzgerald, K. A.; Hornung, V. J. N. i., RIG-I-dependent sensing of poly (dA: dT) through the induction of an RNA polymerase III-transcribed RNA intermediate. **2009**, *10* (10), 1065-1072.
150. Junior, A. G. D.; Sampaio, N. G.; Rehwinkel, J. J. T. i. m., A balancing act: MDA5 in antiviral immunity and autoinflammation. **2019**, *27* (1), 75-85.
151. Reikine, S.; Nguyen, J. B.; Modis, Y. J. F. i. i., Pattern recognition and signaling mechanisms of RIG-I and MDA5. **2014**, *5*, 342.
152. Kato, H.; Takeuchi, O.; Mikamo-Satoh, E.; Hirai, R.; Kawai, T.; Matsushita, K.; Hiiragi, A.; Dermody, T. S.; Fujita, T.; Akira, S. J. T. J. o. e. m., Length-dependent recognition of double-stranded ribonucleic acids by retinoic acid-inducible gene-I and melanoma differentiation-associated gene 5. **2008**, *205* (7), 1601-1610.
153. Pichlmair, A.; Schulz, O.; Tan, C.-P.; Rehwinkel, J.; Kato, H.; Takeuchi, O.; Akira, S.; Way, M.; Schiavo, G.; e Sousa, C. R. J. J. o. v., Activation of MDA5 requires higher-order RNA structures generated during virus infection. **2009**, *83* (20), 10761-10769.
154. Saito, T.; Hirai, R.; Loo, Y.-M.; Owen, D.; Johnson, C. L.; Sinha, S. C.; Akira, S.; Fujita, T.; Gale, M. J. P. o. t. N. A. o. S., Regulation of innate antiviral defenses through a shared repressor domain in RIG-I and LGP2. **2007**, *104* (2), 582-587.
155. Satoh, T.; Kato, H.; Kumagai, Y.; Yoneyama, M.; Sato, S.; Matsushita, K.; Tsujimura, T.; Fujita, T.; Akira, S.; Takeuchi, O. J. P. o. t. N. A. o. S., LGP2 is a positive regulator of RIG-I- and MDA5-mediated antiviral responses. **2010**, *107* (4), 1512-1517.
156. Rothenfusser, S.; Goutagny, N.; DiPerna, G.; Gong, M.; Monks, B. G.; Schoenemeyer, A.; Yamamoto, M.; Akira, S.; Fitzgerald, K. A. J. T. J. o. I., The RNA helicase Lgp2 inhibits TLR-independent sensing of viral replication by retinoic acid-inducible gene-I. **2005**, *175* (8), 5260-5268.
157. Motwani, M.; Pesiridis, S.; Fitzgerald, K. A. J. N. R. G., DNA sensing by the cGAS-STING pathway in health and disease. **2019**, *20* (11), 657-674.
158. Nakhaei, P.; Hiscott, J.; Lin, R. T., STING-ing the Antiviral Pathway. *Journal of Molecular Cell Biology* **2010**, *2* (3), 110-112.
159. Zevini, A.; Olganier, D.; Hiscott, J. J. T. i. i., Crosstalk between cytoplasmic RIG-I and STING sensing pathways. **2017**, *38* (3), 194-205.
160. Tan, R. S.; Ho, B.; Leung, B. P.; Ding, J. L. J. I. r. o. i., TLR cross-talk confers specificity to innate immunity. **2014**, *33* (6), 443-453.
161. Palazzo, M.; Gariboldi, S.; Zanobbio, L.; Dusio, G. F.; Selleri, S.; Bedoni, M.; Balsari, A.; Rumio, C. J. I. i., Cross-talk among Toll-like receptors and their ligands. **2008**, *20* (5), 709-718.
162. Kawai, T.; Akira, S. J. I., Toll-like receptors and their crosstalk with other innate receptors in infection and immunity. **2011**, *34* (5), 637-650.

163. Paterson, B. M.; Roberts, B. E.; Kuff, E. L., Structural gene identification and mapping by DNA-mRNA hybrid-arrested cell-free translation. *Proceedings of the National Academy of Sciences* **1977**, *74* (10), 4370.
164. Geary, R. S.; Norris, D.; Yu, R.; Bennett, C. F., Pharmacokinetics, biodistribution and cell uptake of antisense oligonucleotides. *Advanced Drug Delivery Reviews* **2015**, *87*, 46-51.
165. Rinaldi, C.; Wood, M. J. A., Antisense oligonucleotides: the next frontier for treatment of neurological disorders. *Nature Reviews Neurology* **2018**, *14* (1), 9-21.
166. Uhlmann, E.; Peyman, A., Antisense oligonucleotides - a new therapeutic principle. *Chemical Reviews* **1990**, *90* (4), 543-584.
167. Chan, J. H. P.; Lim, S. H.; Wong, W. S. F., Antisense oligonucleotides: From design to therapeutic application. *Clinical and Experimental Pharmacology and Physiology* **2006**, *33* (5-6), 533-540.
168. Crooke, S. T., Molecular mechanisms of action of antisense drugs. *Biochimica Et Biophysica Acta-Genes Structure and Expression* **1999**, *1489* (1), 31-44.
169. Xie, S. Y.; Li, W.; Ren, Z. R.; Huang, S. Z.; Zeng, F. Y.; Zeng, Y. T., Correction of beta(654)-thalassaemia mice using direct intravenous injection of siRNA and antisense RNA vectors. *International Journal of Hematology* **2011**, *93* (3), 301-310.
170. Hua, Y. M.; Sahashi, K.; Hung, G. N.; Rigo, F.; Passini, M. A.; Bennett, C. F.; Krainer, A. R., Antisense correction of SMN2 splicing in the CNS rescues necrosis in a type III SMA mouse model. *Genes & Development* **2010**, *24* (15), 1634-1644.
171. Passini, M. A.; Bu, J.; Richards, A. M.; Kinnecom, C.; Sardi, S. P.; Stanek, L. M.; Hua, Y. M.; Rigo, F.; Matson, J.; Hung, G.; Kaye, E. M.; Shihabuddin, L. S.; Krainer, A. R.; Bennett, C. F.; Cheng, S. H., Antisense Oligonucleotides Delivered to the Mouse CNS Ameliorate Symptoms of Severe Spinal Muscular Atrophy. *Science Translational Medicine* **2011**, *3* (72).
172. Lu, Q. L.; Rabinowitz, A.; Chen, Y. C.; Yokota, T.; Yin, H. F.; Alter, J.; Jadoon, A.; Bou-Gharios, G.; Partridge, T., Systemic delivery of antisense oligoribonucleotide restores dystrophin expression in body-wide skeletal muscles. *Proceedings of the National Academy of Sciences of the United States of America* **2005**, *102* (1), 198-203.
173. Baker, B. F.; Miraglia, L.; Hagedorn, C. H., Modulation of eukaryotic initiation factor-4e binding to 5'-capped oligoribonucleotides by modified antisense oligonucleotides. *Journal of Biological Chemistry* **1992**, *267* (16), 11495-11499.
174. Vickers, T. A.; Crooke, S. T., The rates of the major steps in the molecular mechanism of RNase H1-dependent antisense oligonucleotide induced degradation of RNA. *Nucleic Acids Research* **2015**, *43* (18), 8955-8963.
175. Anderson, K. P.; Fox, M. C.; BrownDriver, V.; Martin, M. J.; Azad, R. F., Inhibition of human cytomegalovirus immediate-early gene expression by an antisense oligonucleotide complementary to immediate-early RNA. *Antimicrobial Agents and Chemotherapy* **1996**, *40* (9), 2004-2011.
176. Belfort, R.; Goldstein, D. A.; Johnson, D. W.; Mansour, S. E.; Muccioli, C.; Sheppard, J. D.; Mora-Durate, J.; Chan, C. K.; Palestine, A. G.; Perez, J. E.; Cornish, M. J.; Holland, G. N.; Ransome, S. S.; Tufail, A.; Weisz, J. M.; Davis, M. D.; Hubbard, L. D.; Armstrong, J.; Hurlburt, D.; Vanderhoof-Young, M.; Crooke, S. T.; Kisner, D. L.; Chandler, J. W.; Frost, K. R.; Hutcherson, S. L.; Whitley, R. J.; Chandler, J. W.; Grillone, L. R.; Holland, G. N.; Hutcherson, S. L.; Lanz, R.; Vitravene Study, G., A randomized controlled clinical trial of intravitreal fomivirsen for treatment of newly diagnosed peripheral cytomegalovirus retinitis in patients with AIDS. *American Journal of Ophthalmology* **2002**, *133* (4), 467-474.
177. Raal, F. J.; Santos, R. D.; Blom, D. J.; Marais, A. D.; Charng, M. J.; Cromwell, W. C.; Lachmann, R. H.; Gaudet, D.; Tan, J. L.; Chasan-Taber, S.; Tribble, D. L.; Flaim, J. D.; Crooke, S. T., Mipomersen, an apolipoprotein B synthesis inhibitor, for lowering of LDL cholesterol concentrations in patients with homozygous familial hypercholesterolaemia: a randomised, double-blind, placebo-controlled trial. *Lancet* **2010**, *375* (9719), 998-1006.

178. Thomas, G. S.; Cromwell, W. C.; Ali, S.; Chin, W.; Flaim, J. D.; Davidson, M., Mipomersen, an Apolipoprotein B Synthesis Inhibitor, Reduces Atherogenic Lipoproteins in Patients With Severe Hypercholesterolemia at High Cardiovascular Risk. *Journal of the American College of Cardiology* **2013**, *62* (23), 2178-2184.
179. Stein, C. A.; Castanotto, D., FDA-Approved Oligonucleotide Therapies in 2017. *Molecular Therapy* **2017**, *25* (5), 1069-1075.
180. Richardson, P. G.; Soiffer, R. J.; Antin, J. H.; Uno, H.; Jin, Z. Z.; Kurtzberg, J.; Martin, P. L.; Steinbach, G.; Murray, K. F.; Vogelsang, G. B.; Chen, A. R.; Krishnan, A.; Kernan, N. A.; Avigan, D. E.; Spitzer, T. R.; Shulman, H. M.; Di Salvo, D. N.; Revta, C.; Warren, D.; Momtaz, P.; Bradwin, G.; Wei, L. J.; Iacobelli, M.; McDonald, G. B.; Guinan, E. C., Defibrotide for the Treatment of Severe Hepatic Veno-Occlusive Disease and Multiorgan Failure after Stem Cell Transplantation: A Multicenter, Randomized, Dose-Finding Trial. *Biology of Blood and Marrow Transplantation* **2010**, *16* (7), 1005-1017.
181. Lim, K. R. Q.; Maruyama, R.; Yokota, T., Eteplirsen in the treatment of Duchenne muscular dystrophy. *Drug Design Development and Therapy* **2017**, *11*, 533-545.
182. Wurster, C. D.; Ludolph, A. C., Nusinersen for spinal muscular atrophy. *Therapeutic Advances in Neurological Disorders* **2018**, *11*.
183. Agarwal, S.; Habtemariam, B. H.; Goel, V.; Attarwala, H.; Melch, M.; Jiang, X.; Simon, A.; Robbie, G., Pharmacokinetics and pharmacodynamics of givosiran, an investigational RNAi therapeutic for acute intermittent porphyria. *Clinical Pharmacology & Therapeutics* **2019**, *105*, S34-S34.
184. Baker, H., Givosiran for acute intermittent porphyria. *Lancet Gastroenterology & Hepatology* **2019**, *4* (4), 265-265.
185. Zhang, X. P.; Goel, V.; Robbie, G. J., Pharmacokinetics of Patisiran, the First Approved RNA Interference Therapy in Patients With Hereditary Transthyretin-Mediated Amyloidosis. *Journal of Clinical Pharmacology*.
186. Zhang, X. P.; Goel, V.; Attarwala, H.; Sweetser, M. T.; Clausen, V. A.; Robbie, G. J., Patisiran Pharmacokinetics, Pharmacodynamics, and Exposure-Response Analyses in the Phase 3 APOLLO Trial in Patients With Hereditary Transthyretin-Mediated (hATTR) Amyloidosis. *Journal of Clinical Pharmacology*.
187. Setten, R. L.; Rossi, J. J.; Han, S. P., The current state and future directions of RNAi-based therapeutics. *Nature Reviews Drug Discovery* **2019**, *18* (6), 421-446.
188. Paddison, P. J.; Caudy, A. A.; Bernstein, E.; Hannon, G. J.; Conklin, D. S. J. G.; development, Short hairpin RNAs (shRNAs) induce sequence-specific silencing in mammalian cells. **2002**, *16* (8), 948-958.
189. Brummelkamp, T. R.; Bernards, R.; Agami, R. J. s., A system for stable expression of short interfering RNAs in mammalian cells. **2002**, *296* (5567), 550-553.
190. Rupaimoole, R.; Slack, F. J. J. N. r. D. d., MicroRNA therapeutics: towards a new era for the management of cancer and other diseases. **2017**, *16* (3), 203.
191. Janssen, H. L.; Reesink, H. W.; Lawitz, E. J.; Zeuzem, S.; Rodriguez-Torres, M.; Patel, K.; van der Meer, A. J.; Patick, A. K.; Chen, A.; Zhou, Y. J. N. E. J. o. M., Treatment of HCV infection by targeting microRNA. **2013**, *368* (18), 1685-1694.
192. Bracken, C. P.; Scott, H. S.; Goodall, G. J. J. N. R. G., A network-biology perspective of microRNA function and dysfunction in cancer. **2016**, *17* (12), 719.
193. Iorio, M. V.; Croce, C. M. J. E. m. m., MicroRNA dysregulation in cancer: diagnostics, monitoring and therapeutics. A comprehensive review. **2012**, *4* (3), 143-159.
194. Li, Q.; Lowey, B.; Sodroski, C.; Krishnamurthy, S.; Alao, H.; Cha, H.; Chiu, S.; El-Diwany, R.; Ghany, M. G.; Liang, T. J. J. N. c., Cellular microRNA networks regulate host dependency of hepatitis C virus infection. **2017**, *8* (1), 1-16.
195. Krützfeldt, J.; Rajewsky, N.; Braich, R.; Rajeev, K. G.; Tuschl, T.; Manoharan, M.; Stoffel, M. J. n., Silencing of microRNAs in vivo with 'antagomirs'. **2005**, *438* (7068), 685-689.

196. Jopling, C. L.; Yi, M.; Lancaster, A. M.; Lemon, S. M.; Sarnow, P. J. s., Modulation of hepatitis C virus RNA abundance by a liver-specific MicroRNA. **2005**, *309* (5740), 1577-1581.
197. Sharma, V. K.; Sharma, R. K.; Singh, S. K., Antisense oligonucleotides: modifications and clinical trials. *Medchemcomm* **2014**, *5* (10), 1454-1471.
198. Kole, R.; Krainer, A. R.; Altman, S., RNA therapeutics: beyond RNA interference and antisense oligonucleotides. *Nature Reviews Drug Discovery* **2012**, *11* (2), 125-140.
199. Moreno, P. M. D.; Pego, A. P., Therapeutic antisense oligonucleotides against cancer: hurdling to the clinic. *Frontiers in Chemistry* **2014**, *2*.
200. Ozpolat, B.; Sood, A. K.; Lopez-Berestein, G., Nanomedicine based approaches for the delivery of siRNA in cancer. *Journal of Internal Medicine* **2010**, *267* (1), 44-53.
201. Mukalel, A. J.; Riley, R. S.; Zhang, R.; Mitchell, M. J., Nanoparticles for nucleic acid delivery: Applications in cancer immunotherapy. *Cancer Letters* **2019**, *458*, 102-112.
202. Xiao, Y.; Shi, K.; Qu, Y.; Chu, B. Y.; Qian, Z. Y., Engineering Nanoparticles for Targeted Delivery of Nucleic Acid Therapeutics in Tumor. *Molecular Therapy-Methods & Clinical Development* **2019**, *12*, 1-18.
203. Sharma, A. K.; Gupta, L.; Gupta, U., Nanoparticles as nucleic acid delivery vectors. In *Advances in Nanomedicine for the Delivery of Therapeutic Nucleic Acids*, Nimesh, S.; Chandra, R.; Gupta, N., Eds. 2017; pp 13-42.
204. Jayasena, S. D., Aptamers: An emerging class of molecules that rival antibodies in diagnostics. *Clinical Chemistry* **1999**, *45* (9), 1628-1650.
205. Stoltenburg, R.; Reinemann, C.; Strehlitz, B., SELEX-A (r)evolutionary method to generate high-affinity nucleic acid ligands. *Biomolecular Engineering* **2007**, *24* (4), 381-403.
206. Wilson, D. S.; Szostak, J. W., In vitro selection of functional nucleic acids. *Annual Review of Biochemistry* **1999**, *68*, 611-647.
207. Keefe, A. D.; Pai, S.; Ellington, A., Aptamers as therapeutics. *Nature Reviews Drug Discovery* **2010**, *9* (7), 537-550.
208. Nimjee, S. M.; White, R. R.; Becker, R. C.; Sullenger, B. A., Aptamers as Therapeutics. In *Annual Review of Pharmacology and Toxicology, Vol 57*, Insel, P. A., Ed. 2017; Vol. 57, pp 61-79.
209. Tsumoto, K.; Isozaki, Y.; Yagami, H.; Tomita, M. J. I., Future perspectives of therapeutic monoclonal antibodies. **2019**, *11* (2), 119-127.
210. Yan, A. C.; Levy, M. J. n. a. t., Aptamer-mediated delivery and cell-targeting aptamers: room for improvement. **2018**, *28* (3), 194-199.
211. Cerchia, L.; De Franciscis, V. J. T. i. b., Targeting cancer cells with nucleic acid aptamers. **2010**, *28* (10), 517-525.
212. Bouchelouche, K.; Choyke, P. L.; Capala, J. J. D. m., Prostate specific membrane antigen—a target for imaging and therapy with radionuclides. **2010**, *9* (44), 55.
213. Lupold, S. E.; Hicke, B. J.; Lin, Y.; Coffey, D. S., Identification and characterization of nuclease-stabilized RNA molecules that bind human prostate cancer cells via the prostate-specific membrane antigen. *Cancer Research* **2002**, *62* (14), 4029-4033.
214. Dassie, J. P.; Hernandez, L. I.; Thomas, G. S.; Long, M. E.; Rockey, W. M.; Howell, C. A.; Chen, Y. N.; Hernandez, F. J.; Liu, X. Y.; Wilson, M. E.; Allen, L. A.; Vaena, D. A.; Meyerhoff, D. K.; Giangrande, P. H., Targeted Inhibition of Prostate Cancer Metastases with an RNA Aptamer to Prostate-specific Membrane Antigen. *Molecular Therapy* **2014**, *22* (11), 1910-1922.
215. Chu, T. C.; Marks, J. W.; Lavery, L. A.; Faulkner, S.; Rosenblum, M. G.; Ellington, A. D.; Levy, M., Aptamer : toxin conjugates that specifically target prostate tumor cells. *Cancer Research* **2006**, *66* (12), 5989-5992.
216. Bagalkot, V.; Farokhzad, O. C.; Langer, R.; Jon, S., An aptamer-doxorubicin physical conjugate as a novel targeted drug-delivery platform. *Angewandte Chemie-International Edition* **2006**, *45* (48), 8149-8152.

217. Bagalkot, V.; Zhang, L.; Levy-Nissenbaum, E.; Jon, S.; Kantoff, P. W.; Langer, R.; Farokhzad, O. C., Quantum dot - Aptamer conjugates for synchronous cancer imaging, therapy, and sensing of drug delivery based on Bi-fluorescence resonance energy transfer. *Nano Letters* **2007**, *7* (10), 3065-3070.
218. Wang, A. Z.; Bagalkot, V.; Vasilliou, C. C.; Gu, F.; Alexis, F.; Zhang, L.; Shaikh, M.; Yuet, K.; Cima, M. J.; Langer, R.; Kantoff, P. W.; Bander, N. H.; Jon, S. Y.; Farokhzad, O. C., Superparamagnetic iron oxide nanoparticle-aptamer bioconjugates for combined prostate cancer imaging and therapy. *Chemmedchem* **2008**, *3* (9), 1311-1315.
219. Farokhzad, O. C.; Cheng, J. J.; Tepy, B. A.; Sherifi, I.; Jon, S.; Kantoff, P. W.; Richie, J. P.; Langer, R., Targeted nanoparticle-aptamer bioconjugates for cancer chemotherapy in vivo. *Proceedings of the National Academy of Sciences of the United States of America* **2006**, *103* (16), 6315-6320.
220. Rusconi, C. P.; Scardino, E.; Layzer, J.; Pitoc, G. A.; Ortel, T. L.; Monroe, D.; Sullenger, B. A., RNA aptamers as reversible antagonists of coagulation factor IXa. *Nature* **2002**, *419* (6902), 90-94.
221. Dyke, C. K.; Steinhubl, S. R.; Kleiman, N. S.; Cannon, R. O.; Aberle, L. G.; Lin, M.; Myles, S. K.; Melloni, C.; Harrington, R. A.; Alexander, J. H.; Becker, R. C.; Rusconi, C. P., First-in-human experience of an antidote-controlled anticoagulant using RNA aptamer technology - A phase 1a pharmacodynamic evaluation of a drug-antidote pair for the controlled regulation of factor IXa activity. *Circulation* **2006**, *114* (23), 2490-2497.
222. Cohen, M. G.; Purdy, D. A.; Rossi, J. S.; Grinfeld, L. R.; Myles, S. K.; Aberle, L. H.; Greenbaum, A. B.; Fry, E.; Chan, M. Y.; Tonkens, R. M.; Zelenkofske, S.; Alexander, J. H.; Harrington, R. A.; Rusconi, C. P.; Becker, R. C., First Clinical Application of an Actively Reversible Direct Factor IXa Inhibitor as an Anticoagulation Strategy in Patients Undergoing Percutaneous Coronary Intervention. *Circulation* **2010**, *122* (6), 614-622.
223. Bock, L. C.; Griffin, L. C.; Latham, J. A.; Vermaas, E. H.; Toole, J. J., Selection of single-stranded-dna molecules that bind and inhibit human thrombin. *Nature* **1992**, *355* (6360), 564-566.
224. Huang, R. H.; Fremont, D. H.; Diener, J. L.; Schaub, R. G.; Sadler, J. E., A Structural Explanation for the Antithrombotic Activity of ARC1172, a DNA Aptamer that Binds von Willebrand Factor Domain A1. *Structure* **2009**, *17* (11), 1476-1484.
225. Rusconi, C. P.; Roberts, J. D.; Pitoc, G. A.; Nimjee, S. M.; White, R. R.; Quick, G.; Scardino, E.; Fay, W. P.; Sullenger, B. A., Antidote-mediated control of an anticoagulant aptamer in vivo. *Nature Biotechnology* **2004**, *22* (11), 1423-1428.
226. Nimjee, S. M.; Keys, J. R.; Pitoc, G. A.; Quick, G.; Rusconi, C. P.; Sullenger, B. A., A novel antidote-controlled anticoagulant reduces thrombin generation and inflammation and improves cardiac function in cardiopulmonary bypass surgery. *Molecular Therapy* **2006**, *14* (3), 408-415.
227. Akira, S.; Uematsu, S.; Takeuchi, O., Pathogen recognition and innate immunity. *Cell* **2006**, *124* (4), 783-801.
228. Bodera, P.; Stankiewicz, W.; Kocik, J., Synthetic immunostimulatory oligonucleotides in experimental and clinical practice. *Pharmacological Reports* **2012**, *64* (5), 1003-1010.
229. Diebold, S. S.; Kaisho, T.; Hemmi, H.; Akira, S.; Sousa, C. R. E., Innate antiviral responses by means of TLR7-mediated recognition of single-stranded RNA. *Science* **2004**, *303* (5663), 1529-1531.
230. Decker, T.; Schneller, F.; Sparwasser, T.; Tretter, T.; Lipford, G. B.; Wagner, H.; Peschel, C., Immunostimulatory CpG-oligonucleotides cause proliferation, cytokine production, and an immunogenic phenotype in chronic lymphocytic leukemia B cells. *Blood* **2000**, *95* (3), 999-1006.
231. Dilioglou, S.; Cruse, J. M.; Lewis, R. E. J. E.; pathology, m., Function of CD80 and CD86 on monocyte-and stem cell-derived dendritic cells. **2003**, *75* (3), 217-227.

232. Giraldo, D. M.; Hernandez, J. C.; Inchima, S. U. J. I., Impact of in vitro costimulation with TLR2, TLR4 and TLR9 agonists and HIV-1 on antigen-presenting cell activation. **2015**, *58* (2), 122-129.
233. Ferlazzo, G.; Münz, C. J. J. o. c. i., Dendritic cell interactions with NK cells from different tissues. **2009**, *29* (3), 265-273.
234. Ferlazzo, G.; Morandi, B. J. F. i. i., Cross-talks between natural killer cells and distinct subsets of dendritic cells. **2014**, *5*, 159.
235. Lim, T. S.; Mortellaro, A.; Lim, C. T.; Hämmerling, G. J.; Ricciardi-Castagnoli, P. J. T. J. o. I., Mechanical interactions between dendritic cells and T cells correlate with T cell responsiveness. **2011**, *187* (1), 258-265.
236. Bourquin, C.; Schmidt, L.; Lanz, A. L.; Storch, B.; Wurzenberger, C.; Anz, D.; Sandholzer, N.; Mocikat, R.; Berger, M.; Poeck, H.; Hartmann, G.; Hornung, V.; Endres, S., Immunostimulatory RNA Oligonucleotides Induce an Effective Antitumoral NK Cell Response through the TLR7. *Journal of Immunology* **2009**, *183* (10), 6078-6086.
237. Poeck, H.; Besch, R.; Maihoefer, C.; Renn, M.; Tormo, D.; Morskaya, S. S.; Kirschnek, S.; Gaffal, E.; Landsberg, J.; Hellmuth, J.; Schmidt, A.; Anz, D.; Bscheider, M.; Schwerd, T.; Berking, C.; Bourquin, C.; Kalinke, U.; Kremmer, E.; Kato, H.; Akira, S.; Meyers, R.; Hacker, G.; Neuenhahn, M.; Busch, D.; Ruland, J.; Rothenfusser, S.; Prinz, M.; Hornung, V.; Endres, S.; Tuting, T.; Hartmann, G., 5'-triphosphate-siRNA: turning gene silencing and Rig-I activation against melanoma. *Nature Medicine* **2008**, *14* (11), 1256-1263.
238. Jahrsdorfer, B.; Hartmann, G.; Racila, E.; Jackson, W.; Muhlenhoff, L.; Meinhardt, G.; Endres, S.; Link, B. K.; Krieg, A. M.; Weiner, G. J., CpG DNA increases primary malignant B cell expression of costimulatory molecules and target antigens. *Journal of Leukocyte Biology* **2001**, *69* (1), 81-88.
239. Wooldridge, J. E.; Ballas, Z.; Krieg, A. M.; Weiner, G. J., Immunostimulatory oligodeoxynucleotides containing CpG motifs enhance the efficacy of monoclonal antibody therapy of lymphoma. *Blood* **1997**, *89* (8), 2994-2998.
240. Leonard, J. R.; Link, B. K.; Emmanouilides, C.; Gregory, S. A.; Weisdorf, D.; Andrey, J.; Hainsworth, J.; Sparano, J. A.; Tsai, D. E.; Horning, S.; Krieg, A. M.; Weiner, G. J., Phase I trial of toll-like receptor 9 agonist PF-3512676 with and following rituximab in patients with recurrent indolent and aggressive non-hodgkin's lymphoma. *Clinical Cancer Research* **2007**, *13* (20), 6168-6174.
241. Friedberg, J. W.; Kim, H.; McCauley, M.; Hessel, E. M.; Sims, P.; Fisher, D. C.; Nadler, L. M.; Coffman, R. L.; Freedman, A. S., Combination immunotherapy with a CpG oligonucleotide (1018 ISS) and rituximab in patients with non-Hodgkin lymphoma: increased interferon-alpha/beta-inducible gene expression, without significant toxicity. *Blood* **2005**, *105* (2), 489-495.
242. Weeratna, R. D.; Bourne, L. L.; Sullivan, S. M.; Davis, H. L.; Krieg, A. M., Combination of a new TLR9 agonist immunomodulator (CpG 7909) and paclitaxel for treatment of metastatic Lewis Lung Carcinoma (LLC). *Journal of Clinical Oncology* **2004**, *22* (14), 702S-702S.
243. Manegold, C.; van Zandwijk, N.; Szczesna, A.; Zatloukal, P.; Au, J. S. K.; Blasinska-Morawiec, M.; Serwatowski, P.; Krzakowski, M.; Jassem, J.; Tan, E. H.; Benner, R. J.; Ingrosso, A.; Meech, S. J.; Readett, D.; Thatcher, N., A phase III randomized study of gemcitabine and cisplatin with or without PF-3512676 (TLR9 agonist) as first-line treatment of advanced non-small-cell lung cancer. *Annals of Oncology* **2012**, *23* (1), 72-77.
244. Manegold, C.; Gravenor, D.; Woytowicz, D.; Mezger, J.; Hirsh, V.; Albert, G.; Al-Adhami, M.; Readett, D.; Krieg, A. M.; Leichman, C. G., Randomized phase II trial of a toll-like receptor 9 agonist oligodeoxynucleotide, PF-3512676, in combination with first-line taxane plus platinum chemotherapy for advanced-stage non-small-cell lung cancer. *Journal of Clinical Oncology* **2008**, *26* (24), 3979-3986.
245. Manegold, C.; Thatcher, N.; Benner, R. J.; Readett, D.; van Zandwijk, N., Randomized

- phase III trial of gemcitabine/cisplatin with or without PF-3512676 as first line treatment of advanced non-small cell lung cancer (NSCLC). *Journal of Clinical Oncology* **2008**, *26* (15).
246. Speiser, D. E.; Lienard, D.; Rufer, N.; Rubio-Godoy, V.; Rimoldi, D.; Lejeune, F.; Krieg, A. M.; Cerottini, J. C.; Romero, P., Rapid and strong human CD8(+) T cell responses to vaccination with peptide, IFA, and CpG oligodeoxynucleotide 7909. *Journal of Clinical Investigation* **2005**, *115* (3), 739-746.
247. Appay, V.; Jandus, C.; Voelter, V.; Reynard, S.; Coupland, S. E.; Rimoldi, D.; Lienard, D.; Guillaume, P.; Krieg, A. M.; Cerottini, J. C.; Romero, P.; Leyvraz, S.; Rufer, N.; Speiser, D. E., New generation vaccine induces effective melanoma-specific CD8(+) T cells in the circulation but not in the tumor site. *Journal of Immunology* **2006**, *177* (3), 1670-1678.
248. Jin, J. O.; Kim, H.; Huh, Y. H.; Herrmann, A.; Kwak, M., Soft matter DNA nanoparticles hybridized with CpG motifs and peptide nucleic acids enable immunological treatment of cancer. *Journal of Controlled Release* **2019**, *315*, 76-84.
249. Givens, B. E.; Geary, S. M.; Salem, A. K., Nanoparticle-based CpG-oligonucleotide therapy for treating allergic asthma. *Immunotherapy* **2018**, *10* (7), 595-604.
250. Radovic-Moreno, A. F.; Chernyak, N.; Mader, C. C.; Nallagatla, S.; Kang, R. S.; Hao, L. L.; Walker, D. A.; Halo, T. L.; Merkel, T. J.; Rische, C. H.; Anantatmula, S.; Burkhart, M.; Mirkin, C. A.; Gryaznov, S. M., Immunomodulatory spherical nucleic acids. *Proceedings of the National Academy of Sciences of the United States of America* **2015**, *112* (13), 3892-3897.
251. Guo, P. X., The emerging field of RNA nanotechnology. *Nature Nanotechnology* **2010**, *5* (12), 833-842.
252. Kallenbach, N. R.; Ma, R. I.; Seeman, N. C., An immobile nucleic-acid junction constructed from oligonucleotides. *Nature* **1983**, *305* (5937), 829-831.
253. Seeman, N. C., NUCLEIC-ACID JUNCTIONS AND LATTICES. *Journal of Theoretical Biology* **1982**, *99* (2), 237-247.
254. Winfree, E.; Liu, F. R.; Wenzler, L. A.; Seeman, N. C., Design and self-assembly of two-dimensional DNA crystals. *Nature* **1998**, *394* (6693), 539-544.
255. Reif, J. H., The design of autonomous DNA nano-mechanical devices: Walking and rolling DNA. *Natural Computing* **2003**, *2* (4), 439.
256. Chen, Y.; Wang, M. S.; Mao, C. D., An autonomous DNA nanomotor powered by a DNA enzyme. *Angewandte Chemie-International Edition* **2004**, *43* (27), 3554-3557.
257. Shin, J. S.; Pierce, N. A., A synthetic DNA walker for molecular transport. *Journal of the American Chemical Society* **2004**, *126* (35), 10834-10835.
258. Mao, C. D.; LaBean, T. H.; Reif, J. H.; Seeman, N. C., Logical computation using algorithmic self-assembly of DNA triple-crossover molecules. *Nature* **2000**, *407* (6803), 493-496.
259. Adleman, L. M., MOLECULAR COMPUTATION OF SOLUTIONS TO COMBINATORIAL PROBLEMS. *Science* **1994**, *266* (5187), 1021-1024.
260. Rothmund, P. W. K., Folding DNA to create nanoscale shapes and patterns. *Nature* **2006**, *440* (7082), 297-302.
261. Shih, W. M.; Quispe, J. D.; Joyce, G. F., A 1.7-kilobase single-stranded DNA that folds into a nanoscale octahedron. *Nature* **2004**, *427* (6975), 618-621.
262. Westhof, E.; Masquida, B.; Jaeger, L., RNA tectonics: Towards RNA design. *Folding & Design* **1996**, *1* (4), R78-R88.
263. Ishikawa, J.; Furuta, H.; Ikawa, Y. J. W. I. R. R., RNA tectonics (tectoRNA) for RNA nanostructure design and its application in synthetic biology. **2013**, *4* (6), 651-664.
264. Seeman, N. C.; Sleiman, H. F. J. N. R. M., DNA nanotechnology. **2017**, *3* (1), 1-23.
265. Yang, Y.; Han, D.; Nangreave, J.; Liu, Y.; Yan, H. J. A. n., DNA origami with double-stranded DNA as a unified scaffold. **2012**, *6* (9), 8209-8215.
266. Wei, B.; Dai, M.; Yin, P., Complex shapes self-assembled from single-stranded DNA tiles. *Nature* **2012**, *485* (7400), 623-626.
267. Marchi, A. N.; Saaem, I.; Tian, J. D.; LaBean, T. H., One-Pot Assembly of a Hetero-

- dimeric DNA Origami from Chip-Derived Staples and Double-Stranded Scaffold. *Acs Nano* **2013**, *7* (2), 903-910.
268. Douglas, S. M.; Dietz, H.; Liedl, T.; Hogberg, B.; Graf, F.; Shih, W. M., Self-assembly of DNA into nanoscale three-dimensional shapes. *Nature* **2009**, *459* (7245), 414-418.
269. Ke, Y. G.; Sharma, J.; Liu, M. H.; Jahn, K.; Liu, Y.; Yan, H., Scaffolded DNA Origami of a DNA Tetrahedron Molecular Container. *Nano Letters* **2009**, *9* (6), 2445-2447.
270. Endo, M.; Hidaka, K.; Kato, T.; Namba, K.; Sugiyama, H., DNA Prism Structures Constructed by Folding of Multiple Rectangular Arms. *Journal of the American Chemical Society* **2009**, *131* (43), 15570-+.
271. Benson, E.; Mohammed, A.; Gardell, J.; Masich, S.; Czeizler, E.; Orponen, P.; Hogberg, B., DNA rendering of polyhedral meshes at the nanoscale. *Nature* **2015**, *523* (7561), 441-U139.
272. Shi, J.; Bergstrom, D. E. J. A. C. I. E. i. E., Assembly of novel DNA cycles with rigid tetrahedral linkers. **1997**, *36* (1-2), 111-113.
273. Aldaye, F. A.; Sleiman, H. F. J. A. C. I. E., Sequential self-assembly of a DNA hexagon as a template for the organization of gold nanoparticles. **2006**, *45* (14), 2204-2209.
274. Vargas-Baca, I.; Mitra, D.; Zulyniak, H. J.; Banerjee, J.; Sleiman, H. F. J. A. C. I. E., Solid-phase synthesis of transition metal linked, branched oligonucleotides. **2001**, *40* (24), 4629-4632.
275. Raschle, T.; Lin, C.; Jungmann, R.; Shih, W. M.; Wagner, G. J. A. c. b., Controlled co-reconstitution of multiple membrane proteins in lipid bilayer nanodiscs using DNA as a scaffold. **2015**, *10* (11), 2448-2454.
276. Chworos, A.; Severcan, I.; Koyfman, A. Y.; Weinkam, P.; Oroudjev, E.; Hansma, H. G.; Jaeger, L., Building programmable jigsaw puzzles with RNA. *Science* **2004**, *306* (5704), 2068-2072.
277. Fang, Y.; Shu, D.; Xiao, F.; Guo, P. X.; Qin, P. Z., Modular assembly of chimeric phi29 packaging RNAs that support DNA packaging. *Biochemical and Biophysical Research Communications* **2008**, *372* (4), 589-594.
278. Xiao, F.; Zhang, H.; Guo, P. X., Novel mechanism of hexamer ring assembly in protein/RNA interactions revealed by single molecule imaging. *Nucleic Acids Research* **2008**, *36* (20), 6620-6632.
279. Guo, P.; Erickson, S.; Anderson, D., A small viral RNA is required for in vitro packaging of bacteriophage phi 29 DNA. **1987**, *236* (4802), 690-694.
280. Guo, P.; Zhang, C.; Chen, C.; Garver, K.; Trotter, M. J. M. c., Inter-RNA interaction of phage phi29 pRNA to form a hexameric complex for viral DNA transportation. **1998**, *2* (1), 149-155.
281. Geary, C.; Rothmund, P. W. K.; Andersen, E. S., A single-stranded architecture for cotranscriptional folding of RNA nanostructures. *Science* **2014**, *345* (6198), 799-804.
282. Geary, C.; Meunier, P. E.; Schabanel, N.; Seki, S., Oritatami: A Computational Model for Molecular Co-Transcriptional Folding. *International Journal of Molecular Sciences* **2019**, *20* (9).
283. Zuker, M., Mfold web server for nucleic acid folding and hybridization prediction. *Nucleic Acids Research* **2003**, *31* (13), 3406-3415.
284. Waugh, A.; Gendron, P.; Altman, R.; Brown, J. W.; Case, D.; Gautheret, D.; Harvey, S. C.; Leontis, N.; Westbrook, J.; Westhof, E.; Zuker, M.; Major, F., RNAML: A standard syntax for exchanging RNA information. *Rna-a Publication of the Rna Society* **2002**, *8* (6), 707-717.
285. Zuker, M.; Jacobson, A. B., Using reliability information to annotate RNA secondary structures. *Rna* **1998**, *4* (6), 669-679.
286. Bindewald, E.; Afonin, K. A.; Viard, M.; Zakrevsky, P.; Kim, T.; Shapiro, B. A., Multistrand Structure Prediction of Nucleic Acid Assemblies and Design of RNA Switches. *Nano Letters* **2016**, *16* (3), 1726-1735.
287. Zadeh, J. N.; Steenberg, C. D.; Bois, J. S.; Wolfe, B. R.; Pierce, M. B.; Khan, A. R.; Dirks, R. M.; Pierce, N. A., NUPACK: Analysis and Design of Nucleic Acid Systems. *Journal of*

Computational Chemistry **2011**, 32 (1), 170-173.

288. Dirks, R. M.; Pierce, N. A., An algorithm for computing nucleic acid base-pairing probabilities including pseudoknots. *Journal of Computational Chemistry* **2004**, 25 (10), 1295-1304.
289. Dirks, R. M.; Bois, J. S.; Schaeffer, J. M.; Winfree, E.; Pierce, N. A., Thermodynamic analysis of interacting nucleic acid strands. *Siam Review* **2007**, 49 (1), 65-88.
290. Bindewald, E.; Grunewald, C.; Boyle, B.; O'Connor, M.; Shapiro, B. A. J. J. o. M. G.; Modelling, Computational strategies for the automated design of RNA nanoscale structures from building blocks using NanoTiler. **2008**, 27 (3), 299-308.
291. Lin, C.; Liu, Y.; Rinker, S.; Yan, H. J. C., DNA tile based self-assembly: building complex nanoarchitectures. **2006**, 7 (8), 1641-1647.
292. Kosuri, S.; Church, G. M. J. N. m., Large-scale de novo DNA synthesis: technologies and applications. **2014**, 11 (5), 499.
293. Afonin, K. A.; Cieply, D. J.; Leontis, N. B. J. J. o. t. A. C. S., Specific RNA self-assembly with minimal paranemic motifs. **2008**, 130 (1), 93-102.
294. Afonin, K. A.; Bindewald, E.; Yaghoubian, A. J.; Voss, N.; Jacovetty, E.; Shapiro, B. A.; Jaeger, L. J. N. n., In vitro assembly of cubic RNA-based scaffolds designed in silico. **2010**, 5 (9), 676.
295. Grabow, W. W.; Zakrevsky, P.; Afonin, K. A.; Chworos, A.; Shapiro, B. A.; Jaeger, L. J. N. l., Self-assembling RNA nanorings based on RNAI/II inverse kissing complexes. **2011**, 11 (2), 878-887.
296. Parlea, L.; Bindewald, E.; Sharan, R.; Bartlett, N.; Moriarty, D.; Oliver, J.; Afonin, K. A.; Shapiro, B. A. J. M., Ring Catalog: A resource for designing self-assembling RNA nanostructures. **2016**, 103, 128-137.
297. Shu, D.; Shu, Y.; Haque, F.; Abdelmawla, S.; Guo, P. J. N. n., Thermodynamically stable RNA three-way junction for constructing multifunctional nanoparticles for delivery of therapeutics. **2011**, 6 (10), 658.
298. Geary, C.; Chworos, A.; Verzemnieks, E.; Voss, N. R.; Jaeger, L. J. N. l., Composing RNA nanostructures from a syntax of RNA structural modules. **2017**, 17 (11), 7095-7101.
299. Chworos, A. J. R. N., Rational design of RNA nanoparticles and nanoarrays. **2014**, 213-34.
300. Bui, M. N.; Johnson, M. B.; Viard, M.; Satterwhite, E.; Martins, A. N.; Li, Z.; Marriott, I.; Afonin, K. A.; Khisamutdinov, E. F. J. N. N., Biology; Medicine, Versatile RNA tetra-U helix linking motif as a toolkit for nucleic acid nanotechnology. **2017**, 13 (3), 1137-1146.
301. Veneziano, R.; Ratanalert, S.; Zhang, K.; Zhang, F.; Yan, H.; Chiu, W.; Bathe, M. J. S., Designer nanoscale DNA assemblies programmed from the top down. **2016**, 352 (6293), 1534-1534.
302. Jahanban-Esfahlan, A.; Seidi, K.; Jaymand, M.; Schmidt, T. L.; Zare, P.; Javaheri, T.; Jahanban-Esfahlan, R. J. J. o. C. R., Dynamic DNA nanostructures in biomedicine: Beauty, utility and limits. **2019**.
303. Yurke, B.; Turberfield, A. J.; Mills, A. P.; Simmel, F. C.; Neumann, J. L. J. N., A DNA-fuelled molecular machine made of DNA. **2000**, 406 (6796), 605-608.
304. Yan, H.; Zhang, X.; Shen, Z.; Seeman, N. C. J. N., A robust DNA mechanical device controlled by hybridization topology. **2002**, 415 (6867), 62-65.
305. Feng, L.; Park, S. H.; Reif, J. H.; Yan, H. J. A. C. I. E., A two-state DNA lattice switched by DNA nanoactuator. **2003**, 42 (36), 4342-4346.
306. Yin, P.; Choi, H. M.; Calvert, C. R.; Pierce, N. A. J. N., Programming biomolecular self-assembly pathways. **2008**, 451 (7176), 318-322.
307. Dirks, R. M.; Pierce, N. A. J. P. o. t. N. A. o. S., Triggered amplification by hybridization chain reaction. **2004**, 101 (43), 15275-15278.
308. Hochrein, L. M.; Schwarzkopf, M.; Shahgholi, M.; Yin, P.; Pierce, N. A. J. J. o. t. A. C.

- S., Conditional Dicer substrate formation via shape and sequence transduction with small conditional RNAs. **2013**, *135* (46), 17322-17330.
309. Zakrevsky, P.; Parlea, L.; Viard, M.; Bindewald, E.; Afonin, K. A.; Shapiro, B. A., Preparation of a conditional RNA switch. In *RNA Nanostructures*, Springer: 2017; pp 303-324.
310. Martins, A. N.; Ke, W.; Jawahar, V.; Striplin, M.; Striplin, C.; Freed, E. O.; Afonin, K. A., Intracellular Reassociation of RNA–DNA Hybrids that Activates RNAi in HIV-Infected Cells. In *RNA Nanostructures*, Springer: 2017; pp 269-283.
311. Afonin, K. A.; Viard, M.; Tedbury, P.; Bindewald, E.; Parlea, L.; Howington, M.; Valdman, M.; Johns-Boehme, A.; Brainerd, C.; Freed, E. O. J. N. I., The use of minimal RNA toeholds to trigger the activation of multiple functionalities. **2016**, *16* (3), 1746-1753.
312. Halman, J. R.; Satterwhite, E.; Roark, B.; Chandler, M.; Viard, M.; Ivanina, A.; Bindewald, E.; Kasprzak, W. K.; Panigaj, M.; Bui, M. N. J. N. a. r., Functionally-interdependent shape-switching nanoparticles with controllable properties. **2017**, *45* (4), 2210-2220.
313. Chandler, M.; Ke, W.; Halman, J. R.; Panigaj, M.; Afonin, K. A., Reconfigurable nucleic acid materials for cancer therapy. In *Nanooncology*, Springer: 2018; pp 365-385.
314. Ke, W.; Hong, E.; Saito, R. F.; Rangel, M. C.; Wang, J.; Viard, M.; Richardson, M.; Khisamutdinov, E. F.; Panigaj, M.; Dokholyan, N. V. J. N. a. r., RNA–DNA fibers and polygons with controlled immunorecognition activate RNAi, FRET and transcriptional regulation of NF- κ B in human cells. **2019**, *47* (3), 1350-1361.
315. Chandler, M.; Lyalina, T.; Halman, J.; Rackley, L.; Lee, L.; Dang, D.; Ke, W.; Sajja, S.; Woods, S.; Acharya, S. J. M., Broccoli fluorets: split aptamers as a user-friendly fluorescent toolkit for dynamic RNA nanotechnology. **2018**, *23* (12), 3178.
316. Idili, A.; Vallée-Bélisle, A.; Ricci, F., Programmable pH-triggered DNA nanoswitches. *Journal of the American Chemical Society* **2014**, *136* (16), 5836-5839.
317. Zhang, X.; Battig, M. R.; Wang, Y. J. C. C., Programmable hydrogels for the controlled release of therapeutic nucleic acid aptamers via reversible DNA hybridization. **2013**, *49* (83), 9600-9602.
318. Schmidt, T. L.; Koepfel, M. B.; Thevarpadam, J.; Gonçalves, D. P.; Heckel, A. J. S., A light trigger for DNA nanotechnology. **2011**, *7* (15), 2163-2167.
319. Yuan, Q.; Zhang, Y.; Chen, T.; Lu, D.; Zhao, Z.; Zhang, X.; Li, Z.; Yan, C.-H.; Tan, W. J. A. n., Photon-manipulated drug release from a mesoporous nanocontainer controlled by azobenzene-modified nucleic acid. **2012**, *6* (7), 6337-6344.
320. Yang, Y.; Tashiro, R.; Suzuki, Y.; Emura, T.; Hidaka, K.; Sugiyama, H.; Endo, M. J. C. A. E. J., A Photoregulated DNA-Based Rotary System and Direct Observation of Its Rotational Movement. **2017**, *23* (16), 3979-3985.
321. Sherman, W. B.; Seeman, N. C. J. N. I., A precisely controlled DNA biped walking device. **2004**, *4* (7), 1203-1207.
322. Omabegho, T.; Sha, R.; Seeman, N. C. J. S., A bipedal DNA Brownian motor with coordinated legs. **2009**, *324* (5923), 67-71.
323. Chen, J.; Luo, Z.; Sun, C.; Huang, Z.; Zhou, C.; Yin, S.; Duan, Y.; Li, Y. J. T. T. i. A. C., Research Progress of DNA Walker and Its Recent Applications in Biosensor. **2019**, 115626.
324. Goldworthy, V.; LaForce, G.; Abels, S.; Khisamutdinov, E. F. J. N., Fluorogenic RNA aptamers: A nano-platform for fabrication of simple and combinatorial logic gates. **2018**, *8* (12), 984.
325. Sridharan, K.; Gogtay, N. J. J. B. j. o. c. p., Therapeutic nucleic acids: current clinical status. **2016**, *82* (3), 659-672.
326. Stein, C. A.; Castanotto, D. J. M. t., FDA-approved oligonucleotide therapies in 2017. **2017**, *25* (5), 1069-1075.
327. Bajan, S.; Hutvagner, G. J. C., RNA-Based Therapeutics: From Antisense Oligonucleotides to miRNAs. **2020**, *9* (1), 137.
328. Hickerson, R. P.; Vlassov, A. V.; Wang, Q.; Leake, D.; Ilves, H.; Gonzalez-Gonzalez, E.;

- Contag, C. H.; Johnston, B. H.; Kaspar, R. L. J. O., Stability study of unmodified siRNA and relevance to clinical use. **2008**, *18* (4), 345-354.
329. Fedorov, Y.; Anderson, E. M.; Birmingham, A.; Reynolds, A.; Karpilow, J.; Robinson, K.; Leake, D.; Marshall, W. S.; Khvorova, A. J. R., Off-target effects by siRNA can induce toxic phenotype. **2006**, *12* (7), 1188-1196.
330. Cui, D.; Zhang, C.; Liu, B.; Shu, Y.; Du, T.; Shu, D.; Wang, K.; Dai, F.; Liu, Y.; Li, C. J. S. r., Regression of gastric cancer by systemic injection of RNA nanoparticles carrying both ligand and siRNA. **2015**, *5*, 10726.
331. Rychahou, P.; Haque, F.; Shu, Y.; Zaytseva, Y.; Weiss, H. L.; Lee, E. Y.; Mustain, W.; Valentino, J.; Guo, P.; Evers, B. M. J. A. n., Delivery of RNA nanoparticles into colorectal cancer metastases following systemic administration. **2015**, *9* (2), 1108-1116.
332. Lee, T. J.; Haque, F.; Shu, D.; Yoo, J. Y.; Li, H.; Yokel, R. A.; Horbinski, C.; Kim, T. H.; Kim, S.-H.; Kwon, C.-H. J. O., RNA nanoparticle as a vector for targeted siRNA delivery into glioblastoma mouse model. **2015**, *6* (17), 14766.
333. Afonin, K. A.; Viard, M.; Koyfman, A. Y.; Martins, A. N.; Kasprzak, W. K.; Panigaj, M.; Desai, R.; Santhanam, A.; Grabow, W. W.; Jaeger, L. J. N. l., Multifunctional RNA nanoparticles. **2014**, *14* (10), 5662-5671.
334. Halman, J. R.; Kim, K.-T.; Gwak, S.-J.; Pace, R.; Johnson, M. B.; Chandler, M. R.; Rackley, L.; Viard, M.; Marriott, I.; Lee, J. S. J. N. N., Biology; Medicine, A cationic amphiphilic co-polymer as a carrier of nucleic acid nanoparticles (Nanps) for controlled gene silencing, immunostimulation, and biodistribution. **2020**, *23*, 102094.
335. Cruz-Acuña, M.; Halman, J. R.; Afonin, K. A.; Dobson, J.; Rinaldi, C. J. N., Magnetic nanoparticles loaded with functional RNA nanoparticles. **2018**, *10* (37), 17761-17770.
336. Parlea, L.; Puri, A.; Kasprzak, W.; Bindewald, E.; Zakrevsky, P.; Satterwhite, E.; Joseph, K.; Afonin, K. A.; Shapiro, B. A. J. A. c. s., Cellular delivery of RNA nanoparticles. **2016**, *18* (9), 527-547.
337. Shu, D.; Li, H.; Shu, Y.; Xiong, G.; Carson III, W. E.; Haque, F.; Xu, R.; Guo, P. J. A. n., Systemic delivery of anti-miRNA for suppression of triple negative breast cancer utilizing RNA nanotechnology. **2015**, *9* (10), 9731-9740.
338. Daubendiek, S. L.; Ryan, K.; Kool, E. T. J. J. o. t. A. C. S., Rolling-circle RNA synthesis: circular oligonucleotides as efficient substrates for T7 RNA polymerase. **1995**, *117* (29), 7818-7819.
339. Han, D.; Park, Y.; Kim, H.; Lee, J. B. J. N. c., Self-assembly of free-standing RNA membranes. **2014**, *5* (1), 1-7.
340. Kim, H.; Lee, J. S.; Lee, J. B. J. S. r., Generation of siRNA nanosheets for efficient RNA interference. **2016**, *6* (1), 1-7.
341. Roh, Y. H.; Deng, J. Z.; Dreaden, E. C.; Park, J. H.; Yun, D. S.; Shopsowitz, K. E.; Hammond, P. T. J. A. C. I. E., A multi-RNAi microsponge platform for simultaneous controlled delivery of multiple small interfering RNAs. **2016**, *55* (10), 3347-3351.
342. Lee, J. B.; Hong, J.; Bonner, D. K.; Poon, Z.; Hammond, P. T. J. N. m., Self-assembled RNA interference microsponges for efficient siRNA delivery. **2012**, *11* (4), 316-322.
343. Li, H.; Zhang, K.; Pi, F.; Guo, S.; Shlyakhtenko, L.; Chiu, W.; Shu, D.; Guo, P. J. A. m., Controllable self-assembly of RNA tetrahedrons with precise shape and size for cancer targeting. **2016**, *28* (34), 7501-7507.
344. Shu, D.; Khisamutdinov, E.; Zhang, L.; Guo, P. J. N. A. R., Programmable folding of fusion RNA complex driven by the 3WJ motif of phi29 motor pRNA. **2013**, *42* (2), e10.
345. Low, P. S.; Kularatne, S. A. J. C. o. i. c. b., Folate-targeted therapeutic and imaging agents for cancer. **2009**, *13* (3), 256-262.
346. Khisamutdinov, E. F.; Li, H.; Jasinski, D. L.; Chen, J.; Fu, J.; Guo, P. J. N. a. r., Enhancing immunomodulation on innate immunity by shape transition among RNA triangle, square and pentagon nanovehicles. **2014**, *42* (15), 9996-10004.

347. Guo, S.; Xu, C.; Yin, H.; Hill, J.; Pi, F.; Guo, P. J. W. I. R. N.; Nanobiotechnology, Tuning the size, shape and structure of RNA nanoparticles for favorable cancer targeting and immunostimulation. **2020**, *12* (1), e1582.
348. Hong, E.; Halman, J. R.; Shah, A. B.; Khisamutdinov, E. F.; Dobrovolskaia, M. A.; Afonin, K. A. J. N. I., Structure and composition define immunorecognition of nucleic acid nanoparticles. **2018**, *18* (7), 4309-4321.
349. Johnson, M. B.; Halman, J. R.; Satterwhite, E.; Zakharov, A. V.; Bui, M. N.; Benkato, K.; Goldsworthy, V.; Kim, T.; Hong, E.; Dobrovolskaia, M. A. J. S., Programmable nucleic acid based polygons with controlled neuroimmunomodulatory properties for predictive QSAR modeling. **2017**, *13* (42), 1701255.
350. Rackley, L.; Stewart, J. M.; Salotti, J.; Krokhotin, A.; Shah, A.; Halman, J. R.; Juneja, R.; Smollett, J.; Lee, L.; Roark, K. J. A. f. m., RNA fibers as optimized nanoscaffolds for siRNA coordination and reduced immunological recognition. **2018**, *28* (48), 1805959.
351. Juliano, R. L. J. N. a. r., The delivery of therapeutic oligonucleotides. **2016**, *44* (14), 6518-6548.
352. Maeda, H.; Nakamura, H.; Fang, J. J. A. d. d. r., The EPR effect for macromolecular drug delivery to solid tumors: Improvement of tumor uptake, lowering of systemic toxicity, and distinct tumor imaging in vivo. **2013**, *65* (1), 71-79.
353. Komarova, Y.; Malik, A. B., Regulation of endothelial permeability via paracellular and transcellular transport pathways. *Annual review of physiology* **2010**, *72*, 463-493.
354. Tarbell, J. M., Shear stress and the endothelial transport barrier. *Cardiovascular research* **2010**, *87* (2), 320-330.
355. Gordon, S.; Taylor, P. R. J. N. R. I., Monocyte and macrophage heterogeneity. **2005**, *5* (12), 953-964.
356. Haraldsson, B.; Nyström, J.; Deen, W. M. J. P. r., Properties of the glomerular barrier and mechanisms of proteinuria. **2008**, *88* (2), 451-487.
357. Huang, L.; Liu, Y. J. A. r. o. b. e., In vivo delivery of RNAi with lipid-based nanoparticles. **2011**, *13*, 507-530.
358. Leung, A. K.; Tam, Y. Y. C.; Cullis, P. R., Lipid nanoparticles for short interfering RNA delivery. In *Advances in genetics*, Elsevier: 2014; Vol. 88, pp 71-110.
359. Lorenzer, C.; Dirin, M.; Winkler, A.-M.; Baumann, V.; Winkler, J. J. J. o. C. R., Going beyond the liver: progress and challenges of targeted delivery of siRNA therapeutics. **2015**, *203*, 1-15.
360. Ozcan, G.; Ozpolat, B.; Coleman, R. L.; Sood, A. K.; Lopez-Berestein, G. J. A. d. d. r., Preclinical and clinical development of siRNA-based therapeutics. **2015**, *87*, 108-119.
361. Sharma, A.; Madhunapantula, S. V.; Robertson, G. P. J. E. o. o. d. m.; toxicology, Toxicological considerations when creating nanoparticle-based drugs and drug delivery systems. **2012**, *8* (1), 47-69.
362. Akhtar, S. J. E. o. o. d. m.; toxicology, Cationic nanosystems for the delivery of small interfering ribonucleic acid therapeutics: a focus on toxicogenomics. **2010**, *6* (11), 1347-1362.
363. Xue, H. Y.; Liu, S.; Wong, H. L. J. N., Nanotoxicity: a key obstacle to clinical translation of siRNA-based nanomedicine. **2014**, *9* (2), 295-312.
364. Suk, J. S.; Xu, Q.; Kim, N.; Hanes, J.; Ensign, L. M., PEGylation as a strategy for improving nanoparticle-based drug and gene delivery. *Advanced drug delivery reviews* **2016**, *99*, 28-51.
365. Richards, D. A.; Maruani, A.; Chudasama, V., Antibody fragments as nanoparticle targeting ligands: a step in the right direction. *Chemical science* **2017**, *8* (1), 63-77.
366. Xue, W.; Dahlman, J. E.; Tammela, T.; Khan, O. F.; Sood, S.; Dave, A.; Cai, W.; Chirino, L. M.; Yang, G. R.; Bronson, R. J. P. o. t. N. A. o. S., Small RNA combination therapy for lung cancer. **2014**, *111* (34), E3553-E3561.
367. Katakowski, J. A.; Mukherjee, G.; Wilner, S. E.; Maier, K. E.; Harrison, M. T.;

- DiLorenzo, T. P.; Levy, M.; Palliser, D. J. M. T., Delivery of siRNAs to dendritic cells using DEC205-targeted lipid nanoparticles to inhibit immune responses. **2016**, *24* (1), 146-155.
368. Ramishetti, S.; Kedmi, R.; Goldsmith, M.; Leonard, F.; Sprague, A. G.; Godin, B.; Gozin, M.; Cullis, P. R.; Dykxhoorn, D. M.; Peer, D. J. A. n., Systemic gene silencing in primary T lymphocytes using targeted lipid nanoparticles. **2015**, *9* (7), 6706-6716.
369. Gupta, K.; Afonin, K. A.; Viard, M.; Herrero, V.; Kasprzak, W.; Kagiampakis, I.; Kim, T.; Koyfman, A. Y.; Puri, A.; Stepler, M. J. J. o. C. R., Bolaamphiphiles as carriers for siRNA delivery: From chemical syntheses to practical applications. **2015**, *213*, 142-151.
370. Merkel, O. M.; Kissel, T. J. J. o. C. R., Quo vadis polyplex? **2014**, *190*, 415-423.
371. Parveen, S.; Sahoo, S. K., Polymeric nanoparticles for cancer therapy. *Journal of drug targeting* **2008**, *16* (2), 108-123.
372. Kesharwani, P.; Banerjee, S.; Gupta, U.; Amin, M. C. I. M.; Padhye, S.; Sarkar, F. H.; Iyer, A. K. J. M. T., PAMAM dendrimers as promising nanocarriers for RNAi therapeutics. **2015**, *18* (10), 565-572.
373. Serrano-Sevilla, I.; Artiga, Á.; Mitchell, S. G.; De Matteis, L.; de la Fuente, J. M. J. M., Natural polysaccharides for siRNA delivery: Nanocarriers based on chitosan, hyaluronic acid, and their derivatives. **2019**, *24* (14), 2570.
374. Reis, C. P.; Neufeld, R. J.; Ribeiro, A. J.; Veiga, F., Nanoencapsulation I. Methods for preparation of drug-loaded polymeric nanoparticles. *Nanomedicine: Nanotechnology, Biology and Medicine* **2006**, *2* (1), 8-21.
375. Vicente, S.; Peleteiro, M.; Gonzalez-Aramundiz, J. V.; Díaz-Freitas, B.; Martínez-Pulgarín, S.; Neissa, J. I.; Escribano, J. M.; Sanchez, A.; González-Fernández, Á.; Alonso, M. J., Highly versatile immunostimulating nanocapsules for specific immune potentiation. *Nanomedicine* **2014**, *9* (15), 2273-2289.
376. Jiang, Y.; Huo, S.; Hardie, J.; Liang, X.-J.; Rotello, V. M. J. E. o. o. d. d., Progress and perspective of inorganic nanoparticle-based siRNA delivery systems. **2016**, *13* (4), 547-559.
377. Narayan, R.; Nayak, U. Y.; Raichur, A. M.; Garg, S. J. P., Mesoporous silica nanoparticles: A comprehensive review on synthesis and recent advances. **2018**, *10* (3), 118.
378. Vivero-Escoto, J. L.; Jeffords, L. M.; Dréau, D.; Alvarez-Berrios, M.; Mukherjee, P. In *Mucin1 antibody-conjugated dye-doped mesoporous silica nanoparticles for breast cancer detection in vivo*, Colloidal Nanoparticles for Biomedical Applications XII, International Society for Optics and Photonics: 2017; p 100780B.
379. Alvarez-Berrios, M. P.; Vivero-Escoto, J. L. J. I. j. o. n., In vitro evaluation of folic acid-conjugated redox-responsive mesoporous silica nanoparticles for the delivery of cisplatin. **2016**, *11*, 6251.
380. Dréau, D.; Moore, L. J.; Alvarez-Berrios, M. P.; Tarannum, M.; Mukherjee, P.; Vivero-Escoto, J. L. J. o. b. n., Mucin-1-antibody-conjugated mesoporous silica nanoparticles for selective breast cancer detection in a mucin-1 transgenic murine mouse model. **2016**, *12* (12), 2172-2184.
381. Manzano, M.; Vallet-Regí, M. J. A. F. M., Mesoporous Silica Nanoparticles for Drug Delivery. **2019**, 1902634.
382. Santos, H. A.; Bimbo, L. M.; Peltonen, L.; Hirvonen, J., Inorganic nanoparticles in targeted drug delivery and imaging. In *Targeted Drug Delivery: Concepts and Design*, Springer: 2015; pp 571-613.

2 Chapter 2: Functionally-interdependent shape-switching nanoparticles with controllable properties

2.1 Introduction

Nucleic acids (RNA and DNA) have been acknowledged as an important building material for nanotechnology due to their biocompatibility and programmability. The option of both canonical and non-canonical base pairings tremendously expands the diverse set of RNA structural motifs available as building blocks¹⁻¹³. Programmable multi-tasking as well as the ability to dynamically respond to the environment make nucleic acids an attractive material for tailor-made applications in both biotechnology and personalized therapy.

In one decade, a wide array of artificially designed dynamic DNA assemblies have been shown to respond to a broader spectrum of physicochemical stimuli or ligands. Rationally designed DNA nanomachines can carry out a rotary motion by switching from B- to Z-DNA at high ionic strength¹⁴, sense the pH¹⁵⁻¹⁶, and respond to changes from visible to UV light¹⁷. DNA “walkers” are capable of directional movement based on strand displacement¹⁸⁻¹⁹, enzymatic activity²⁰⁻²¹, or in accordance with the prescriptive DNA origami landscapes²². DNA boxes with a programmable lid²³ and DNA “nanorobots”²⁴ can be used for delivery and release of different cargos. Recently, a DNA

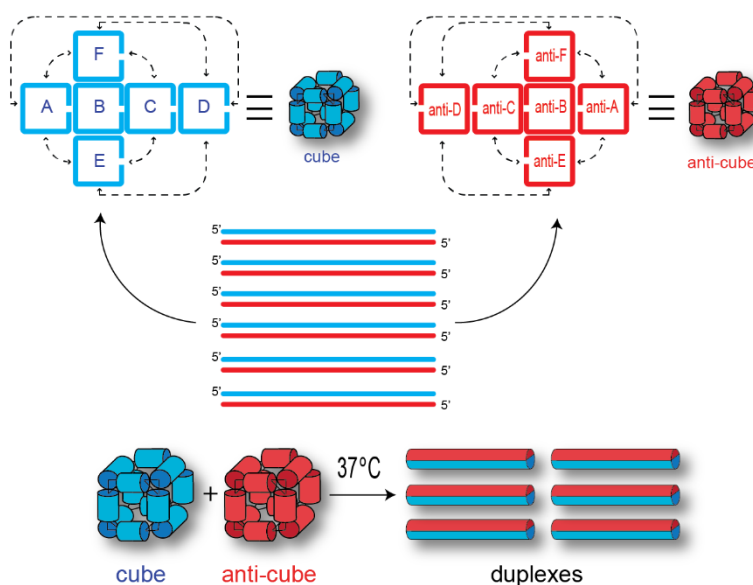


Figure 5. Schematics depicting the design principles of complementary nucleic acid nanoparticles.

cube that selectively forms a flat 2D structure after hybridization to a specific fusion gene that is characteristic for a prostate cancer cell line was engineered. While authors have demonstrated that the cubes are taken up by a number of cell lines, the dynamic response has only been shown *in vitro*²⁵. Although numerous creative innovations of dynamic DNA nanoassemblies have been described, the majority are only functional *in vitro* and their immediate practical applications in living systems remain unclear.

In addition to being carriers of genetic information, RNAs are now recognized to function as natural scaffolds, enzymes, switches, aptamers, and regulators of gene expression and editing. The emerging field of RNA nanotechnology applies the current knowledge related to the structure and function of natural and artificial RNAs to further address specific biomedical challenges by engineering nanodevices that can interact with cellular machinery^{2, 26}. Building dynamic RNA nanoparticles that can communicate with one another will further improve the operation of functional systems. In fact, metabolite and cofactor responsive riboswitches and ribozymes as well as temperature-sensing RNA thermometers are some examples of dynamic RNAs autogenic in nature²⁷⁻³⁰. Recently, we reported two approaches of dynamic RNA³¹ and RNA-DNA hybrid³² nanostructures that conditionally activate gene silencing in diseased cells *in vitro* and *in vivo*. The first approach is based on computer-generated two-stranded RNA switches that are activated only in the presence of specific mRNAs through interaction with a single-stranded (ss) RNA toehold of the switch³¹. The second approach is based on RNA-DNA hybrids with split-functionalities activated only when two complementary copies are introduced into the same cell. Strand exchange, with subsequent intracellular activation of functionalities, is promoted by the interaction of complementary ssDNA³² or ssRNA³³ toeholds. This concept was further used by other research groups for various applications³⁴⁻³⁵. The simultaneous delivery and release of multiple functionalities was achieved by including them all into the longer hybrids³⁶. Alternatively, RNA and/or DNA nanoscaffolds can be decorated with multiple hybrids and activated by adding individual cognate DNA/RNA hybrids³⁷⁻³⁸. This approach, however, requires the simultaneous

presence of the nanoparticle and six individual cognate hybrids in the same cell to activate six functionalities. While efficient, previously described nanodevices typically demand intensive computer-assisted design and the use of specifically programmed toeholds.

Here, we set out to design a series of interdependent complementary nucleic acid nanoparticles that take advantage of dynamic interaction and shape-switching to activate multiple functionalities. As opposed to previously described work, this new approach does not require any toeholds to initiate the interactions and their design principles are simplified. Additionally, only two particles are required to simultaneously activate multiple functionalities. The novel interrelated nanoparticles are designed by simply taking the reverse complements of the existing RNA scaffolds and assembling them into the “anti-scaffolds,” as schematically explained in Fig. 9. As a proof of concept, nucleic acid cubes¹ and their reverse complements, anti-cubes, are extensively characterized in this work (Fig. 6A). The interaction of cubes with anti-cubes at physiological conditions leads to conformational changes and to the swift formation of multiple duplexes or fibers that can further activate transcription, *Förster* resonance energy transfer (FRET), aptamers, and specific gene silencing. We show that the immunostimulatory activity, thermodynamic stability, resistance to nuclease degradation, re-association rate, and cost of production for complementary nanoparticles vary tremendously depending on their composition (*e.g.*, DNA vs RNA). In addition, RNA hexameric rings³⁹ and recently engineered RNA and DNA triangle⁴⁰ scaffolds and their corresponding anti-scaffolds are explored.

2.2 Methods

2.2.1 Nanoparticle assembly and purification.

All nanoparticles were assembled by combining individual monomer components in equimolar concentrations. For cubes, the mixture of oligonucleotides in double-deionized water (ddiH₂O) was heated to 95 °C for 2 minutes, followed by snap-cooling to 45 °C and incubation for 20 minutes. For rings, mixtures were heated to 95 °C for 2 minutes, followed by snap cooling on ice for 2 minutes, and incubation at 30 °C for 30 minutes. An assembly buffer (1X

concentration: 89 mM tris-borate (pH 8.3), 2 mM MgCl₂, 50 mM KCl) was added following the heating step to all assemblies. For triangular complexes the mixtures in TMS buffer (1X concentration: 50 mM tris (pH 8.0), 100 mM NaCl and 10 mM MgCl₂) were heated to 80 °C for 2 min and slow cooled (over 1 h) to 4 °C.

For activation of co-transcriptional assembly of RNA cubes, DNA cubes (in Figure 2 C6sP: dA-T7, dB-T7, dC-T7, dD-T7, dE-T7, dF-T7, tP4C at 1:1:1:1:1:1:6 ratio; at 100 nM final) and anti-cubes (in Figure 2 A6sP: anti-dA-T7, anti-dB-T7, anti-dC-T7, anti-dD-T7, anti-dE-T7, anti-dF-T7, tP4AC at 1:1:1:1:1:1:6 ratio; at 100 nM final) with six *split promoters* were either incubated individually or mixed together for 3.5 hours in the presence of T7 RNA polymerase, 100 mM DTT, and transcription buffer (400 mM HEPES-KOH, 10 mM Spermidine, 200 mM DTT, 120 mM MgCl₂). For co-transcriptional assembly of RNA cubes, DNA cubes (in Figure 2 C6P: dA-T7, dB-T7, dC-T7, dD-T7, dE-T7, dF-T7, P4C at 1:1:1:1:1:1:6 ratio; at 100 nM final) and anti-cubes (in Figure 2 A6P: anti-dA-T7, anti-dB-T7, anti-dC-T7, anti-dD-T7, anti-dE-T7, anti-dF-T7, P4AC at 1:1:1:1:1:1:6 ratio; at 100 nM final) with six *complete T7 promoters* were incubated individually for 3.5 hours in transcription mixture. For purification, 8% non-denaturing PAGE (37.5:1) was used in the presence of 89 mM tris-borate, pH 8.3, 2 mM MgCl₂. Nanoparticle bands were visualized with UV lamp (short wavelength), cut and eluted with assembly buffer for purification. The extinction coefficients of nanoparticles were calculated as the summation of extinction coefficients of individual sequences comprising them. Electrophoretic mobility shift assays were performed for all assemblies on 8% non-denaturing native PAGE (37.5:1, 2 mM MgCl₂) and visualized with a Bio-Rad ChemiDoc MP System using total staining with ethidium bromide or fluorescently labeled oligonucleotides. Native-PAGE was run for 1 hour at 4 °C, 300 Volts.

2.2.2 UV-melting experiments.

Temperature-dependent absorption measurements were recorded at 260 nm on an Agilent 8453 spectrophotometer coupled with the Agilent 89090 Peltier Temperature Controller. This

configuration contains a diode-array system to enhance the collection of all spectra. The instrument was calibrated by adding 100 μL of assembly buffer into a Starna Cells 100 μL sub-micro quartz fluorometer cell cuvette. Nanoparticles (compositions of cubes are shown in Fig. 7) were diluted in assembly buffer for a final concentration and volume of 250 nM and 100 μL , respectively. The temperature was gradually increased from 20-25 $^{\circ}\text{C}$ to 60-85 $^{\circ}\text{C}$ and the absorbance was recorded every 1 $^{\circ}\text{C}$ increment while the temperature was held constant for 10 seconds. The Agilent UV/vis software was used to plot the melting temperature (T_m) based on the average between the initial and final absorbance values selected from the temperature range from the initial increase of the slope until a plateau was observed. The data was analyzed using Origin[®] Pro 2016 Graphing and Analysis software with a Boltzmann sigmoidal curve fit. All experiments were repeated at least three times and presented as the mean \pm SD.

2.2.3 Kinetics of re-association determination.

To determine the kinetics, gel purified Cy5-tagged DNA anti-cube (and Alexa 488 labeled RNA cube) was mixed with different compositions of cubes (compositions of cubes are shown in Fig. 7) and were aliquoted at set time points to assess the extent of re-association. Based on the analysis of T_m curves, the relative rates of re-association were measured at 25 $^{\circ}\text{C}$ to ensure the complete assembly of all nanoparticles. For RNA cube and RNA anti-cubes, the re-association was measured at 25 $^{\circ}\text{C}$ and at 37 $^{\circ}\text{C}$. In order to ensure the complete re-association, the cubes without fluorescent tags were used in 10X excess (1 μM final). Upon addition of the cubes, the solution was pipetted up and down rapidly and equal aliquots were taken at specified time points, mixed with equal volume of loading buffer (50% glycerol, 1X assembly buffer), and placed on dry ice to preserve the current stage of re-association. Samples were loaded in reverse order onto 8% native-PAGE at 4 $^{\circ}\text{C}$. Results were visualized with a Bio-Rad ChemiDoc MP System with a Cy5 filter. The bands were quantified to determine the re-association kinetics using Image Lab[™] Software. All experiments were repeated at least three times and presented as the mean \pm SD.

2.2.4 Primary human peripheral blood mononuclear cell and whole blood culture for analysis of interferon and cytokine secretion.

Blood from pre-screened healthy donor volunteers was collected under National Cancer Institute, Frederick Protocol OH99-C-N046 using BD vacutainer tubes containing Li-heparin as the anticoagulant. The blood was used within 1-1.5 h after collection and was kept at room temperature (RT). Whole blood was used for the analysis of chemokines and pro-inflammatory cytokines, while PBMC cultures, in which myeloid cells producing type I interferon are more concentrated than in whole blood, were used for the analysis of type I interferon. The cultures were performed according to the standardized protocol NCL-ITA-10 (http://ncl.cancer.gov/NCL_Method_ITA-10.pdf). Supernatants were analyzed using a chemiluminescence based multiplex system (Quansys, Logan, UT) according to the manufacturer's instructions. Two independent samples were prepared for each nanoparticle (compositions of RNA, RNA/DNA and DNA cubes were the same as shown in Fig. 7) and tested in at least two individual donors. Each supernatant was analyzed in duplicate on multiplex plate. The positive control for interferon assays was a synthetic class A CpG oligonucleotide ODN 2216. Bacterial lipopolysaccharide (LPS) from *E.coli* strain K-12 was used as positive control for whole blood assay measuring pro-inflammatory cytokines. Presented is the mean \pm SD of individual samples (N=2) for each individual donor.

2.2.5 Nuclease digestion assays.

Assembled nanoparticles (compositions of cubes are shown in Fig. 7) containing either RNA or DNA strands labeled with Alexa 488 at the 3'-end were used in chemical stability studies. For RNase digestion assays, RNase I_f (New England Biolabs) that cleaves at all RNA dinucleotide bonds leaving a 5' hydroxyl and 2', 3' cyclic monophosphate, was used according to the manufacturer's protocols. For DNase digestion assays, RQ1 RNase-free DNase (Promega) that cleaves both double-stranded and single-stranded DNA endonucleolytically, producing 3'-OH oligonucleotides, was used according to the manufacturer's protocols. For blood stability assays,

freshly drawn human blood serum (blood was allowed to coagulate, then spun down and supernatant was collected) was immediately aliquoted and frozen at -80 °C. Different Alexa 488 labeled nanocubes (assembled at 1 μ M final) were incubated with RNase, DNase at 37 °C for 10 min, and with 1% (v/v) human blood serum at 37 °C for 3 min. The bands of treated samples were quantified using Image Lab TM Software and compared to the bands of corresponding untreated nanoparticles to determine the relative degradation. All experiments were repeated at least three times and presented as the mean \pm SD.

2.2.6 Computational predictions and 3D modeling.

Computational predictions of T_{ms} were performed for the different combinations of RNA and DNA strands using the HyperFold program. Predictions were performed at temperatures between 20 °C and 70 °C using steps of 2 °C intervals. For each temperature, the free energy corresponding to the ensemble of all nucleic acid structures for which all six strands are forming a complex was computed. Using linear interpolation, the temperature corresponding to a free energy of zero was determined. Additional structure predictions were performed at 10 °C in order to obtain the idealized secondary structures shown in Figure 9.

The all-RNA cube model is identical to that which was built with the aid of our program called NanoTiler, (<https://binkley2.ncifcrf.gov/users/bshapiro/software.html>) and scaled to bring it into better agreement with the experimental data^{1,2}. The RNA/DNA hybrid cubes and DNA cube models utilize the RNA cube as a spatial reference, but were created independently in PyMOL Molecular Graphics System (Schrödinger, LLC., <http://www.pymol.org/>) with custom scripts connecting B-form (pure DNA) and A-form (Hybrid and pure RNA) helices and single-stranded corner linker fragments pre-generated in Accelrys Discovery Studio Visualizer 4.0 (Accelrys Software, Inc; <http://accelrys.com>). The DNA/RNA hybrid cube model shown in Figure 1B that was built from 3 RNA and 3 DNA strands mixes the B-form and A-form helices in one cube (2 pure DNA B-form helices, 2 pure RNA A-form helices and 8 DNA/RNA helices). All preliminary models were structurally cleaned-up with implicit solvent Generalized Born

energy minimization in Amber14 with the RNA and DNA specific components of the force field ff14SB³⁻⁸. In addition, all models were subjected to 50 ns long explicit solvent molecular dynamics (TIP3P water model, Berendsen thermostat, PME method for long distance interactions and 9Å non-bonded cutoff⁹⁻¹¹ simulations) that verified their robustness, i.e. maintenance of the designed base pairing under full cube dynamic distortions (results not shown).

The RNA, RNA/DNA, and DNA cube models were built using PyMol. The triangle models were built with the aid of NanoTiler (<https://binkley2.ncifcrf.gov/users/bshapiro/software.html>).

2.2.7 Activation of FRET

To determine the re-association of nanoparticles *in vitro*, FRET measurements were performed using a FluoroMax3 (Jobin-Yvon, Horiba). For all measurements, the excitation wavelength was set at 460 nm and the excitation and emission slit widths were set at 2 nm. For tracking the DS RNA formation, DS sense and antisense strands were modified with Alexa 488 and Alexa 546 fluorophores, respectively. To follow the kinetics of re-association, purified DNA nanoparticles containing DS sense strands were first incubated for two minutes at 37 °C and nanoparticles assembled with DS antisense strands were then added in equimolar amounts. At 460 nm excitation, the emissions were simultaneously recorded at 520 nm and 570 nm every 30 seconds to follow the DS RNA formation through FRET. This was completed for nanoparticles with and without Lipofectamine 2000 (L2K) added in the concentrations corresponding to the transfection experiments. For reporter DNA release in co-transcriptional production experiments, static measurements were performed after 3 hours of incubation of equimolar amounts of the two fluorescently labeled DNA nanoparticles. Since the reporter strands are relatively short (tP4C: 5'-ATAGTGAGTCG-Alexa 488; tP4AC:5'-Alexa 546-CgACTCACTAT) with T_m s below 37 °C, FRET was measured at 20 °C. Low T_m can also explain the appearance of two bands, due to melting, on re-association gel in Figure 2B.

2.2.8 AFM imaging and sample preparation

To determine the re-association of nanoparticles *in vitro*, FRET measurements were

performed using a FluoroMax3 (Jobin-Yvon, Horiba). For all measurements, the excitation wavelength was set at 460 nm and the excitation and emission slit widths were set at 2 nm. For tracking the DS RNA formation, DS sense and antisense strands were modified with Alexa 488 and Alexa 546 fluorophores, respectively. To follow the kinetics of re-association, purified DNA nanoparticles containing DS sense strands were first incubated for two minutes at 37 °C and nanoparticles assembled with DS antisense strands were then added in equimolar amounts. At 460 nm excitation, the emissions were simultaneously recorded at 520 nm and 570 nm every 30 seconds to follow the DS RNA formation through FRET. This was completed for nanoparticles with and without Lipofectamine 2000 (L2K) added in the concentrations corresponding to the transfection experiments. For reporter DNA release in co-transcriptional production experiments, static measurements were performed after 3 hours of incubation of equimolar amounts of the two fluorescently labeled DNA nanoparticles. Since the reporter strands are relatively short (tP4C: 5'-ATAGTGAGTCG-Alexa 488; tP4AC:5'-Alexa 546-CgACTCACTAT) with T_m s below 37 °C, FRET was measured at 20 °C. Low T_m can also explain the appearance of two bands, due to melting, on re-association gel in Figure 2B⁴¹⁻⁴².

2.2.9 Transfection of human cell lines

For cell culture experiments with nanoparticles, human breast cancer MDA-MB-231 (with or without eGFP), human prostate cancer PC-3, and human cervical cancer HeLa cell lines were grown in D-MEM (MDA-MB-231 and HeLa) and RPMI (PC-3) media at 37 °C in a 5% CO₂ incubator. The media was supplemented with 10% FBS and penicillin-streptomycin. All transfection experiments were carried out using L2K purchased from Invitrogen according to manufacturer's protocol. Solution of purified nanoparticles (100X concentration) were pre-incubated at RT with L2K for 30 mins. Prior to each transfection, the cell media was changed to OPTI-MEM (from RPMI or D-MEM) and prepared nanoparticles with L2K complexes were added to the final 1X concentration. The cells were incubated for 4 hours followed by a media change (RPMI or D-MEM).

2.2.10 Fluorescent microscopy

To assess the intracellular interaction and shape change of nanoparticles, FRET measurements were performed using an LSM 710 confocal microscope (Carl Zeiss) with a 63x, 1.4 NA magnification lens. PC-3 cells were plated in glass bottom petri dishes (Ibidi) and transfected with fluorescently labeled complementary cubes and anti-cubes used in FRET studies. The next day, the samples were fixed in 4% paraformaldehyde at RT. Images of the cells were then taken to assess the appearance of FRET within the sample.

2.2.11 Flow Cytometry

For specific gene silencing experiments, human breast cancer cells expressing GFP (MDA-MB-231/GFP) were cultured at 2×10^4 or 3×10^4 cells per well respectively in either 12 or 24 well plates. 72 hours post-transfections, cells were removed from plates using trypsin, centrifuged, and re-suspended in 1X PBS. Silencing of GFP was assessed using BD Accuri C6 flow cytometer. Non-treated cells were used as control. At least 15,000 events were collected for each sample and analyzed. CellQuest or the CFlow Sampler software were used to retrieve the geometric mean fluorescence intensity (gMFI) and the standard error of the mean.

2.2.12 Cell proliferation assay

The viability of cells after transfection with purified cognate nanoparticles designed to release DS RNAs against PLK1 and BCL2 was assessed through the CellTiter 96[®] Aqueous One assay (Promega, Madison) following manufacturer's protocol. Upon addition of the CellTiter reagents to the cells in DMEM, the absorbance (490 nm) of the resorufin-forming compound was measured after three hours of incubation at 37 °C.

2.2.13 Statistics

Statistical significance was determined using a Student's two-tailed t-test conducted with GraphPad Prism Software. A p-value of less than 0.05 was considered to be statistically significant.

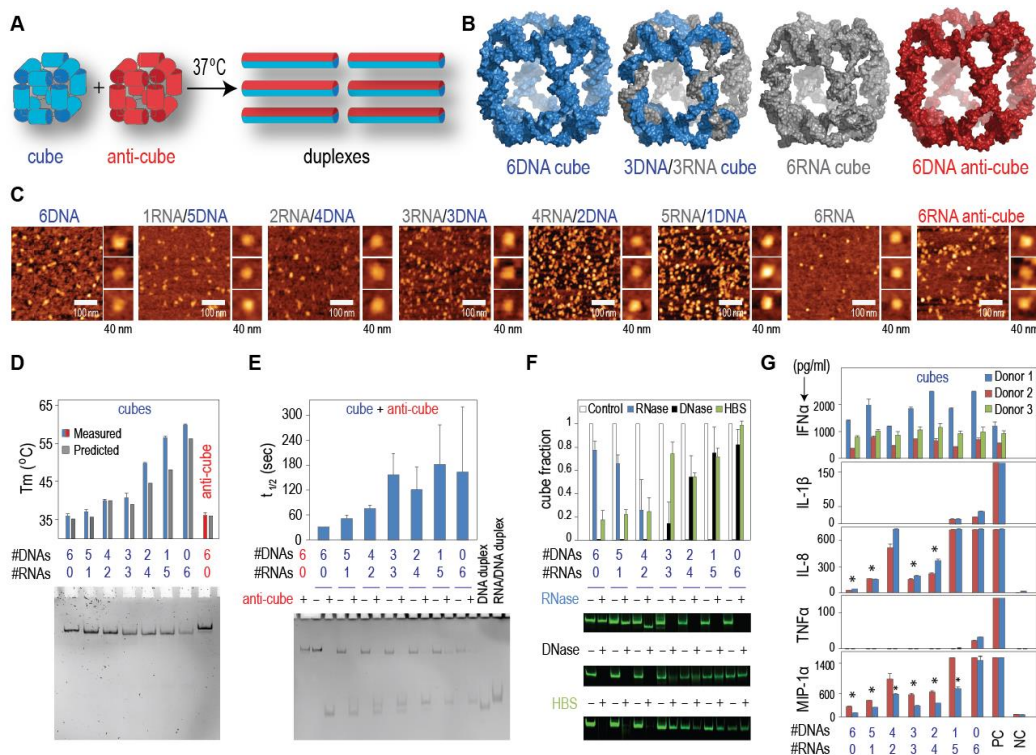


Figure 6. Fine-tunable isothermal re-association of complementary shape-switching nanoparticles. **(A)** Schematic representation of re-association between the complementary cube and anti-cube nanoparticles. **(B)** 3D models of nanoparticles. **(C)** AFM images of RNA, RNA/DNA, DNA cubes and RNA anti-cube. **(D)** Experimental and predicted melting temperatures of nanoparticles controlled by their compositions and native-PAGE with corresponding assemblies. Error bars indicate s.d.; N=3 **(E)** Relative re-association rates of RNA, RNA/DNA, and DNA cubes with DNA anti-cubes measured at 25 °C and native-PAGE with corresponding re-associations visualized after 30 mins of incubation. Error bars indicate s.d.; N=3. **(F)** Relative stabilities of nanoparticles in the presence of DNase, RNase, and human blood serum. Results are normalized to corresponding non-treated samples. Error bars indicate s.d.; N=3. **(G)** Immunostimulatory properties of RNA, RNA/DNA, and DNA shape-switching nanoparticles delivered using Lipofectamine 2000. Error bars indicate s.d.; N=2. Statistically significant results (compared to PC) are indicated with asterisks (p-value < 0.05). For IL-1 β and TNF α all results are statistically significant. In **(D-E)**, note that the higher number of RNA strands per nanoparticle weakens the extent of total staining.

2.3 Results and Discussion

2.3.1 Complementary nanoparticles have controlled rates of re-association and fine-tunable thermodynamic, chemical, and immunogenic properties

An important feature of rationally designed cubes is their ability to efficiently assemble with different ratios of RNA and DNA strands entering their composition (Fig. 6B). This design flexibility together with the difference in physicochemical properties between RNA and DNA allows for fine-tuning of the thermodynamic, kinetic, and chemical properties of the interacting

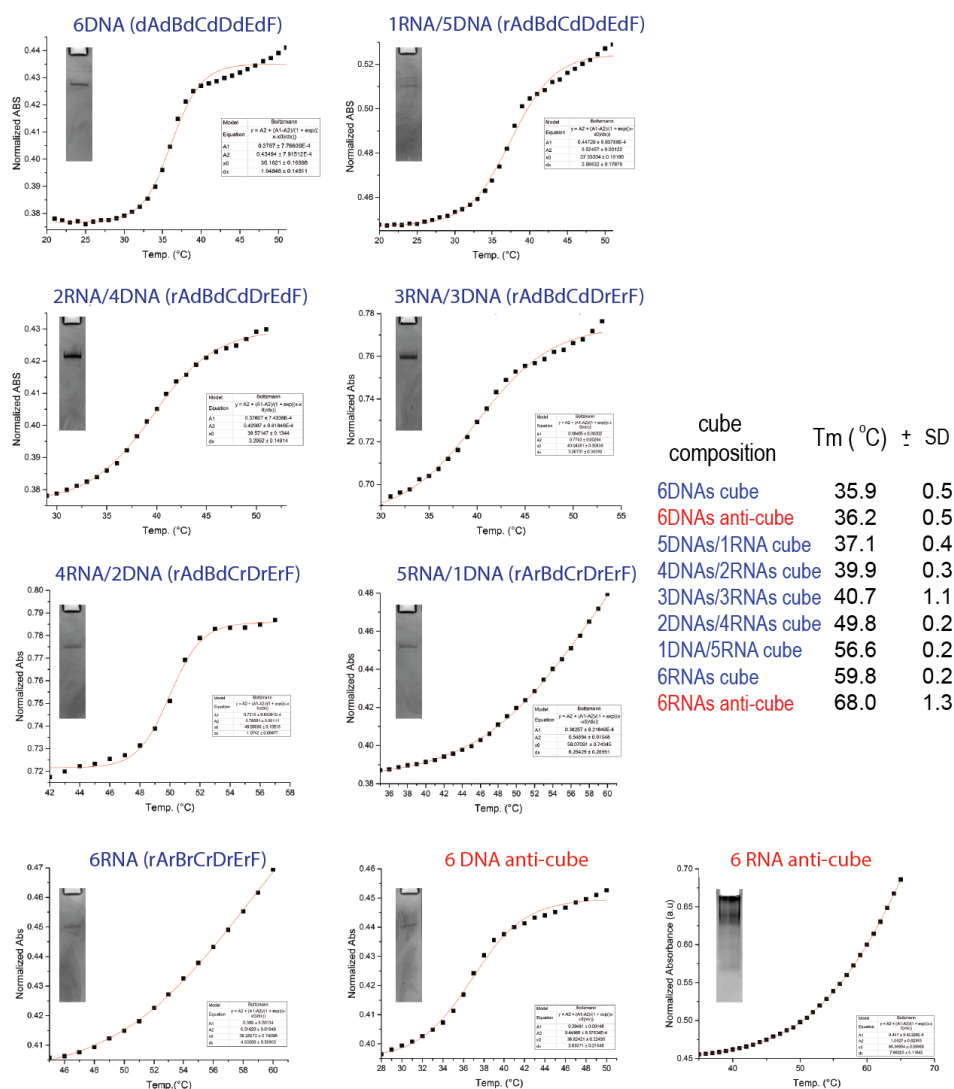


Figure 7. Melting temperatures measured by UV-melt for varying compositions of cube and anti-cube RNA, RNA/DNA, and DNA nanoparticles. EtBr total staining native-PAGE show the assemblies of corresponding compositions. Error is presented as s.d.; N=3.

nanoparticles (Fig. 6D-F). To prove this concept, seven cubes with different ratios of RNA and DNA strands in their compositions were examined. It is worth mentioning that the costs of tested nanoparticles increase by approximately a factor of two with the introduction of each RNA strand into the assembly. The assemblies of all cubes were confirmed by non-denaturing polyacrylamide gel electrophoresis (native-PAGE) and visualized by AFM (Fig. 6C). The resolution of AFM does not allow for analysis of structural details of our assemblies, but all the cube nanoparticles appear to be uniform in size and shape and monodisperse. As expected, the relative thermodynamic stability of nanoparticles increased with the higher number of RNA strands introduced into assembly, with the melting temperatures (T_m) ranging from ~ 36 °C for DNA cubes to ~ 60 °C for

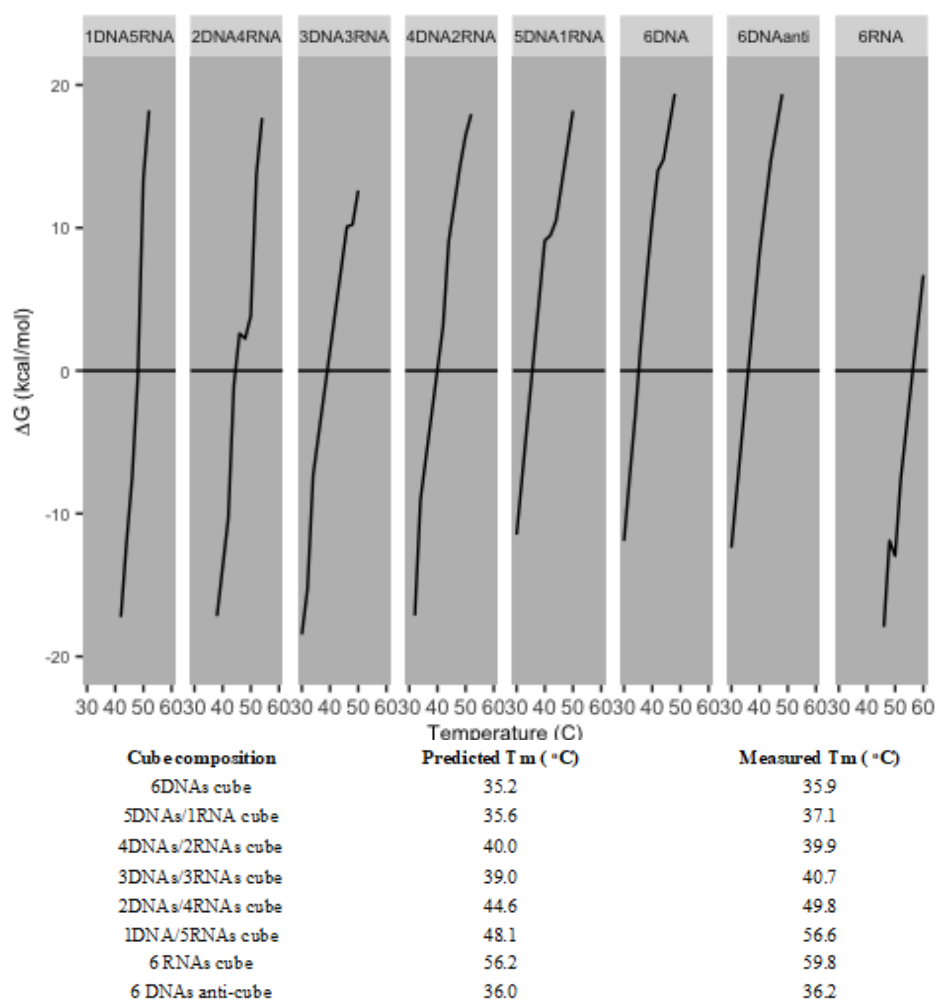


Figure 8. Predicted free energy of nucleic acid cube structures (at 250 nM concentration) as a function of temperature.

RNA cubes. Computational predictions using the new version of Hyperfold³¹ accurately confirmed the experimental results (Fig. 6D and 7-8).

Upon re-association of two complementary nanoparticles, the formation of duplexes

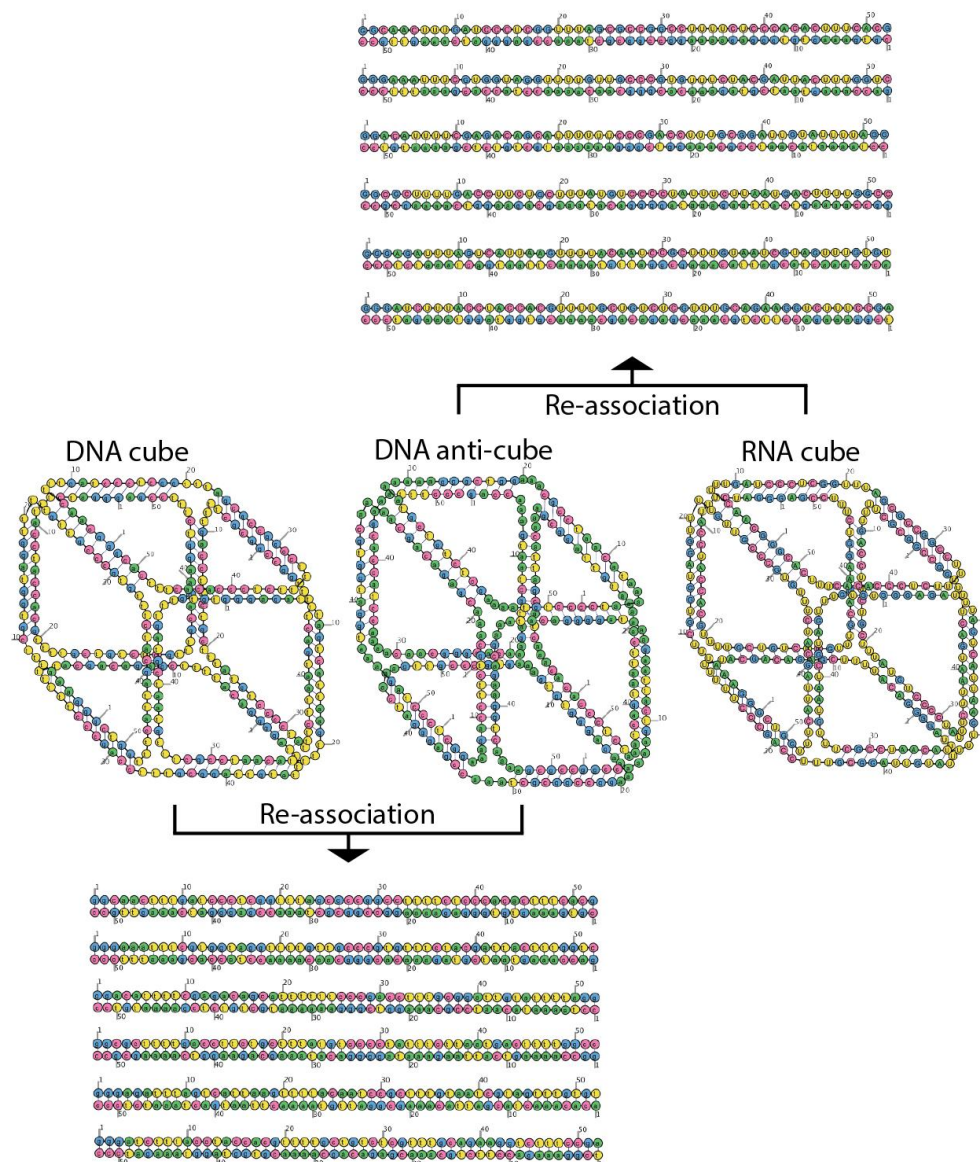


Figure 9. Computationally predicted secondary structures of RNA cube, DNA anti-cube and hybrid duplexes formed during their re-association. As described in the Methods section, secondary structure predictions were generated using HyperFold for a variety of different temperatures and different combinations of RNA and DNA strands. The depicted secondary structures are idealized secondary structures, but they are also identical to the secondary structures for low temperatures (10 °C). At higher temperatures, the predicted cube structures are similar, but some helices (especially helices consisting of only 4 or 6 base pairs) are predicted to be unfolded. This tendency is more pronounced for DNA strands compared to RNA strands.

consisting of cube and anti-cube strands was observed (Fig. 6E). The re-association of the equimolar concentrations of the cognate cubes after 30 mins of incubation was demonstrated via native-PAGE. The intact cubes had lower mobility compared to corresponding duplexes. The re-association of cognate cubes was thermodynamically driven and did not require any toehold interactions (conclusions, Thermodynamics of re-associating cubes). As described in the Methods, secondary structures for different cubes and the products of their re-associations can now be automatically predicted and generated using HyperFold (Fig. 9). The kinetics experiments (Fig. 6E and 10) demonstrated the capability to directly alter the rates of re-association by changes in the nucleic acid makeup. The higher number of RNA strands in cube composition delayed the re-association. As expected, the re-association of RNA cubes and RNA anti-cubes was the most retarded ($t_{1/2}$ ~16 min, Fig. 18). This notion was supported by the measured T_m s. The relative chemical stability and the resistance to nuclease degradation can also be tuned by changing the composition of cube (Fig. 6F).

Although synthetic RNA and DNA nanoparticles are biodegradable and commonly considered highly biocompatible, various therapeutic RNA and DNA motifs have been found to trigger the human innate immune system, leading to the induction of pro-inflammatory cytokines and type I interferons, thus complicating the translation of these novel therapeutics from bench to clinic⁴³. Consequences of such immune reaction may be severe and lead to the patient's death. For example, the Phase I clinical trial of MRX34, a nanoparticle formulated miRNA, was halted in September 2016 due to the severe cytokine storm reaction in 5 patients participating in the study (<http://investor.mirnarx.com/releasedetail.cfm?ReleaseID=990204>). To estimate immunological compatibility of DNA and RNA cubes with varying ratios of RNA to DNA strands, we assessed the immune response to these particles. This was done in primary human peripheral blood mononuclear cell cultures by measuring the activation and secretion of type I interferon (IFN α) as well as various pro-inflammatory cytokines and chemokines including IL-1 β , TNF α , IL-8, and MIP-1 α (Fig. 6G). IFN α , IL-1 β , and TNF α are common biomarkers used to estimate the pro-

inflammatory potential of nucleic acids during both normal immune responses to viral pathogens and during autoimmune responses to host nucleic acids⁴⁴⁻⁴⁵. The same markers were used in

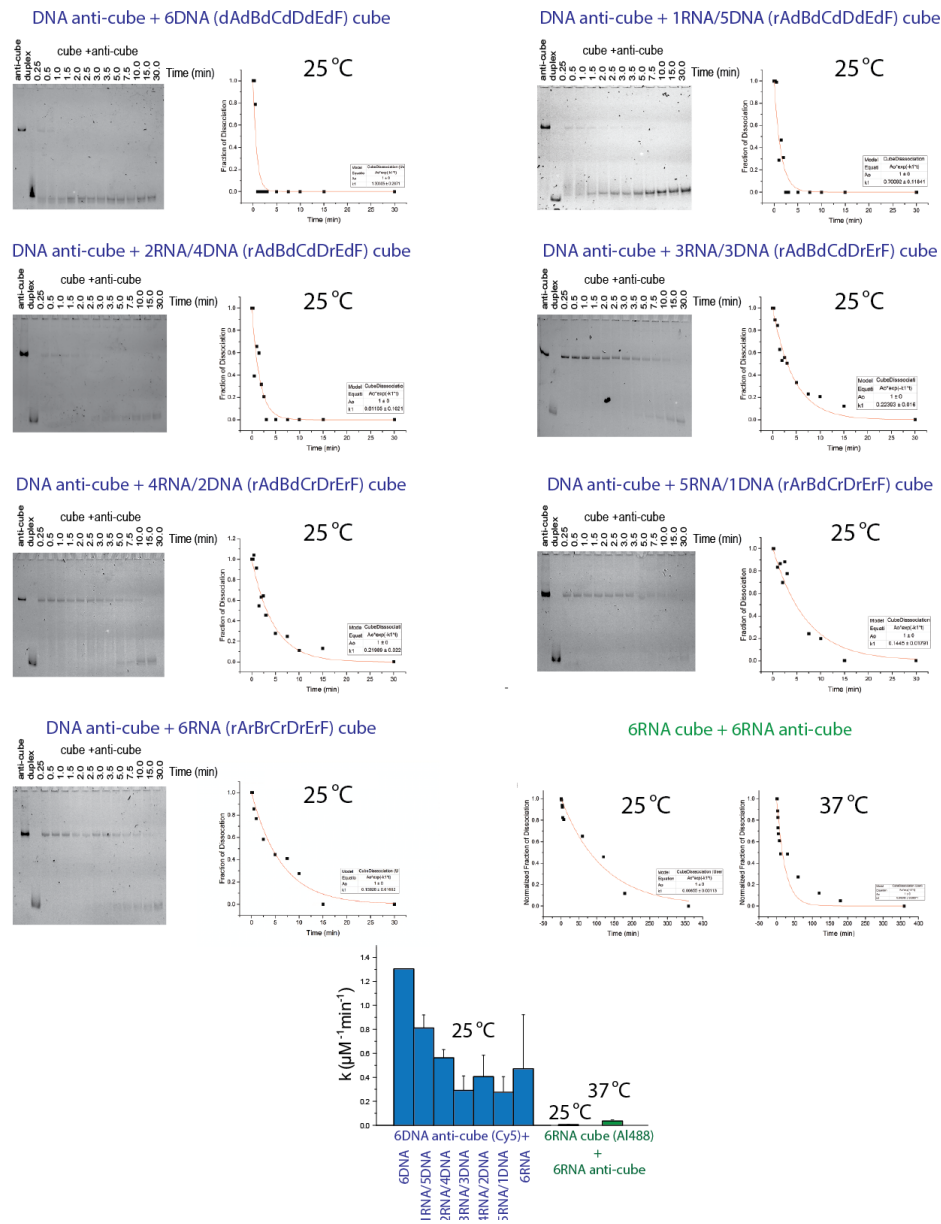


Figure 10. Relative rates of re-association measured for different compositions of nanoparticles using native-PAGE. In all experiments with DNA anti-cube (blue), gel purified anti-cube was fluorescently labeled with Cy5. For RNA anti-cube (green), RNA cube was labeled with Alexa 488. All re-association constants are summarized below. Error is presented as s.d.; N=3

(pre)clinical studies to estimate the safety of RNA therapeutics⁴⁶. We expanded this commonly used test panel by adding pro-inflammatory chemokines IL-8 and MIP-1 α ⁴⁷. To deliver nanoparticles to cells, we used Lipofectamine 2000. Such complexation was used for consistency

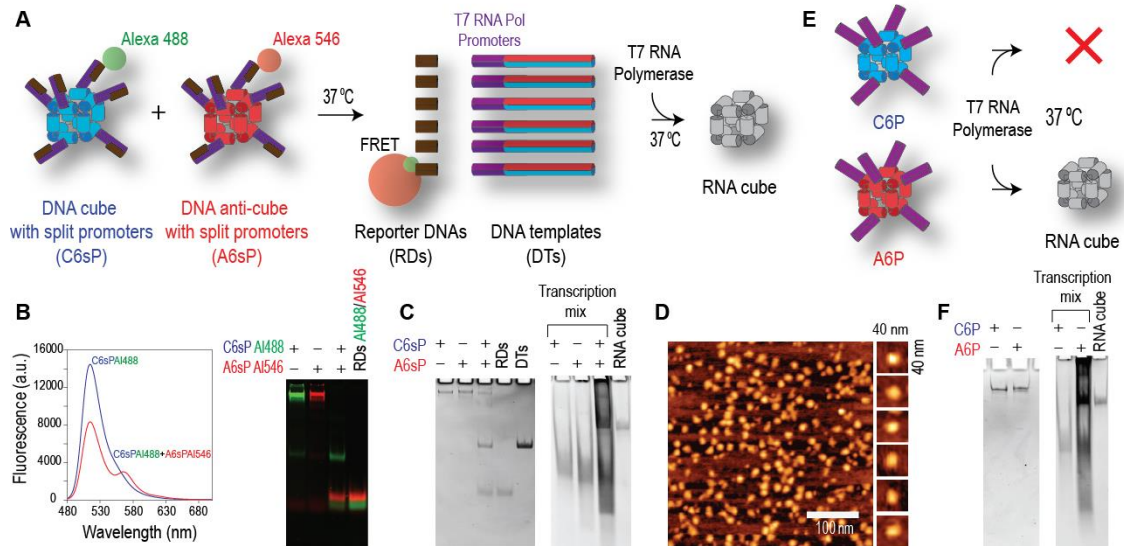


Figure 11. Isothermal re-association of complementary DNA nanoparticles activates co-transcriptional production of RNA nanoparticles. (A) Schematics of re-association between the complementary DNA cubes and anti-cubes carrying split and therefore inactive T7 RNA polymerase promoters. The re-association of DNA cubes in transcription mixture releases DNA templates with active promoters and allows for co-transcriptional assembly of RNA cubes. (B-C) Native-PAGE and fluorescence experiments visualizing re-association of shape-switching purified DNA cubes and DNA anti-cubes, resulting in formation of DNA templates with activated T7 RNA polymerase promoters and further co-transcriptional assembly of RNA cubes. (D) Co-transcriptionally assembled RNA cubes eluted from native-PAGE and imaged by AFM. (E) RNA cubes can only be formed co-transcriptionally using DNA anti-cubes decorated with six complete T7 RNA Polymerase promoters (A6P) and not from DNA cubes (C6P) due to the directionality of the promoter sequences. (F) Native-PAGE showing the co-transcriptional production of RNA cubes from DNA anti-cubes with six promoters. Following 4 hours of incubation, all transcription mixtures were treated with DNase to remove any residual DNA.

with other cellular experiments presented in this study, and because expression of the immune receptors sensing nucleic acids predominantly present in the intracellular compartments (*e.g.*, endosomes, cytosol). Although all tested constructs induced the expression of IFN α , IL-8, and MIP-1 α , cubes containing six RNA strands were more potent immune stimulants compared to other tested particles. The level of type I interferon induced by RNA cubes was comparable to positive control, a synthetic CpG oligonucleotide (ODN 2216) used as a potent vaccine adjuvant. Therefore, if interferon induction was used as a marker of immunogenicity, RNA cubes could be qualified as promising adjuvants. A similar trend was observed in the cases of pro-inflammatory cytokines IL-1 β and TNF α , which were induced only by cubes containing five or six RNA strands. The response, however, was much lower compared to the positive control, a bacterial lipopolysaccharide. High

levels of these cytokines are responsible for septic shock syndrome, while their low level is typically induced by vaccine adjuvants. The levels observed with RNA cubes were insignificant in terms of the cytokine storm or septic shock, but were at levels which may contribute to immunogenicity, thus additionally qualifying RNA cubes for a potential vaccine adjuvant application. The levels of chemokines IL-8 and MIP-1 α were raised proportionally with an

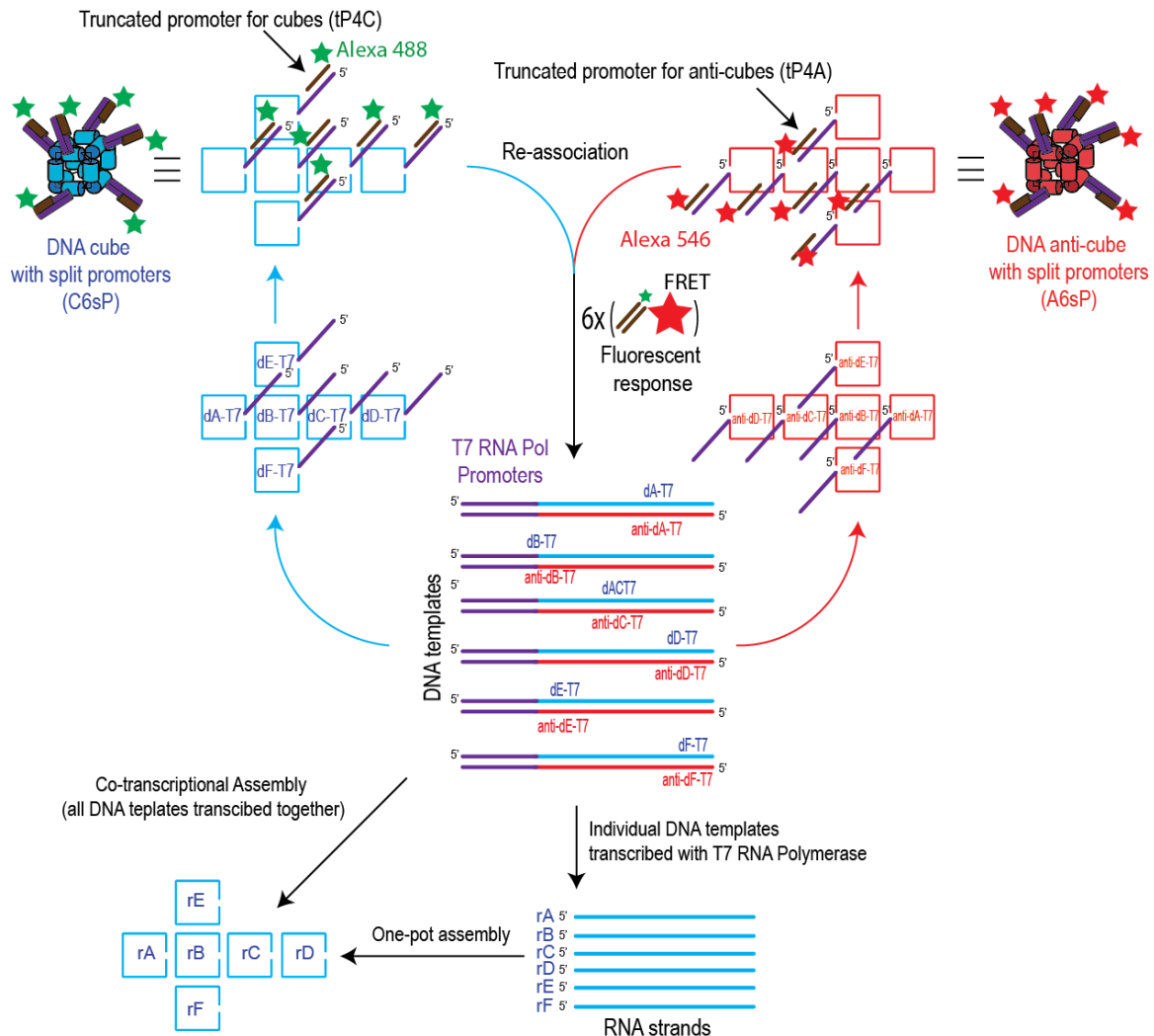


Figure 12. Design and working principles of complementary nanoparticles activating the in vitro transcription upon their re-association.

increasing number of RNA strands, except for the 2DNA/4RNA cube, which was as potent as cubes containing a higher number of RNA strands. This data suggested greater immunostimulatory potential of RNA cubes and is consistent with our earlier report³⁷. This finding also demonstrated

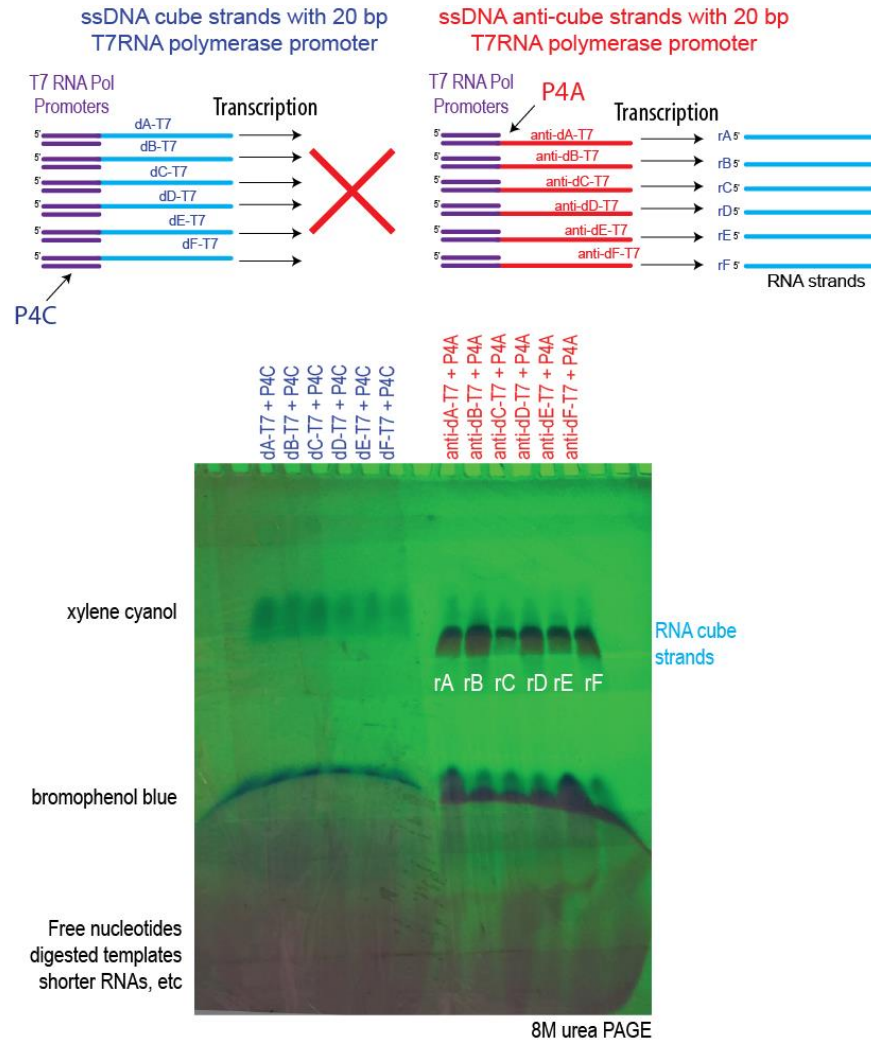


Figure 13. Denaturing 8M urea PAGE demonstrates the relative yields of transcribed individual ssDNA strands of cubes and anti-cube with dsDNA promoter for T7 RNA Polymerase and schematics explaining the process. The bands are visualized by UV shadowing.

that the reduction in number of RNA strands is a viable strategy for reducing any undesirable immunostimulation of these nanoparticles if they are used for systemic delivery. It further suggested that by simply optimizing the ratio between RNA and DNA strands, resulting assemblies that did not induce pro-inflammatory cytokines (*e.g.*, DNA cubes) could be used for drug delivery while RNA cubes with optimal immunomodulatory properties could be used for vaccines and immunotherapy. The precise mechanism of the immune recognition of the particles reported herein is a subject for a separate mechanistic study.

2.3.2 Re-association of complementary DNA nanoparticles triggers co-transcriptional formation of RNA nanoparticles

The ability to activate the simultaneous transcription of multiple RNAs and further co-transcriptional assembly of RNA nanostructures is an important step towards the intracellular production of RNA nanoparticles. The endogenous production of functional RNA nanoparticles in mammalian cells will substantially increase their yields while eliminating the complexity of assembly protocols and reducing possible endotoxin contamination. In the attempt to control the transcription with complementary nanoparticles, all six DNA strands of cube and anti-cube were modified with split 20 bps T7 RNA polymerase promoters (Fig. 11A and 12). T7 RNA polymerase

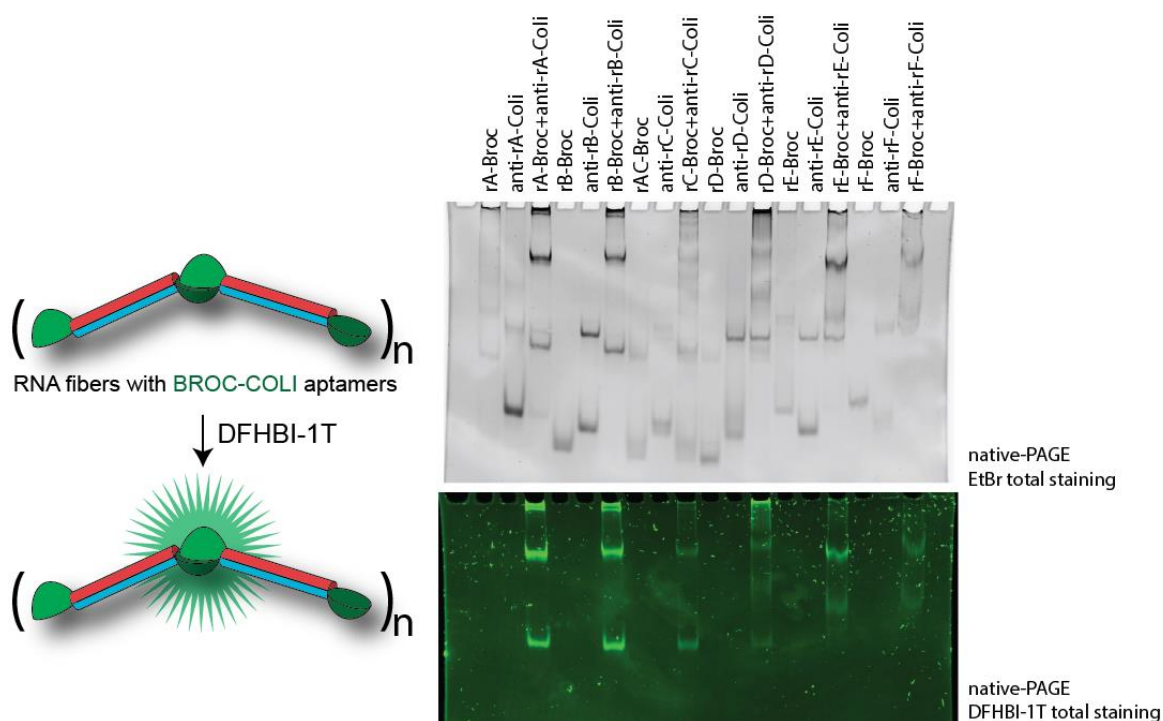


Figure 14. Activation of functional aptamers with isothermal re-association of shape-switching nanoparticles. (A) Schematics of isothermal re-association and re-assembly of aptamers. (B) Total EtBr and DFHBI-1T stained native-PAGE demonstrates fiber formation and aptamer activation on re-association of cognate cubes. (C) AFM images of the aptamer containing fibers. (D) Re-association and fiber formation can be traced by measuring fluorescence of DFHBI-1T in vitro. Error bars indicate s.d.; N=3.

is a single-subunit enzyme that can be expressed in mammalian cells⁴⁸ and does not require any additional factors for accurate transcription. In the current design, the presence of both

complementary DNA cubes in a transcription mixture was required to undergo shape-switching and formation of dsDNA templates with active T7 RNA polymerase promoters whose further transcription leads to the assembly of RNA cubes. Short reporter DNAs were used to provide an optical response upon re-association (Fig. 11B). The co-transcriptionally assembled RNA cubes can be gel purified (Fig. 11C) and visualized by AFM (Fig. 11D). Even though the co-transcriptional assembly of RNA cubes was efficiently triggered by the re-association of two parent DNA cubes, the run-off transcription of multiple individual DNA templates may not be ideal for co-transcriptional assembly of RNA nanoparticles in the intracellular environment due to potential degradation or compartmentalization of some DNAs, causing stoichiometry problems with transcribed RNA units. To overcome this possible problem, the DNA anti-cube decorated with six complete T7 promoters (Fig. 11E) can be used. We then have an assembly of individually potent ssDNA templates (Fig. 13) required for the co-transcriptional production of RNA cubes (Fig. 11F). The advantage of this approach is the precise control over the stoichiometry of the DNA templates

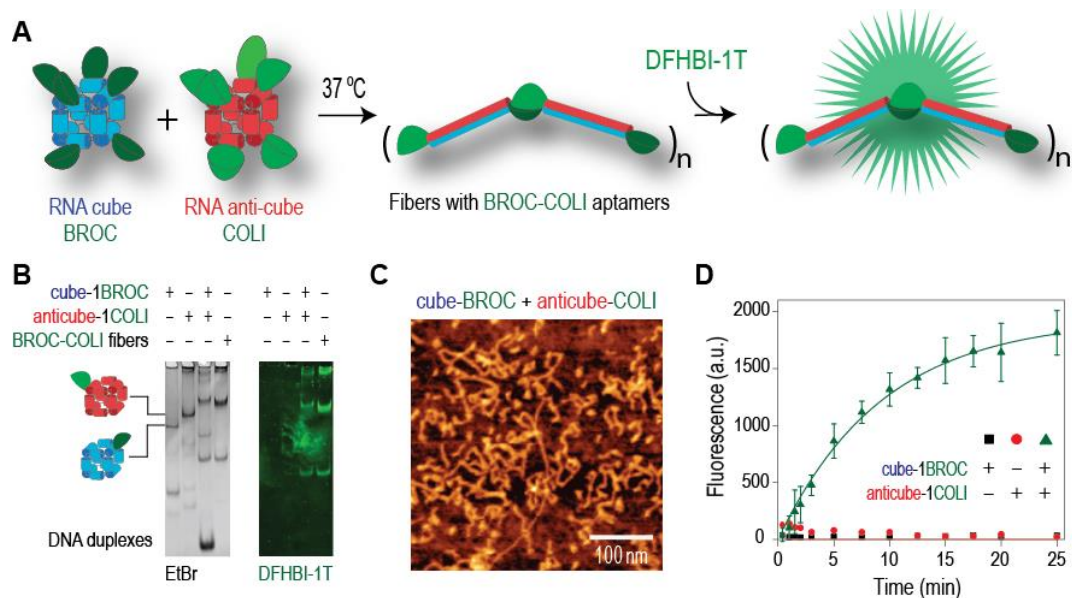


Figure 15. Fiber formation and simultaneous activation of multiple BROCCOLI aptamers. Schematics of activation of aptamers and total EtBr and DFHBI-1T stained native-PAGE demonstrates fiber formation and aptamer activation when stained with DFHBI-1T

and their local availability for transcription. These results paved the way for further development of the intracellular co-transcriptional production of RNA nanoparticles.

2.3.3 Re-association of complementary DNA nanoparticles triggers activation of embedded split RNA aptamers

Broccoli is a synthetic RNA aptamer which binds to the fluorophore DFHBI-1T to mimic the fluorescent spectrum of green fluorescent protein (GFP)⁴⁹. We hypothesized that the splitting of the Broccoli aptamer sequence into two separate non-functional strands (named Broc and Coli)

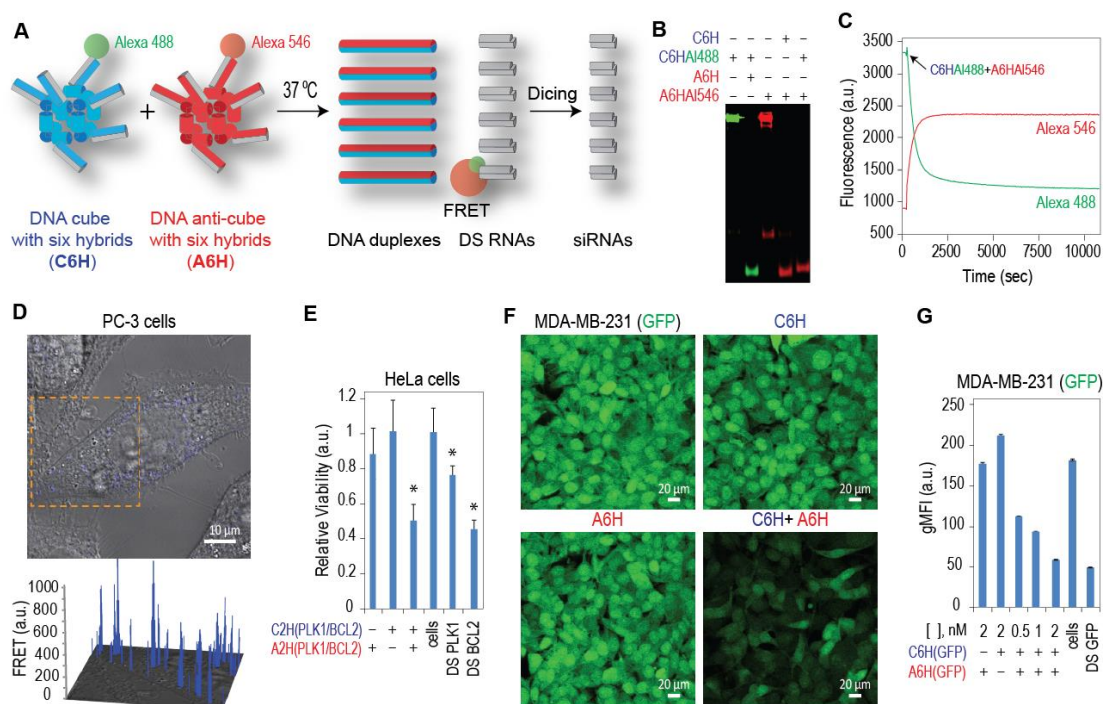


Figure 16. Activation of RNA interference and intracellular FRET with complementary shape-switching nanoparticles. (A) Schematics of isothermal re-association and activation of FRET and RNAi. (B) In vitro re-association of fluorescently labeled cubes and anti-cubes with split DS RNAs was visualized by native-PAGE. (C) FRET time traces during re-association of fluorescently labeled Alexa 488 and Alexa 546 cubes and anti-cubes carrying split Dicer Substrate RNAs (DS RNAs). (D) For intracellular FRET experiments, human prostate cancer (PC-3) cells were co-transfected with fluorescently labeled cubes and anti-cubes and images were taken on the next day. (E) Cell viability assay for HeLa cells transfected with nanoparticles (at 5 nM final) designed to release two DS RNAs against PLK1 and BCL2. Error bars indicate s.d.; N=3. Statistically significant results (compared to control cells) are indicated with asterisks (p-value < 0.05). (F-G) GFP knockdown assays for human breast cancer cells expressing enhanced GFP (MDA-MB-231/GFP). Prior to transfection, formation of the nanocubes was verified by total EtBr staining of native-PAGE. Three days after the transfection of cells, GFP expression was analyzed with fluorescent microscopy (F) and flow cytometry (G). As the control, pre-formed DS RNAs (at 2 nM final) against PLK1, BCL2, and GFP were used for HeLa and MDA-MB-231 cells respectively. At concentrations higher than 10 nM, some gene silencing was observed for cubes carrying antisense DS RNAs (data not shown). Note that the individual cubes and anti-cubes cause no decrease in GFP production. gMFI corresponds to the geometric mean fluorescence intensity. Error bars denote SEM.

can be used for monitoring the cube and anti-cube interaction and shape-switching that leads to Broc and Coli re-assembly into an active fluorescent aptamer (Fig. 14A). Furthermore, this approach demonstrates the general strategy for conditional re-activation of disconnected functional ssRNAs with complex secondary structure. As predicted, the interaction of Broc-cubes with Coli-anti-cubes leads to the formation of fiber-like structures (Fig. 14B-C) containing re-assembled Broc-Coli aptamers, thus providing an alternative optical response of interdependent nanocube interactions. The response was confirmed by native-PAGE (Fig. 14B and 15) and fluorescent measurements (Fig. 14D). Flow cytometry analysis of human cervical cancer cells co-transfected with complementary nanoparticles bearing the split aptamer strands revealed some Broc-Coli re-association into the functional structure, however the difference was not statistically significant compared to just cells treated with the dye (data not shown).

2.3.4 Re-association of complementary nanoparticles triggers activation of energy transfer and RNA interference in cells

RNAi is a naturally occurring post-transcriptional gene regulation process which represses the expression of specific genes⁵⁰. Therefore, exploiting endogenous RNAi mechanisms by externally delivered RNAi inducers is a promising tool in biotechnology and therapy. To have additional control over the initiation of targeted gene silencing is an important step forward leading towards the construction of intracellular logic gates and smart nanoparticles. We decorated two sets of cognate DNA cubes and anti-cubes with split Dicer Substrate (DS) RNAs against either (i) BCL2 and PLK1⁵¹, well-validated molecular targets whose down-regulation induces apoptosis⁵²⁻⁵³, or (ii) GFP⁵⁴. The re-association of the cube and anti-cube nanoparticles led to the formation of DS RNAs that could be further activated through dicing by releasing the functional siRNAs (Fig. 16A). Additionally, split DS RNAs can be fluorescently labeled with dyes (*e.g.*, Alexa 488 and Alexa 546) chosen to undergo FRET. Thus, the shape-switching of labeled nanoparticles was not only directly visualized by native-PAGE (Fig. 16B), but also assessed in real time using FRET (Fig. 16C). With the same approach, the intracellular re-association of cubes and anti-cubes in human

prostate, breast, and cervical cancer cells was traced by FRET (Fig. 16D and 17). For activation of RNA interference, human cervical cancer cells were treated with nanoparticles releasing BCL2 and PLK1 DS RNAs (Fig. 4E and 18A). The cell viability was significantly decreased when both cubes

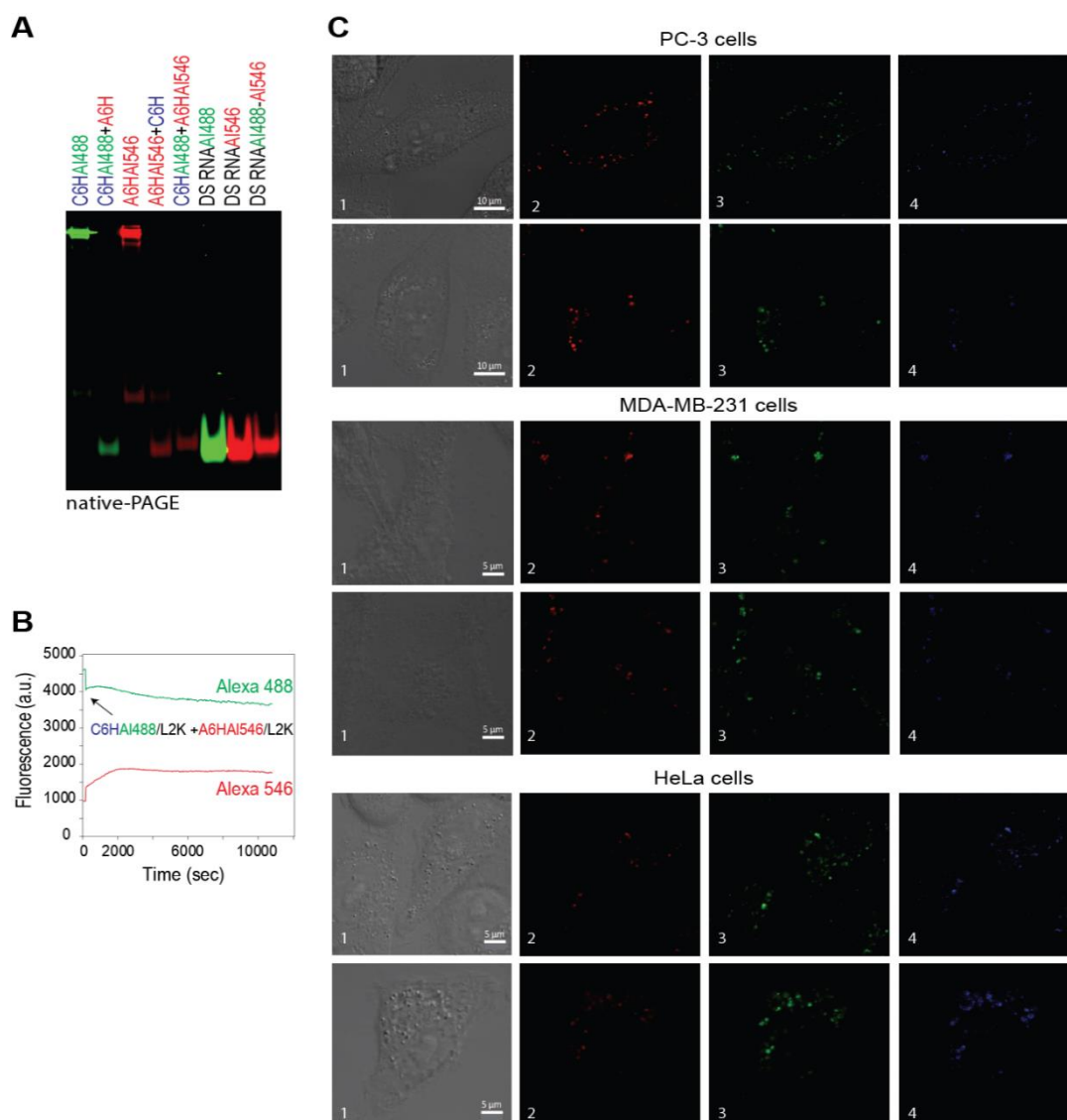


Figure 17. Activation of FRET with complementary shape switching nanoparticles. (A) *In vitro* re-association of fluorescently labeled cubes and anti-cubes with split Dicer Substrate (DS) RNAs was visualized by native-PAGE. (B) Fluorescence time traces show no re-association between the fluorescently labeled Alexa 488 and Alexa 546 cubes and anti-cubes carrying split DS RNAs when associated with Lipofectamine 2000 (L2K). (C) For intracellular FRET experiments, human prostate cancer (PC-3) and breast cancer (MDA-MB-231) cells were co-transfected with fluorescently labeled cubes and anti-cubes and images were taken the next day. Numbers at each image correspond to (1) differential interference contrast images, (2) Alexa 488 emission, (3) Alexa 546 emission, (4) bleed-through corrected FRET image.

were introduced, while individual cubes did not show much effect. To show the generality of the RNAi induction approach, GFP-expressing breast cancer cells were treated with complementary cubes releasing DS RNAs targeting GFP. The extent of GFP silencing was assessed with fluorescent microscopy and quantified by flow cytometry (Fig. 16F-G). The results showed an

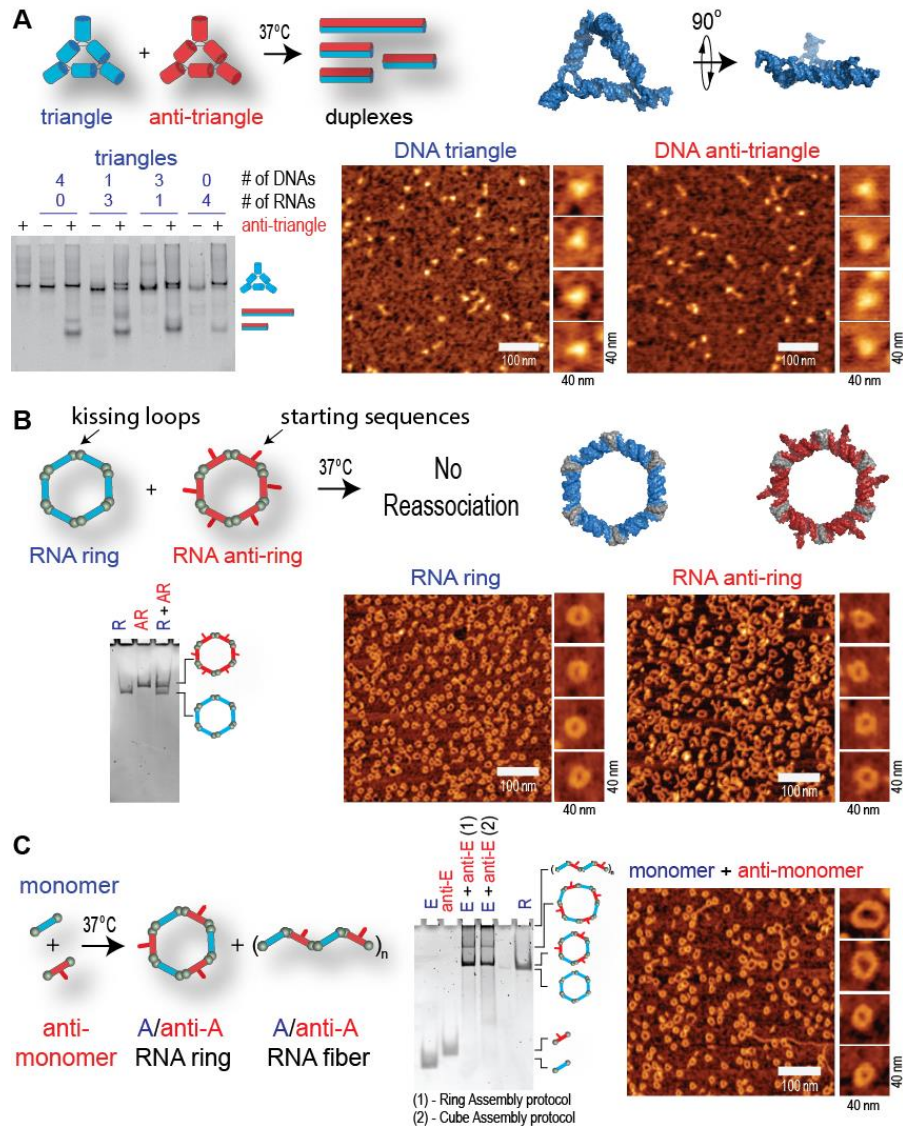


Figure 18 Ring and anti-ring nanoparticles do not re-associate but cognate monomers form rings and fibers. (A) Schematics of isothermal re-association of triangles and anti-triangles. AFM of triangles and anti-triangles and native-PAGE of re-associated anti-triangles with triangles after 30 mins of incubation. (B) AFM images of RNA rings and anti-rings and native-PAGE showing that they do not interact. (C) The individual monomers of rings and anti-rings form the mixture of hexameric rings and fiber-like structures as shown by native-PAGE and AFM.

efficient knock-down of GFP production upon the intracellular re-association of cubes and anti-cubes functionalized with six split DS RNAs. In comparison, transfection of cells with individual cubes or anti-cubes did not result in GFP silencing. Re-association occurs intracellularly, as suggested by FRET showing that individual cubes and anti-cubes associated with transfection agent do not re-associate in solution (Fig. 17B). Efficient GFP silencing was observed at picomolar concentrations of complementary cubes (Fig. 18B).

2.3.5 Other examples of complementary nanoparticles

With the same design principles, several additional complementary nanoparticles were created by using previously characterized RNA triangles⁴⁰ and RNA rings³⁹ and their reverse complements (Fig. 19). We expected that co-incubation of the cognate pairs will lead to the similar collapse of each structure and recombination of smaller subunits as seen in the cube and anti-cube pairs. However, while native-PAGE results showed that the incubation of triangles with anti-triangles led to the shape-switching (Fig. 19A), the rings and anti-rings did not interact (Fig. 19B). The explanation was offered by comparing ring designing principles with the cube and triangle structures. RNA nanorings did not have exposed single bases like cubes and triangles have in their

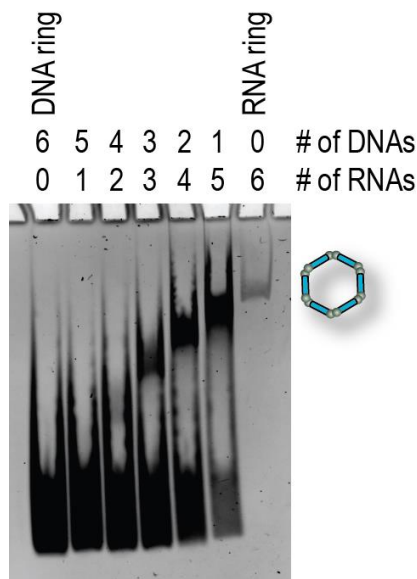


Figure 19. Assembly of RNA and DNA ring monomers show no assembly for nanorings due to lack of kissing loop interactions

corners; rather, the rings were formed through interstrand RNA-RNA “kissing loops” (KL). Therefore, due to the absence of exposed bases, the reverse complement strands were unable to elicit shape-switching, and each ring remains intact as is visualized using native-PAGE stained with ethidium bromide (Fig. 19B). The use of RNA tertiary interacting motifs (KL) also prevented rings from forming RNA/DNA or DNA/DNA structures (Fig. 20), as opposed to cubes and triangles. The use of complementary rings provided a simple way of expanding the library of the novel programmable nanoscaffolds based on the existing nanodesigns, thus eliminating any laborious computational design and experimental verification. Although the intact rings would not interact, their individual subunits were complementary and formed both hexameric and octameric rings as well as elongated fiber-like structures as verified by native-PAGE and AFM (Fig. 5C and 21A). The fabrication of these structures was accomplished using both the established ring and cube assembly protocol, which differ only in the incubation profile. Depending on the kissing loop sequence, the formation of either fibers (*e.g.*, A and anti-A) or rings (*e.g.*, F and anti-F) can be promoted (Fig. 21A). The formation of functional fibers and rings was achieved by functionalizing one of the monomers (Fig. 21B).

Thermodynamics of re-associating cubes

At 20 °C, 250 nM, we obtained the following free energies of predicted structures for the following nucleic acid strand combinations:

Structure	Free Energy (kcal/mol)
RNA cube	-125.01
DNA cube	-41.04
DNA anti-cube	-41
RNA/DNAa duplexes	-305.67
DNA/DNAa duplexes	-318.61

For the re-association of RNA cube and DNA anti-cube we obtain:

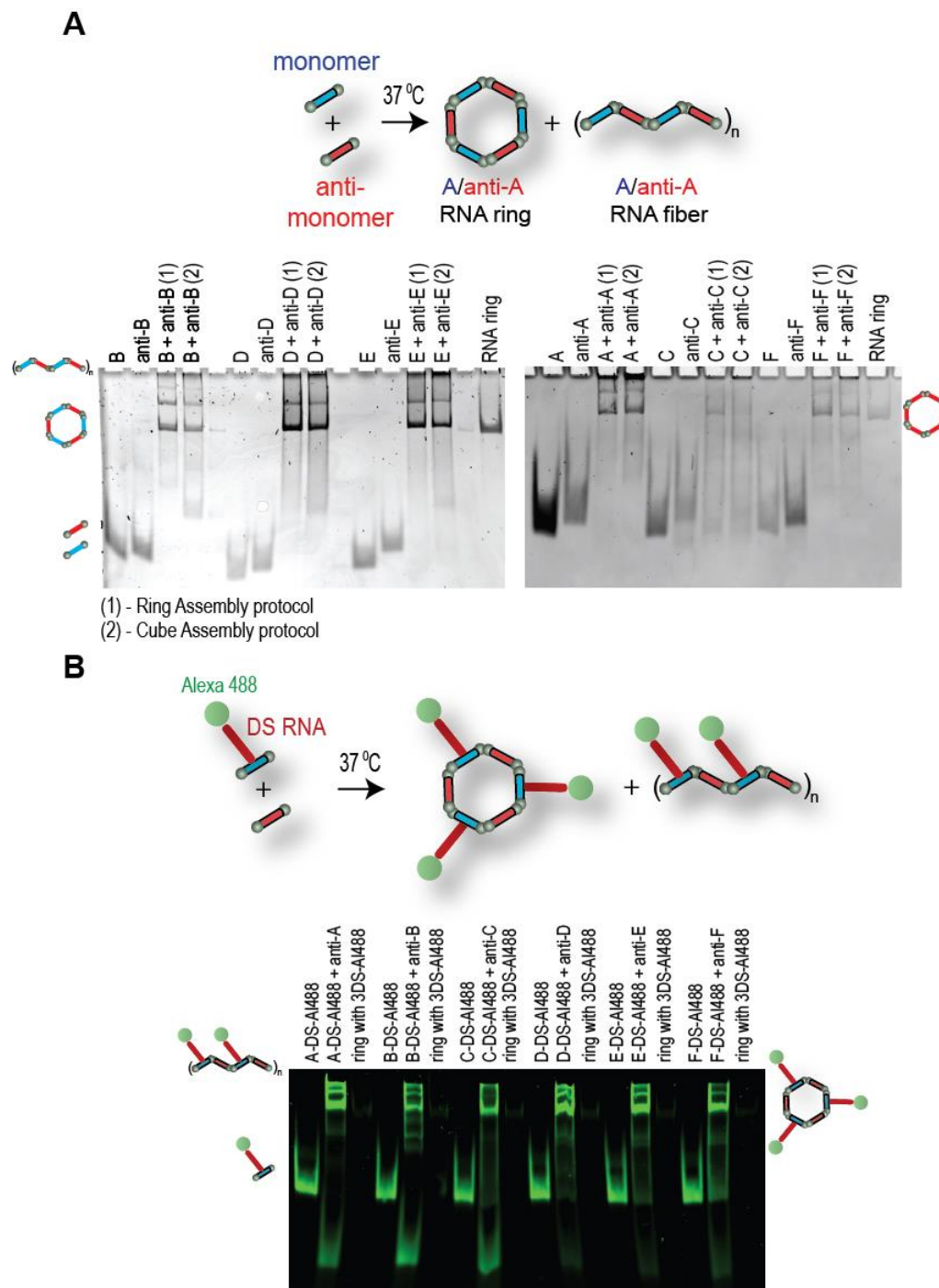


Figure 20. Contrary to assembled rings, individual ring monomers and anti-ring monomers form a mixture of ring and fiber structures as shown by native-PAGE. (A) Assemblies of non-functionalized monomers. Two different assembly protocols explained in methods were tested. Depending on the kissing loop sequence the formation either of fibers (e.g., A and anti-A) or rings (e.g., F and anti-F) can be promoted. (B) Assembly of monomers functionalized with DS RNAs and Alexa 488 led to the formation of functional fibers and rings.

$$\Delta\Delta G = \Delta G_{RNA/DNAa} - \Delta G_{RNA} - \Delta G_{DNAa}$$

$$\Delta\Delta G = -305.67\text{kcal/mol} - (-125.01)\text{kcal/mol} - (-41)\text{kcal/mol} = -139.67\text{kcal/mol}$$

In contrast, for the re-association of the DNA cube with the DNA anti-cube we obtain:

$$\Delta\Delta G = \Delta G_{DNA/DNAa} - \Delta G_{DNA} - \Delta G_{DNAa}$$

$$\Delta\Delta G = -318.61\text{kcal/mol} - (-41.04)\text{kcal/mol} - (-41)\text{kcal/mol} = -236.57\text{kcal/mol}$$

There appears to be a large energetic difference: while the RNA/DNA hybrid duplexes are similar in energy compared to DNA/DNA duplexes, it is the RNA cube that is energetically far more stable compared to the DNA cube and less apt to participate in the re-association reaction.

Another role may be at play; the DNA cube is more likely to be partially unfolded compared to the RNA cube, thus providing additional toehold-like regions that may aid the re-association.

However, the kinetics of re-association were tracked experimentally at 25 °C, which is below the T_m of DNA cubes (Fig. 8).

Both of these effects are contributing to the experimentally observed tendency, that the DNA cube combined with the DNA anti-cube are re-associating far more readily compared to the RNA cube combined with the DNA anti-cube.

2.4 Conclusion

Diverse examples of mutual relations between interdependent entities exist in nature both at the levels of ecosystems and individual molecular interactions. Herein, we present a new concept of dynamic interdependent nucleic acid nanoparticles. Our approach relies on the physical interaction of two complementary nanoparticles with controllable thermodynamic and chemical properties. Our findings also suggest that by simply optimizing the ratio between RNA and DNA strands entering the composition of assemblies, one can create nanoparticles with optimal immunomodulatory properties when activation of the immune system is desirable (*e.g.*, vaccines and immunotherapy). However, other types of RNA nanoparticles may expose different immunomodulatory properties⁵⁵. After interaction of the cognate nanoparticles both *in vitro* and in

human cells, as demonstrated in three different cell lines, constructs undergo isothermal shape-switching resulting in activation of one or more functionalities including RNAi, optical response, transcription, and split aptamer re-assembly. Importantly, only two nanoparticles are required to simultaneously activate multiple functionalities and no ssRNA or ssDNA toeholds are needed to initiate the interaction. Moreover, in the case of co-transcriptional assemblies, only one specifically designed DNA nanoparticle is needed to efficiently produce an RNA counterpart. Overall, the presented strategy allows for the use of simple, multifunctional, and conditionally activated nanoparticles and provides a promising future for their use in nanobioscience.

2.4.1 Sequences used in this project

DNA cube with three Ts at each corner

dA

5'-GGCAACTTTGATCCCTCGGTTTAGCGCCGGCCTTTTCTCCCACACTTTCACG

dB

5'-GGGAAATTTTCGTGGTAGGTTTTGTTGCCCGTGTTTCTACGATTACTTTGGTC

dC

5'-GGACATTTTCGAGACAGCATTTTTTCCCGACCTTTGCGGATTGTATTTTAGG

dD

5'-GGCGCTTTTGACCTTCTGCTTTATGTCCCCTATTTCTTAATGACTTTTGGCC

dE

5'-GGGAGATTTAGTCATTAAGTTTTACAATCCGCTTTGTAATCGTAGTTTGTGT

dF

5'-GGGATCTTTACCTACCACGTTTTGCTGTCTCGTTTGCAGAAGGTCTTTCCGA

Fluorescently labeled DNA cube strand

dD-Alexa 488

5'-GGCGCTTTTGACCTTCTGCTTTATGTCCCCTATTTCTTAATGACTTTTGGCC-Alexa
488

DNA anti-cube with three As at each corner

anti-dA

5'-CGTGAAAGTGTGGGAGAAAAGGCCGGCGCTAAACCGAGGGATCAAAGTTGCC

anti-dB

5'-GACCAAAGTAATCGTAGAAACACGGGCAACAAAACCTACCACGAAATTTCCC

anti-dC

5'-CCTAAAATACAATCCGCAAAGGTCGGGAAAAAATGCTGTCTCGAAAATGTCC

anti-dD

5'-GGCCAAAAGTCATTAAGAAATAGGGGACATAAAGCAGAAGGTCAAAGCGCC

anti-dE

5'-ACACAAACTACGATTACAAAGCGGATTGTA AAACTTAATGACTAAATCTCCC

anti-dF

5'-TCGAAAAGACCTTCTGCAAACGAGACAGCAAAACGTGGTAGGTAAAGATCCC

Fluorescently labeled anti-DNA cube strand**anti-dA-Cy5**

5'-CGTGAAGTGTGGGAGAAAAGGCCGGCGCTAAACCGAGGGATCAAAGTTGCC-Cy5

RNA cube with three Us at each corner²**rA**

5'-GGCAACUUUGAUCCUCGGUUUAGCGCCGGCCUUUCUCCACACUUUCACG

rB

5'-GGGAAAUUCGUGGUAGGUUUUGUUGCCCGUGUUUCUACGAUUACUUUGGUC

rC

5'-GGACAUUUUCGAGACAGCAUUUUUCCCGACCUUUGCGGAUUGUAUUUUAGG

rD

5'-GGCGCUUUUGACCUUCUGCUUUUAUGUCCCCUAUUUCUUAUGACUUUUGGCC

rE

5'-GGGAGAUUUAGUCAUUAAGUUUUACAAUCCGCUUUGUAAUCGUAGUUUGUGU

rF

5'-GGGAUCUUUACCUACCACGUUUUGCUGUCUCGUUUGCAGAAGGUCUUUCCGA

Fluorescently labeled RNA cube strand**rD-Alexa 488**

5'-GGCGCUUUUGACCUUCUGCUUUUAUGUCCCCUAUUUCUUAUGACUUUUGGCC-Alexa 488

RNA anti-cube with three As at each corner

(lower case nucleotides were added for higher in vitro transcription yields)

anti-rA

5'-ggCGUGAAAGUGUGGGAGAAAAGGCCGGCGCUAAACCGAGGGGAUCAAGUUGCC

anti-rB

5'-ggGACCAAAGUAAUCGUAGAAACACGGGCAACAAAACCUACCACGAAAUUCCC

anti-rC

5'-

ggaCCUAAAAUACAAUCCGCAAAGGUCGGGAAAAAAUGCUGUCUCGAAAAUGUCC

anti-rD

5'-gGGCCAAAAGUCAUUAAGAAAUAGGGGACAUAAGCAGAAGGUCAAAAGCGCC

anti-rE

5'-ggACACAAACUACGAUUACAAAGCGGAUUGUAAAACUUAUGACUAAAUCUCCC

anti-rF

5'-

gggaUCGGAAAGACCUUCUGCAAACGAGACAGCAAAACGUGGUAGGUAAAGAUGCC

**DNA cube with three Ts at each corner and with T7RNA polymerase promoter
(underlined)****dA-T7**

5'TTCTAATACGACTCACTATAGGCAACTTTGATCCCTCGGTTTAGCGCCGGCCTTTTC
TCCACACTTTCACG

dB-T7

5'TTCTAATACGACTCACTATAGGGAAATTTTCGTGGTAGGTTTTGTTGCCCGTGTCT
ACGATTACTTTGGTC

dC-T7

5'TTCTAATACGACTCACTATAGGACATTTTCGAGACAGCATTTTTCCCGACCTTGC
GGATTGTATTTTAGG

dD-T7

5'TTCTAATACGACTCACTATAGGCGCTTTTGACCTTCTGCTTTATGTCCCCTATTTCT
AATGACTTTTGGCC

dE-T7

5'TTCTAATACGACTCACTATAGGGAGATTTAGTCATTAAGTTTTACAATCCGCTTGT
AATCGTAGTTTGTGT

dF-T7

5'TTCTAATACGACTCACTATAGGGATCTTTACCTACCACGTTTTGCTGTCTCGTTTGC
AGAAGGTCTTCCGA

Complementary strand for active 20 bps T7 promoter attached to cubes

Promoter for cubes (P4C)

5'-TATAGTGAGTCGTATTAGAA

Truncated strand (with Alexa 488) for split, inactive, T7 promoter attached to cubes

Truncated promoter for cubes (tP4C)

5'-ATAGTGAGTCG-Alexa 488

DNA anti-cube with three As at each corner with T7RNA polymerase promoter

anti-dA-T7

5'CGTGAAAGTGTGGGAGAAAAGGCCGGCGCTAAACCGAGGGATCAAAGTTGCCTAT
AGTGAGTCGTATTAGAA

anti-dB-T7

5'GACCAAAGTAATCGTAGAAACACGGGCAACAAAACCTACCACGAAATTTCCCTAT
AGTGAGTCGTATTAGAA

anti-dC-T7

5'CCTAAAATACAATCCGCAAAGGTCGGGAAAAAATGCTGTCTCGAAAATGTCCTAT
AGTGAGTCGTATTAGAA

anti-dD-T7

5'GGCCAAAAGTCATTAAGAAATAGGGGACATAAAGCAGAAGGTCAAAGCGCCTAT
AGTGAGTCGTATTAGAA

anti-dE-T7

5'ACACAAACTACGATTACAAAGCGGATTGTAAACTTAATGACTAAATCTCCCTATA
GTGAGTCGTATTAGAA

anti-dF-T7

5'TCGGAAAGACCTTCTGCAAACGAGACAGCAAACGTGGTAGGTAAAGATCCCTAT
AGTGAGTCGTATTAGAA

Complementary strand for 20 bps T7 promoter attached to anti-cubes

Promoter for anti-cubes (P4AC)

5'-TTCTAATACgACTCACTATA

**Truncated strand (with Alexa 546) for split, inactive, T7 promoter attached to anti-cubes
Truncated promoter for cubes (tP4AC)**

5'-Alexa 546-CgACTCACTAT

Split F30 BROCCOLI aptamer

(5'-gggaa sequences were added for higher in vitro transcription yields)

F30 broccoli¹⁵

5'gggaaagUUGCCAUGUGUAUGUGGGAGACGGUCGGGUCCAGAUAUUCGUAUCUGUC
GAGUAGAGUGUGGGCUCCCACAUACUCUGAUGAUCCUUCGGGAUCAUUCAUGGCA
A

Split aptamer:

BROC

5'gggaaaUUGCCAUGUGUAUGUGGGAGACGGUCGGGUCCAGAUAAU

COLI

5'gggaaaCGUAUCUGUCGAGUAGAGUGUGGGCUCCCACAUACUCUGAUGAUCCUUCG
GGAUCAUUCAUGGCAA

**RNA cube with three Us at each corner and BROC to form fibers with embedded aptamers
on re-association with anti-cubes**

(5'-gggaa sequences were added for higher in vitro transcription yields)

rA_BROC_fiber

5'gggaaUUGCCAUGUGUAUGUGGGAGACGGUCGGGUCCAGAUAAUUGGCAACUUUGA
UCCCUCGGUUUAGCGCCGCCUUUCUCCCACACUUUCACG

rB_BROC_fiber

5'gggaaUUGCCAUGUGUAUGUGGGAGACGGUCGGGUCCAGAUAAUUGGAAAUUUCG
UGGUAGGUUUUGUUGCCCGUGUUUCUACGAUUACUUUGGUC

rC_BROC_fiber

5'gggaaUUGCCAUGUGUAUGUGGGAGACGGUCGGGUCCAGAUAAUUGGACAUUUUCG
AGACAGCAUUUUUCCCGACCUUUGCGGAUUGUAUUUUAGG

rD_BROC_fiber

5'gggaaUUGCCAUGUGUAUGUGGGAGACGGUCGGGUCCAGAUAAUUGGCGCUUUUGA
CCUUCUGCUUUUAUGUCCCCUAUUUCUAAUGACUUUUUGGCC

rE_BROC_fiber_terminal

5'gggaaUUGCCAUGUGUAUGUGGGAGACGGUCGGGUCCAGAUAAUUGGAGAUUUAG
UCAUUAAGUUUUACAUCCGCUUUGUAAUCGUAGUUUGUUGCAUGUGUAU
GUGGGAGACGGUCGGGUCCAGAUAAU

RNA anti-cube with three As at each corner and COLI

(5'-gggaa sequences were added for higher in vitro transcription yields)

anti-rA_COLI

5'gggaaCGUAUCUGUCGAGUAGAGUGUGGGCUCCCACAUACUCUGAUGAUCCUUCG
GGAUCAUUCAUGGCAACGUGAAAGUGUGGGAGAAAAGGCCGCGCUAAACCGAGG
GAUCAAGUUGCC

anti-rB_COLI

5'gggaaCGUAUCUGUCGAGUAGAGUGUGGGCUCCCACAUACUCUGAUGAUCCUUCG
GGAUCAUUCAUGGCAAGACCAAAGUAAUCGUAGAAACACGGGCAACAAAACCUAC
CACGAAAUUUCCC

anti-rC_COLI

5'gggaaCGUAUCUGUCGAGUAGAGUGUGGGCUCCCACAUACUCUGAUGAUCCUUCG

GGAUCAUUCAUGGCAACCUAAAAUACAAUCCGCAAAGGUCGGGAAAAAUGCUGU
CUCGAAAAUGUCC

anti-rD_COLI

5'gggaaCGUAUCUGUCGAGUAGAGUGUGGGCUCCACAUACUCUGAUGAUCCUUCG
GGAUCAUUCAUGGCAAGGCCAAAAGUCAUUAAGAAAUAGGGGACAUAAAGCAGA
AGGUCAAAGCGCC

anti-rE_COLI

5'gggaaCGUAUCUGUCGAGUAGAGUGUGGGCUCCACAUACUCUGAUGAUCCUUCG
GGAUCAUUCAUGGCAAACACAAACUACGAUUACAAAGCGGAUUGUAAAACUUAU
GACUAAAUCUCC

anti-rF_COLI

5'gggaaCGUAUCUGUCGAGUAGAGUGUGGGCUCCACAUACUCUGAUGAUCCUUCG
GGAUCAUUCAUGGCAAUCGGAAAGACCUUCUGCAAACGAGACAGCAAACGUGGU
AGGUAAAAGAUC

DNA cubes and anti-cubes designed to release DS RNA against GFP¹⁶ upon re-association.

DNA cube with three Ts at each corner carrying sense DS RNA (GFP)

dA-DS GFP

5'CGGTGGTGCAGATGAACTTCAGGGTCAttGGCAACTTTGATCCCTCGGTTTAGCGCC
GGCCTTTTCTCCACACTTTCACG

dB-DS GFP

5'CGGTGGTGCAGATGAACTTCAGGGTCAttGGGAAATTCGTGGTAGGTTTTGTTGCC
CGTGTCTTACGATTACTTTGGTC

dC-DS GFP

5'CGGTGGTGCAGATGAACTTCAGGGTCAttGGACATTTTCGAGACAGCATTTTTTCCC
GACCTTTGCGGATTGTATTTAGG

dD-DS GFP

5'CGGTGGTGCAGATGAACTTCAGGGTCAttGGCGCTTTTGACCTTCTGCTTTATGTCCC
CTATTTCTTAATGACTTTTGGCC

dE-DS GFP

5'CGGTGGTGCAGATGAACTTCAGGGTCAttGGGAGATTTAGTCATTAAGTTTTACAAT
CCGCTTTGTAATCGTAGTTTGTGT

dF-DS GFP

5'CGGTGGTGCAGATGAACTTCAGGGTCAttGGGATCTTTACCTACCACGTTTTGCTGTC
TCGTTTGCAGAAGGTCTTTCCGA

DNA anti-cube with three As at each corner carrying antisense DS RNA (GFP)

anti-dA-antisense DS GFP

5'CGTGAAAGTGTGGGAGAAAAGGCCGGCGCTAAACCGAGGGATCAAAGTTGCCaaT
GACCCTGAAGTTCATCTGCACCACCG

anti-dB-antisense DS GFP

5'GACCAAAGTAATCGTAGAAACACGGGCAACAAAACCTACCACGAAATTTCCCaaTG
ACCCTGAAGTTCATCTGCACCACCG

anti-dC-antisense DS GFP

5'CCTAAAATACAATCCGCAAAGGTTCGGGAAAAAATGCTGTCTCGAAAATGTCCaaTG
ACCCTGAAGTTCATCTGCACCACCG

anti-dD-antisense DS GFP

5'GGCCAAAAGTCATTAAGAAATAGGGGACATAAAGCAGAAGGTCAAAGCGCCaaT
GACCCTGAAGTTCATCTGCACCACCG

anti-dE-antisense DS GFP

5'ACACAAACTACGATTACAAAGCGGATTGTAAACTTAATGACTAAATCTCCCaaTG
ACCCTGAAGTTCATCTGCACCACCG

anti-dF-antisense DS GFP

5'TCGGAAAGACCTTCTGCAAACGAGACAGCAAACGTGGTAGGTAAAGATCCCaaTG
ACCCTGAAGTTCATCTGCACCACCG

DS RNA against GFP¹⁶**DS RNA sense**

5'-pACCCUGAAGUUCAUCUGCACCACCG

DS RNA antisense

5'-CGGUGGUGCAGAUGAACUUCAGGGUCA

Fluorescently labeled RNA**DS RNA sense 3'-end labeled with Alexa488**

5'-pACCCUGAAGUUCAUCUGCACCACCG-Alexa488

DS RNA antisense 5'-end labeled with Alexa546

5'-Alexa546-CGGUGGUGCAGAUGAACUUCAGGGUCA

DNA cubes and anti-cubes designed to release DS RNA against PLK1 and BCL2 upon re-association**DNA cube with three Ts at each corner carrying sense DS RNA****dA-DS PLK1 sense**

5'TCGTCATTAAGCAGCTCGTTAATGGTttGGCAACTTTGATCCCTCGGTTTAGCGCCGG
CCTTTTCTCCACACTTTCACG

dB-DS BCL2 sense

5'CTGCGACAGCTTATAATGGATGTACTTttGGGAAATTTTCGTGGTAGGTTTTGTTGCC
GTGTTTCTACGATTACTTTGGTC

DNA anti-cube with three As at each corner carrying antisense DS RNA**anti-dA DS PLK1 antisense**

5'CGTGAAAGTGTGGGAGAAAAGGCCGCGCTAAACCGAGGGATCAAAGTTGCCaaA
CCATTAACGAGCTGCTTAATGACGA

anti-dB DS BCL2 antisense

5'GACCAAAGTAATCGTAGAAACACGGGCAACAAAACCTACCACGAAATTTCCaaaa
GTACATCCATTATAAGCTGTCGACG

DS RNA against PLK1 designed based on the validate siRNA sequences¹⁷**DS RNA sense**

5'-pCCAUUAACGAGCUGCUUAAUGACGA

DS RNA antisense

5'-UCGUCAUUAAGCAGCUCGUUAAUGGUU

DS RNA against BCL2 designed based on the validate siRNA sequences¹⁸**DS RNA sense**

5'-pGUACAUCCAUAUAAGCUGUCGCAG

DS RNA antisense

5'-CUGCGACAGCUUAAUUAUGGAUGUACUU

Ring/Anti-ring nanoparticles

RNA ring¹⁹

nrA

5'-GGGAACCGUCCACUGGUUCCCGCUACGAGAGCCUGCCUCGUAGC

nrB

5'-GGGAACCGCAGGCUGGUUCCCGCUACGAGAGAACGCCUCGUAGC

nrC

5'-GGGAACCGCGUUCUGGUUCCCGCUACGAGACGUCUCCUCGUAGC

nrD

5'-GGGAACCGAGACGUGGUUCCCGCUACGAGUCGUGGUCUCGUAGC

nrE

5'-GGGAACCACCACGAGGUUCCCGCUACGAGAACCAUCCUCGUAGC

nrF

5'-GGGAACCGAUGGUUGGUUCCCGCUACGAGAGUGGACCUCGUAGC

RNA anti-ring

(5'-gggaa sequences were added for higher in vitro transcription yields)

nrA

5'-gggaaGCUACGAGGCAGGCUCUCGUAGCGGGAACCAGUGGACGGUUCCC

nrB

5'-gggaaGCUACGAGGCGUUCUCUCGUAGCGGGAACCAGCCUGCGGUUCCC

nrC

5'-gggaaGCUACGAGGAGACGUCUCGUAGCGGGAACCAGAACGCGGUUCCC

nrD

5'-gggaaGCUACGAGACCACGACUCGUAGCGGGAACCACGUCUCGGUUCCC

nrE

5'-gggaaGCUACGAGGAUGGUUCUCGUAGCGGGAACCUCGUGGUGGUUCCC

nrF

5'-gggaaGCUACGAGGUCCACUCUCGUAGCGGGAACCAACCAUCGGUUCCC

DNA anti-nanoring with T7RNA POL PROMOTER

Anti-nrA-T7

5'-GCTACGAGGCAGGCTCTCGTAGCGGGAACCAGTGGACGGTTCCTATAGTGAGTC
GTATTAGAA

Anti-nrB-T7

5'-GCTACGAGGCGTTCTCTCGTAGCGGGAACCAGCCTGCGGTTCCCTATAGTGAGTCG
TATTAGAA

Anti-nrC-T7

5'-GCTACGAGGAGACGTCTCGTAGCGGGAACCAGAACGCGGTTCCCTATAGTGAGTC
GTATTAGAA

Anti-nrD-T7

5'-GCTACGAGACCACGACTCGTAGCGGGAACCACGTCTCGGTTCCCTATAGTGAGTCG
TATTAGAA

Anti-nrE-T7

5'-GCTACGAGGATGGTTCTCGTAGCGGGAACCTCGTGGTGGTTCCTATAGTGAGTCG
TATTAGAA

Anti-nrF-T7

5'GCTACGAGGTCCACTCTCGTAGCGGGAACCAACCATCGGTTCCCTATAGTGAGTCG
TATTAGAA

Triangle/Anti-triangle nanoparticles**RNA triangle****rA**

5'GGAUGCUGGUACUUUUGAAACAUUUCGAGUCGCGAGGGUUUCCCAUCGUUGGC
CCGU AUCGCGUUUUCUUAUGAAGA

rB

5'-GGUCGCGACCUUCUUUUCUUCGCGACUCGAAAUGUUUCUUUUCGAGGUCGCCC

rC

5'-
GGAUCUUUCGCCUUUUCGCGAUACGGGCCAACGAUGGGUUUUGAAGGUCGCGAC

rD

5'-GGGCGACCUCGUUUUGUACCAGCAUCCUCUUCAUAAGUUUUGGCGAAAGAUC

DNA triangle**dA**

5'GGATGCTGGTACTTTTGAAACATTTTCGAGTCGCGAGGGTTTTCCCATCGTTGGCCC
GTATCGCGTTTTCTTATGAAGA

dB

5'-GGTCGCGACCTTCTTTTCCCTCGCGACTCGAAATGTTTCTTTTCGAGGTCGCCC

dC

5'-GGATCTTTCGCCTTTTCGCGATACGGGCCAACGATGGGTTTTGAAGGTCGCGAC

dD

5'-GGGCGACCTCGTTTTGTACCAGCATCCTCTTCATAAGTTTTGGCGAAAGATCC

DNA anti-triangle**Anti-dA**

5'TCTTCATAAGAAAAGGCGATACGGGCCAACGATGGGAAAACCCTCGCGACTCGAA
ATGTTTCAAAGTACCAGCATCC

Anti-dB

5'-GGGCGACCTCGAAAAGAAACATTTTCGAGTCGCGAGGGAAAAGAAGGTCGCGACC

Anti-dC

5'-TCGCGACCTTCAAACCCATCGTTGGCCCGTATCGCCAAAACGCGAAAGATCC

Anti-dD

5'-GATCTTTCGCGAAAACCTTATGAAGAGGATGCTGGTACAAAACGAGGTCGCCC

2.5 References

1. Afonin, K. A.; Bindewald, E.; Yaghoubian, A. J.; Voss, N.; Jacovetty, E.; Shapiro, B. A.; Jaeger, L., In vitro assembly of cubic RNA-based scaffolds designed in silico. *Nature nanotechnology* **2010**, *5* (9), 676-682.
2. Guo, P., The emerging field of RNA nanotechnology. *Nature nanotechnology* **2010**, *5* (12), 833-42.
3. Guo, P.; Zhang, C.; Chen, C.; Garver, K.; Trottier, M., Inter-RNA interaction of phage phi29 pRNA to form a hexameric complex for viral DNA transportation. *Mol Cell* **1998**, *2* (1), 149-55.
4. Haque, F.; Shu, D.; Shu, Y.; Shlyakhtenko, L. S.; Rychahou, P. G.; Evers, B. M.; Guo, P., Ultrastable synergistic tetravalent RNA nanoparticles for targeting to cancers. *Nano today* **2012**, *7* (4), 245-257.
5. Khisamutdinov, E. F.; Jasinski, D. L.; Guo, P., RNA as a boiling-resistant anionic polymer material to build robust structures with defined shape and stoichiometry. *ACS Nano* **2014**, *8* (5), 4771-81.
6. He, Y.; Ye, T.; Su, M.; Zhang, C.; Ribbe, A. E.; Jiang, W.; Mao, C., Hierarchical self-assembly of DNA into symmetric supramolecular polyhedra. *Nature* **2008**, *452* (7184), 198-201.
7. Yu, J.; Liu, Z.; Jiang, W.; Wang, G.; Mao, C., De novo design of an RNA tile that self-assembles into a homo-octameric nanoprism. *Nat Commun* **2015**, *6*, 5724.
8. Geary, C.; Rothmund, P. W.; Andersen, E. S., RNA nanostructures. A single-stranded architecture for cotranscriptional folding of RNA nanostructures. *Science* **2014**, *345* (6198), 799-804.
9. Rothmund, P. W. K., Folding DNA to create nanoscale shapes and patterns. *Nature* **2006**, *440* (7082), 297-302.
10. Ohno, H.; Kobayashi, T.; Kabata, R.; Endo, K.; Iwasa, T.; Yoshimura, S. H.; Takeyasu, K.; Inoue, T.; Saito, H., Synthetic RNA-protein complex shaped like an equilateral triangle. *Nature nanotechnology* **2011**, *6* (2), 116-20.
11. Osada, E.; Suzuki, Y.; Hidaka, K.; Ohno, H.; Sugiyama, H.; Endo, M.; Saito, H., Engineering RNA-protein complexes with different shapes for imaging and therapeutic applications. *ACS Nano* **2014**, *8* (8), 8130-40.
12. Pinheiro, A. V.; Han, D.; Shih, W. M.; Yan, H., Challenges and opportunities for structural DNA nanotechnology. *Nature nanotechnology* **2011**, *6* (12), 763-72.
13. Lee, H.; Lytton-Jean, A. K.; Chen, Y.; Love, K. T.; Park, A. I.; Karagiannis, E. D.; Sehgal, A.; Querbes, W.; Zurenko, C. S.; Jayaraman, M.; Peng, C. G.; Charisse, K.; Borodovsky, A.; Manoharan, M.; Donahoe, J. S.; Truelove, J.; Nahrendorf, M.; Langer, R.; Anderson, D. G., Molecularly self-assembled nucleic acid nanoparticles for targeted in vivo siRNA delivery. *Nature nanotechnology* **2012**, *7* (6), 389-93.
14. Mao, C.; Sun, W.; Shen, Z.; Seeman, N. C., A nanomechanical device based on the B-Z transition of DNA. *Nature* **1999**, *397* (6715), 144-146.
15. Modi, S.; M, G. S.; Goswami, D.; Gupta, G. D.; Mayor, S.; Krishnan, Y., A DNA nanomachine that maps spatial and temporal pH changes inside living cells. *Nature nanotechnology* **2009**, *4* (5), 325-30.
16. Modi, S.; Nizak, C.; Surana, S.; Halder, S.; Krishnan, Y., Two DNA nanomachines map pH changes along intersecting endocytic pathways inside the same cell. *Nature nanotechnology* **2013**, *8* (6), 459-467.
17. Zhou, M.; Liang, X.; Mochizuki, T.; Asanuma, H., A light-driven DNA nanomachine for the efficient photoswitching of RNA digestion. *Angew. Chem. Int. Ed. Engl.* **2010**, *49* (12), 2167-2170.
18. Yurke, B.; Turberfield, A. J.; Mills, A. P.; Simmel, F. C.; Neumann, J. L., A DNA-fuelled molecular machine made of DNA. *Nature* **2000**, *406* (6796), 605-608.

19. Shin, J.-S.; Pierce, N. A., A synthetic DNA walker for molecular transport. *J. Am. Chem. Soc.* **2004**, *126* (35), 10834-10835.
20. Bath, J.; Green, S. J.; Turberfield, A. J., A free-running DNA motor powered by a nicking enzyme. *Angew. Chem. Int. Ed. Engl.* **2005**, *44* (28), 4358-4361.
21. Chen, Y.; Wang, M.; Mao, C., An autonomous DNA nanomotor powered by a DNA enzyme. *Angew. Chem. Int. Ed. Engl.* **2004**, *43* (27), 3554-3557.
22. Lund, K.; Manzo, A. J.; Dabby, N.; Michelotti, N.; Johnson-Buck, A.; Nangreave, J.; Taylor, S.; Pei, R.; Stojanovic, M. N.; Walter, N. G.; Winfree, E.; Yan, H., Molecular robots guided by prescriptive landscapes. *Nature* **2010**, *465* (7295), 206-10.
23. Andersen, E. S.; Dong, M.; Nielsen, M. M.; Jahn, K.; Subramani, R.; Mamdouh, W.; Golas, M. M.; Sander, B.; Stark, H.; Oliveira, C. L.; Pedersen, J. S.; Birkedal, V.; Besenbacher, F.; Gothelf, K. V.; Kjems, J., Self-assembly of a nanoscale DNA box with a controllable lid. *Nature* **2009**, *459* (7243), 73-6.
24. Douglas, S. M.; Bachelet, I.; Church, G. M., A logic-gated nanorobot for targeted transport of molecular payloads. *Science* **2012**, *335* (6070), 831-834.
25. Bujold, K. E.; Fakhoury, J.; Edwardson, T. G. W.; Carneiro, K. M. M.; Briard, J. N.; Godin, A. G.; Amrein, L.; Hamblin, G. D.; Panasci, L. C.; Wiseman, P. W.; Sleiman, H. F., Sequence-responsive unzipping DNA cubes with tunable cellular uptake profiles. *Chem. Sci.* **2014**, *5* (6), 2449-2455.
26. Afonin, K. A.; Lindsay, B.; Shapiro, B. A., Engineered RNA Nanodesigns for Applications in RNA Nanotechnology. *RNA nanotechnology* **2013**, 1-15.
27. Jimenez, R. M.; Polanco, J. A.; Luptak, A., Chemistry and Biology of Self-Cleaving Ribozymes. *Trends Biochem Sci* **2015**, *40* (11), 648-61.
28. Mironov, A. S.; Gusarov, I.; Rafikov, R.; Lopez, L. E.; Shatalin, K.; Kreneva, R. A.; Perumov, D. A.; Nudler, E., Sensing small molecules by nascent RNA: a mechanism to control transcription in bacteria. *Cell* **2002**, *111* (5), 747-756.
29. Righetti, F.; Nuss, A. M.; Twittenhoff, C.; Beele, S.; Urban, K.; Will, S.; Bernhart, S. H.; Stadler, P. F.; Dersch, P.; Narberhaus, F., Temperature-responsive in vitro RNA structure of *Yersinia pseudotuberculosis*. *Proc Natl Acad Sci U S A* **2016**, *113* (26), 7237-42.
30. Winkler, W. C.; Cohen-Chalamish, S.; Breaker, R. R., An mRNA structure that controls gene expression by binding FMN. *Proc. Natl. Acad. Sci. U.S.A.* **2002**, *99* (25), 15908-15913.
31. Bindewald, E.; Afonin, K. A.; Viard, M.; Zakrevsky, P.; Kim, T.; Shapiro, B. A., Multistrand Structure Prediction of Nucleic Acid Assemblies and Design of RNA Switches. *Nano letters* **2016**, *16* (3), 1726-35.
32. Afonin, K. A.; Viard, M.; Martins, A. N.; Lockett, S. J.; Maciag, A. E.; Freed, E. O.; Heldman, E.; Jaeger, L.; Blumenthal, R.; Shapiro, B. A., Activation of different split functionalities on re-association of RNA-DNA hybrids. *Nature nanotechnology* **2013**, *8* (4), 296-304.
33. Afonin, K. A.; Viard, M.; Tedbury, P.; Bindewald, E.; Parlea, L.; Howington, M.; Valdman, M.; Johns-Boehme, A.; Brainerd, C.; Freed, E. O.; Shapiro, B. A., The Use of Minimal RNA Toeholds to Trigger the Activation of Multiple Functionalities. *Nano letters* **2016**, *16* (3), 1746-53.
34. Groves, B.; Chen, Y. J.; Zurla, C.; Pochekailov, S.; Kirschman, J. L.; Santangelo, P. J.; Seelig, G., Computing in mammalian cells with nucleic acid strand exchange. *Nature nanotechnology* **2016**, *11* (3), 287-94.
35. Rogers, T. A.; Andrews, G. E.; Jaeger, L.; Grabow, W. W., Fluorescent monitoring of RNA assembly and processing using the split-spinach aptamer. *ACS Synth Biol* **2015**, *4* (2), 162-6.
36. Afonin, K. A.; Desai, R.; Viard, M.; Kireeva, M. L.; Bindewald, E.; Case, C. L.; Maciag, A. E.; Kasprzak, W. K.; Kim, T.; Sappe, A.; Stepler, M.; Kewalramani, V. N.; Kashlev, M.; Blumenthal, R.; Shapiro, B. A., Co-transcriptional production of RNA-DNA hybrids for

- simultaneous release of multiple split functionalities. *Nucleic acids research* **2014**, *42* (3), 2085-2097.
37. Afonin, K. A.; Viard, M.; Kagiampakis, I.; Case, C. L.; Dobrovolskaia, M. A.; Hofmann, J.; Vrzak, A.; Kireeva, M.; Kasprzak, W. K.; KewalRamani, V. N.; Shapiro, B. A., Triggering of RNA Interference with RNA-RNA, RNA-DNA, and DNA-RNA Nanoparticles. *Acs Nano* **2015**, *9* (1), 251-259.
38. Afonin, K. A.; Viard, M.; Koyfman, A. Y.; Martins, A. N.; Kasprzak, W. K.; Panigaj, M.; Desai, R.; Santhanam, A.; Grabow, W. W.; Jaeger, L.; Heldman, E.; Reiser, J.; Chiu, W.; Freed, E. O.; Shapiro, B. A., Multifunctional RNA nanoparticles. *Nano letters* **2014**, *14* (10), 5662-71.
39. Grabow, W. W.; Zakrevsky, P.; Afonin, K. A.; Chworos, A.; Shapiro, B. A.; Jaeger, L., Self-assembling RNA nanorings based on RNAI/II inverse kissing complexes. *Nano letters* **2011**, *11* (2), 878-87.
40. Bui, M. N.; Johnson, M. B.; Viard, M.; Satterwhite, E.; Martins, A. N.; Ramey, H.; Marriott, I.; Li, Z.; Afonin, K. A.; Khisamutdinov, E., Versatile RNA Tetra-U Helix Linking Motif as a Toolkit for Nucleic Acid Nanotechnology. *submitted* **2016**.
41. Shlyakhtenko, L. S.; Gall, A. A.; Lyubchenko, Y. L., Mica functionalization for imaging of DNA and protein-DNA complexes with atomic force microscopy. *Methods in molecular biology* **2013**, *931*, 295-312.
42. Shlyakhtenko, L. S.; Gall, A. A.; Filonov, A.; Cerovac, Z.; Lushnikov, A.; Lyubchenko, Y. L., Silatrane-based surface chemistry for immobilization of DNA, protein-DNA complexes and other biological materials. *Ultramicroscopy* **2003**, *97* (1-4), 279-287.
43. Dobrovolskaia, M. A.; McNeil, S. E., Immunological and hematological toxicities challenging clinical translation of nucleic acid-based therapeutics. *Expert opinion on biological therapy* **2015**, *15* (7), 1023-48.
44. Blanco, P.; Palucka, A. K.; Pascual, V.; Banchereau, J., Dendritic cells and cytokines in human inflammatory and autoimmune diseases. *Cytokine & growth factor reviews* **2008**, *19* (1), 41-52.
45. Takanohashi, A.; Prust, M.; Wang, J.; Gordish-Dressman, H.; Bloom, M.; Rice, G. I.; Schmidt, J. L.; Crow, Y. J.; Lebon, P.; Kuijpers, T. W.; Nagaraju, K.; Vanderver, A., Elevation of proinflammatory cytokines in patients with Aicardi-Goutieres syndrome. *Neurology* **2013**, *80* (11), 997-1002.
46. Zamanian-Daryoush, M.; Marques, J. T.; Gantier, M. P.; Behlke, M. A.; John, M.; Rayman, P.; Finke, J.; Williams, B. R., Determinants of cytokine induction by small interfering RNA in human peripheral blood mononuclear cells. *Journal of interferon & cytokine research : the official journal of the International Society for Interferon and Cytokine Research* **2008**, *28* (4), 221-33.
47. Turner, M. D.; Nedjai, B.; Hurst, T.; Pennington, D. J., Cytokines and chemokines: At the crossroads of cell signalling and inflammatory disease. *Biochimica et biophysica acta* **2014**, *1843* (11), 2563-2582.
48. Elroy-Stein, O.; Moss, B., Cytoplasmic expression system based on constitutive synthesis of bacteriophage T7 RNA polymerase in mammalian cells. *Proc Natl Acad Sci U S A* **1990**, *87* (17), 6743-7.
49. Filonov, G. S.; Moon, J. D.; Svensen, N.; Jaffrey, S. R., Broccoli: rapid selection of an RNA mimic of green fluorescent protein by fluorescence-based selection and directed evolution. *J. Am. Chem. Soc.* **2014**, *136* (46), 16299-16308.
50. Fire, A.; Xu, S.; Montgomery, M. K.; Kostas, S. A.; Driver, S. E.; Mello, C. C., Potent and specific genetic interference by double-stranded RNA in *Caenorhabditis elegans*. *Nature* **1998**, *391* (6669), 806-11.
51. Stewart, J. M.; Viard, M.; Subramanian, H. K.; Roark, B. K.; Afonin, K. A.; Franco, E., Programmable RNA microstructures for coordinated delivery of siRNAs. *Nanoscale* **2016**, *8* (40), 17542-17550.

52. Reagan-Shaw, S.; Ahmad, N., Silencing of polo-like kinase (Plk) 1 via siRNA causes induction of apoptosis and impairment of mitosis machinery in human prostate cancer cells: implications for the treatment of prostate cancer. *The FASEB journal* **2005**, *19* (6), 611-613.
53. Ruckert, F.; Samm, N.; Lehner, A. K.; Saeger, H. D.; Grutzmann, R.; Pilarsky, C., Simultaneous gene silencing of Bcl-2, XIAP and Survivin re-sensitizes pancreatic cancer cells towards apoptosis. *BMC cancer* **2010**, *10*, 379.
54. Rose, S. D.; Kim, D. H.; Amarzguioui, M.; Heidel, J. D.; Collingwood, M. A.; Davis, M. E.; Rossi, J. J.; Behlke, M. A., Functional polarity is introduced by Dicer processing of short substrate RNAs. *Nucleic acids research* **2005**, *33* (13), 4140-56.
55. Khisamutdinov, E. F.; Li, H.; Jasinski, D. L.; Chen, J.; Fu, J.; Guo, P., Enhancing immunomodulation on innate immunity by shape transition among RNA triangle, square and pentagon nanovehicles. *Nucleic acids research* **2014**, *42* (15), 9996-10004.

3 Chapter 3: Programmable Nucleic Acid-based Polygons with Controlled Neuroimmunomodulatory Properties for Predictive QSAR Modeling

3.1 Introduction

The field of nanotherapeutics is exponentially growing due to the ability of nanoparticles to overcome many of the limitations noted for traditional small and macromolecular drugs. Nanotechnology is increasingly used in drug delivery due to the unique physical and chemical properties of nanoparticles, such as hydrophobicity, size, surface charge, and the presence of targeting moieties. These properties can overcome barriers that commonly limit the efficacy of traditional small and macromolecular drugs. The development of therapeutic nucleic acids (TNAs) that have rapidly evolved from conventional (*e.g.*, siRNAs) to nanotechnology-formulated concepts (*e.g.*, siRNAs incorporated into liposomes) and to the more controllable new generation of nano-TNAs represents one such example of utilizing benefits of nanotechnology for improving the quality of traditional therapeutics. These nano-TNAs rely on rationally designed nucleic acids (RNA, DNA or their chemical analogs) to engineer well-defined, fully programmable, and self-assembling nanoparticles, in which the nucleic acids serve as both a carrier and an active pharmaceutical ingredient¹⁻²³. One major limitation to the clinical use of conventional TNAs is their immunostimulatory properties including the induction of cytokines, chemokines, and type I and II interferons. Translational considerations for nano-TNA have been discussed before, and among other areas, include an understanding of the immunological properties²⁴. The ability to predict the effects of the nano-TNAs on the immune system would allow maximizing their therapeutic index. For example, diseases of the central nervous system (CNS) are extremely difficult to treat due to the highly selective permeability of the blood brain barrier. Moreover, the neuroinflammation, which has been implicated in degenerative CNS pathologies such as multiple sclerosis, Alzheimer's disease, and Parkinson's disease²⁵, may also arise from delivery of therapeutic agents with undesirable immunostimulation into the brain, and therefore may counteract the efficacy of these drugs. Nano-TNAs have the potential to overcome both of these

barriers. Their delivery to the brain can be achieved by previously characterized carriers, such as bolaamphiphiles²⁶⁻³⁰, and rational design of nano-TNAs can help avoid the undesirable neuroinflammation. Therefore, it is necessary to characterize the immunomodulatory effects of nano-TNAs on resident CNS cells such as microglia and astrocytes that are essential for the initiation and progression of immune responses in the CNS³¹ through the production of various inflammatory cytokines³²⁻³⁴. Earlier studies by our research groups and others revealed that while some types of nano-TNAs do not induce an immunological response, the immunogenicity of other assemblies strongly depends on their connectivity and composition^{4, 35-37}. Recently, we introduced a novel design strategy that allows for the simple and efficient construction of RNA nanoparticles³⁸. The assemblies, exemplified by nano-triangles, are solely based on Watson-Crick interactions and therefore, can be made not only of RNAs but also of DNAs and even RNA and DNA mixtures. The alterations in composition significantly affect the thermodynamic and chemical stabilities of nanoparticles as well as their immunological properties.

In the present study, we expanded the library of nanoparticles from triangle to hexagon with the same connectivity rules and assessed the effect of the nano-TNA size and composition on their immunomodulatory activity in human glia-like cells. For these purposes, RNA triangles (~75 kDa) were compared to RNA tetragons (~100 kDa), RNA pentagons (~125 kDa), and RNA hexagons (~150 kDa). Similarly, we compared corresponding DNA polygons and two types of different RNA/DNA hybrids for each polygon. We demonstrate that nucleic acid polygons primarily stimulate an interferon response in contrast to a damaging inflammatory cytokine response. Additionally, we report that nucleic acid composition significantly alters the amount of type I interferons release by microglia-like cells. Together these data suggest that nano-TNAs may be specifically engineered to minimize detrimental inflammatory responses while promoting beneficial host immunity. Finally, to establish a set of design rules that allow engineering of nucleic acid-based polygons with predicted immunological activities for further confirmative biological screening experiments, we applied a QSAR modeling technique to the experimental dataset

generated for 16 polygons.

3.2 Methods

3.2.1 Assembly of polygons and their characterization.

The nucleic acid sequences for construction of a polygon library containing 16 candidates were computationally designed using 2D folding programs including Mfold³⁹ and NUPACK⁴⁰⁻⁴³. The nucleic acid strands encoding the composition of polygons are listed in the conclusions section. All DNAs were purchased from IDT (idtdna.com) and all RNA strands were produced from PCR-amplified DNA templates using *in vitro* run-off transcription. Briefly, synthetic DNAs coding for the sequence of the designed RNA were amplified by PCR using primers containing the T7 RNA polymerase promoter. Resulting DNA templates were transcribed with T7 RNA polymerase. Transcription was performed in 80 mM HEPES-KOH, pH 7.5; 2.5 mM spermidine; 50 mM DTT; 25 mM MgCl₂; 5 mM NTPs; 0.2 μM of DNA templates, and “home-made” T7 RNA polymerase ~100 units/μL. Transcription was stopped with RQ1 DNase. Transcribed RNAs were purified with a denaturing urea gel electrophoresis (PAGE) (15% acrylamide, 8M urea). The RNAs were eluted from gel slices overnight at 4°C into 1 × TBE buffer containing 300 mM NaCl. After precipitating the RNA in 2.5 volumes of 100% ethanol, samples were rinsed with 90% ethanol, vacuum dried, and dissolved in double-deionized water.

The polygons were assembled one pot from an equimolar mixture of nucleic acid strands (1 μM) in 1 × TMS buffer (80 mM Tris-HCl pH = 8.0, 100 mM NaCl, 5 mM MgCl₂) with subsequent heating and cooling processes (annealing) from 80 °C to 4 °C in 20 min. All assemblies were tested with 7% native-PAGE and/or 3 % agarose gels. Native-PAGE ran for 1 hour at 4 °C at a constant 90 V and then were stained with ethidium bromide before imaging with the Bio-Rad ChemiDoc MP system.

3.2.2 3D modeling

3D models of each RNA polygon were built using Discovery Studio Visualizer⁴⁴. The energy minimization was applied for structural refinement of each polygon, using the ff10 force field and

the Amber12 molecular dynamics package^{14, 45}.

3.2.3 Atomic force microscopy (AFM)

Assembled RNA polygons (5 μ L of 50 nM stock) were deposited on APS modified mica, incubated for \sim 2 min and air dried, as described previously. AFM visualization was performed using a MultiMode AFM Nanoscope IV system (Bruker Instruments, Santa Barbara, CA) in tapping mode. The images were recorded with a 1.5 Hz scanning rate using a TESPA-300 probe from Bruker with a resonance frequency of 320 kHz and spring constant of about 40 N/m. Images were processed by the FemtoScan Online software package (Advanced Technologies Center, Moscow, Russia)⁴⁶⁻⁴⁷.

3.2.4 Dynamic Light Scattering (DLS)

The average hydrodynamic radii for assembled polygons (at 1 μ M final concentration) were measured in a micro-cuvette (Starna Cells, Inc) using Zetasizer nano-ZS (Malvern Instrument, LTD). All measurements were done at room temperature according to instrumentation protocol.

3.2.5 Degradation assay in fetal bovine serum (FBS)

The experiment was conducted by incubation of nucleic acid polygons (1 μ M) in an aqueous 2% (v/v) FBS solution at 37 $^{\circ}$ C, and aliquots (10 μ L) were collected at 1, 5, 10, 20, 40, 60, and 90 min. Aliquots were immediately snap-frozen on dry ice to prevent any further degradation by nucleases presented in FBS. The collected samples were analyzed by a 7% native PAGE. We used ImageJ software to evaluate the fractions of remaining polygons by integrating the intensities of the bands corresponding to NPs. Integration areas for each time point were compared to the integration area for the control polygon of the same concentration in the absence of FBS. Plots were generated using OriginPro 8 Software where the remaining fraction (%) of polygons was plotted against FBS exposure time (min). An exponential decay function was used to fit data points following $F_{(t)} = F_0 * e^{(-t/\tau)}$, where $F_{(t)}$ and F_0 are the fractions at time t and at initial time 0 respectively; τ is exponential decay time constant.

3.2.6 Equilibrium dissociation constant (K_D) measurements

To measure the apparent K_D for polygon assemblies, titration experiments were carried out. For this, fixed concentrations (10 nM) of IR-700 conjugated dT2 or rT2 strands were titrated with various concentrations (0.01 nM – 1000 nM) of the corresponding triangle, tetragon, pentagon or hexagon short side oligonucleotides. For instance, for DNA triangle, 10 nM IR-700 dT2 were mixed with mixtures of unlabeled [dT1, dT3, dT4] at 0.1, 0.5, 1, 5, 10, 50, 100, 500, and 1000 nM. The samples were annealed and analyzed with a 7% native-PAGE. The quantified polygon fractions (f) were plotted versus the total concentration (C_t) of the polygons. Non-linear sigmoidal curve fitting was applied to the data from two independent experiments using Origin 8.0 software. The general equilibrium equation for multi-strand nucleic acid components was used according to

$$K_D = \frac{\left(\frac{C_t}{2n}\right)^{n-1} \times (1-f)^n}{f}$$

where n = numbers of oligonucleotide strands: triangle n = 4, tetragon n = 5, pentagon n = 6, hexagon n = 7. The bands corresponding to polygons were quantified using ImageJ software. The yield for each polygon was calculated by dividing the corresponding quantified value for triangles by the total sum of the values for all monomers, dimers, and trimers present in the lane.

3.2.7 Structural integrity of polygons associated with Lipofectamine 2000 (L2K)

To ensure that all polygons remain intact during the transfection experiments, polygons (at 1 μM) were incubated with 2 μL of L2K at 25 °C for 30 minutes. Polygon/L2K complexes (4 μL) were then mixed with 2 μL of Triton X-100 (Sigma Aldrich) for an additional 30 minutes at 25 °C. All samples were analyzed by 7% native-PAGE and visualized by AFM (Figure 23 and 25).

3.2.8 Transfections

The human microglia-like cell line, hμglia or hHμ, was a generous gift from the laboratory of Dr. Jonathan Karn (Case Western Reserve University)⁴⁸. Primary human microglia cells purchased from ScienCell were immortalized using SV40 and hTert antigens and sorted for the microglial/macrophage cell marker CD11b. These cells were grown in Dulbecco's Modified Eagle's Medium (DMEM) supplemented with 5% FBS and 100 U/ml penicillin-100 μg/ml

streptomycin at 37 °C with 5% CO₂. The human astrocyte-like cell line, U87 MG (ATCC HTB-14) was grown in Eagle's Minimum Essential Medium (EMEM) supplemented with 10 % FBS, 1 mM sodium pyruvate, and 100 U/ml penicillin with 100 µg/ml streptomycin at 37 °C 5 % CO₂. Transfection of U87 MG cells and hHµ cells was conducted using Lipofectamine 2000 (L2K) (Invitrogen). Polygons or the positive controls poly dA:dT naked and poly I:C naked (Invivogen) were pre-incubated with L2K and Opti-MEM medium prior to transfection. Cells were transfected with polygon/L2K complexes at a final concentration of polygons of 5 nM or 25 nM or with positive control/L2K complexes at a final concentration of 1 µg/ml. Media used for transfection was either DMEM supplemented with 5% FBS or EMEM supplemented with 10% FBS and 1 mM sodium pyruvate. Four hours post transfection the cell culture media was changed to media additionally supplemented with 100 U/ml penicillin with 100 µg/ml streptomycin. The cell supernatants were collected for further analysis twenty-four hours post transfection.

3.2.9 Cell Viability

hHµ cells were plated in a 96 well plate at 5,000 cells per well (six wells per each sample) and polygons were transfected at a final concentration of either 5 nM or 25 nM. The cells were then incubated for four hours at 37° C and 5% CO₂ and the transfection media was replaced with the fresh one. Twenty-four hours post transfection, 20 µL of CellTiter-Blue (Promega) was added to each well and incubated for 2.5 hours. Absorbance was measured at 490 nM using a Tecan Ultra (Tecan) plate reader and normalized to solutions transfected only with L2K.

3.2.10 Relative uptake efficiencies in hHµ

hHµ wells were plated in a 24 well plate at 50,000 cells per well and polygons tagged with IR-700 were transfected. The cells were then incubated in the solution for four hours at 37 °C and 5% CO₂ prior to media change. Twenty-four hours post transfection, cells were treated with Cell Dissociation Buffer (Gibco) and analyzed using a BD Accuri C6 Flow Cytometer. Untreated cells were used as control.

3.2.11 Enzyme-linked Immunosorbent Assay (ELISA)

Specific capture ELISAs were performed to quantify concentrations of human IL-6, IL-8, and IFN- β as previously described by our laboratory⁴⁹. A commercially available ELISA kit was used to measure IL-8 (R&D Systems). The IL-6 ELISA was conducted using a rat anti-human IL-6 capture antibody (BD Pharmingen) and a biotinylated rat anti-human IL-6 detection antibody (BD Pharmingen). The IFN- β ELISA was carried out using a polyclonal rabbit anti-human IFN- β capture antibody (Abcam) and a biotinylated polyclonal rabbit anti-human IFN- β detection antibody (Abcam). Bound antibody was detected using streptavidin-horseradish peroxidase (BD Biosciences) followed by the addition of tetramethylbenzidine (TMB) substrate. H₂SO₄ was used to stop the reaction and absorbance was measured at 450 nm. Dilutions of recombinant cytokines for IL-6 and IFN- β (BD Pharmingen, Abcam) were used to generate a standard curve. The concentration of each cytokine was determined by extrapolation of absorbances in the study samples to that in the standard curve prepared from known concentrations of the relevant cytokine.

3.2.12 Limulus Amoebocyte Lysate (LAL) assay

The LAL assay was utilized to assess preparation contamination with the bacterial endotoxin, lipopolysaccharide. The polygons were tested at several dilutions according to a standardized procedure described earlier (https://ncl.cancer.gov/sites/default/files/protocols/NCL_Method_STE-1.2.pdf)². Controls included the addition of known quantities of an endotoxin standard to nanoparticle samples to rule out potential nanoparticle interference with the assay. Reported values are from dilutions that demonstrated acceptable spike recovery and did not interfere with the assay.

3.2.13 Statistics

Experimental results were normalized to the L2K alone treated control and presented as the mean +/- SEM. Statistical significance was determined using a Student's two-tailed t-test conducted with GraphPad Prism Software. A P-value of less than 0.05 was considered to be statistically significant.

3.2.14 Quantitative Structure-Activity Relationship (QSAR) modeling.

In this study, 16 polygonal nanoparticles (both RNA- and DNA-based) were used for the construction of quantitative structure-activity relationships (QSAR). Three types of immune responses were identified based on the levels of IFN- β , IL-6, and IL-8 release experimentally measured from hH μ cells, and we used these activity values for QSAR modeling. The physicochemical properties and immune-response activities (observed and predicted) of studied polygons are presented in Tables 3 and 4.

3.2.15 QSAR approach

For the development of the QSAR model we used two types of descriptors: physicochemical properties of constructed nanoparticles and sequence-based descriptors generated by Word2vec⁵⁰ approach as well as Random Forest (RF)⁵¹ technique for model building.

3.2.16 Descriptors

To generate the sequence-based descriptors we have used the Word2vec approach implemented in the KNIME analytic platform⁵². Word2vec is a two-layer neural network which is trained to reconstruct the linguistic contexts of words. As input Word2vec uses text and as an output, it produces a continuous vector space where semantically similar words are mapped to nearby points. Thus, sequences of nanoparticles were transformed into the vectors of real numbers of ten dimensions using nucleotides as the words. In addition to sequence-based descriptors, we also used the six physicochemical properties of constructed nanoparticles: molecular weight, GC content (%), diameter (nm), T_m (°C), decay time (min) and K_D (nM).

3.2.17 Machine learning method

For the development of QSAR models, we used the RF implemented in the KNIME analytic platform⁵³, which is a modern and predictive machine learning approach. RF is an ensemble of decision trees and more trees reduce the variance. The classification from each tree can be thought of as a vote; the most votes determine the classification. The regression output was calculated as a mean value of all trees. Each tree was grown as the following: A random sample of nanoparticles

(67%) was selected from the initial modeling set as the training set for the current tree. Not selected samples were used as a test set called an out-of-bag (OOB), which typically is 33% of initial modeling data. The randomly selected descriptors from the training set were used to split the nodes in the tree. Each tree is grown until it reaches the maximum tree depth parameter. The internal model evaluation was done according to the performance with the OOB set. To construct the best RF model, the following parameters were considered during a 5-fold cross validation procedure (5-fold CV): the number of trees (100), and the number of descriptors (16).

3.2.18 Model construction and validation

To estimate the predictivity of the developed models we used 5-fold external cross-validation procedure (5-fold CV)⁵⁴. During this procedure the initial data set was randomly divided into 5 parts. Four parts were used as the training set for model building and the remaining part was used as the test set for the assessment of external predictive accuracy. In addition, the Y-randomization (shuffling of the dependent values) was performed during 5-fold CV to assure that the accuracy of the model was not obtained due to chance correlations.

3.2.19 Evaluation of the model prediction accuracy

To estimate the accuracy of prediction the following statistical parameters were calculated:

1) Determination coefficient

$$R^2 = 1 - \frac{\sum_{n=1}^n (\hat{Y}_i - Y_i)^2}{\sum_{n=1}^n (Y_i - \bar{Y})^2}$$

where \hat{Y}_i is predicted value for each particular object, \bar{Y} is average activity value from the training set, and n is the number of objects in the training set.

2) Root mean square error

$$RMSE = \frac{1}{n} \sum_{n=1}^n (\hat{Y}_i - Y_i)^2$$

where \hat{Y}_i is predicted value for each particular compound and n is the number of objects in the training set.

3.3 Results and discussion

We constructed four types of equilateral polygons that can self-assemble from single-stranded

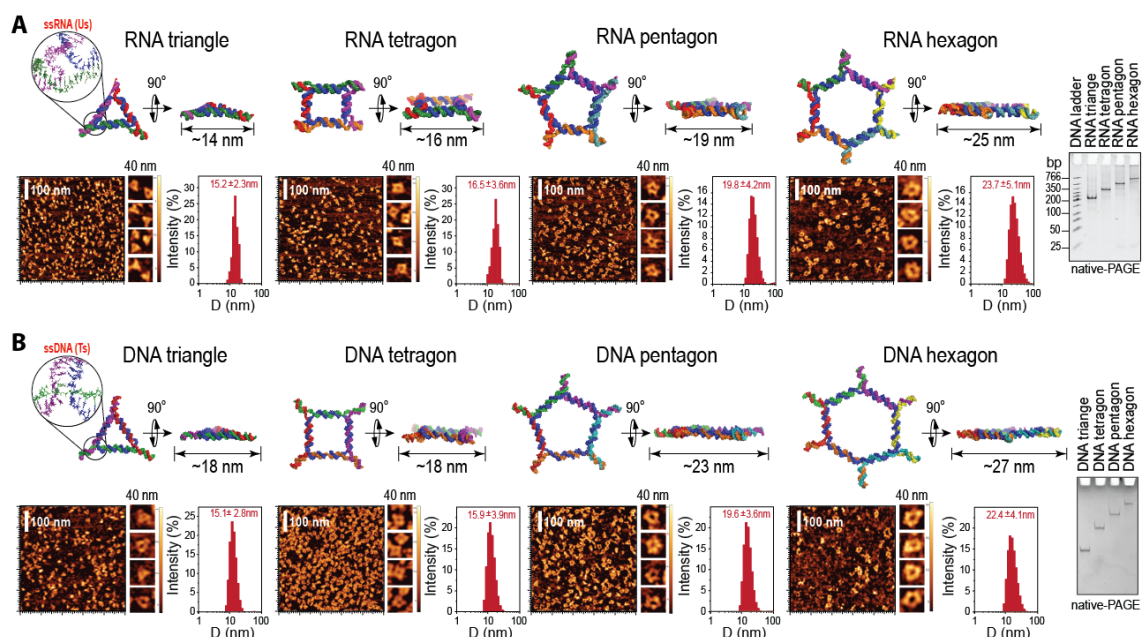


Figure 21. Programmable nucleic acid RNA (**A**) and DNA (**B**) polygons. Each panel presents energy minimized 3D models of RNA and DNA nanoparticles (identical sequences are colored the same), with corresponding AFM images, hydrodynamic radii measured by DLS (presented as \pm SEM), and ethidium bromide total staining native-PAGE results.

longer central and shorter side strands. All polygons, while being different in size, number of sides, and the total number of strands entering their assemblies, have minimal variance in their sequence signatures (Figure 22A). For example, polygons with n number of sides would share the sequences with $n-1$ polygons but have an extra short side strand and an elongated central strand in their assembly. Polygons assembled *via* one-pot assembly were extensively analyzed by gels (Figures 22, 23B, and 24) with the average yield estimated to be greater than 90%. The type of polygon was determined by the sequence of the longer strand. Thus the assembly of the particular shape is guided by the addition of the corresponding central strand to a mixture of all short RNAs. The structural evaluation of the assemblies by AFM and DLS provide additional evidence of formation of the designed polygon structures (Figure 22). AFM studies revealed that the shapes of resulting polygons were similar to their computed 3D models. The hydrodynamic diameters of polygons in aqueous solution were measured to be ~15 nm, ~16 nm, ~20 nm, and ~24 nm for triangles,

tetragons, pentagons, and hexagons, respectively. These experimental results were in agreement with the predicted sizes.

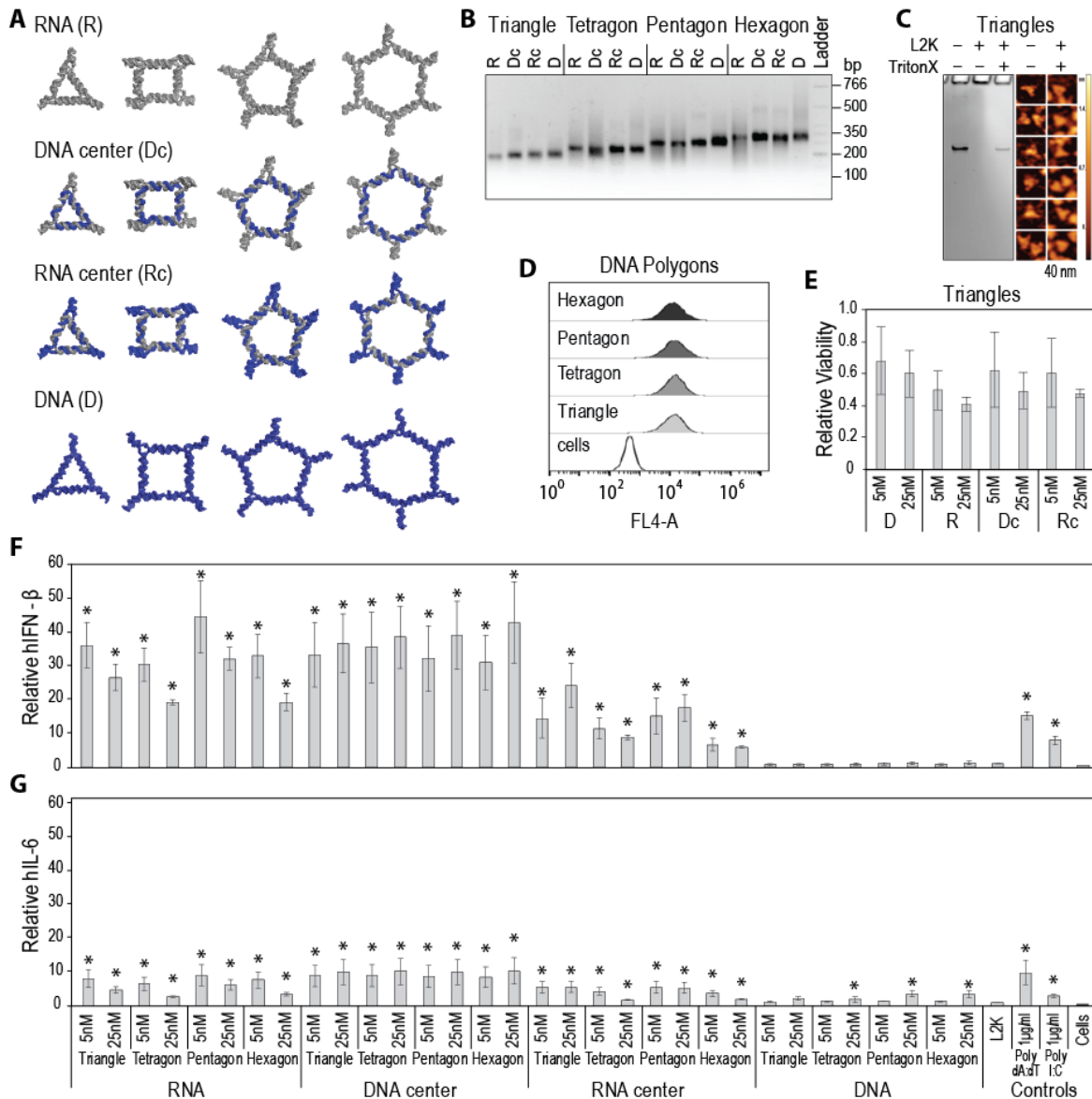


Figure 22. Cell culture experiments with programmable polygons. Human microglia-like cell lines were transfected with polygons at a final concentration of 5 nM and 25 nM. (A) 3D models of tested polygons with RNA strands shown in grey and DNA strands in blue. (B) Assemblies all polygons visualized by agarose gel. (C) Structural integrity of polygons associated with Lipofectamine 2000 (L2K) confirmed by the release studies with Triton X100. The results are analyzed by native-PAGE and visualized by AFM. (D) Relative cellular uptakes assessed by flow cytometry and (E) cell viability assays. (F-G) 24 hours post transfection with 16 RNA, DNA and RNA/DNA polygons, cell supernatants were collected and levels of IFN- β (F) and IL-6 (G) production were assessed by specific-capture ELISA. In C, E, and F, results were normalized to transfection reagent alone treated cells (L2K) and presented as the mean \pm SEM. Statistically significant results are indicated with asterisks (p value $<$ 0.05).

Due to the design principles that rely only on canonical Watson-Crick interactions, polygons have an ability to efficiently assemble not only from RNAs but also from DNAs as well as from different ratios of RNA and DNA strands. This composition flexibility offers a rapid, convenient, and cost effective way to engineer different polygons with tunable physicochemical properties dictated by the nature of RNA and DNA. For example, by using various combinations of just 20

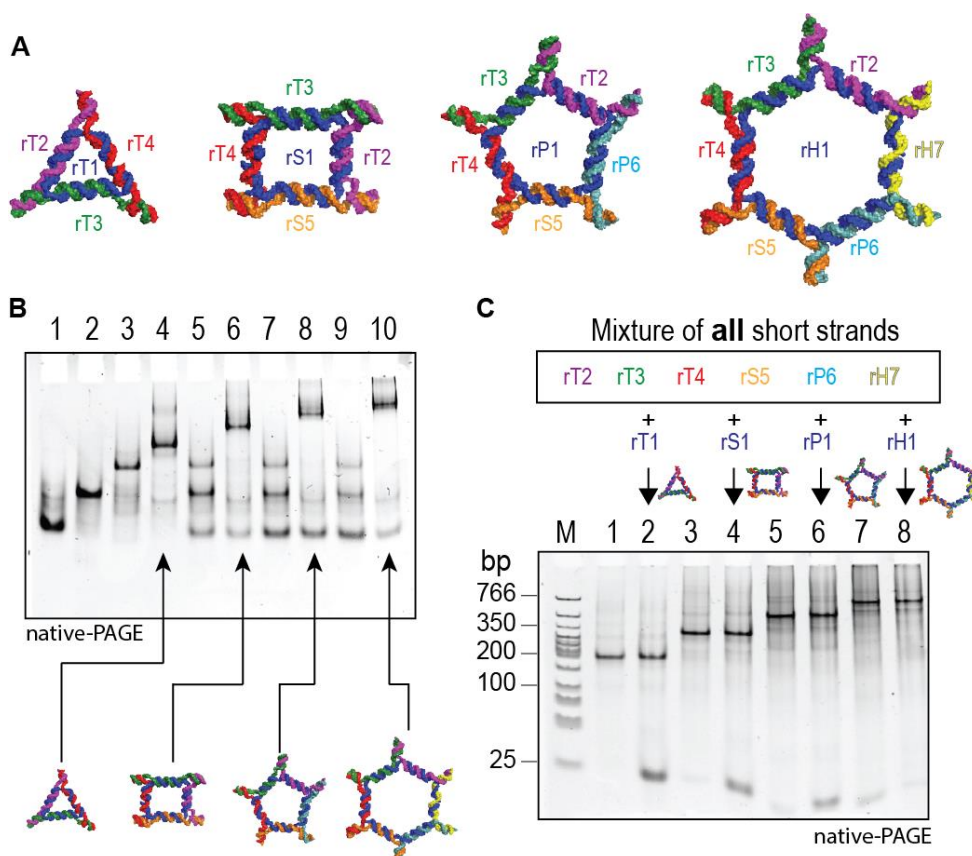


Figure 23. (A) 3D models of polygons with corresponding sequence annotations. (B) Self-assembly properties of RNA polygons in the presence and absence of central (blue) strands evaluated on 7% non-denaturing PAGE. Lanes 1 – 3 correspond to monomer, dimer and trimer stepwise association of RNA strands. Lane 4 corresponds to triangle with strand rT1. Lanes 5 and 6 correspond to square with and without central strand rS1. Lanes 7 and 8 correspond to pentagon with and without central strand rP1. Lanes 9 and 10 correspond to hexagon with and without central strand rH1. (C) Self-assembly properties of RNA polygons from the same mixture of short strands (rT2, rT3, rT4, rS5, rP6, rH7) and different central strands. Lane M is a DNA step ladder (Low Molecular Weight from NEB). Lanes 2, 4, 6, and 7 are corresponding assembly of Triangle, Square, Pentagon and Hexagon formations driven by the presence of rT1, rS1, rP1, and rH1, respectively. Lanes 1, 3, 5, and 8 are corresponding pre-assembled control RNA polygons.

different RNA and DNA strands (10 each), it becomes possible to easily assemble a total of 240

unique RNA, DNA, and RNA/DNA hybrid polygons (16 triangles, 32 tetragons, 64 pentagons, and 128 hexagons). To show the feasibility of this approach, we have synthesized 16 polygons (Figure 2) made of all RNAs, all DNAs, only central strand RNA, and only central strand DNA and then further extensively characterized their properties and tested their immunogenicity. For all polygons, relative sizes (D), melting temperatures (T_m), dissociation constants (K_D), and stabilities in blood serum (τ) were measured and the results are summarized in Table 2.

Prior to the immunological studies, the levels of endotoxin in prepared samples were assessed. Endotoxin is a component of the cell wall of Gram-negative bacteria and is a common contaminant in biotechnology and nanotechnology therapeutics⁵⁵. Common sources of endotoxin are laboratory glassware, spatulas used to weigh out reagents, water, commercially available enzymes and oligonucleotides. Autoclaving kills bacteria, but does not eliminate endotoxin. Likewise, water purification systems remove ions, but not endotoxin. It is common knowledge in the area of nanotechnology that as much as 30-50% of nanoparticles fail during preclinical stage due to endotoxin contamination. Since endotoxins are potent immunostimulants, which may induce production of proinflammatory cytokines, we tested polygons for the presence of this contaminant using LAL assay. The level of endotoxin in all tested samples was below 0.05 EU/mL of 10 nM stock, which corresponds to less than 5 pg/mL concentration in our in vitro assays. The results are shown in Table 1. These levels of endotoxin are insufficient to elicit significant production of pro-inflammatory cytokines by glial cells.

Table 1. Endotoxin in the test samples was measured by kinetic turbidity LAL. Spike recovery between 50 and 200% indicates that the tested nanoparticle did not interfere with the assay and the value of endotoxin shown in the middle column is valid.

Material tested	Endotoxin (EU/mL)	Spike recovery (%)
RNA triangle	0.0146	101
RNA square	<0.05	115
RNA pentagon	0.0319	125
RNA hexagon	0.0386	121
DNA triangle	<0.005	93
DNA square	<0.005	118
DNA pentagon	0.00929	123
DNA hexagon	<0.005	144

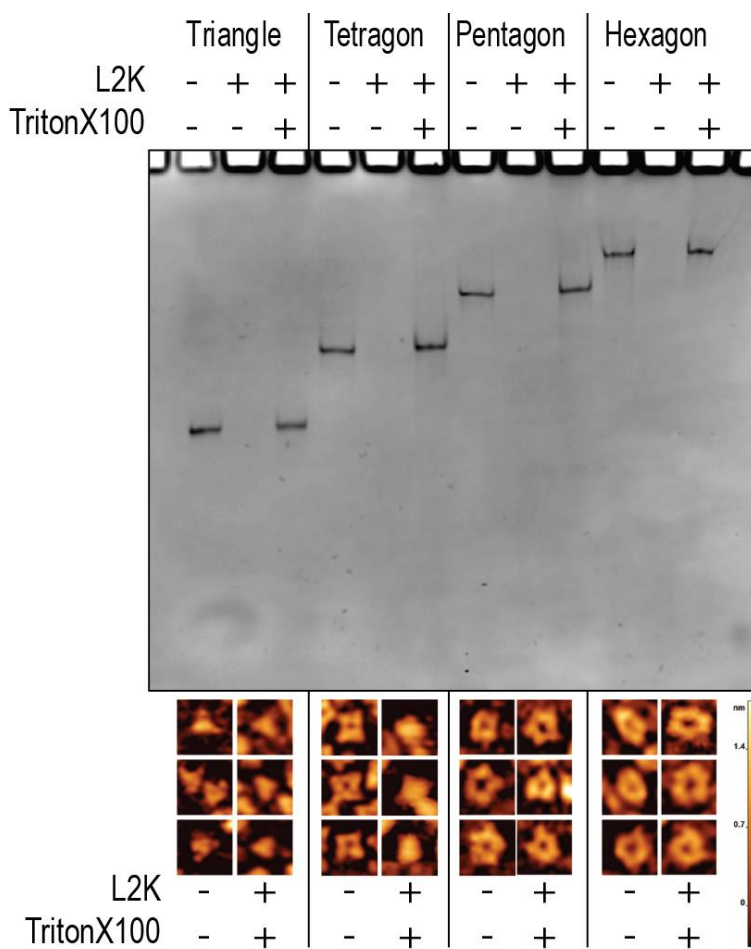


Figure 24. Experiments confirming structural integrity of DNA polygons associated with Lipofectamine 2000 (L2K). L2K complexes with polygons were prepared and then treated with Triton X100. All samples were analyzed by ethidium bromide total staining native-PAGE and visualized by AFM.

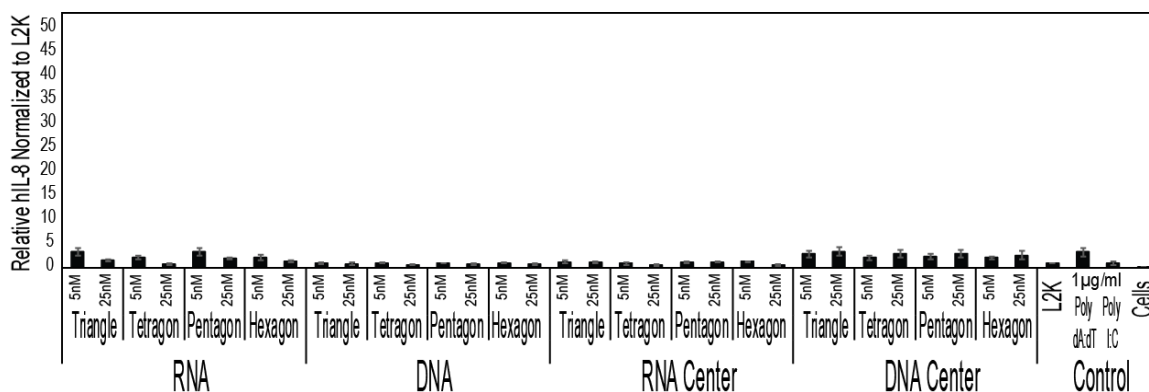


Figure 25. Human microglia-like cell lines were transfected with nanoparticles at a final concentration of 5nM and 25nM. 24 hours post transfection cell supernatants were collected and levels of IL-8, were assessed by specific-capture ELISA. Results are normalized to L2K control and presented as the mean \pm SEM.

Currently, one of the primary limitations in the translation of TNAs to the clinic is the stimulation of both off-target effects and immunotoxicity. In addition, treatment of CNS diseases is especially difficult due to an inability of therapies to cross the blood brain barrier and the sensitivity of the CNS to inflammatory damage. The TNAs discussed in this study can be complexed with lipid-based carriers that permit delivery to target cells within the CNS. Importantly, the carrier does not alter the structure of polygons (Figure 23C and Figure 25). In the CNS, glial cells are key initiators of immune responses. Glial cells use a variety of cell surface, endosomal, and cytosolic receptors to sense pathogen-associated molecular patterns (PAMPs) such as nucleic acids. Due to the complexing of TNAs with lipid-based carriers, we predict TNAs will be identified by endosomal and/or cytosolic nucleic acid sensors. Therefore, in order to determine the immunomodulatory activity of TNA polygons that differ in their nucleic acid composition, human microglia-like cells and astrocyte-like cells were transfected side-by-side with 16 different polygons or positive controls and inflammatory mediator release was determined by specific capture ELISA (Figures 23 and 26). The positive controls selected were poly dA:dT, a synthetic analog of B-DNA recognized by DNA sensors; and poly (I:C) a synthetic dsRNA polymer recognized by RNA sensors. We observed no significant release of IFN- β or IL-6 from astrocyte-like cells transfected with nano-TNAs (data not shown). Interestingly, transfection of microglia-

like cells with 12 out of the 16 polygons resulted in significant IFN- β release with minimal IL-6 or IL-8 production compared to the transfection reagent alone control. We observed no statistically significant difference in the release of IL-6 and IL-8 for polygons compared to our positive controls poly dA:dT and poly (I:C). These data suggest that these polygons primarily promote an interferon response rather than a damaging inflammatory cytokine production. The cytokine responses to these polygons did not show a clear dose dependency, potentially due to ligand saturation effects or reductions in cell viability resulting from greater activation and terminal differentiation of these cells, although it should be noted that such reductions were not statistically significant (Figure 23E).

Additionally, we observed that the nucleic acid composition of the TNA polygons significantly affected the release of inflammatory mediators. We observed that the polygons composed exclusively of RNA, or those that had central strand of RNA or DNA, stimulated a robust 10 to 40-fold increase in IFN- β responses compared to transfection reagent alone control. Additionally, compared to our positive controls, RNA and DNA center polygons induced a significant increase in the release of IFN- β further indicating the potency of these polygons as an interferon stimulus. In contrast, polygons composed exclusively of DNA do not stimulate significant IFN- β release above our transfection reagent alone control and induced significantly less release of IFN- β compared to our positive controls. These data suggest an RNA composition is required to stimulate an interferon response. Additionally, our data indicate DNA polygons are more immunologically quiescent compared to other polygon compositions and our positive controls. Interestingly, we observed a trend in inflammatory mediator responses attributable to polygon type for nano-TNAs composed exclusively of RNA, or TNAs composed of DNA with an RNA center. For these compositions, triangle and pentagon structures tended to simulate more IFN- β release compared to tetragon and hexagon compositions, suggesting a role for polygon type in cytokine production. However, further investigations will be required to definitively establish the role of polygon type in immune mediator release. Overall, these results hold promise for the development of these novel polygon nano-TNAs for clinical use given that their nucleic acid composition may dictate the

cytokine response of the recipient. For example, all polygons composed solely of DNA elicit minimal inflammatory cytokine responses, thus avoiding the negative effects often associated with

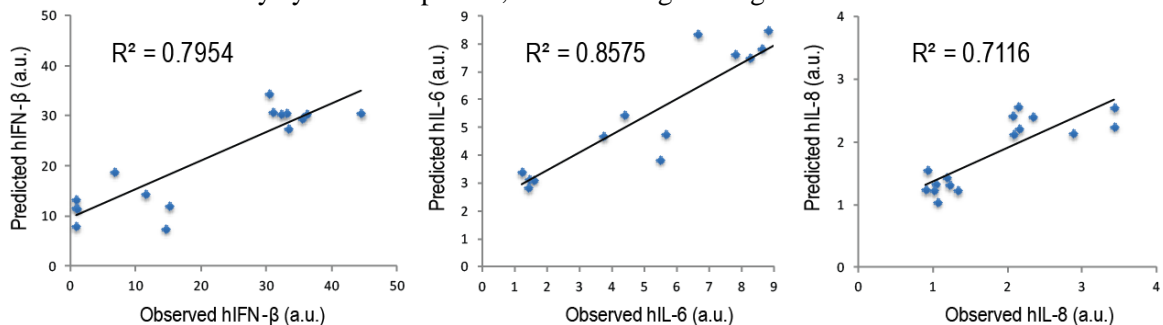


Figure 26. Examples of model accuracy estimations for IFN- β , IL-6, and IL-8 datasets obtained by 5-fold Cross Validation procedure.

nanoparticle delivery, while RNA polygons may have use as adjuvants due to their ability to stimulate interferon responses. As such, these nano-TNAs provide an opportunity to engineer specific therapies for a variety of medical purposes.

To construct a model that allows engineering of nucleic acid-based polygons with predicted immunological activities for further biological screening, we applied QSAR modeling technique to the experimental dataset of the 16 polygons (Figure 27). The two types of descriptors together with

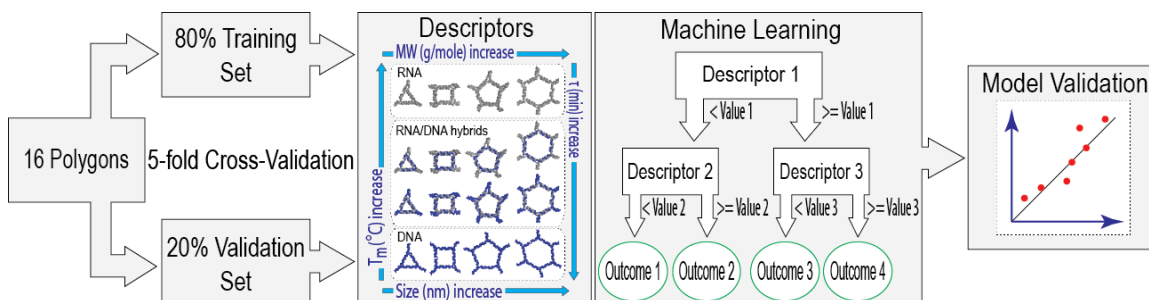


Figure 27. Schematic representation of quantitative structure-activity relationship (QSAR) modeling used in this project.

Random Forest were used for developing of QSAR models. To investigate the informativeness of the descriptors we built three separate models. The first model was based only on the physicochemical properties. The second model was based only on the sequence-based descriptors and the third model was based on both physicochemical properties together with sequence-based descriptors. The performance of each model was evaluated by 5-fold CV procedure (Figure 28).

The statistical characteristics of the generated models are presented in Table 2.

Table 2. Model accuracy estimated during 5-fold cross validation procedure.

Descriptors	IFN- β			IL-6			IL-8		
	R ²	RMSE	R ² _y	R ²	RMSE	R ² _y	R ²	RMSE	R ² _y
	rand			rand			rand		
physicochemical (PC)	0.728	7.806	-0.318	0.803	1.333	-0.252	0.669	0.486	-0.358
sequence-based (Seq)	0.392	11.66	-0.649	0.353	2.415	-0.674	0.539	0.574	-0.706
PC and Seq	0.696	8.225	-0.540	0.682	1.694	-0.469	0.565	0.558	-0.614

As shown in Table 2, the models constructed using two types of descriptors together demonstrated strong predictive power. All models showed negative determination coefficients after y-randomization procedures, proving the lack of correlations by chance. The models based only on sequence descriptors showed poor predictivity for IFN- β and IL-6 responses, and moderate predictivity for IL-8. The best predictive accuracy was obtained using only the physicochemical descriptors. These results are not surprising since the developed polygons have little variation across their sequences. However, the sequence information still showed some effect in the models, especially for IL-8 responses, and might play a significant role in predicting the behavior of polygons with more diverse shapes and structures. Thus, to predict immune responses to novel structure-diverse polygons, the models based on both descriptor types, as well as models based only on physicochemical descriptors, should be applied to predict nano-TNA immunomodulatory activity.

As mentioned above, the best prediction results were obtained using the physicochemical descriptors. Besides yielding good accuracy, these types of descriptors allow mining for clear interpretations of the developed models. Since the RF algorithm was used to build the QSAR models, the contribution of each descriptor into the tree-based model can be readily calculated. Thus, for each descriptor, we calculated an importance value as a ratio of the number of models, which used the descriptor as a split of the tree to the number of times the descriptor was the candidate for splitting. The sum of the importance values for all descriptors was scaled to 100% for comparison purposes. The results obtained are presented in Table 3.

Table 3. Descriptor's contribution into the Random Forest models. Bold and italic font represents the most important descriptors.

	IFN-β	IL-6	IL-8
<i>MW</i>	20.54%	19.29%	19.38%
GC content	11.94%	5.96%	6.98%
Size (diameter)	2.99%	2.98%	5.99%
<i>T_m, °C</i>	24.01%	25.04%	21.88%
<i>τ, min</i>	31.30%	30.38%	31.38%
<i>K_D, nM</i>	9.23%	16.36%	14.39%

Table 3 shows that *MW*, *T_m*, and *τ* provide the major contributors to the RF models across all immune response activities. These important descriptors have interesting relationships with biological activities. It can be seen that DNA-based nanoparticles that have lower *T_m* values also induce low immune responses. Interestingly, the low decay time (30 min and less) for most of the nanoparticles corresponded to higher immune-response values. Although clear relationships between the physicochemical properties of nanoparticles and biological activities were discovered during modeling, future extension of the data set will improve the predictivity of these models and increase the confidence level in result interpretation.

3.4 Conclusion

In conclusion, we have developed novel nano-TNA platforms that are highly reconfigurable in both their physicochemical and immunological properties. These nano-TNAs can be specifically designed with the desired size, shape, melting temperature, enzymatic decay rates, and immunomodulatory activity. Our data strongly indicate that the nucleic acid composition of the nano-TNAs, specifically the combination of RNA to DNA, determines many of the physicochemical and immunological properties. Our data indicates that the properties of RNA and DNA determine stability factors including *T_m* and *τ* . Here, we demonstrate that nucleic acid composition also determines immunomodulatory activity. Nano-TNAs with an RNA composition

stimulate a robust interferon response and minimal inflammatory cytokine release. In contrast, nano-TNAs composed solely of DNA stimulate minimal interferon and inflammatory cytokine release. Additionally, we observed a trend for polygon type to contribute to the robustness of the immunological response. While our current data focuses on defining the role of polygon type and composition in initiating an immune response using one transfection reagent for delivery, preliminary experiments conducted using two additional transfection reagents display similar trends in the cytokine profile released in response to polygon transfection (Figure 29). These results

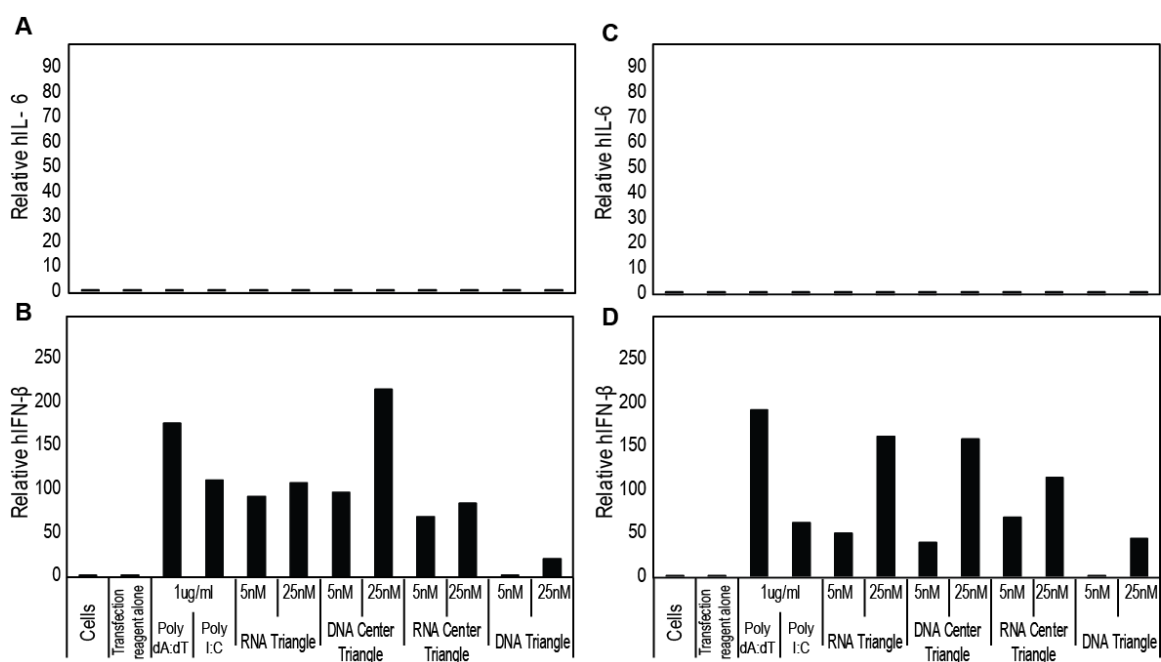


Figure 28. Human microglia-like cell lines were transfected with nanoparticles at a final concentration of 5 nM and 25 nM using the transfection reagents jetPrime (A-B) or Mirus TransIT-X2 (B-C) and following the manufacturer's protocols. 24 hours post transfection with RNA, DNA and RNA/DNA polygons, cell supernatants were collected and levels of IL-6 (A, C) and IFN- β (B, D) production were assessed by specific-capture ELISA. Results were normalized to transfection reagent alone treated cells. Data shown is an N=1.

suggest that the conclusions from our current data could be applied to additional carriers. However, future studies are necessary to fully investigate the role of lipid-based carriers in delivery and initiation of polygon induced immune responses in order to translate these nano-TNAs to clinical use. Interestingly, by developing QSAR models we were able to demonstrate that the physicochemical properties of the nano-TNAs, which are determined by the ratio of RNA and

DNA, are the best predictors of immunological activity. Specifically, MW, T_m , and τ predict nano-TNA immunomodulatory activity. The QSAR models have also allowed for the generation of a library of nano-TNAs and their predicted immunological activity. Most importantly, the construction of this library provides a set of design principles for nano-TNAs. These design principles allow engineering nano-TNAs with specific physicochemical and immunological properties for desired medical applications. The flexibility of designing nano-TNAs with differing RNA and DNA composition as well as polygon type provides the potential for efficient and cost-

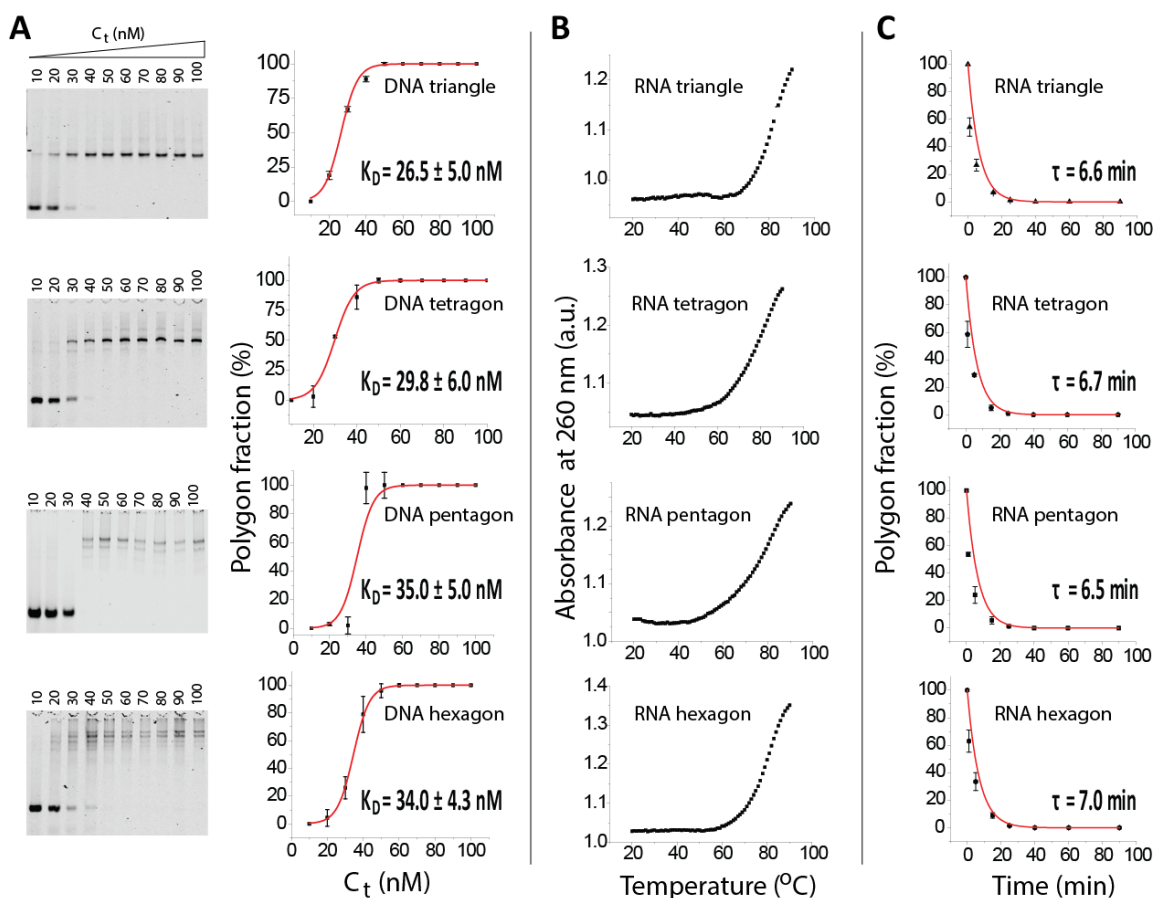


Figure 29. Examples of experimental determination of dissociation constants (K_D), melting temperatures (T_m), and stabilities in blood serum (τ). (A) For equilibrium dissociation constant (K_D) assay: fixed amounts of IR-700 labeled dT2 was titrated with increasing amount of unlabeled strands corresponding to triangle, tetragon, pentagon, and hexagon. The assembled polygons were subjected to 7% native-PAGE analysis shown on left. Titration curve fitting data is demonstrated on the right with corresponding apparent K_D values (+/- SEM). (B) Representative UV-melting curves for RNA polygons. Sigmoidal curves exhibited one transition at $T_m \sim 80^{\circ}$ C in all cases. The exact melting temperatures for polygons were determined from first derivative plots of corresponding melting curves. (C) Time dependent degradation profiles for RNA polygons (at 1 μ M) in 2% (v/v) FBS at 37 $^{\circ}$ C.

effective development of an extensive library of nano-TNAs with an array of physicochemical and immunological properties. Studies are ongoing to identify the molecular mechanisms, such as cytosolic nucleic acid sensors, that underlie the immune responses of these cells to our nano-TNAs. The ability to tailor these key nano-TNA properties to therapeutic applications brings us one step closer to a more personalized medical treatment plan for patients for a myriad of diseases and conditions.

Table 4. The data set for 16 polygons used for QSAR modeling.

Polygons	MW (g/mole)	GC content (%)	D (nm)	T_m (°C)	τ (min)	K_D (nM)	IFN-β (a.u.)	IL-6 (a.u.)	IL-8 (a.u.)
RNA Triangle	76208.3	~31	~15	~79	~7	~10	~36.16	~8.23	~3.4
RNA Tetragon	101133.1	~33	~17	~83	~7	~10	~30.45	~6.65	~2.15
RNA Pentagon	126057.8	~33.5	~20	~82	~7	~10	~44.49	~9.21	~3.43
RNA Hexagon	150997.6	~32.3	~24	~83	~7	~10	~32.98	~7.80	~2.13
DNA Triangle	73450.5	~31	~15	~59	~60	~30	~0.82	~1.20	~0.90
DNA Tetragon	97435.9	~33	~16	~61	~60	~30	~0.93	~1.44	~1.06
DNA Pentagon	121421.3	~33.5	~19	~60	~60	~30	~1.01	~1.59	~1.01
DNA Hexagon	145407.8	~32.3	~23	~62	~60	~30	~0.82	~1.42	~1.03
R_Center Triangle	74319.7	~31	~14	~70	~30	~10	~14.51	~5.64	~1.22
R_Center Tetragon	98608.9	~33	~16	~73	~60	~10	~11.52	~4.38	~0.92
R_Center Pentagon	122884	~33.5	~19	~69	~60	~10	~15.16	~5.47	~1.17
R_Center Hexagon	147188.2	~32.3	~25	~71	~60	~10	~6.75	~3.73	~1.32
D_Center Triangle	75339.1	~31	~14	~68	~15	~50	~33.37	~9.06	~2.88
D_Center Tetragon	99960.1	~33	~15	~74	~20	~50	~35.46	~9.08	~2.06
D_Center Pentagon	124595.1	~33.5	~19	~72	~20	~50	~32.20	~8.82	~2.34
D_Center Hexagon	149217.2	~32.3	~25	~73	~20	~50	~30.93	~8.63	~2.07

Table 5. Immunogenic values experimentally observed and predicted with QSAR model based on physicochemical descriptors.

	Observed IFN- β (a.u.)	Predicted IFN- β (a.u.)	Observed IL-6 (a.u.)	Predicted IL-6 (a.u.)	Observed IL-8 (a.u.)	Predicted IL-8 (a.u.)
RNA Triangle	~36.16	~30.35	~8.23	~7.52	~3.4	~2.55
RNA Square	~30.45	~34.39	~6.65	~8.36	~2.15	~2.20
RNA Pentagon	~44.49	~30.54	~9.21	~7.35	~3.43	~2.24
RNA Hexagon	~32.98	~30.44	~7.80	~7.62	~2.13	~2.56
R_Center Triangle	~0.82	~7.52	~1.20	~4.78	~0.90	~1.32
R_Center Square	~0.93	~14.47	~1.44	~5.47	~1.06	~1.54
R_Center Pentagon	~1.01	~11.93	~1.59	~3.83	~1.01	~1.43
R_Center Hexagon	~0.82	~18.91	~1.42	~4.67	~1.03	~1.21
DNA Triangle	~14.51	~11.74	~5.64	~3.38	~1.22	~1.24
DNA Square	~11.52	~7.97	~4.38	~3.15	~0.92	~1.04
DNA Pentagon	~15.16	~11.43	~5.47	~3.12	~1.17	~1.22
DNA Hexagon	~6.75	~13.28	~3.73	~2.83	~1.32	~1.32
D_Center Triangle	~33.37	~27.46	~9.06	~7.68	~2.88	~2.13
D_Center Square	~35.46	~29.31	~9.08	~7.93	~2.06	~2.41
D_Center Pentagon	~32.20	~30.33	~8.82	~8.46	~2.34	~2.39
D_Center Hexagon	~30.93	~30.80	~8.63	~7.81	~2.07	~2.11

3.4.1 Sequences used in this project

Compositions of 16 polygons used in this project:

RNA polygons:

RNA Triangle 5'→3'

rT1:

GGAUGCUGGUACUUUUGAAACAUUUCGAGUCGCGAGGGUUUUCCCAUCGUUGGCC
CGUAUCGCGUUUUCUUAUGAAGA

rT2:

GGUCGCGACCUUCUUUUCCCUCGCGACUCGAAAUGUUUCUUUUCGAGGUCGCCC

rT3:

GGAUCUUUCGCCUUUUCGCGAUACGGGCCAACGAUGGGUUUUGAAGGUCGCGAC

rT4:

GGGCGACCUCGUUUUGUACCAGCAUCCUCUUCAUAAGUUUUGGCGAAAGAUC

RNA Square 5'→3'

rS1:GGAUGCUGGUACUUUUGUUGGCCGAGACCAUAUCCCGGUUUUGAAACAUUUC
GAGUCGCGAGGGUUUUCCCAUCGUUGGCCCGUAUCGCGUUUUCUUAUGAAGA

rT2:

GGUCGCGACCUUCUUUUCCCUCGCGACUCGAAAUGUUUCUUUUCGAGGUCGCCC

rT3:

GGAUCUUUCGCCUUUUCGCGAUACGGGCCAACGAUGGGUUUUGAAGGUCGCGAC

rT4:

GGGCGACCUCGUUUUGUACCAGCAUCCUCUUCAUAAGUUUUGGCGAAAGAUC

rS5: GGGCGACCUCGUUUUCCGGGAUAUGGUCUCGGCCAACUUUUCGAGGUCGCCC

RNA Pentagon 5'→3'

rP1:GGAUGCUGGUACUUUUUGUUGGCCGAGACCAUAUCCCGGUUUUGGGCCAACUCU
 UAGCGUGUCCGUUUUGAAACAUUUCGAGUCGCGAGGGUUUUCCCAUCGUUGGCC
 GUAUCGCGUUUUCUUAUGAAGA

rT2:

GGUCGCGACCUUCUUUUCCCUCGCGACUCGAAAUGUUUCUUUUCGAGGUCGCCC

rT3:

GGAUCUUUCGCCUUUUUCGCGAUACGGGCCAACGAUGGGUUUUUGAAGGUCGCGAC

rT4:

GGGCGACCUCGUUUUGUACCAGCAUCCUCUUCAUAAGUUUUGGCGAAAGAUC

rS5: GGGCGACCUCGUUUUCCGGGAUAUGGUCUCGGCCAACUUUUCGAGGUCGCCC

rP6: GGGCGACCUCGUUUUCGGACACGCUAAGAGUUGGCCUUUUUCGAGGUCGCCC

RNA Hexagon 5'→3'

rH1:GGAUGCUGGUACUUUUUGUUGGCCGAGACCAUAUCCCGGUUUUGGGCCAACUC
 UUAGCGUGUCCGUUUUGGGGCCGAUAUCGAACCGGGUGUUUUGAAACAUUUCGAG
 UCGCGAGGGUUUUCCCAUCGUUGGCCCGUAUCGCGUUUUCUUAUGAAGA

rT2:

GGUCGCGACCUUCUUUUCCCUCGCGACUCGAAAUGUUUCUUUUCGAGGUCGCCC

rT3:

GGAUCUUUCGCCUUUUUCGCGAUACGGGCCAACGAUGGGUUUUUGAAGGUCGCGAC

rT4:

GGGCGACCUCGUUUUGUACCAGCAUCCUCUUCAUAAGUUUUGGCGAAAGAUC

rS5: GGGCGACCUCGUUUUCCGGGAUAUGGUCUCGGCCAACUUUUCGAGGUCGCCC

rP6: GGGCGACCUCGUUUUCGGACACGCUAAGAGUUGGCCUUUUUCGAGGUCGCCC

rH7: GGGCGACCUCGUUUUCACCCGGUUCGAUAUCGGCCCCUUUUCGAGGUCGCCC

DNA polygons:**DNA Triangle 5'→3'**

dT1:

GGATGCTGGTACTTTTTGAAACATTTTCGAGTCGCGAGGGTTTTCCCATCGTTGGCCCGT
 ATCGCGTTTTCTTATGAAGA

dT2: GGTCGCGACCTTCTTTTTCCCTCGCGACTCGAAATGTTTCTTTTTCGAGGTCGCCC

dT3: GGATCTTTCGCCTTTTCGCGATACGGGCCAACGATGGGTTTTGAAGGTCGCGAC

dT4: GGGCGACCTCGTTTTGTACCAGCATCCTCTTCATAAGTTTTGGCGAAAGATCC

DNA Square 5'→3'

dS1:GGATGCTGGTACTTTTTGTTGGCCGAGACCATATCCCGGTTTTGAAACATTTTCGAG
 TCGCGAGGGTTTTCCCATCGTTGGCCCGTATCGCGTTTTCTTATGAAGA

dT2: GGTCGCGACCTTCTTTTTCCCTCGCGACTCGAAATGTTTCTTTTTCGAGGTCGCCC

dT3: GGATCTTTCGCCTTTTCGCGATACGGGCCAACGATGGGTTTTGAAGGTCGCGAC

dT4: GGGCGACCTCGTTTTGTACCAGCATCCTCTTCATAAGTTTTGGCGAAAGATCC

dS5: GGGCGACCTCGTTTTCCGGGATATGGTCTCGGCCAACTTTTTCGAGGTCGCCC

DNA Pentagon 5'→3'

dP1:GGATGCTGGTACTTTTTGTTGGCCGAGACCATATCCCGGTTTTGGGCCAACTCTTA
 GCGTGTCCGTTTTGAAACATTTTCGAGTCGCGAGGGTTTTCCCATCGTTGGCCCGTATC
 GCGTTTTCTTATGAAGA

dT2: GGTCGCGACCTTCTTTTTCCCTCGCGACTCGAAATGTTTCTTTTTCGAGGTCGCCC

dT3: GGATCTTTCGCCTTTTCGCGATACGGGCCAACGATGGGTTTTGAAGGTCGCGAC

dT4: GGGCGACCTCGTTTTGTACCAGCATCCTCTTCATAAGTTTTGGCGAAAGATCC

dS5: GGGCGACCTCGTTTTCCGGGATATGGTCTCGGCCAACTTTTTCGAGGTCGCCC

dP6: GGGCGACCTCGTTTTCGGACACGCTAAGAGTTGGCCCTTTTTCGAGGTCGCCC

DNA Hexagon 5'→3'

dH1:GGATGCTGGTACTTTTTGTTGGCCGAGACCATATCCCGGTTTTGGGCCAACTCTTA

GCGTGTCCGTTTTGGGGCCGATATCGAACC GGGTGTTTTTGAAACATTTTCGAGTCGCG
 AGGGTTTTCCCATCGTTGGCCCGTATCGCGTTTTCTTATGAAGA
 dT2: GGTCGCGACCTTCTTTTCCCTCGCGACTCGAAATGTTTCTTTTCGAGGTCGCCC
 dT3: GGATCTTTCGCCTTTTCGCGATACGGGCCAACGATGGGTTTTGAAGGTCGCGAC
 dT4: GGGCGACCTCGTTTTGTACCAGCATCCTCTTCATAAGTTTTGGCGAAAGATCC
 dS5: GGGCGACCTCGTTTTCCGGGATATGGTCTCGGCCAACTTTTCGAGGTCGCCC
 dP6: GGGCGACCTCGTTTTCGGACACGCTAAGAGTTGGCCCTTTTCGAGGTCGCCC
 dH7: GGGCGACCTCGTTTTCACCCGGTTCGATATCGGCCCTTTTCGAGGTCGCCC

DNA center Polygons:

DNA_center Triangle 5'→3'

dT1:GGATGCTGGTACTTTTTGAAACATTTTCGAGTCGCGAGGGTTTTCCCATCGTTGGCC
 CGTATCGCGTTTTCTTATGAAGA

rT2:

GGUCGCGACCUUCUUUUCCCUCGCGACUCGAAAUGUUUCUUUUCGAGGUCGCCC

rT3:

GGAUCUUUCGCCUUUUCGCGAUACGGGCCAACGAUGGGUUUUGAAGGUCGCGAC

rT4:

GGGCGACCUCGUUUUGUACCAGCAUCCUCUUCAUAAGUUUUGGCGAAAGAUC

DNA_center Square 5'→3'

dS1:GGATGCTGGTACTTTTTGTTGGCCGAGACCATATCCCGGTTTTGAAACATTTTCGAG
 TCGCGAGGGTTTTCCCATCGTTGGCCCGTATCGCGTTTTCTTATGAAGA

rT2:

GGUCGCGACCUUCUUUUCCCUCGCGACUCGAAAUGUUUCUUUUCGAGGUCGCCC

rT3:

GGAUCUUUCGCCUUUUCGCGAUACGGGCCAACGAUGGGUUUUGAAGGUCGCGAC

rT4:

GGGCGACCUCGUUUUGUACCAGCAUCCUCUUCAUAAGUUUUGGCGAAAGAUC

rS5: GGGCGACCUCGUUUUUCCGGGAUAUGGUCUCGGCCAACUUUUCGAGGUCGCCC

DNA_center Pentagon 5'→3'

dP1:GGATGCTGGTACTTTTTGTTGGCCGAGACCATATCCCGGTTTTGGGCCAACTCTTA
 GCGTGTCCGTTTTGAAACATTTTCGAGTCGCGAGGGTTTTCCCATCGTTGGCCCGTATC
 GCGTTTTCTTATGAAGA

rT2:

GGUCGCGACCUUCUUUUCCCUCGCGACUCGAAAUGUUUCUUUUCGAGGUCGCCC

rT3:

GGAUCUUUCGCCUUUUCGCGAUACGGGCCAACGAUGGGUUUUGAAGGUCGCGAC

rT4:

GGGCGACCUCGUUUUGUACCAGCAUCCUCUUCAUAAGUUUUGGCGAAAGAUC

rS5: GGGCGACCUCGUUUUUCCGGGAUAUGGUCUCGGCCAACUUUUCGAGGUCGCCC

rP6: GGGCGACCUCGUUUUUCGGACACGCUAAGAGUUGGCCUUUUCGAGGUCGCCC

DNA_center Hexagon 5'→3'

dH1:GGATGCTGGTACTTTTTGTTGGCCGAGACCATATCCCGGTTTTGGGCCAACTCTTA
 GCGTGTCCGTTTTGGGGCCGATATCGAACC GGGTGTTTTTGAAACATTTTCGAGTCGCG
 AGGGTTTTCCCATCGTTGGCCCGTATCGCGTTTTCTTATGAAGA

rT2:

GGUCGCGACCUUCUUUUCCCUCGCGACUCGAAAUGUUUCUUUUCGAGGUCGCCC

rT3:

GGAUCUUUCGCCUUUUCGCGAUACGGGCCAACGAUGGGUUUUGAAGGUCGCGAC

rT4:

GGGCGACCUCGUUUUGUACCAGCAUCCUCUUCAUAAGUUUUGGCGAAAGAUC

rS5: GGGCGACCUCGUUUUUCCGGGAUAUGGUCUCGGCCAACUUUUCGAGGUCGCCC

rP6: GGGCGACCUCGUUUUCGGACACGCUAAGAGUUGGCCCUUUUCGAGGUCGCCC
 rH7: GGGCGACCUCGUUUUCACCCGGUUCGAUAUCGGCCCUUUUCGAGGUCGCCC

RNA center polygons:

RNA_center Triangle 5'→3'

rT1:

GGAUGCUGGUACUUUUGAAACAUUUCGAGUCGCGAGGGUUUUCUCAUCGUUGGCC
 CGUAUCGCGUUUUCUUAUGAAGA

dT2: GGTCGCGACCTTCTTTTCCCTCGCGACTCGAAATGTTTCTTTTCGAGGTCGCCC

dT3: GGATCTTTCGCCTTTTCGCGATACGGGCCAACGATGGGTTTTGAAGGTCGCGAC

dT4: GGGCGACCTCGTTTTGTACCAGCATCCTCTTCATAAGTTTTGGCGAAAGATCC

RNA_center Square 5'→3'

rS1:GGAUGCUGGUACUUUUGUUGGCCGAGACCAUAUCCCGGUUUUGAAACAUUUC
 GAGUCGCGAGGGUUUUCUCAUCGUUGGCCCGUAUCGCGUUUUCUUAUGAAGA

dT2: GGTCGCGACCTTCTTTTCCCTCGCGACTCGAAATGTTTCTTTTCGAGGTCGCCC

dT3: GGATCTTTCGCCTTTTCGCGATACGGGCCAACGATGGGTTTTGAAGGTCGCGAC

dT4: GGGCGACCTCGTTTTGTACCAGCATCCTCTTCATAAGTTTTGGCGAAAGATCC

dS5: GGGCGACCTCGTTTTCCGGGATATGGTCTCGGCCAACTTTTTCGAGGTCGCCC

RNA_center Pentagon 5'→3'

rP1:GGAUGCUGGUACUUUUGUUGGCCGAGACCAUAUCCCGGUUUUGGGCCAACUCU
 UAGCGUGUCCGUUUUGAAACAUUUCGAGUCGCGAGGGUUUUCUCAUCGUUGGCC
 GUAUCGCGUUUUCUUAUGAAGA

dT2: GGTCGCGACCTTCTTTTCCCTCGCGACTCGAAATGTTTCTTTTCGAGGTCGCCC

dT3: GGATCTTTCGCCTTTTCGCGATACGGGCCAACGATGGGTTTTGAAGGTCGCGAC

dT4: GGGCGACCTCGTTTTGTACCAGCATCCTCTTCATAAGTTTTGGCGAAAGATCC

dS5: GGGCGACCTCGTTTTCCGGGATATGGTCTCGGCCAACTTTTTCGAGGTCGCCC

dP6: GGGCGACCTCGTTTTCGGACACGCTAAGAGTTGGCCCTTTTCGAGGTCGCCC

RNA_center Hexagon 5'→3'

rH1:GGAUGCUGGUACUUUUGUUGGCCGAGACCAUAUCCCGGUUUUGGGCCAACUC
 UUAGCGUGUCCGUUUUGGGGCCGAUAUCGAACCGGUGUUUUGAAACAUUUCGAG
 UCGCGAGGGUUUUCUCAUCGUUGGCCCGUAUCGCGUUUUCUUAUGAAGA

dT2: GGTCGCGACCTTCTTTTCCCTCGCGACTCGAAATGTTTCTTTTCGAGGTCGCCC

dT3: GGATCTTTCGCCTTTTCGCGATACGGGCCAACGATGGGTTTTGAAGGTCGCGAC

dT4: GGGCGACCTCGTTTTGTACCAGCATCCTCTTCATAAGTTTTGGCGAAAGATCC

dS5: GGGCGACCTCGTTTTCCGGGATATGGTCTCGGCCAACTTTTTCGAGGTCGCCC

dP6: GGGCGACCTCGTTTTCGGACACGCTAAGAGTTGGCCCTTTTCGAGGTCGCCC

dH7: GGGCGACCTCGTTTTACCCGGTTCGATATCGGCCCTTTTCGAGGTCGCCC

Fluorescently labeled strand used in all uptake experiments:

dT2 IR-700: IR-700dye-

GGTCGCGACCTTCTTTTCCCTCGCGACTCGAAATGTTTCTTTTCGAGGTCGCCC

3.5 References

1. Jasinski, D.; Haque, F.; Binzel, D. W.; Guo, P., The Advancement of the Emerging Field of RNA Nanotechnology. *ACS Nano* **2017**.
2. Afonin, K. A.; Grabow, W. W.; Walker, F. M.; Bindewald, E.; Dobrovolskaia, M. A.; Shapiro, B. A.; Jaeger, L., Design and self-assembly of siRNA-functionalized RNA nanoparticles for use in automated nanomedicine. *Nat Protoc* **2011**, *6* (12), 2022-2034.
3. Afonin, K. A.; Kasprzak, W. K.; Bindewald, E.; Kireeva, M.; Viard, M.; Kashlev, M.; Shapiro, B. A., In silico design and enzymatic synthesis of functional RNA nanoparticles. *Acc. Chem. Res.* **2014**, *47* (6), 1731-1741.
4. Afonin, K. A.; Viard, M.; Kagiampakis, I.; Case, C. L.; Dobrovolskaia, M. A.; Hofmann, J.; Vrzak, A.; Kireeva, M.; Kasprzak, W. K.; KewalRamani, V. N.; Shapiro, B. A., Triggering of RNA Interference with RNA-RNA, RNA-DNA, and DNA-RNA Nanoparticles. *Acs Nano* **2015**, *9* (1), 251-259.
5. Afonin, K. A.; Viard, M.; Koyfman, A. Y.; Martins, A. N.; Kasprzak, W. K.; Panigaj, M.; Desai, R.; Santhanam, A.; Grabow, W. W.; Jaeger, L.; Heldman, E.; Reiser, J.; Chiu, W.; Freed, E. O.; Shapiro, B. A., Multifunctional RNA nanoparticles. *Nano letters* **2014**, *14* (10), 5662-71.
6. Afonin, K. A.; Viard, M.; Martins, A. N.; Lockett, S. J.; Maciag, A. E.; Freed, E. O.; Heldman, E.; Jaeger, L.; Blumenthal, R.; Shapiro, B. A., Activation of different split functionalities on re-association of RNA-DNA hybrids. *Nature nanotechnology* **2013**, *8* (4), 296-304.
7. Guo, P., The emerging field of RNA nanotechnology. *Nature nanotechnology* **2010**, *5* (12), 833-42.
8. Feng, L.; Li, S. K.; Liu, H.; Liu, C. Y.; LaSance, K.; Haque, F.; Shu, D.; Guo, P., Ocular delivery of pRNA nanoparticles: distribution and clearance after subconjunctival injection. *Pharmaceutical research* **2014**, *31* (4), 1046-58.
9. Jasinski, D. L.; Khisamutdinov, E. F.; Lyubchenko, Y. L.; Guo, P., Physicochemically tunable polyfunctionalized RNA square architecture with fluorogenic and ribozymatic properties. *ACS Nano* **2014**, *8* (8), 7620-9.
10. Rychahou, P.; Haque, F.; Shu, Y.; Zaytseva, Y.; Weiss, H. L.; Lee, E. Y.; Mustain, W.; Valentino, J.; Guo, P.; Evers, B. M., Delivery of RNA nanoparticles into colorectal cancer metastases following systemic administration. *ACS Nano* **2015**, *9* (2), 1108-16.
11. Shu, D.; Li, H.; Shu, Y.; Xiong, G.; Carson, W. E.; Haque, F.; Xu, R.; Guo, P., Systemic Delivery of Anti-miRNA for Suppression of Triple Negative Breast Cancer Utilizing RNA Nanotechnology. *ACS Nano* **2015**.
12. Shu, Y.; Haque, F.; Shu, D.; Li, W.; Zhu, Z.; Kotb, M.; Lyubchenko, Y.; Guo, P., Fabrication of 14 different RNA nanoparticles for specific tumor targeting without accumulation in normal organs. *RNA* **2013**, *19* (6), 767-77.
13. Stewart, J. M.; Viard, M.; Subramanian, H. K.; Roark, B. K.; Afonin, K. A.; Franco, E., Programmable RNA microstructures for coordinated delivery of siRNAs. *Nanoscale* **2016**, *8* (40), 17542-17550.
14. Steinbrecher, T.; Latzer, J.; Case, D. A., Revised AMBER parameters for bioorganic phosphates. *J Chem Theory Comput* **2012**, *8* (11), 4405-4412.
15. Lee, J. B.; Hong, J.; Bonner, D. K.; Poon, Z.; Hammond, P. T., Self-assembled RNA interference microsponges for efficient siRNA delivery. *Nat Mater* **2012**, *11* (4), 316-22.
16. Roh, Y. H.; Lee, J. B.; Shopsowitz, K. E.; Dreaden, E. C.; Morton, S. W.; Poon, Z.; Hong, J.; Yamin, I.; Bonner, D. K.; Hammond, P. T., Layer-by-layer assembled antisense DNA microsphere particles for efficient delivery of cancer therapeutics. *ACS Nano* **2014**, *8* (10), 9767-80.
17. Kim, H.; Lee, J. S.; Lee, J. B., Generation of siRNA Nanosheets for Efficient RNA Interference. *Sci Rep* **2016**, *6*, 25146.

18. Lee, H.; Lytton-Jean, A. K.; Chen, Y.; Love, K. T.; Park, A. I.; Karagiannis, E. D.; Sehgal, A.; Querbes, W.; Zurenko, C. S.; Jayaraman, M.; Peng, C. G.; Charisse, K.; Borodovsky, A.; Manoharan, M.; Donahoe, J. S.; Truelove, J.; Nahrendorf, M.; Langer, R.; Anderson, D. G., Molecularly self-assembled nucleic acid nanoparticles for targeted in vivo siRNA delivery. *Nature nanotechnology* **2012**, *7* (6), 389-93.
19. Lee, H.; Lytton-Jean, A. K. R.; Chen, Y.; Love, K. T.; Park, A. I.; Karagiannis, E. D.; Sehgal, A.; Querbes, W.; Zurenko, C. S.; Jayaraman, M.; Peng, C. G.; Charisse, K.; Borodovsky, A.; Manoharan, M.; Donahoe, J. S.; Truelove, J.; Nahrendorf, M.; Langer, R.; Anderson, D. G., Molecularly self-assembled nucleic acid nanoparticles for targeted in vivo siRNA delivery. *Nature nanotechnology* **2012**, *7* (6), 389-393.
20. Liu, X.; Xu, Y.; Yu, T.; Clifford, C.; Liu, Y.; Yan, H.; Chang, Y., A DNA nanostructure platform for directed assembly of synthetic vaccines. *Nano letters* **2012**, *12* (8), 4254-9.
21. Schuller, V. J.; Heidegger, S.; Sandholzer, N.; Nickels, P. C.; Suhartha, N. A.; Endres, S.; Bourquin, C.; Liedl, T., Cellular immunostimulation by CpG-sequence-coated DNA origami structures. *ACS Nano* **2011**, *5* (12), 9696-702.
22. Kumar, V.; Palazzolo, S.; Bayda, S.; Corona, G.; Toffoli, G.; Rizzolio, F., DNA Nanotechnology for Cancer Therapy. *Theranostics* **2016**, *6* (5), 710-25.
23. Rangnekar, A.; Nash, J. A.; Goodfred, B.; Yingling, Y. G.; LaBean, T. H., Design of Potent and Controllable Anticoagulants Using DNA Aptamers and Nanostructures. *Molecules* **2016**, *21* (2).
24. Dobrovolskaia, M. A., Self-assembled DNA/RNA nanoparticles as a new generation of therapeutic nucleic acids: immunological compatibility and other translational considerations. *DNA and RNA Nanotechnology* **2016**, *3* (7), 1-10.
25. Chen, W. W.; Zhang, X.; Huang, W. J., Role of neuroinflammation in neurodegenerative diseases (Review). *Mol Med Rep* **2016**, *13* (4), 3391-6.
26. Grinberg, S.; Linder, C.; Heldman, E., Progress in lipid-based nanoparticles for cancer therapy. *Crit Rev Oncog* **2014**, *19* (3-4), 247-60.
27. Gupta, K.; Afonin, K. A.; Viard, M.; Herrero, V.; Kasprzak, W.; Kagiampakis, I.; Kim, T.; Koyfman, A. Y.; Puri, A.; Stepler, M.; Sappe, A.; KewalRamani, V. N.; Grinberg, S.; Linder, C.; Heldman, E.; Blumenthal, R.; Shapiro, B. A., Bolaamphiphiles as carriers for siRNA delivery: From chemical syntheses to practical applications. *J Control Release* **2015**, *213*, 142-151.
28. Kim, T.; Afonin, K. A.; Viard, M.; Koyfman, A. Y.; Sparks, S.; Heldman, E.; Grinberg, S.; Linder, C.; Blumenthal, R. P.; Shapiro, B. A., In Silico, In Vitro, and In Vivo Studies Indicate the Potential Use of Bolaamphiphiles for Therapeutic siRNAs Delivery. *Mol Ther Nucleic Acids* **2013**, *2*, e80.
29. Popov, M.; Abu Hammad, I.; Bachar, T.; Grinberg, S.; Linder, C.; Stepensky, D.; Heldman, E., Delivery of analgesic peptides to the brain by nano-sized bolaamphiphilic vesicles made of monolayer membranes. *European journal of pharmaceuticals and biopharmaceutics : official journal of Arbeitsgemeinschaft fur Pharmazeutische Verfahrenstechnik e.V* **2013**, *85* (3 Pt A), 381-9.
30. Popov, M.; Grinberg, S.; Linder, C.; Waner, T.; Levi-Hevroni, B.; Deckelbaum, R. J.; Heldman, E., Site-directed decapsulation of bolaamphiphilic vesicles with enzymatic cleavable surface groups. *J Control Release* **2012**, *160* (2), 306-14.
31. Ransohoff, R. M.; Brown, M. A., Innate immunity in the central nervous system. *J Clin Invest* **2012**, *122* (4), 1164-71.
32. Perry, V. H.; Holmes, C., Microglial priming in neurodegenerative disease. *Nat Rev Neurol* **2014**, *10* (4), 217-24.
33. Ramesh, G.; MacLean, A. G.; Philipp, M. T., Cytokines and chemokines at the crossroads of neuroinflammation, neurodegeneration, and neuropathic pain. *Mediators Inflamm* **2013**, *2013*, 480739.
34. Sofroniew, M. V., Astrocyte barriers to neurotoxic inflammation. *Nat Rev Neurosci* **2015**,

16 (5), 249-63.

35. Afonin, K. A.; Desai, R.; Viard, M.; Kireeva, M. L.; Bindewald, E.; Case, C. L.; Maciag, A. E.; Kasprzak, W. K.; Kim, T.; Sappe, A.; Stepler, M.; Kewalramani, V. N.; Kashlev, M.; Blumenthal, R.; Shapiro, B. A., Co-transcriptional production of RNA-DNA hybrids for simultaneous release of multiple split functionalities. *Nucleic acids research* **2014**, *42* (3), 2085-2097.
36. Halman, J. R.; Satterwhite, E.; Roark, B.; Chandler, M.; Viard, M.; Ivanina, A.; Bindewald, E.; Kasprzak, W. K.; Panigaj, M.; Bui, M. N.; Lu, J. S.; Miller, J.; Khisamutdinov, E. F.; Shapiro, B. A.; Dobrovolskaia, M. A.; Afonin, K. A., Functionally-interdependent shape-switching nanoparticles with controllable properties. *Nucleic acids research* **2017**.
37. Khisamutdinov, E. F.; Li, H.; Jasinski, D. L.; Chen, J.; Fu, J.; Guo, P., Enhancing immunomodulation on innate immunity by shape transition among RNA triangle, square and pentagon nanovehicles. *Nucleic acids research* **2014**, *42* (15), 9996-10004.
38. Bui, M. N.; Brittany Johnson, M.; Viard, M.; Satterwhite, E.; Martins, A. N.; Li, Z.; Marriott, I.; Afonin, K. A.; Khisamutdinov, E. F., Versatile RNA tetra-U helix linking motif as a toolkit for nucleic acid nanotechnology. *Nanomedicine* **2017**.
39. Zuker, M., Mfold web server for nucleic acid folding and hybridization prediction. *Nucleic acids research* **2003**, *31* (13), 3406-15.
40. Zadeh, J. N.; Steenberg, C. D.; Bois, J. S.; Wolfe, B. R.; Pierce, M. B.; Khan, A. R.; Dirks, R. M.; Pierce, N. A., NUPACK: Analysis and design of nucleic acid systems. *J Comput Chem* **2010**, *32* (1), 170-3.
41. Dirks, R. M.; Lin, M.; Winfree, E.; Pierce, N. A., Paradigms for computational nucleic acid design. *Nucleic acids research* **2004**, *32* (4), 1392-403.
42. Wolfe, B. R.; Pierce, N. A., Sequence Design for a Test Tube of Interacting Nucleic Acid Strands. *ACS Synth Biol* **2015**, *4* (10), 1086-100.
43. Zadeh, J. N.; Wolfe, B. R.; Pierce, N. A., Nucleic acid sequence design via efficient ensemble defect optimization. *J Comput Chem* **2011**, *32* (3), 439-52.
44. Dassault Systèmes BIOVIA, D. S. M. E., Release 2017, San Diego: Dassault Systèmes, 2016.
45. Case, D. A.; Cheatham, T. E., 3rd; Darden, T.; Gohlke, H.; Luo, R.; Merz, K. M., Jr.; Onufriev, A.; Simmerling, C.; Wang, B.; Woods, R. J., The Amber biomolecular simulation programs. *J Comput Chem* **2005**, *26* (16), 1668-88.
46. Shlyakhtenko, L. S.; Gall, A. A.; Lyubchenko, Y. L., Mica functionalization for imaging of DNA and protein-DNA complexes with atomic force microscopy. *Methods in molecular biology* **2013**, *931*, 295-312.
47. Shlyakhtenko, L. S.; Gall, A. A.; Filonov, A.; Cerovac, Z.; Lushnikov, A.; Lyubchenko, Y. L., Silatrane-based surface chemistry for immobilization of DNA, protein-DNA complexes and other biological materials. *Ultramicroscopy* **2003**, *97* (1-4), 279-287.
48. Garcia-Mesa, Y.; Jay, T. R.; Checkley, M. A.; Luttge, B.; Dobrowolski, C.; Valadkhan, S.; Landreth, G. E.; Karn, J.; Alvarez-Carbonell, D., Immortalization of primary microglia: a new platform to study HIV regulation in the central nervous system. *J Neurovirol* **2017**, *23* (1), 47-66.
49. Chauhan, V. S.; Sterka, D. G., Jr.; Gray, D. L.; Bost, K. L.; Marriott, I., Neurogenic exacerbation of microglial and astrocyte responses to *Neisseria meningitidis* and *Borrelia burgdorferi*. *Journal of immunology* **2008**, *180* (12), 8241-9.
50. Mikolov, T.; Chen, K.; Corrado, G.; Dean, J., Efficient Estimation of Word Representations in Vector Space. *ArXiv13013781 Cs* **2013**.
51. Breiman, L., Random Forests. *Mach Learn* **2001**, *45* (1), 5-32.
52. Warr, W. A., Scientific workflow systems: Pipeline Pilot and KNIME. *J Comput Aided Mol Des* **2012**, *26* (7), 801-4.
53. Zakharov, A. V.; Peach, M. L.; Sitzmann, M.; Filippov, I. V.; McCartney, H. J.; Smith, L. H.; Pugliese, A.; Nicklaus, M. C., Computational tools and resources for metabolism-related

property predictions. 2. Application to prediction of half-life time in human liver microsomes. *Future Med Chem* **2012**, *4* (15), 1933-44.

54. Tropsha, A., Best Practices for QSAR Model Development, Validation, and Exploitation. *Mol Inform* **2010**, *29* (6-7), 476-88.

55. Dobrovolskaia, M. A., Pre-clinical immunotoxicity studies of nanotechnology-formulated drugs: Challenges, considerations and strategy. *J Control Release* **2015**, *220* (Pt B), 571-83.

4 Chapter 4: A cationic amphiphilic co-polymer as a carrier of nucleic acid nanoparticles (NANPs) for controlled gene silencing, immunostimulation, and biodistribution

4.1 Introduction

Therapeutic nucleic acids (TNAs) have garnered considerable attention as potential therapeutics for assorted diseases. RNA interference (RNAi) inducers, aptamers, and immunostimulatory nucleic acids have been studied for their ability to treat both endogenous and infectious diseases. The latest success of the first RNAi-based therapeutic agent (Patisiran)¹, FDA-approved in 2018, makes advances in the composition and delivery of TNAs timely and important²⁻⁵. Recently, a new generation of nucleic acid-based nanoparticles (NANPs) functionalized with TNAs has been introduced. NANPs are composed of multiple nucleic acid strands programmed to self-assemble into defined 3D structures⁶ with further possibilities for embedded functionalities⁷⁻¹³. Various self-assembling NANPs have been generated to both increase stability and enzymatic resistance, as well as to coalesce multiple pharmaceuticals¹⁴⁻²⁰. The ability to finely control the size, shape, multivalency, and therapeutic payload makes NANP technology an attractive option for biomedical applications. Despite advances, hurdles to the rapid translation of NANPs from benchtop to clinic include their poor resistance to enzymatic degradation in blood serum, their inability to cross biological membranes, and the potential for deleterious immune responses²¹⁻²². Therefore, combining potent customizable therapeutic NANPs with stable, non-toxic, and non-immunogenic carriers would greatly increase the clinical potential of such agents for the treatment of a plethora of diseases; however, the effects of NANP size, shape, and composition on relative delivery efficiency with the same carrier have not yet been determined.

A number of effective TNA carriers composed of a wide variety of materials have been investigated to combat the difficulties associated with the use of NANPs and each possesses distinct features²³⁻²⁶. In addition, each new formulation varies in terms of toxicity, biodistribution, accumulation, *in vivo* stability, and excretion. Furthermore, different formulations have shown

varied success in crossing the blood brain barrier (BBB), a major challenge for the treatment of central nervous system (CNS) diseases. Finally, the drug loading capabilities of each formulation varies, allowing for various payload magnitudes to be delivered in a single multi-modal platform.

Cationic lipids, liposomes, and polymers, including polyethylenimine (PEI), poly (β -amino esters), and polyamidoamine (PAMAM) dendrimers, have been evaluated as non-viral vectors for pDNA and small RNA therapeutics²⁷⁻²⁹. Among these carriers, branched PEI (bPEI; 25kDa), considered the gold standard for gene transfection, has exhibited the highest transfection efficiency among non-viral vectors in serum-free conditions due to its ability to form stable polyplexes with nucleic acids and its buffering capacity, which facilitates its endosomal escape via the proton sponge effect³⁰. However, the low transfection efficiency of bPEI in the presence of serum limits its potential for use as a vector *in vivo*.

In the present work, we employed the previously described cationic amphiphilic co-polymer, poly (lactide-co-glycolide)-graft-polyethylenimine (PgP)³¹⁻³² as a carrier for a series of NANPs of different shapes and sizes that include three-dimensional cubic^{14-15,33-35}, planar ring-like³⁶⁻³⁹, and fibrous^{36,40} RNA self-assembling NANPs. PgP, a micelle-forming co-polymer composed of poly (lactic-co-glycolic acid) (PLGA) and bPEI, has previously been characterized and demonstrated to be an efficient carrier of siRNA and pDNA *in vitro* in various cell lines and in the rat normal spinal cord *in vivo*³². PgP has also been demonstrated to deliver siRNA targeting RhoA to spinal cord lesion sites in a rat model of compression injury, achieving sustained RhoA gene expression knockdown for up to four weeks and supporting its efficacy as an *in vivo* TNA delivery system⁴¹. Here, we investigated the effect of NANP size, shape, and composition on PgP/NANP polyplex stability, intracellular uptake, silencing efficiency, toxicity, immunostimulatory activity, hemocompatibility, and biodistribution, *in vitro* and/or *in vivo*. Figure 31 illustrates the experimental design of the current work.

4.2 Methods

4.2.1 Synthesis of PgP and NANPs

PgP was synthesized as previously described using PLGA (4kDa, 50:50, Durect Corporation Pelham, AL) and bPEI (MW 25 kDa, Sigma). DNA templates and primers were purchased from Integrated DNA Technologies (Coralville, Iowa) and polymerase chain reaction (PCR) was performed using primers containing the T7 RNA polymerase promoter sequence to amplify the DNA template. To obtain RNAs, *in vitro* transcription was performed for four hours at 37 °C using T7 RNA polymerase in a buffer containing 80 mM HEPES-KOH (pH 7.5), 2.5 mM spermidine, 50 mM DTT, 2 mM MgCl₂, 25 mM rNTPs, 0.2 μM DNA templates and ~100 units/μL of T7 RNA polymerase enzyme (isolated in house). Transcription was stopped using RQ1 DNase (Promega, WI). RNAs were purified using a denaturing urea gel (PAGE, 10% acrylamide, 8 M urea). Gel pieces containing RNAs were excised from the gel and the RNA was eluted overnight at 4 °C in 1 X TBE buffer with 300 mM NaCl. The following day, RNAs were precipitated in 2.5 X volumes of ethanol, followed by a 90% ethanol wash. RNAs were dried using vacuum centrifugation and suspended in endotoxin-free double-deionized water. All NANPs were assembled using previously published protocols. Briefly, functional RNA rings and fibers were assembled by mixing individual monomers at an equimolar ratio, heating to 95 °C for 2 min, snap cooling on ice for 2 min, adding 20% volume of 5 X assembly buffer (final concentration: 89 mM TB (pH 8.2), 50 mM KCl, 2 mM MgCl₂), and further incubated for 30 min at 30 °C. Functional RNA cubes were assembled by mixing all constituent strands at an equimolar ratio and heating to 95 °C for 2 min. The samples were then snap cooled to 45 °C and incubated for 2 min. Finally, 5X assembly buffer was added and the assembly mixture was further incubated at 45 °C for an additional 30 min.

4.2.2 Nuclease protection assay of PgP/DNA duplex polyplexes

Briefly, DNA duplex (200 nM final) tagged with Alexa488 and Iowa Black quencher (PgP/DNA-AI488/IWB) was incubated with PgP at various N/P ratios at 37 °C for 30 minutes (30

μL final). Following complexation, 3 μL of RQ1 DNase (Promega, WI) was added to the solution. The fluorescence was measured every thirty seconds using a Bio-Rad C1000 Touch Thermal Cycler and CFX96 Real Time System (Bio-Rad, Hercules, California).

4.2.3 Physical characterization of NANPs

To evaluate the structure of assembled NANPs, 5 μL (50 nM) of each particle was deposited on APS-modified mica, incubated for ~ 2 min and air-dried, as described previously according to established protocols. Briefly, AFM was performed using a MultiMode AFM Nanoscope IV system (Bruker Instruments, Santa Barbara, CA) in tapping mode. The images were recorded with a 1.5 Hz scanning rate using a TESPA-300 probe from Bruker with a resonance frequency of 320 kHz and spring constant of about 40 N/m. Images were processed by the FemtoScan Online software package (Advanced Technologies Center, Moscow, Russia). Non-denaturing polyacrylamide gel electrophoresis (Native-PAGE) was performed using 8% acrylamide, 37.5:1 acrylamide/bis-acrylamide, run at 4° C. A heparin competition assay was performed to ensure structural integrity was maintained. For this assay, each NANP was bound to PgP at a 30:1 N/P ratio, then released by electrostatic competition with heparin, and run through Native-PAGE.

4.2.4 Fluorescent microscopy and cellular uptake

Confocal microscopy images were taken using a LSM710 confocal microscope (Carl Zeiss, Germany) equipped with a 63X/1.4 magnification lens. In order to confirm an endosomal uptake pathway of the PgP complexed RNA, PgP/DS RNA-A1546 were transfected into MDA-MB-231 cells and incubated for 6 hours, at which point they were washed three times with PBS and fixed with 4% paraformaldehyde for 20 minutes at room temperature. For uptake analysis, A1546 was imaged by exciting the sample with a DPSS 561 laser and collecting emission at wavelengths of 566 and 640 nm, respectively. For co-localization, the cells were permeabilized with Tween 20 (0.2% for 30 minutes at room temperature), blocked with 1% BSA, and stained with an antibody directed against Rab5 (Santa Cruz, Dallas, TX) and a secondary antibody labeled with

Alexa 647 (Molecular Probes, CA). For Alexa 647 imaging, a 633 nm Helium Neon laser was used for excitation at 638 nm and the emission was collected at a wavelength of 755 nm.

4.2.5 Specific gene silencing and cell viability

MDA-MB-231/GFP cells were cultured in DMEM supplemented with 10% FBS and 100 U/mL penicillin-100 µg/mL streptomycin at 37 °C 5% CO₂. Cells were seeded in 24-well plates at 20,000 cells per well and allowed to adhere overnight. The following day, 50 nM of NANP (GFP) was combined with PgP at an N/P ratio of 30:1 for 30 minutes at 37 °C. The PgP/NANP(GFP) polyplexes were then added to the cells by mixing with FBS supplemented DMEM. After 72 hours of incubation, fluorescent imaging was conducted using an EVOS FL with 10X magnification, and quantitative fluorescence was measured using flow cytometry (BD Accuri C6) measuring 10,000 events per condition.

B35 neuroblastoma cells (CRL-2754, ATCC, Manassas, VA) at a density of 8×10^4 cells/well were seeded in 24-well plates in 10% serum-supplemented medium and cultured overnight to allow cells adhere to the plate. PgP/NANP(RhoA) polyplexes (1 µg of various NANPs) were prepared by mixing PgP and NANPs(RhoA) at an N/P ratio of 30:1. PgP/NT-siRNA at an N/P ratio of 30:1 was prepared as a negative control and Lipofectamine 3000/DS RNA(RhoA) was prepared according to manufacturer's protocol and was used as a positive control. Non-transfected cells were also used as a control. The cells were transfected with polyplexes in medium containing 10% FBS, incubated for 24 hours, and then the media containing polyplexes was removed and replaced by fresh medium containing 10% FBS. The cells were then incubated for an additional 48 hours. At 72 hours post-transfection, the cells were lysed and total RNA was isolated using RNeasy mini kit (Qiagen, Germany). The isolated RNA quality and QUANTity were evaluated by Take 3 using a BioTek synergy microplate reader (BioTek, Synergy HT). Complementary DNA (cDNA) was synthesized by reverse transcription reactions with isolated total RNA (1.0 µg) using MultiScribe™ reverse transcriptase with random primers (High Capacity cDNA Reverse Transcription Kit; Applied Biosystems, Foster city, CA). Real-time PCR was

performed using target-specific primers (final concentration: 0.5 μ M) and SYBR Green PCR kit in a Rotorgene Q thermal cycler (Qiagen). Glyceraldehyde-3-phosphate dehydrogenase (GAPDH) was used as an endogenous control. Primers for RhoA: forward primer: 5'-CAA GGA CCA GTT CCC AGA GG -3', reverse primer: 5'-GCT GTG TCC CAT AAA GCC AAC-3'. Primers for GAPDH: forward primer: 5'- ATG GCC TTC CGT GTT CCT AC-3'; reverse primer: 5'-TAG CCC AGG ATG CCC TTT AG -3'. Relative mRNA expression levels of RhoA were calculated using the $2^{-\Delta\Delta C_t}$ method. The minus RT (reverse transcriptase) reactions were performed on a representative subset of samples to confirm no genomic DNA contamination. Reaction specificities were verified by melting curve analysis.

4.2.6 Immunostimulation in vitro

THP1-Dual™ cells (Invivogen, CA) are monocytes engineered to express secreted alkaline phosphatase (SEAP) when NF- κ B is stimulated and luciferase when the IRF pathway is stimulated. THP1-Dual™ cells were plated at 40,000 cells per well in a 96 well-plate and immediately transfected with PgP/NANP(GFP) complexes at 100 nM with a 30:1 N/P ratio. R848 (1 μ g/mL) and poly I:C (0.5 μ g/mL) were used as positive controls. After 24 hours of incubation, 20 μ L of the suspension media was mixed with 50 μ L of QUANTI-Luc™ (Invivogen) and the luminescence was immediately measured. Furthermore, 20 μ L of supernatant media was then mixed with 180 μ L of QUANTI-Blue™ (Invivogen, CA) and incubated for two hours at 37 °C and the absorbance at 620 nm was measured.

HEK-Blue™ hTLR (Invivogen, CA) cells are HEK 293 cells engineered to express a single TLR with an NF- κ B-inducible SEAP reporter gene. Both HEK-Blue™ hTLR -3 and -7 cells were maintained under selective antibiotics as recommended by the manufacturer and were plated in 96-well plates at 40,000 cells per well. The cells were then transfected with 100 nM PgP/NANP(GFP) at a 30:1 N/P ratio for 24 hours. R848 was used as a positive control for hTLR7, and poly I:C for hTLR3. Following incubation, 20 μ L of the supernatant media was mixed with 180 μ L of QUANTI-Blue™ detection media (Invitrogen, CA) for 2 hours and the absorbance was measured at 620 nm.

4.2.7 Hemolysis assay in vitro

To evaluate the blood compatibility of various PgP/NANP polyplexes, a hemolysis assay was performed by adapting a protocol used by Aravindan and co-workers. Polyplexes were prepared by mixing PgP with various functionalized NANPs (cubes, rings, and fibers) carrying DS RNAs against GFP (an N/P ratio of 30:1) and individual DS RNAs against GFP (an N/P ratio of 30:1) for comparison. Briefly, rat blood (4 mL) was collected in a heparinized tube via cardiac puncture and centrifuged at 700 X g for 20 minutes at 4 °C. The buffy coat and plasma was removed and then the erythrocyte (red blood cell) pellet was washed three times with PBS (pH 7.4) by centrifuging at 1000 X g for 10 minutes at 4 °C. Erythrocytes were re-suspended in a 3% (w/v) solution in PBS. Equal volumes of erythrocyte solution and PgP/NANP(GFP) polyplexes (80 µL each) were mixed and incubated for 1 hour at 37 °C. Following incubation, suspensions were centrifuged at 1000 X g for 10 minutes and the pellet and supernatant were separated. The pellet was resuspended in PBS and the morphology of erythrocytes was imaged using an inverted microscope (Zeiss Axiovert 200, Göttingen, Germany). The supernatant (100 µL) was transferred to a 96 well plate and absorbance was measured at 540 nm using a Synergy HT plate reader (Biotek, Winooski, VT). PBS and Triton X-100 treatments were used as controls for 0 and 100% hemolysis. Hemolysis was QUANTIFIED using the following formula:

$$\frac{A_{Sample} - A_{PBS}}{A_{Triton-X} - A_{PBS}} \times 100\%$$

where A_{Sample} , A_{PBS} , A_{Triton} are the absorbances of the sample, PBS, and Triton X-100, respectively.

4.2.8 Biodistribution of PgP/NANP polyplexes after systemic injection

To visualize the biodistribution of PgP/NANP polyplexes, the hydrophobic fluorescent dye 1,1-dioctadecyl-3,3,3,3-tetramethyl indo tricarboyanine iodide (DiR, PromoCell GmbH, Germany) was loaded in the core of PgP by the solvent evaporation method, followed by complexation with either cubes, rings, or fibers functionalized with DS RNAs against GFP or free

DS RNAs. Briefly, DiR dye was dissolved in acetone and the DiR solution was added into a PgP solution (10 mg/mL) and then incubated for 4 hours at room temperature under constant stirring. After loading, the DiR-PgP solution was incubated overnight to evaporate acetone (final DiR concentration: 250 μ g/mL). The DiR-PgP solution was filtered (0.2 μ m pore size) to remove unloaded DiR dye. Various DiR-PgP/NANP (50 μ g RNA) polyplexes at an N/P ratio 30:1 were prepared by mixing various NANP solutions with DiR-PgP and incubated at 37 °C for 30 min. Male CD-1 mice (7-8 weeks-old, Charles River Laboratories, MA) were anesthetized using isoflurane gas and various DiR-PgP/NANP polyplexes (2 mg/kg, RNA per body weight) were injected via tail vein. PgP complexed to DS RNA was used for comparison and untreated mice were used as a control group. At 1, 2, 6, and 24 hours post-injection, the animals were imaged by a live animal fluorescence imaging system (IVIS Luminar XR, Caliper Life Sciences) under anesthesia with isoflurane gas. At 24 hours post-injection, the animals were euthanized by CO₂ and their organs (liver, heart, lungs, spleen, kidneys, and brain) were harvested for *ex vivo* organ imaging and determination of the fluorescence intensity of the region of interest (ROI). The % of organ distribution was calculated as the fluorescence of the organ normalized by the total fluorescence of the total organs. quantification of organ accumulation of polyplexes was compared for the five groups using analysis of variance with a significance level of 0.05.

4.2.9 Statistics

Experimental results are presented as the mean \pm SEM. Statistical significance was determined using one-way Anova using GraphPad Prism Software Version 7.

4.3 Results

4.3.1 PgP/DNA stability, binding, and nuclease protection assay

For cost efficiency, all initial *in vitro* optimization experiments were performed using Alexa 488-labeled DNAs rather than labeled RNA. To identify the formation of stable complexes of PgP and DNA duplexes (Fig. 32A), a fixed amount of fluorescently tagged DNA duplex was

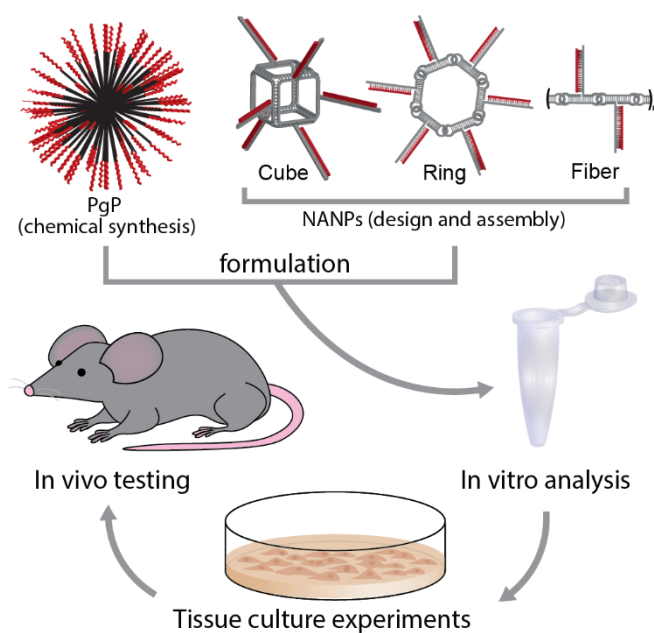


Figure 30. Experimental design of the current work.

mixed with PgP at varying N/P ratios and run through a 2% (w/v) agarose gel. Duplexes not complexed with PgP migrated freely through the gels, while the mobility of duplexes electrostatically complexed with PgP was limited. Complete retardation was observed at an N:P

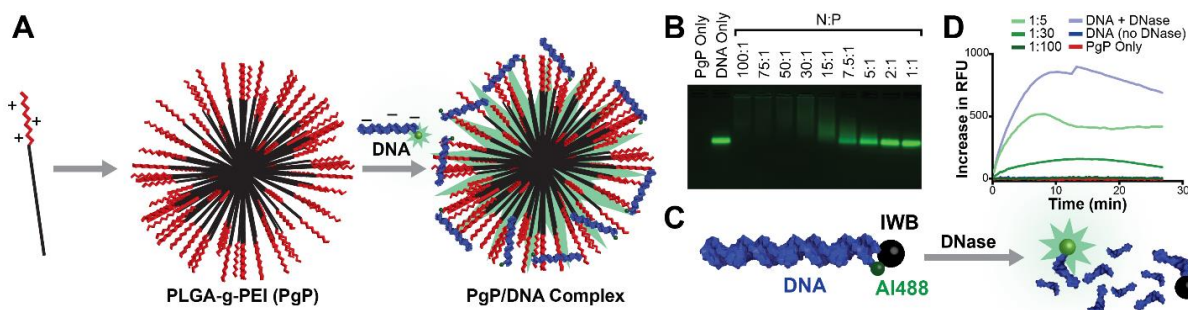


Figure 31. Binding of DNA to PgP leads to protection from nuclease activity. (A) Schematic showing electrostatically-driven PgP binding to nucleic acids, (B) gel retardation of various PgP/DNA polyplexes prepared using various PgP/DNA ratios (N/P ratio), and (C-D) nuclease protection assay of PgP/DNA polyplexes after incubation with DNase I.

ratio of 30:1 (Fig. 32B). Above this ratio, additional PgP did not demonstrate any difference in the gel. This demonstrated a visual representation of the PgP's maximum loading capacity and confirmed attachment of PgP to nucleic acids. Next, we investigated the ability of the PgP to protect the nucleic acid cargo from enzymatic degradation. DNA duplexes tagged with Alexa 488 at the 5'-side and Iowa Black quencher at the corresponding 3'-side were treated with RQ1 DNase (Fig. 32C-D). In untreated duplexes, the close proximity of Iowa Black completely quenched the fluorescence of Alexa 488. However, upon DNase treatment, the degradation of duplexes and further spatial separation of fluorophore and quencher led to activation of the fluorescent signal. PgP was shown to successfully shield the attached nucleic acids from enzymatic activity for several hours, as evidenced by the minimal increase in fluorescence as compared to the rapidly increasing signal in that of free duplexes.

4.3.2 Intracellular uptake of PgP/RNA or PgP/DNA complexes

To confirm intracellular uptake and localization, PgP complexed with Alexa 488-labeled DS RNAs (PgP/RNA-AI488) were added to breast cancer cells (MDA-MB-231). MDA-MB-231 cells are an immortalized triple negative breast cancer cell line used frequently in the study of cancer therapeutics. The cells proliferate quickly, and are frequently studied as transfection targets for nucleic acid therapeutics. Confocal microscopy showed that PgP/RNA-AI488 polyplexes were successfully internalized into the cells and distributed in the cytoplasm for extended periods of time (Fig. 33A). To confirm that the PgP was taken in via endocytosis, cells were again exposed to PgP/RNA-AI488 and co-localization with protein Rab5, which localizes around endosomes to promote trafficking⁴², was demonstrated (Fig. 2B). The co-localization of the Alexa 488 (green) and the anti-Rab5 antibodies (red) demonstrates that the PgP/RNA-AI488 polyplexes were taken up and processed via an endosomal pathway. To further confirm this observation, MDA-MB-231 cells were exposed to PgP/RNA-AI488 or PgP/DNA-AI488 at either 37 °C or 4 °C (Fig. 33C). Endocytosis is a temperature-dependent process that has been previously demonstrated to be absent in cells under 4 °C conditions⁴³. Our flow cytometry and microscopy results show that cells

exposed to PgP/DNA-A1488 or PgP/RNA-A1488 complexes at 4 °C showed a negligible increase in fluorescence, while those transfected with the same sample at 37 °C showed a marked increase in fluorescence (Fig 33C-D). These data therefore support our hypothesis that PgP/DNA and PgP/RNA polyplexes are taken into cells via endocytosis.

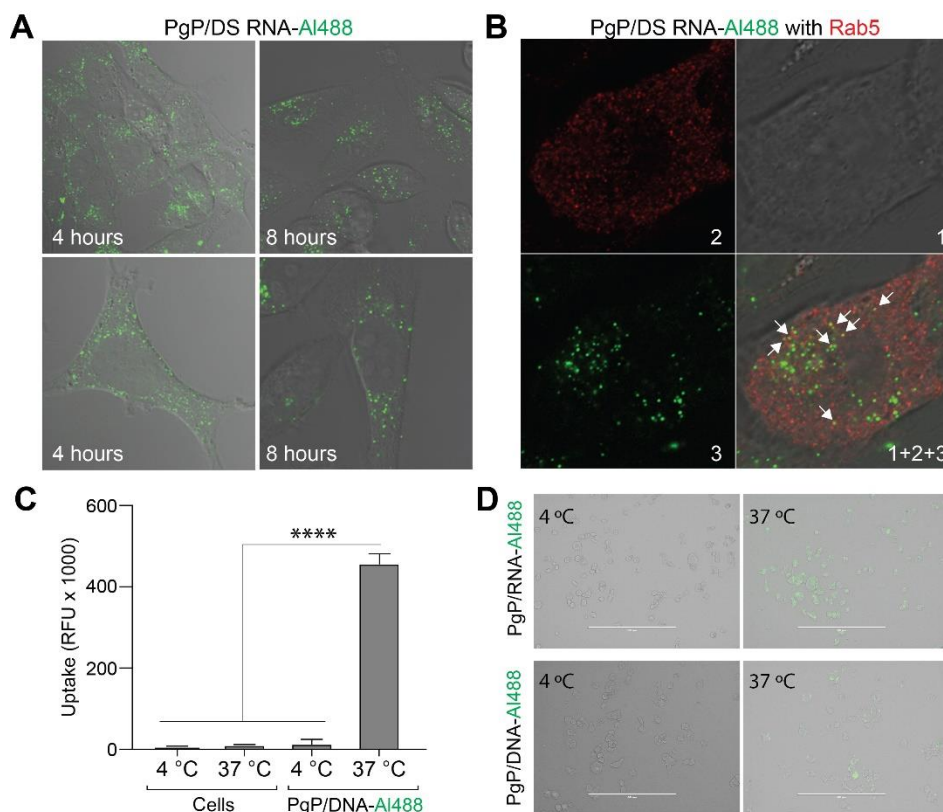


Figure 32. Intracellular uptake of PgP/DS RNA polyplexes assessed in MDA-MB-231 human breast cancer cells. (A) Visualization of intracellular uptake of polyplexes by confocal microscope; (B) Co-localization of polyplexes with early endosomal marker Rab5 confirms an endocytic pathway of internalization; (C) Flow cytometry measuring the effect of temperature on intracellular uptake of polyplexes (**** denotes $p < 0.0005$); (D) Fluorescent microscopy and bright-field overlay of MDA-MB-231 human breast cancer cells transfected with either PgP/DS RNA-A1488 or PgP/DNA-A1488 at either 4 °C or 37 °C, 6 hours after transfection.

4.3.3 Characterization of PgP/NANP polyplexes

The NANPs included in this study were generated utilizing various design strategies and were formulated to assemble into robust constructs with distinct connectivity, shapes, and sizes. Three-dimensional hexameric RNA cubes assemble via intermolecular Watson-Crick base pairing, while planar hexameric RNA rings and linear RNA fibers both assemble via magnesium-dependent

intramolecular Watson-Crick base pairing to facilitate intermolecular kissing loop interactions (120° ColE1-like for rings and 180° HIV-like for fibers). The cubic RNA structures are designed to form solely due to intermolecular forces, avoiding secondary structures within individual strands and forming a 3D cube. The rings and fibers are designed to fold via intramolecular interactions, exposing kissing loops for strand-strand interactions to form a planar ring. By extending the individual strands of each scaffold, cubes, rings, and fibers, can be functionalized with DS RNAs

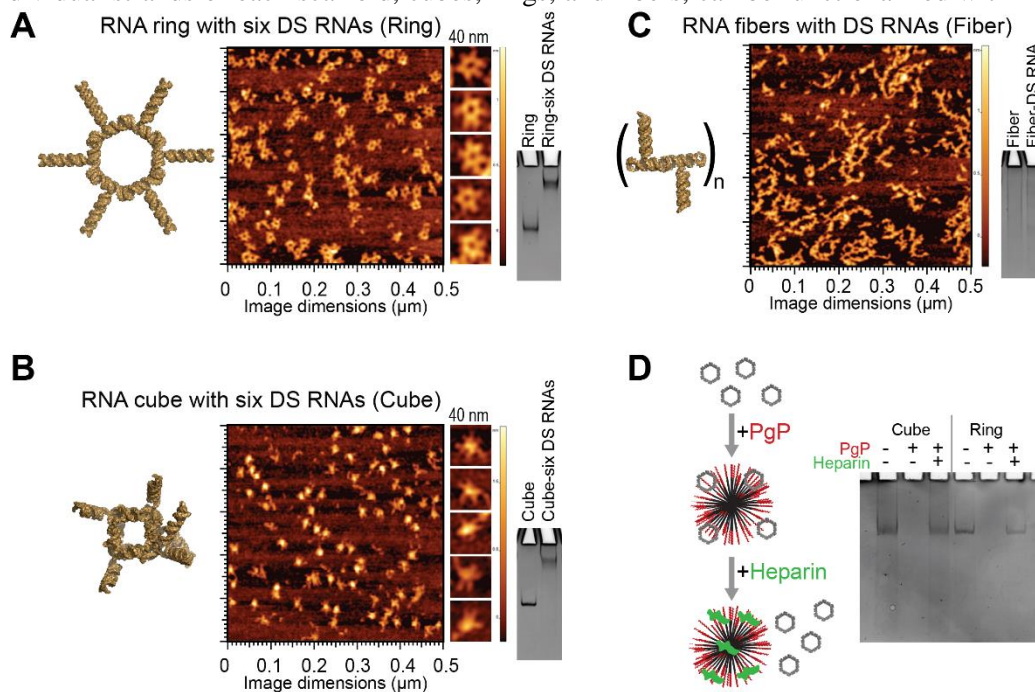


Figure 33. Characterization of various functionalized NANPs by AFM and native-PAGE: (A) RNA rings functionalized with six Dicer substrate (DS) RNAs, (B) RNA cubes functionalized with six DS RNAs, and (C) DS functionalized RNA fibers. (D) Native-PAGE results confirm the integrity of NANPs upon heparin-assisted release from PgP polyplexes.

against any target and generated via one-pot assembly as previously described^{15, 21, 37}. The assemblies of resulting functional NANPs can then be confirmed by both gel electrophoresis (native-PAGE) and atomic force microscopy (AFM) as shown in Fig. 34A-C. An important aspect of this study was to determine the effect of functional NANP compositions on their delivery and efficacy. As such, it was essential to demonstrate that the NANPs stay intact following release from PgP. A heparin competition assay was performed to disrupt the PgP/NANP interaction and release the NANP following PgP binding. Gel electrophoresis demonstrates that the model NANPs remain

intact following their release (Fig. 34D).

4.3.4 Gene silencing with PgP/NANP(GFP or RhoA) polyplexes

We have previously demonstrated that NANPs functionalized with DS RNA against GFP efficiently silence GFP expression when transfected into various cell lines using common transfection agents such as Lipofectamine 2000^{11-12, 21, 38, 44}. To confirm the efficacy of PgP as a delivery agent, we transfected the breast cancer cell line MDA-MB-231/GFP with the panel of PgP/NANP(GFP) polyplexes. The NANPs with multiple DS RNAs against GFP, as well as individual GFP DS RNA complexed with PgP, were shown to successfully silence the expression of GFP as demonstrated by fluorescent microscopy and flow cytometry (Fig. 35A-B), without significant changes in cell viability (Fig. 35C). All transfections were performed at concentrations normalized to the amounts of DS RNAs (50 nM). Despite their structural differences, no NANP was determined to be significantly better than the others. To further demonstrate therapeutic potential in central nervous system injury repair, NANPs decorated with DS RNAs targeting RhoA were tested in rat neuroblastoma (B35) cells. Previously, PgP complexed with siRNA against RhoA has been demonstrated to treat spinal cord injuries in rats⁴¹. We sought to determine whether RhoA DS RNA-functionalized NANPs (Fig. 36A) have enhanced silencing capabilities versus conventional DS RNAs. PgP/NANPs(RhoA) were transfected into B35 cells and uptake was confirmed (Fig. 36B). We identified that fibers functionalized with RhoA DS RNAs induced greater knockdown than cube NANPs, ring NANPs, or standard RhoA siRNA duplexes (Fig. 36C). This enhanced knockdown occurred in the absence of significant changes in cell viability (data not shown).

4.3.5 Hemocompatibility and immunotoxicity of PgP/NANP polyplexes

To assess the potential for detrimental toxicity that would limit the therapeutic potential of

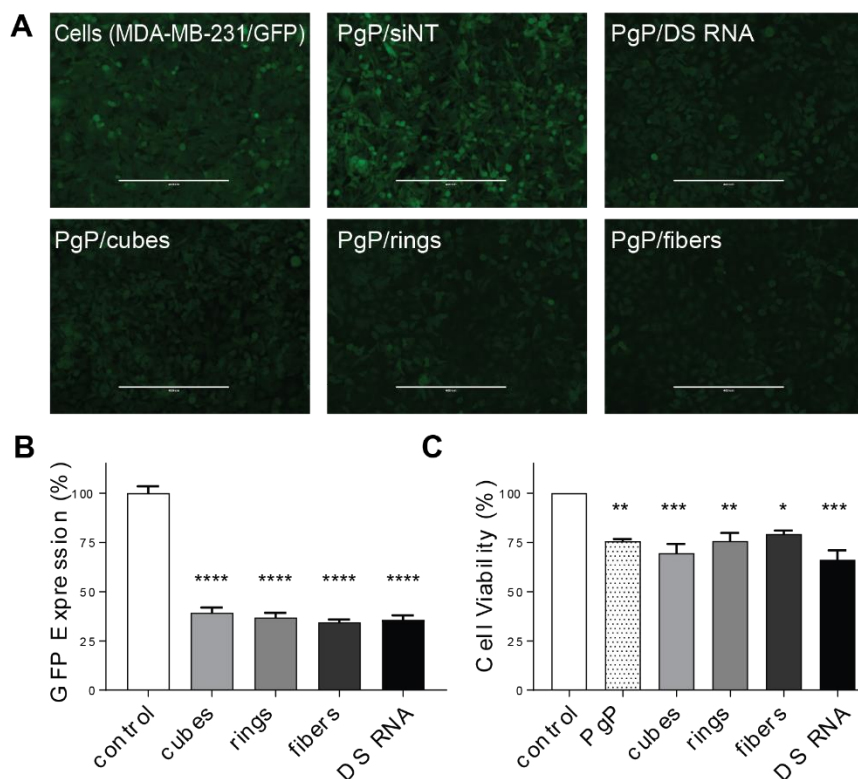


Figure 34. Specific gene silencing with PgP/NANP(GFP) polyplexes and cell viability assays tested against GFP expressing breast cancer cells (MDA-MB-231/GFP). Fluorescent microscopy (A) shows representative images of GFP knockdown by PgP/NANP(GFP) polyplexes. (B) GFP knockdown efficiency by cubes (PgP/cubes(GFP)), rings (PgP/rings(GFP)), and fibers (PgP/fibers(GFP)) are compared to free DS RNAs(GFP) and negative control (siNT), PgP only (0.1 mg/mL) used as an additional control. (N=3, **** denotes statistically significant vs. untreated cells with $p < 0.0005$, # denotes statistical significance vs. cubes with $p < 0.05$). (C) Cell viability by PgP/NANP(GFP) polyplexes (N=3, * denotes statistical significance with $p < 0.05$, ** with $p < 0.005$, *** with $p < 0.005$).

PgP/NANP polyplexes, we have assessed the hemocompatibility of these complexes by incubating them with rat erythrocytes and investigating their effects on blood cell morphology. We observed that erythrocytes treated with Triton X-100 showed complete hemolysis, while the morphology of erythrocytes treated with various PgP/NANP polyplexes were intact and hemolysis was not significantly different than that of erythrocytes treated with PBS (Table 5). Figure 37A shows the

representative images of erythrocytes treated with PBS, Triton X-100, and various PgP/NANP polyplexes.

Another important pharmaceutical consideration is immunostimulatory activity. Previously, NANPs have been shown to elicit the secretion of a number of pro-inflammatory cytokines and chemokines ^{6, 21, 45}. In addition, we conducted a quantitative structure-activity relationship study using hμglia cells to identify physicochemical contributors to

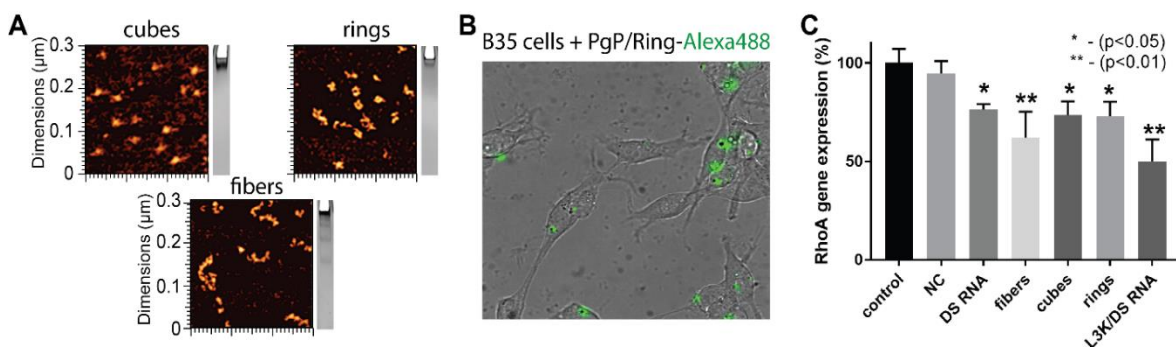


Figure 35. (A) AFM images of RhoA NANPs and (B,C) specific gene silencing with PgP/NANP polyplexes targeting RhoA in rat neuroblastoma cells (B35). In all experiments, cubes (PgP/cubes(RhoA)), rings (PgP/rings(RhoA)), fibers (PgP/fibers(RhoA)), and individual DS RNAs(RhoA) are compared. Negative control siRNA (siNT) and DS RNA transfected with Lipofectamine 3000 (L3K) are used as controls. Intracellular uptake of fluorescently labeled PgP/Ring-A1488 by confocal microscopy (A) and RhoA gene silencing assessed by RT PCR (B).

immunostimulatory activity ⁴⁵. These studies, however, were limited to commercially available carriers such as L2K, which has no potential for clinical use. We therefore investigated the immunogenic properties of PgP/NANPs and determined whether structural differences influenced them. NANPs were delivered to hμglia cells using PgP or L2K and the release of the cytokines interleukin-6 (IL-6) and interferon-beta (IFN-β) was determined at 24 hours post-exposure by specific capture ELISAs. Poly I:C and poly dA:dT, known inducers of immune responses, were used as positive controls in these studies. Delivery of NANPs with L2K induced the release of

both IL-6 and IFN- β . Interestingly, cube and ring-shaped NANPs complexed with PgP induced the

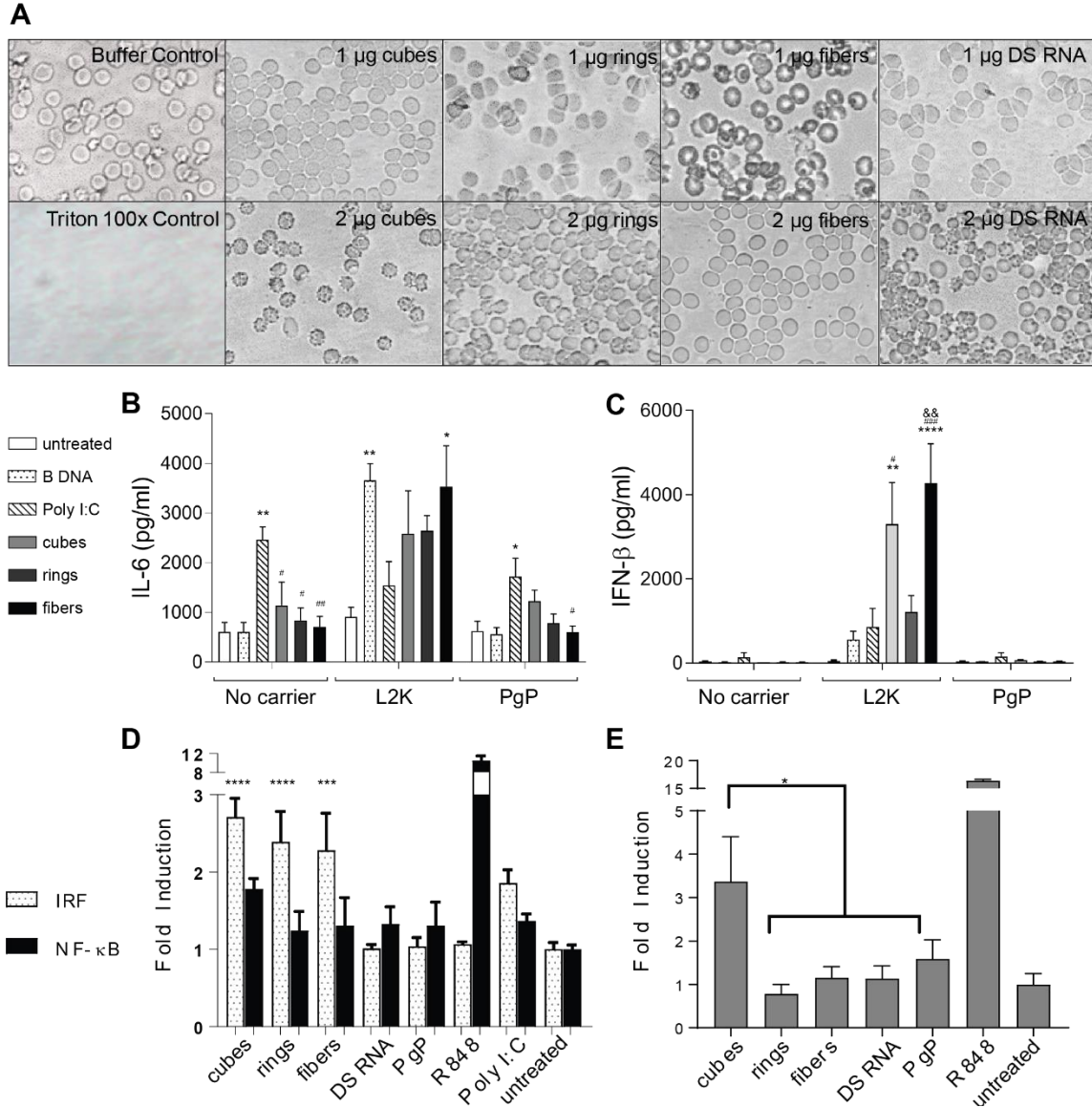


Figure 36. Blood compatibility and immunostimulation with PgP/NANP(GFP) polyplexes. In all experiments, cubes (PgP/cubes(GFP)), rings (PgP/rings(GFP)), fibers (PgP/fibers(GFP)), and individual DS RNAs(GFP) are compared. (A) Hemolysis assay was conducted using primary rat erythrocytes and demonstrated no lysis. (B-C) Immunostimulation of PgP/NANP(GFP) polyplexes measured via ELISA of inflammatory cytokines and type I interferons in h μ glia cells. (D) IRF and NF- κ B stimulation as measured by luciferase production and SEAP production, respectively, in THP1-DualTM cells, and (E) TLR stimulation from polyplexes as measured by SEAP secretion from HEK-BlueTM hTLR7 cells. In B and C, statistical significance relevant to cells, poly I:C, and ring is denoted by *, #, and & respectively (*/# $p < 0.05$, **/###/&& $p < 0.005$, ### $p < 0.001$, **** $p < 0.0001$). (D) The role of IRF and NF- κ B stimulation were measured using THP1-DualTM cells. Statistical significance compared to cells denoted by *** with $p < 0.0005$ and **** with $p < 0.0001$). (E) HEK-BlueTM hTLR7 cells were transfected with the various PgP/NANP complexes and the TLR stimulation was measured using QUANTI-BlueTM detection media (* denotes $p < 0.005$).

same release of IL-6 compared to a positive control, while fibers induced a significantly lower response (Fig. 37B), thus indicating that the structure of NANPs can influence the immunostimulatory properties of polyplexes. Additionally, we observed that the delivery of NANPs or positive controls complexed with PgP showed much lower IL-6 and IFN- β release than transfection using L2K. Only cubes delivered with PgP stimulated detectable release of IL-6 and IFN- β when compared to positive control, indicating a link between NANP structure and immunogenic properties consistent with previous observations ⁶. Importantly, these data suggest that delivery of NANPs with PgP may reduce potentially detrimental immunogenicity when

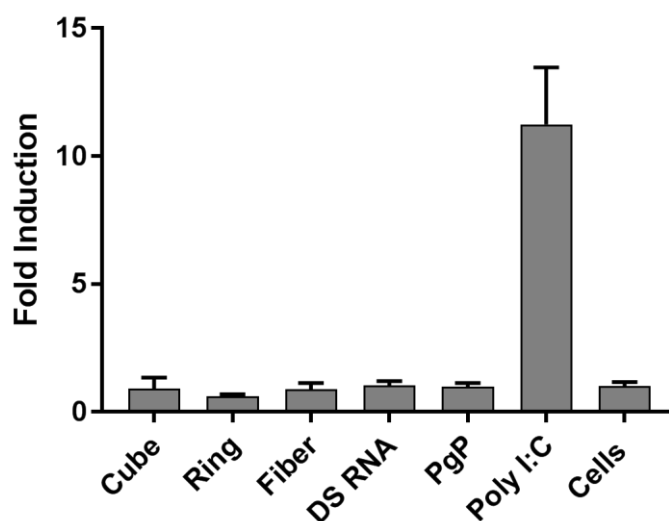


Figure 37. hTLR3 stimulation as measured by HEK-Blue™ hTLR3 cells. Positive control Poly I:C stimulates a response whereas none of the PgP/NANPs trigger hTLR3 activation. In all experiments, cubes (PgP/cubes(GFP)), rings (PgP/rings(GFP)), fibers (PgP/fibers(GFP)), and individual DS RNAs(GFP) are compared.

compared to the conventional polycationic lipid-like carriers.

Furthermore, the specific contribution made by cellular signaling pathways and individual toll-like receptors (TLR) to NANP-induced responses was evaluated using HEK-Blue™ hTLR and THP1-Dual™ cells. Engineered THP1-Dual™ cells express either SEAP or secreted luciferase upon activation of either NF- κ B or IRF pathways, respectively. Our results demonstrate that the

majority of the response elicited by the PgP/NANP constructs occurs via the IRF pathway (Fig 37D). The HEK-Blue™ hTLR cell model expresses a single human TLR, which upon stimulation activates the production of SEAP for further QUANTifiable detection. TLRs 3, 7, and 8 are responsible for RNA detection in endosomal compartments, with TLR3 recognizing dsRNA and TLRs 7 and 8 responsible for ssRNA detection. Therefore, we selected TLR3 and TLR7 receptor-expressing *in vitro* models for use in the present study. Our data demonstrate that the TLR7-mediated immune stimulation is mainly caused by the PgP/cube polyplexes (Fig 37E) while other NANPs demonstrated negligible stimulation. Additionally, TLR3 did not show any utilization in PgP/NANP recognition (Figure 38). Overall, these results are consistent with our studies on L2K-mediated NANP delivery in human PBMCs^{6, 46}.

4.3.6 Biodistribution of PgP/NANP polyplexes after systemic *in vivo* administration

Biodistribution of various DiR-PgP/NANP polyplexes in CD-1 mice was monitored over 24 hours after intravenous injection using an IVIS live animal imaging system (Fig. 39). As shown in Figure 7A, the PgP/NANP polyplexes were distributed throughout the body after 24 hours. Interestingly, we observed strong signals in the head by *in vivo* animal imaging (Fig. 39A), suggesting that PgP/NANP polyplexes might be capable of crossing the BBB. However, only low-level signal expression was detectable in brain tissue *ex vivo* (Figure 39B, right), and the same analysis showed that the majority of the polyplexes were located in the liver, spleen, and lungs (Figure 6B, left). Figure 39C shows the percent organ biodistribution, with a rank order of distribution of liver (>70%), spleen, and then lung, with minor distribution to other organs. We observed that the percentage biodistribution of both DiR-PgP/cube(GFP) and DiR-PgP/ring(GFP) polyplexes to the liver and lung was significantly higher than DS RNA. Interestingly, we observed that all DiR-PgP/NANP polyplexes were detectable in brain tissue for up to 24 hours post-administration, but it should be noted that their percentage distribution to this site was less than 1%. Clearly, further studies will be required to confirm the BBB penetrance of PgP/NANP polyplexes.

4.4 Discussion

A principle goal of this study was to determine how the shape and structure of functional NANPs affects the stability and efficacy of PgP/NANP polyplexes. The RNA nanoparticle structures were selected due to their differences in assembly and shape; the cubes, rings, and fibers differ in terms of dimensionality. The cubes are a globular-type structure (3D), whereas the rings are planar (2D), and the fibers form long chains of various lengths (1D). The fibers can be considered a more pliant structure, which could lead to increased binding to PgP due to ease of bending to conform to various surfaces. Such features could impact the delivery and therapeutic efficacy of each NANP. In order for duplexes, fibers, or rings to successfully bind to PgP, simple bending is needed for the entire structure to be electrostatically bound to the surface; however, due to their three dimensional globular-type structure, cubes could require greater deformation in order to successfully bind to PgP. While PgP-bound NANPs may undergo some transient deformation, we determined that the NANPs remain intact and reassume their original shapes when released.

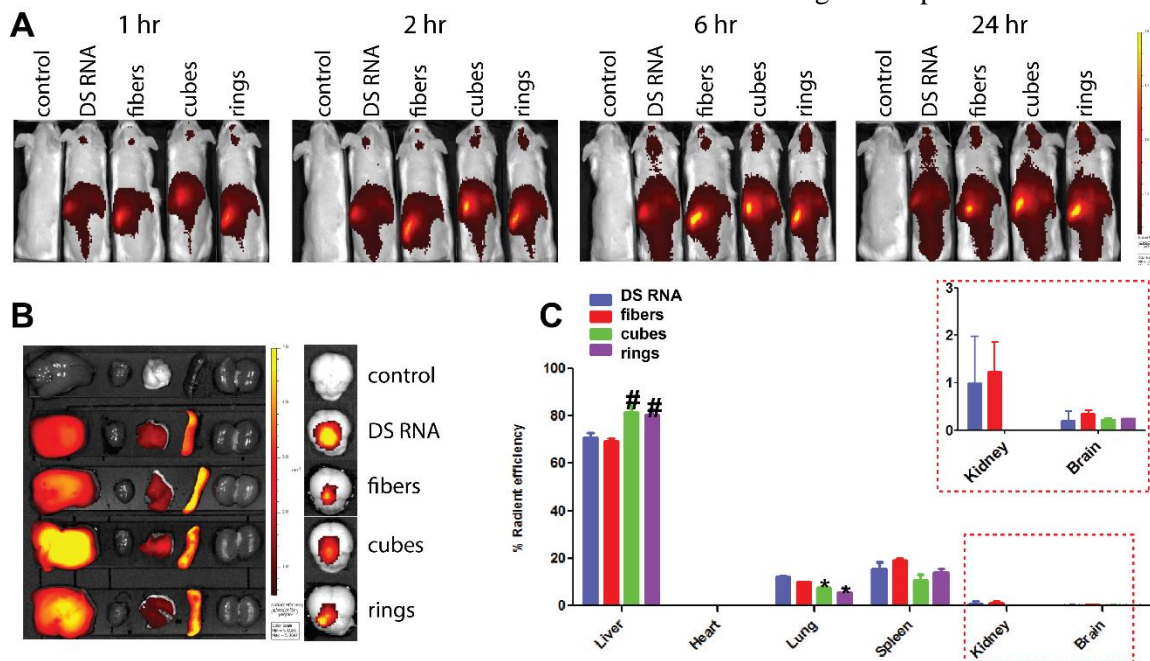


Figure 38. Biodistribution of various PgP/NANPs after systemic injection via tail vein in mice. The results were analyzed *in vivo* (A), and *ex vivo* (B-C). Significant difference ($p < 0.05$) when compared to PgP/DS RNA for PgP/NANPs' accumulation in lungs (*) and in livers (#) are shown.

We administered our polyplexes systemically via tail-vein injection into mice to evaluate the role of the NANP structure in their biodistribution. We determined that the polyplexes accumulated mainly in the liver and spleen and that such accumulation was independent of NANP shape. However, perhaps the most promising result from our biodistribution studies was that all structures were found, at least to some extent, to traverse the BBB into the brain (Figs. 7A and E). The delivery of bioactive compounds to the brain is a major challenge in the treatment of various maladies as the BBB is highly selective, which limits access by most nanoparticles and conventional therapeutics. As such, our results suggest that that PgP, an amphiphilic micelle-forming block copolymer, might be suitable as a nucleic acid delivery carrier to administer NANPs of various shapes across the BBB to the CNS.

A major obstacle to the therapeutic use of nanoparticles with various chemical compositions is the sensitivity of the CNS to off-target/immunotoxic effects as resident glial cells initiate and propagate immune responses in the CNS. As such, optimizing a therapeutic to enhance efficacy while limiting immunotoxicity is paramount for the generation of a successful platform. Here, we transfected hμglia cells with NANPs using L2K or PgP and measured the secretion of key immune mediators. We observed that NANPs delivered using L2K stimulated the release of both IL-6 and IFN-β. Similar to our previous studies with NANPs composed of RNA, we primarily observed a robust type I IFN response with only modest inflammatory cytokine responses⁴⁵. In contrast, we observed no statistically significant release of IL-6 or IFN-α in response to NANPs delivered using PgP. Only cubes delivered with PgP stimulated a detectable release of immune mediators. Consistent with this finding, cubes were demonstrated to be the only NANP capable of stimulating TLR7 when delivered via PgP. The ability of cubes, but not other structures, to elicit immune mediator release has been observed previously^{6,46} and could be attributable to the globular nature of these nucleic acid nanostructures as opposed to the planar or fibrous structures of rings and fibers. Additionally, our data suggests that the delivery of TNAs via PgP reduces the immunogenicity of such complexes, raising the exciting possibility that this carrier could limit the

detrimental immune responses previously associated with nanoparticle administration. Alternatively, several groups have used immunostimulatory nucleic acids to purposefully provoke an immune response for therapeutic action. Unmethylated cytosine-phosphate-guanosine (CpG) motifs have been delivered using nanoparticles to elicit a response via TLR 9 for targeted immune responses⁴⁷⁻⁴⁸. Other research has used NANPs with chemical modifications of various shapes to modulate the immune response⁴⁹. This additional control over not only the therapeutic payload but also the immunostimulant potential lends another unforeseen layer of control over their application, allowing for desired immunostimulation with specific gene silencing on a structure and carrier dependent basis.

Table 6. Hemocompatibility of various PgP/NANP polyplexes at N/P ratio of 30/1 on rat erythrocytes in vitro. % hemolysis= (A sample-A PBS) / (A Tritonx-100-A PBS) X 100

	Abs at 540nm			
	sample 1	sample 2	sample 3	% hemolysis
Triton X-100	0.63	0.621	0.684	100±6.68%
PBS	0.136	0.142	0.136	0.59±0.68%
PgP 6 µg (Equivalent to 1 µg NANP)	0.109	0.107	0.102	0.1±0.6%
PgP 12 µg (Equivalent to 2 µg NANP)	0.068	0.065	0.07	-2.48±0.15%
PgP/rings(GFP) 1µg	0.095	0.096	0.088	-8.24±0.85%
PgP/rings(GFP) 2µg	0.127	0.115	0.114	-3.20±1.42%
PgP/cubes(GFP) 1µg	0.119	0.094	0.104	-5.70±2.47%
PgP/cubes(GFP) 2µg	0.14	0.143	0.141	1.24±0.30%
PgP/fibers (GFP) 1µg	0.097	0.125	0.092	-5.95±3.49%
PgP/fibers(GFP) 2µg	0.128	0.134	0.145	0.13±1.69%
PgP/DS RNA(GFP) 1µg	0.116	0.106	0.11	-4.77±0.99%
PgP/DS RNA(GFP) 2µg	0.139	0.148	0.141	1.50±0.93%

4.5 Conclusion

Here we have demonstrated and evaluated the use of functional NANPs complexed to polymeric carriers for the efficient delivery of TNAs. We show uptake and silencing efficacy in a manner that is not significantly impacted by the shape or size of the conjugated nucleic acid nanoparticle. Additionally, we show that the immunostimulatory activity of these polyplexes is markedly lower than that seen with other complexes employing the same NANPs. Expanding the

arsenal of TNAs complexed with PgP to include miRNAs, aptamers, and siRNAs directed against other genes could prove highly useful in the treatment of currently intractable diseases and injuries. The present demonstration that nanostructured nucleic acids complexed to PgP are effective, non-toxic, and non-immunogenic support their further development as pharmaceuticals.

4.5.1 Sequences used in this project

All sequences are shown 5' → 3'

Six-stranded DNA cube without functionalization:

Strand A

GGCAACTTTGATCCCTCGGTTTAGCGCCGGCCTTTTCTCCCACACTTTCACG

Strand B

GGGAAATTTTCGTGGTAGGTTTTGTTGCCCGTGTTTCTACGATTACTTTGGTC

Strand C

GGACATTTTCGAGACAGCATTTTTTCCCGACCTTTGCGGATTGTATTTTAGG

Strand D

GGCGCTTTTGACCTTCTGCTTTATGTCCCCTATTTCTTAATGACTTTTGGCC

Strand E

GGGAGATTTAGTCATTAAGTTTTACAATCCGCTTTGTAATCGTAGTTTGTGT

Strand F

GGGATCTTTACCTACCACGTTTTGCTGTCTCGTTTGCAGAAGGTCTTTCCGA

Six-stranded RNA ring functionalized with six DS RNAs against GFP

Strand A

GGGAACCGUCCACUGGUUCCCGCUACGAGAGCCUGCCUCGUAGC

Strand B

GGGAACCGCAGGCUGGUUCCCGCUACGAGAGAACGCCUCGUAGC

Strand C

GGGAACCGCGUUCUGGUUCCCGCUACGAGACGUCUCCUCGUAGC

Strand D

GGGAACCGAGACGUGGUUCCCGCUACGAGUCGUGGUCUCGUAGC

Strand E

GGGAACCACGAGGUUCCCGCUACGAGAACCAUCCUCGUAGC

Strand F

GGGAACCGAUGGUUGGUUCCCGCUACGAGAGUGGACCUCGUAGC

Six-stranded RNA cube functionalized with six DS RNAs against GFP:

Strand A

GGCAACUUUGAUCCUCGGUUUAGCGCCGGCCUUUUCUCCACACUUUCAGUUC

GGUGGUGCAGAUGAACUUCAGGGUCA

Strand B

GGGAAUUUCGUGGUAGGUUUUGUUGCCCGUGUUUCUACGAUUACUUUGGUCUUC

GGUGGUGCAGAUGAACUUCAGGGUCA

Strand C

GGACAUUUUCGAGACAGCAUUUUUCCCGACCUUUGCGGAUUGUAUUUUAGGUUC

GGUGGUGCAGAUGAACUUCAGGGUCA

Strand D

GGCGCUUUUGACCUUCUGCUUUUAUGUCCCCUAUUUCUUA AUGACUUUUGGCCUUC
GGUGGUGCAGAUGAACUUCAGGGUCA

Strand E

GGGAGAUUUAGUCAUUAAGUUUUACAAUCCGCUUUGUAAUCGUAGUUUGUGUUU
CGGUGGUGCAGAUGAACUUCAGGGUCA

Strand F

GGGAUCUUUACCUACCACGUUUUGCUGUCUCGUUUGCAGAAGGUCUUUCCGAUUC
GGUGGUGCAGAUGAACUUCAGGGUCA

Six-stranded RNA ring functionalized with six DS RNAs against GFP:**Strand A**

GGGAACCGUCCACUGGUUCCCGCUACGAGAGCCUGCCUCGUAGCUUCGGUGGUGC
AGAUGAACUUCAGGGUCA

Strand B

GGGAACCGCAGGCUGGUUCCCGCUACGAGAGAACGCCUCGUAGCUUCGGUGGUGC
AGAUGAACUUCAGGGUCA

Strand C

GGGAACCGCGUUCUGGUUCCCGCUACGAGACGUCUCCUCGUAGCUUCGGUGGUGC
AGAUGAACUUCAGGGUCA

Strand D

GGGAACCGAGACGUGGUUCCCGCUACGAGUCGUGGUCUCGUAGCUUCGGUGGUGC
AGAUGAACUUCAGGGUCA

Strand E

GGGAACCACACGAGGUUCCCGCUACGAGAACCAUCCUCGUAGCUUCGGUGGUGC
AGAUGAACUUCAGGGUCA

Strand F

GGGAACCGAUGGUUGGUUCCCGCUACGAGAGUGGACCUCGUAGCUUCGGUGGUGC
AGAUGAACUUCAGGGUCA

RNA fiber functionalized with DS RNAs against GFP:**Strand A**

GGGAAUCCAAGGAGGCAGGAUUCCCGUCACAGAAGGAGGCACUGUGAC

Strand B

GGGAACGUAAGCCUCCAACGUUCCCGGAUGC UAAGCCUCCAAGCAUCCUUUGGUG
GUGCAGAUGAACUUCAGGGUCA

GFP Sense

pACCCUGAAGUUCAUCUGCACCACCG

“p” denotes phosphate

GFP Antisense

CGGUGGUGCAGAUGAACUUCAGGGUCA

Six-stranded RNA cube functionalized with six DS RNAs against RhoA:**Strand A**

GGCAACUUUGAUCCUCGGUUUAGCGCCGGCCUUUUCUCCACACUUUCAGUUC
CUGCUUCAUUUUGGCUAACUCCCGCCUU

Strand B

GGGAAUUUCGUGGUAGGUUUUGUUGCCCGUGUUUCUACGAUUACUUUGGUCUUC
CUGCUUCAUUUUGGCUAACUCCCGCCUU

Strand C

GGACAUUUUCGAGACAGCAUUUUUCCCCGACCUUUGCGGAUUGUAUUUUAGGUUC
CUGCUUCAUUUUGGCUAACUCCCGCCU

Strand D

GGCGCUUUUGACCUUCUGCUUUUUGUCCCCUAUUUCUUAUGACUUUUGGCCUUC
CUGCUUCAUUUUGGCUAACUCCCGCCU

Strand E

GGGAGAUUUAGUCAUUAAGUUUUACAAUCCGCUUUGUAAUCGUAGUUUGUGUUU
CCUGCUUCAUUUUGGCUAACUCCCGCCU

Strand F

GGGAUCUUUACCUACCACGUUUUGCUGUCUGUUUGCAGAAGGUCUUUCCGAUUC
CUGCUUCAUUUUGGCUAACUCCCGCCU

Six-stranded RNA ring functionalized with six DS RNAs against RhoA:**Strand A**

GGGAAUCCGUCCACUGGAUUCCCGUCACAGAGCCUGCCUGUGACUUCCUGCUUCA
UUUUGGCUAACUCCCGCCU

Strand B

GGGAAUCCGCAGGCUGGAUUCCCGUCACAGAGAACGCCUGUGACUUCCUGCUUCA
UUUUGGCUAACUCCCGCCU

Strand C

GGGAAUCCGCGUUCUGGAUUCCCGUCACAGACGUCUCCUGUGACUUCCUGCUUCA
UUUUGGCUAACUCCCGCCU

Strand D

GGGAAUCCGAGACGUGGAUUCCCGUCACAGUCGUGGUCUGUGACUUCCUGCUUCA
UUUUGGCUAACUCCCGCCU

Strand E

GGGAAUCCACCACGAGGAUUCCCGUCACAGAACCAUCCUGUGACUUCCUGCUUCA
UUUUGGCUAACUCCCGCCU

Strand F

GGGAAUCCGAUGGUUGGAUUCCCGUCACAGAGUGGACCUGUGACUUCCUGCUUCA
UUUUGGCUAACUCCCGCCU

RNA fiber functionalized with DS RNAs against RhoA:**Strand A**

GGGAAUCCAAGGAGGCAGGAUUCCCGUCACAGAAGGAGGCACUGUGAC

Strand B

GGGAACGUAAGCCUCCAACGUUCCCGGAUGCUAAGCCUCCAAGCAUCCUCCUGC
UUCAUUUUGGCUAACUCCCGCCU

RhoA Sense

pGGCGGAGUUAGCCAAAUGAAGCAGG

RhoA Antisense

CCUGCUUCAUUUUGGCUAACUCCCGCCU

GFP Sense with Alexa 488

pACCCUGAAGUUCAUCUGCACCACCG-Alexa488

DNA-Sense-AI488

GGAGACCGTGACCGGTGGTGCAGATGAACTTCAGGGTCATT-Alexa488

DNA-Anti-Sense-Iowa Black

Iowa Black Quencher-TGACCCTGAAGTTCATCTGCACCACCGGTCACGGTCTCC

DNA-Anti-Sense

TGACCCTGAAGTTCATCTGCACCACCGGTCACGGTCTCC

4.6 References

1. Adams, D.; Gonzalez-Duarte, A.; O'Riordan, W. D.; Yang, C. C.; Ueda, M.; Kristen, A. V.; Tournev, I.; Schmidt, H. H.; Coelho, T.; Berk, J. L.; Lin, K. P.; Vita, G.; Attarian, S.; Plante-Bordeneuve, V.; Mezei, M. M.; Campistol, J. M.; Buades, J.; Brannagan, T. H., 3rd; Kim, B. J.; Oh, J.; Parman, Y.; Sekijima, Y.; Hawkins, P. N.; Solomon, S. D.; Polydefkis, M.; Dyck, P. J.; Gandhi, P. J.; Goyal, S.; Chen, J.; Strahs, A. L.; Nochur, S. V.; Sweetser, M. T.; Garg, P. P.; Vaishnav, A. K.; Gollob, J. A.; Suhr, O. B., Patisiran, an RNAi Therapeutic, for Hereditary Transthyretin Amyloidosis. *N Engl J Med* **2018**, *379* (1), 11-21.
2. Bramsen, J. B.; Kjems, J., Chemical modification of small interfering RNA. *Methods in molecular biology (Clifton, N.J)* **2011**, *721*, 77-103.
3. Bramsen, J. B.; Kjems, J., Development of Therapeutic-Grade Small Interfering RNAs by Chemical Engineering. *Frontiers in genetics* **2012**, *3* (154), 154.
4. Pecot, C. V.; Calin, G. A.; Coleman, R. L.; Lopez-Berestein, G.; Sood, A. K., RNA interference in the clinic: challenges and future directions. *Nature Reviews Cancer* **2011**, *11* (1), 59-67.
5. Fire, A.; Xu, S.; Montgomery, M. K.; Kostas, S. A.; Driver, S. E.; Mello, C. C., Potent and specific genetic interference by double-stranded RNA in *Caenorhabditis elegans*. *Nature* **1998**, *391* (6669), 806-11.
6. Hong, E. P.; Halman, J. R.; Shah, A. B.; Khisamutdinov, E. F.; Dobrovolskaia, M. A.; Afonin, K. A., Structure and Composition Define Immunorecognition of Nucleic Acid Nanoparticles. *Nano Letters* **2018**, *18* (7), 4309-4321.
7. Guo, P., The emerging field of RNA nanotechnology. *Nature nanotechnology* **2010**, *5* (12), 833-42.
8. Jasinski, D.; Haque, F.; Binzel, D. W.; Guo, P., Advancement of the Emerging Field of RNA Nanotechnology. *ACS Nano* **2017**, *11* (2), 1142-1164.
9. Binzel, D. W.; Shu, Y.; Li, H.; Sun, M.; Zhang, Q.; Shu, D.; Guo, B.; Guo, P., Specific Delivery of MiRNA for High Efficient Inhibition of Prostate Cancer by RNA Nanotechnology. *Molecular therapy : the journal of the American Society of Gene Therapy* **2016**, *24* (7), 1267-77.
10. Shukla, G. C.; Haque, F.; Tor, Y.; Wilhelmsson, L. M.; Toulme, J. J.; Isambert, H.; Guo, P.; Rossi, J. J.; Tenenbaum, S. A.; Shapiro, B. A., A Boost for the Emerging Field of RNA Nanotechnology. *ACS Nano* **2011**, *5* (5), 3405-3418.
11. Bui, M. N.; Brittany Johnson, M.; Viard, M.; Satterwhite, E.; Martins, A. N.; Li, Z.; Marriott, I.; Afonin, K. A.; Khisamutdinov, E. F., Versatile RNA tetra-U helix linking motif as a toolkit for nucleic acid nanotechnology. *Nanomedicine* **2017**, *13* (3), 1137-1146.
12. Stewart, J. M.; Viard, M.; Subramanian, H. K.; Roark, B. K.; Afonin, K. A.; Franco, E., Programmable RNA microstructures for coordinated delivery of siRNAs. *Nanoscale* **2016**, *8* (40), 17542-17550.
13. Parlea, L.; Puri, A.; Kasprzak, W.; Bindewald, E.; Zakrevsky, P.; Satterwhite, E.; Joseph, K.; Afonin, K. A.; Shapiro, B. A., Cellular Delivery of RNA Nanoparticles. *ACS combinatorial science* **2016**, *18* (9), 527-47.
14. Afonin, K. A.; Bindewald, E.; Yaghoubian, A. J.; Voss, N.; Jacovetty, E.; Shapiro, B. A.; Jaeger, L., In vitro assembly of cubic RNA-based scaffolds designed in silico. *Nature nanotechnology* **2010**, *5* (9), 676-682.
15. Afonin, K. A.; Grabow, W. W.; Walker, F. M.; Bindewald, E.; Dobrovolskaia, M. A.; Shapiro, B. A.; Jaeger, L., Design and self-assembly of siRNA-functionalized RNA nanoparticles for use in automated nanomedicine. *Nat Protoc* **2011**, *6* (12), 2022-2034.
16. Haque, F.; Shu, D.; Shu, Y.; Shlyakhtenko, L. S.; Rychahou, P. G.; Evers, B. M.; Guo, P., Ultrastable synergistic tetravalent RNA nanoparticles for targeting to cancers. *Nano today* **2012**, *7* (4), 245-257.
17. Khisamutdinov, E. F.; Jasinski, D. L.; Guo, P., RNA as a boiling-resistant anionic

polymer material to build robust structures with defined shape and stoichiometry. *ACS Nano* **2014**, *8* (5), 4771-81.

18. Khisamutdinov, E. F.; Li, H.; Jasinski, D. L.; Chen, J.; Fu, J.; Guo, P., Enhancing immunomodulation on innate immunity by shape transition among RNA triangle, square and pentagon nanovehicles. *Nucleic Acids Res* **2014**, *42* (15), 9996-10004.
19. Lee, H.; Lytton-Jean, A. K. R.; Chen, Y.; Love, K. T.; Park, A. I.; Karagiannis, E. D.; Sehgal, A.; Querbes, W.; Zurenko, C. S.; Jayaraman, M.; Peng, C. G.; Charisse, K.; Borodovsky, A.; Manoharan, M.; Donahoe, J. S.; Truelove, J.; Nahrendorf, M.; Langer, R.; Anderson, D. G., Molecularly self-assembled nucleic acid nanoparticles for targeted in vivo siRNA delivery. *Nature nanotechnology* **2012**, *7* (6), 389-393.
20. Osada, E.; Suzuki, Y.; Hidaka, K.; Ohno, H.; Sugiyama, H.; Endo, M.; Saito, H., Engineering RNA-protein complexes with different shapes for imaging and therapeutic applications. *ACS Nano* **2014**, *8* (8), 8130-40.
21. Halman, J. R.; Satterwhite, E.; Roark, B.; Chandler, M.; Viard, M.; Ivanina, A.; Bindewald, E.; Kasprzak, W. K.; Panigaj, M.; Bui, M. N.; Lu, J. S.; Miller, J.; Khisamutdinov, E. F.; Shapiro, B. A.; Dobrovolskaia, M. A.; Afonin, K. A., Functionally-interdependent shape-switching nanoparticles with controllable properties. *Nucleic acids research* **2017**, *45* (4), 2210-2220.
22. Afonin, K. A.; Kasprzak, W. K.; Bindewald, E.; Kireeva, M.; Viard, M.; Kashlev, M.; Shapiro, B. A., In silico design and enzymatic synthesis of functional RNA nanoparticles. *Acc. Chem. Res.* **2014**, *47* (6), 1731-1741.
23. Wilczewska, A. Z.; Niemirowicz, K.; Markiewicz, K. H.; Car, H., Nanoparticles as drug delivery systems. *Pharmacological Reports* **2012**, *64* (5), 1020-1037.
24. De Jong, W. H.; Borm, P. J. A., Drug delivery and nanoparticles: Applications and hazards. *International Journal of Nanomedicine* **2008**, *3* (2), 133-149.
25. Egusquiaguirre, S. P.; Igartua, M.; Hernandez, R. M.; Pedraz, J. L., Nanoparticle delivery systems for cancer therapy: advances in clinical and preclinical research. *Clinical & Translational Oncology* **2012**, *14* (2), 83-93.
26. Cruz-Acuna, M.; Halman, J. R.; Afonin, K. A.; Dobson, J.; Rinaldi, C., Magnetic nanoparticles loaded with functional RNA nanoparticles. *Nanoscale* **2018**, *10* (37), 17761-17770.
27. Cutlar, L.; Zhou, D. Z.; Hu, X. J.; Duarte, B.; Greiser, U.; Larcher, F.; Wang, W. X., A non-viral gene therapy for treatment of recessive dystrophic epidermolysis bullosa. *Experimental Dermatology* **2016**, *25* (10), 818-820.
28. Mintzer, M. A.; Simanek, E. E., Nonviral Vectors for Gene Delivery. *Chemical Reviews* **2009**, *109* (2), 259-302.
29. Yin, H.; Kanasty, R. L.; Eltoukhy, A. A.; Vegas, A. J.; Dorkin, J. R.; Anderson, D. G., Non-viral vectors for gene-based therapy. *Nature Reviews Genetics* **2014**, *15* (8), 541-555.
30. Boussif, O.; Lezoualc'h, F.; Zanta, M. A.; Mergny, M. D.; Scherman, D.; Demeneix, B.; Behr, J. P., A versatile vector for gene and oligonucleotide transfer into cells in culture and in vivo: polyethylenimine. *Proceedings of the National Academy of Sciences of the United States of America* **1995**, *92* (16), 7297-301.
31. Gwak, S. J.; Macks, C.; Bae, S.; Cecil, N.; Lee, J. S., Physicochemical stability and transfection efficiency of cationic amphiphilic copolymer/pDNA polyplexes for spinal cord injury repair. *Scientific Reports* **2017**, *7*, 11247.
32. Gwak, S. J.; Nice, J.; Zhang, J.; Green, B.; Macks, C.; Bae, S.; Webb, K.; Lee, J. S., Cationic, amphiphilic copolymer micelles as nucleic acid carriers for enhanced transfection in rat spinal cord. *Acta Biomaterialia* **2016**, *35*, 98-108.
33. Afonin, K. A.; Viard, M.; Kagiampakis, I.; Case, C. L.; Dobrovolskaia, M. A.; Hofmann, J.; Vrzak, A.; Kireeva, M.; Kasprzak, W. K.; KewalRamani, V. N.; Shapiro, B. A., Triggering of RNA Interference with RNA-RNA, RNA-DNA, and DNA-RNA Nanoparticles. *Acs Nano* **2015**, *9* (1), 251-259.

34. Afonin, K. A.; Kasprzak, W.; Bindewald, E.; Puppala, P. S.; Diehl, A. R.; Hall, K. T.; Kim, T. J.; Zimmermann, M. T.; Jernigan, R. L.; Jaeger, L.; Shapiro, B. A., Computational and experimental characterization of RNA cubic nanoscaffolds. *Methods* **2014**, *67* (2), 256-265.
35. Afonin, K. A.; Kireeva, M.; Grabow, W. W.; Kashlev, M.; Jaeger, L.; Shapiro, B. A., Co-transcriptional assembly of chemically modified RNA nanoparticles functionalized with siRNAs. *Nano Lett* **2012**, *12* (10), 5192-5.
36. Grabow, W. W.; Zakrevsky, P.; Afonin, K. A.; Chworos, A.; Shapiro, B. A.; Jaeger, L., Self-assembling RNA nanorings based on RNAI/II inverse kissing complexes. *Nano Lett* **2011**, *11* (2), 878-87.
37. Afonin, K. A.; Viard, M.; Koyfman, A. Y.; Martins, A. N.; Kasprzak, W. K.; Panigaj, M.; Desai, R.; Santhanam, A.; Grabow, W. W.; Jaeger, L.; Heldman, E.; Reiser, J.; Chiu, W.; Freed, E. O.; Shapiro, B. A., Multifunctional RNA nanoparticles. *Nano Lett* **2014**, *14* (10), 5662-71.
38. Afonin, K. A.; Viard, M.; Tedbury, P.; Bindewald, E.; Parlea, L.; Howington, M.; Valdman, M.; Johns-Boehme, A.; Brainerd, C.; Freed, E. O.; Shapiro, B. A., The Use of Minimal RNA Toeholds to Trigger the Activation of Multiple Functionalities. *Nano Lett* **2016**, *16* (3), 1746-53.
39. Sajja, S.; Chandler, M.; Fedorov, D.; Kasprzak, W. K.; Lushnikov, A.; Viard, M.; Shah, A.; Dang, D.; Dahl, J.; Worku, B.; Dobrovolskaia, M. A.; Krasnoslobodtsev, A.; Shapiro, B. A.; Afonin, K. A., Dynamic Behavior of RNA Nanoparticles Analyzed by AFM on a Mica/Air Interface. *Langmuir* **2018**, *34* (49), 15099-15108.
40. Rackley, L.; Stewart, J. M.; Salotti, J.; Krokhotin, A.; Shah, A.; Halman, J. R.; Juneja, R.; Smollett, J.; Lee, L.; Roark, K.; Viard, M.; Tarannum, M.; Vivero-Escoto, J.; Johnson, P. F.; Dobrovolskaia, M. A.; Dokholyan, N. V.; Franco, E.; Afonin, K. A., RNA Fibers as Optimized Nanoscaffolds for siRNA Coordination and Reduced Immunological Recognition. *Advanced Functional Materials* **2018**, *28* (48), 1805959.
41. Gwak, S. J.; Macks, C.; Jeong, D. U.; Kindy, M.; Lynn, M.; Webb, K.; Lee, J. S., RhoA knockdown by cationic amphiphilic copolymer/siRhoA polyplexes enhances axonal regeneration in rat spinal cord injury model. *Biomaterials* **2017**, *121*, 155-166.
42. Jovic, M.; Sharma, M.; Rahajeng, J.; Caplan, S., The early endosome: a busy sorting station for proteins at the crossroads. *Histology and histopathology* **2010**, *25* (1), 99-112.
43. Weigel, P. H.; Oka, J. A., Temperature-dependence of endocytosis mediated by the asialoglycoprotein receptor in isolated rat hepatocytes - evidence for 2 potentially rate-limiting steps. *Journal of Biological Chemistry* **1981**, *256* (6), 2615-2617.
44. Afonin, K. A.; Viard, M.; Martins, A. N.; Lockett, S. J.; Maciag, A. E.; Freed, E. O.; Heldman, E.; Jaeger, L.; Blumenthal, R.; Shapiro, B. A., Activation of different split functionalities on re-association of RNA-DNA hybrids. *Nature nanotechnology* **2013**, *8* (4), 296-304.
45. Johnson, M. B.; Halman, J. R.; Satterwhite, E.; Zakharov, A. V.; Bui, M. N.; Benkato, K.; Goldsworthy, V.; Kim, T.; Hong, E.; Dobrovolskaia, M. A.; Khisamutdinov, E. F.; Marriott, I.; Afonin, K. A., Programmable Nucleic Acid Based Polygons with Controlled Neuroimmunomodulatory Properties for Predictive QSAR Modeling. *Small* **2017**, *13* (42).
46. Hong, E.; Halman, J. R.; Shah, A.; Cedrone, E.; Truong, N.; Afonin, K. A.; Dobrovolskaia, M. A., Toll-Like Receptor-Mediated Recognition of Nucleic Acid Nanoparticles (NANPs) in Human Primary Blood Cells. *Molecules (Basel, Switzerland)* **2019**, *24* (6), 1094.
47. Givens, B. E.; Geary, S. M.; Salem, A. K., Nanoparticle-based CpG-oligonucleotide therapy for treating allergic asthma. *Immunotherapy* **2018**, *10* (7), 595-604.
48. Hanagata, N., Structure-dependent immunostimulatory effect of CpG oligodeoxynucleotides and their delivery system. *International Journal of Nanomedicine* **2012**, *7*, 2181-2195.
49. Khisamutdinov, E. F.; Li, H.; Jasinski, D. L.; Chen, J.; Fu, J.; Guo, P. X., Enhancing immunomodulation on innate immunity by shape transition among RNA triangle, square and

pentagon nanovehicles. *Nucleic Acids Research* **2014**, 42 (15), 9996-10004.

5 Chapter 5: Conclusions

Nucleic acid nanotechnology has become a burgeoning field, enabling the design of complex therapeutics, biosensors, and molecular machines. From the late twentieth century to present, advancements in the design, prediction, and understanding of nucleic acid structures have propelled this bottom-up nanotechnology-based therapy to the precipice of the clinical approval; however, issues with stability, delivery, and immunostimulation have hindered its advance. This dissertation presents three independent articles which make progress in addressing these issues, elucidating new strategies for designing dynamic NANPs, predicting the immunostimulatory properties of NANPs, and designing a novel carrier system for their delivery.

In the first study, a strand-displacement approach is used to enable the activation of several functionalities including aptamer formation, FRET, RNAi, and transcription. This method demonstrates the ability to conditionally activate a desired functionality only in the presence of two cognate NANPs, acting as an AND gate. Furthermore, the re-association of the two NANPs, as well as their individual properties can be tuned greatly by their composition. Among the tunable properties are their melting temperature, re-association kinetics, and immunostimulatory properties. This approach allows for a desired functionality to be activated only when the two cognate NANPs are combined, allowing for the possibility of targeted, conditionally activated therapeutics.

The second study uses a QSAR approach for analyzing the immunostimulatory potential of NANPs. Specifically, a set of sixteen NANPs with similar design principles but different overall shapes and chemical compositions are examined for their ability to provoke an immune response in human microglial cells. Using physicochemical and sequence-based descriptors such as GC-content, melting temperature, mass, and size, a model was generated with the ability to modestly predict the immunostimulatory properties for a set of NANPs with similar design. It was determined that the stability of the NANP contributes greatly to its immunostimulatory properties, generating several additional questions regarding the cellular processing and

intracellular stability of the nanostructured nucleic acids.

Finally, the third study describes the design and evaluation of a novel polymeric nanoparticle for the delivery of therapeutic NANPs. In this study, P_gP is used for its ability to protect and delivery various NANPs carrying different therapeutic payloads. The polymeric carrier was demonstrated to efficiently electrostatically complex with the NANPs, protect it from nuclease activity, and release an intact product. Furthermore, the delivery of the NANPs was achieved and their therapeutic activity confirmed by RNAi of two different genes, as well as their differential ability to provoke an immune response. Additionally, the distribution of these complexes was studied, demonstrating early evidence of biodistribution based on NANP shape.

Efficacy, biocompatibility, and customizability have driven therapeutic nucleic acids into becoming a clinical reality. Several ASOs, miRNAs, and siRNAs are now available in the clinic, but many have floundered in clinical trials due to immunostimulation and off-target effects. Nucleic acid nanotechnology offers an alternative to traditional NANPs, bringing higher stability, multivalence, and a greater degree of customizability. Undoubtedly, progress in NANP technologies will enable their use as efficient therapeutics for a number of diseases, leading to a new wave of personalized medicine.